Mid-America Earthquake Center

Project ST-4 Final Report

Response Modification Applications for Essential Facilities

by

J. I. Craig, B. J. Goodno, P. Towashiraporn and J. Park

Georgia Institute of Technology

School of Civil and Environmental Engineering

Atlanta, Georgia 30332-0355

March 2002

This research was conducted at the Georgia Institute of Technology and was supported through the Mid-America Earthquake Center by the National Science Foundation under grant ECC-9701785.

Table of Contents

List of Figures

List of Tables

Summary

This study examined the application of passive energy dissipation systems for response modification of essential facilities in the Mid-America region. Essential facilities are defined as buildings that support functions related to post-earthquake emergency response and disaster management. For such buildings simply insuring life safety and preventing collapse are not sufficient, and the buildings must remain operational during or suitable for immediate occupancy after a major earthquake. A regional inventory of essential facilities (MAE Center project SE-1) revealed that unreinforced masonry (URM) is the most common type of construction for essential facilities, and such material is well known to be highly vulnerable to strong earthquakes. As a result, response modification for this type of building, and particularly for low-rise firehouses, was the focus of this study.

Tapered metallic flexures were examined as passive damping devices for response modification purposes. Metallic hysteresis offers good energy dissipation with excellent long-term stability and reliability, and therefore is particularly well-suited for scenarios with infrequent earthquakes. Passive energy dissipation has not been considered for response modification of URM structures because of the very high initial elastic in-plane stiffnesses of URM walls. However, a large number of URM essential facilities commonly include flexible wooden floor and roof diaphragms that couple the URM walls into structures that are more flexible (and complex) than the URM walls alone.

Three response modification concepts were investigated. Type 1 is activated by relative displacements between the in-plane walls and the diaphragm. Type 2 is activated by relative displacements between the diaphragm and the ground, and Type 3 is activated by the relative in-plane displacements within a wall. Only Type 1 and 2 configurations were studied in this report. The passive energy dissipation devices were designed using an energy-based criterion with the objective being to maximize the ratio of the energy dissipated in the devices to the total input seismic energy subject to selected constraints on peak forces and dynamic ductility.

An efficient and simple approach was developed for modeling the in-plane response of perforated URM walls. The wall is decomposed into characteristic regions such as piers and spandrels, and the in-plane behavior of each region is modeled by a single nonlinear spring with empirically determined properties. These nonlinear springs are then assembled into a 2-D

parallel-series composite spring model for the complete wall. The boundary conditions for each of these components are modeled by using either an "effective height" or an "effective end stiffness." An additional factor based on overall wall aspect ratio is applied to reflect overall in-plane bending. The model was calibrated against plane stress solutions and was verified by comparison with experimental results. Good agreement was found for the wall stiffness and strength. Finally, a simple 2-D lumped-parameter building model was developed in DRAIN-2DX and ABAQUS using these in-plane wall models with springs to model the shear deformation modes for flexible floor/roof diaphragms. No consideration was given to out-of-plane wall stiffness but the masses were considered.

The response modification concepts were evaluated using a highly idealized laboratory test model (MAE Center project ST-10) and a full-scale test structure (project ST-11/22). The results verified that incorporation of properly designed passive energy dissipators in the rehabilitation of certain kinds of URM structures lowered energy dissipation demand in the main structure, reduced seismic response, and lessened the possibility of damage. Given the inherently stiff nature of URM structures, this approach can only be applied in cases where sufficient deformation can be developed to fully activate typical metallic hysteretic dampers considered in this study. The primary benefit was a significant reduction in out-of-plane wall deformation induced by a flexible floor diaphragm. The effectiveness of this approach was reduced when the diaphragm stiffness for shear mode deformation was more than about 8% of the in-plane wall stiffness, but this is well above the stiffnesses of typical floor and roof diaphragms. Thus the use of a passive energy dissipator as outlined in this study could be considered as a part of a rehabilitation scheme that aims to reduce the deleterious effects of an overly flexible diaphragm system.

Finally, the probabilistic nature of the problem, specifically the variation in building configuration for a regional class of buildings such as firehouses, was taken into account. Fragility curves and damage probability matrices were used to describe the likelihood of damages under different ground shaking intensities. This research made use of meta-modeling techniques through a combined response surface methodology and Monte Carlo simulation approach to include randomness in configurations over a class of buildings in a region. Improvement in the seismic responses when a passive energy dissipation system is implemented were shown to lead to a lowered probability of damage in the buildings..

1 INTRODUCTION

This report summarizes research carried out under Project ST-4 at the Mid America Earthquake Center (MAEC) to explore and develop response modification approaches that might be suitable for use in rehabilitation of essential facilities typically found in Mid-America. This region encompasses the Midwest, and particularly the New Madrid seismic area along the middle Mississippi River region of the central US. The earthquake hazard in this region is largely defined by infrequent but large and potentially high-consequence events such as the major earthquakes which occurred near New Madrid, MO in 1811-1812.

Hazard mitigation for infrequent but major earthquakes presents significant challenges to the structural engineer. For hazards with very low probabilities of occurrence over the practical life of a structure, seismically resistant design for new structures may be difficult to justify, and it is even more difficult to devise practical strategies to reduce the risk to a large inventory of very vulnerable legacy structures. Such is the case for much of the US Midwest where, for example, one to two story unreinforced masonry (URM) structures are widely found, and yet a major earthquake occurred less than 200 years ago.

The situation is perhaps more clearly defined when one considers the relative differences in magnitudes between what could be taken as a reasonable expected earthquake for design purposes versus what the most extreme event might be. More specifically, for the New Madrid seismic region, the peak accelerations for the "extreme" or Maximum Considered Earthquake (MCE or an earthquake with a 2% in 50 year probability) are more than 3 times larger than for the BSE-1 (Basic Safety Earthquake-1 or 10% in 50 year probability) [FEMA, 2000]. These differences are much less pronounced for US regions of greater (and more predictable) seismicity such as the West Coast.

This presents challenging engineering problems for both new designs as well as rehabilitation projects. A reasonable rehabilitation objective might be, for example, to achieve a Basic Safety Objective (BSO) defined as providing collapse prevention for the MCE while insuring Life Safety Performance for the BSE-1 earthquake [FEMA 2000]. For essential facilities, which are defined as those buildings and facilities that must remain operational immediately following an earthquake, the performance levels must be much higher and should include Operational

Performance (Level 1a) for a BSE-1 hazard and Immediate Occupancy Performance (Level 1b) for the MCE hazard [FEMA 2000].

Any study of response modification approaches for rehabilitation of essential facilities must also consider the type or types of structures that are most commonly used for such facilities. Essential facilities might house any kind of emergency response or post-disaster recovery management operations. Typically these would include fire houses, police stations, emergency management offices, schools, and hospitals. The facilities themselves could range from relatively small buildings for police stations or firehouses to much larger multistory structures for hospitals. The focus of this project was specifically on the smaller, low-rise structures associated with police and fire stations. In the Midwest, such structures are most likely to be two stories or less and constructed largely of unreinforced masonry (URM) [French 2000].

Low rise URM structures are usually characterized by their relatively stiff yet quite brittle structural behavior. URM walls usually exhibit very high in-plane elastic stiffness and very little out-of-plane stiffness. Out-of-plane failures are generally quite brittle unless significant compressive loads are present, but in-plane cracking can lead to relatively ductile behavior of perforated walls if significant pier rocking is developed. A good deal of interest has been devoted to rehabilitation and retrofit methods for URM walls, and this is the subject of a related MAEC project (ST-6) [Abrams 2001]. However, many of the URM essential facilities considered in the present study are constructed with wooden floor and roof diaphragms that are rather flexible and are often poorly tied into the walls. As a result, such URM structures are often complex. For example, while URM walls might adequately resist in-plane seismic forces, the flexible diaphragm can transfer significant out-of-plane forces into orthogonal URM walls, giving rise to connection failures or out-of-plane wall cracking or collapse. The situation is even more complicated for irregular structures.

The present Project ST-4 study focused on the application of passive response modification as a strategy for rehabilitating URM structures with flexible diaphragms that are characteristic of many essential facilities in the Midwest. Normally, passive energy dissipation would not be considered for use in URM structures because of their relatively high elastic stiffness (and consequent small deflections), but the presence of very flexible wood floor and roof diaphragms in these structures can provide a basis for using this approach. In particular, passive energy dissipators (PED's) constructed using metallic hysteretic dissipation mechanisms are considered

in view of the very long recurrence intervals that are characteristic of the seismic hazard in the Midwest (the MCE with a 2% probability in 50 years has a return period of just under 2,500 years and the BSE-1 at 10% in 50years is 474 years).

Prior research at Georgia Tech has attempted to assess the effectiveness of seismic response modification using passive control devices [Pinelli, et al, 1993; Weston, et al, 2002; Dogan, et al, 2002]. The earliest work considered the application of passive response modification using architectural cladding with hysteretic damping being developed in the connection subsystem. Response reductions of as much as 50% from baseline values could be achieved for medium and tall buildings with steel frame structures. More recent work for a 20 story building [Goodno, et al. 1998;] showed that in a new design, use of similar PED's incorporated in the cladding connection subsystem could result in as much as a 15% reduction in the weight of the steel frame for similar performance levels.

1.1 Research Objectives and Scope

The primary objective of this research was to investigate response modification approaches for essential facilities typical of those constructed in the Midwest. Specifically, the research studied the use of passive damping systems, specifically hysteretic damping systems, to control and modify the seismic response of low rise URM structures that are typical of these types of structures. The objective were not to develop a particular rehabilitation approach, but rather to investigate how effective passive response modification methods might be when applied to these URM structures. Innovative schemes using metallic dampers that are activated by structural deformations of flexible wood floor and roof diaphragms that are commonly incorporated in these buildings were developed. Appropriate damping system design criteria for optimal overall performance were also developed, and in this context, optimal means that damage in the main structural components was minimal or none. At the same time, a significant reduction in the overall seismic demands is expected.

Since randomness is a defining characteristic of earthquakes and modeling uncertainties are inherent in the problem, especially when trying to consider a "typical" essential facility, further detailed analyses considering the probabilistic properties of the problem were pursued. Rather than simply evaluate the use of PED's in a deterministic fashion for a "typical" URM essential facility, a probabilistic approach to consider the variability in such structures and in the demand

across the New Madrid area was developed. A meta-modeling approach based on use of Monte Carlo simulations utilizing response surfaces [Mavris, et al, 1995, 1996] to represent more detailed nonlinear structural analysis models was developed. The performance of baseline and modified buildings are characterized by fragility curves and these were used to assess the expected improvements.

1.2 Regional Inventory

Essential facilities are defined as buildings that support functions related to post-earthquake emergency response and disaster management such as fire stations, police stations, emergency shelters, hospitals, etc. As a consequence, the unimpeded availability and functionality of essential facilities during and immediately following an earthquake is a top priority.

An accurate understanding of the structural characteristics of essential facilities in the New Madrid area is the first step in addressing this problem. A regional assessment of essential facilities was carried out by French and Olshansky [2000] to assemble a building inventory. Over 5000 such buildings were identified and more than 1300 of these were inventoried visually and/or by telephone. It was found that nearly a third of these facilities (see Table 1-1) are constructed of unreinforced masonry and are two stories or less in height. In fact, this is by far the largest structural grouping by a factor of nearly 3 times over steel frame construction which accounts for about 12% of the total. It follows, then, that any study of response modification approaches for essential facilities must consider the application to these kinds of structures which are highly vulnerable to earthquakes.

Table 1-1: Number of Facilities by Structure Types from French and Olshansky [2000]

Structure Types	Number	Percent
C1 – Concrete	9	0.7
C2 – Concrete	78	6.0
C3 – Concrete Frame	83	6.4
MH – Mobile Home	17	1.3
PC1 – Precast Concrete	10	0.8
PC2 – Precast Concrete	5	0.4
RM1 – Reinforced Masonry	72	5.5
RM2 – Reinforced Masonry	30	2.3
S1 – Steel Frame	54	4.1
S2 – Steel Frame	21	1.6
S3 – Prefabricated Steel	91	7.0
S4 – Steel Frame	22	1.7

S5 – Steel Frame	163	12.5
URM – Unreinforced Masonry	428	32.8
W1 – Wood Frame	81	6.2
W2 – Wood Frame	43	3.3
Unknown	99	7.6
Total	**1306**	**100**

1.3 Passive Approaches

1.3.1 Background

Conventional seismic design philosophy is based on the concept of balancing demand with capacity. The structures are designed to ensure that the ductility demands developed in structural members are balanced by the ductility capacities of those members. The structural members dissipate the seismic energy by undergoing large inelastic deformation, which leads to damage in those structural members. This design philosophy concentrates on preventing structural collapse, but higher levels of performance (*e.g.* Immediate Occupancy) may be required of modern buildings. For example, the interstory drifts required to achieve significant energy dissipation in the ductile structural members are often large and may result in severe damage to nonstructural components. Substantial damage to nonstructural components could affect the overall performance of the structures and preclude achieving Life Safety or Immediate Occupancy levels of performance. Passive energy dissipation concepts have been proposed to address this situation by limiting damage mainly to the pre-designed energy dissipation devices while reducing interstory drift and thereby improving overall performance.

For roughly 25 years, it has been recognized by both researchers and practitioners that incorporating passive energy dissipation (PED) devices into buildings would improve their dynamic response (*i.e.* displacements, accelerations, *etc*.) When the input energy (seismic or wind) is applied to the structures, the passive energy dissipation devices consume a portion of that input energy, thereby reducing energy dissipation demand in the primary structural elements. As a result, damage in the main structural elements is minimized. Unlike the situation with active and semi-active control systems, there is no need for external power sources to operate passive energy dissipation systems. The PED devices can also be used as protective systems in buildings under wind as well as earthquake forces.

Many different types of passive energy dissipation devices have been used in seismic protection applications for buildings. Metallic energy dissipation devices are based on the plastic deformation of the metallic materials, such as mild steel. Friction dampers dissipate energy through the friction that develops between two solid bodies sliding relative to one another. Viscoelastic dampers use highly dissipative polymeric materials which dissipate energy when subjected to shear deformations. Other forms of passive energy dissipation devices include viscous fluid dampers, tuned mass dampers, and tuned liquid dampers, none of which will be covered in this report.

In recent years, extensive efforts have been made to apply passive energy dissipation devices to actual structures. A large number of PED devices have been successfully installed in structures in highly seismic regions throughout the world. Examples of passive energy dissipation systems are presented in the following sections.

1.3.2 Metallic Dampers

One of the most effective mechanisms for dissipating input seismic energy in a structure is through the inelastic deformation of metallic materials under time-dependent cyclic loading. Mild structural steel is a popular choice for the metallic energy dissipation device because of its relatively high stiffness in the elastic region and potential of dissipating energy in the post-yielding region. Alternative materials include leads and shape-memory alloys. Numerous experimental and analytical studies have been conducted to determine the properties and behaviors of these devices.

Past Developments

The idea of utilizing metallic hysteretic dampers to dissipate a portion of the input energy in structures began in early 1970s. Kelly, Skinner, and Heine [1972], and Skinner, Kelly, and Heine [1973, 1975] reported on the conceptual and experimental development of three special mechanical devices to be incorporated into a structure specifically to passively absorb energy generated by an earthquake (see Figure 1-1):

(a) Rolling- bending thin U-shaped strips;

(b) Torsional energy absorbers; and,

(c) Flexural energy absorbers.

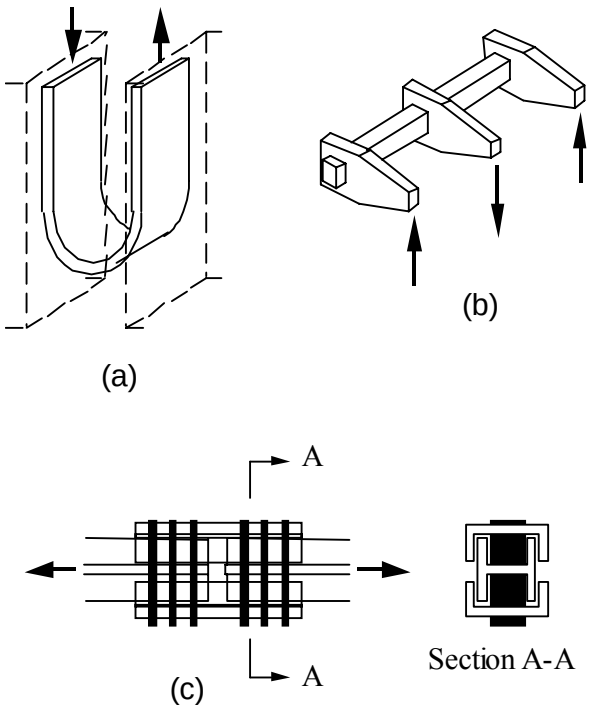

Figure 1-1: Metallic Damper Geometries: (a) U-Shaped Strips, (b) Torsional Energy Absorber, and (c) Flexural Energy Absorber. From Kelly et al. [1972]

The U-shaped steel strips (Figure 1-1a) interact between adjacent surfaces with parallel relative movement. Plastic deformation occurs when the strip changes from straight to curved. Different specimens were tested under controlled cyclic displacements. The peak load, dissipated energy and the total number of cycles to failure depended on the thickness, radius and width of the device. The torsional bar (Figure 1-1b) uses a combination of torsion and bending, and therefore was designed for use between surfaces moving away from each other in foundations or shear wall systems. The flexural device (Figure 1-1c) uses bending of short rectangular beams, and therefore was designed for use in diagonal bracing to provide the energy absorption normally developed in the vicinity of beam-column connections. This flexural device is not as efficient in energy absorption nor as fatigue resistant as the torsional bar, but it can be easily located and readily replaced in the event of earthquake damage.

Test results showed that, if dimensioned to achieve sufficient ductility and to avoid low-cycle fatigue, the energy-absorption capacity of these three devices could significantly augment that of a conventional building structure. The torsional device was the most efficient energy absorber, with lifetimes in the range of 100 to 1000 cycles. Skinner, Beck, and Bycroft [1975], showed

that these hysteretic dampers could be combined with base isolation systems, and used for the isolation of bridges, nuclear reactors, and other special structures.

Tyler [1978a, 1978b] proposed the concept of the tapered energy dissipation device. It is also a flexural device where the taper is shaped so that the stress is uniformly distributed over the whole length of the device. He proposed two types of tapered cantilever beams. The round type (Figure 1-2) provides damping in any arbitrary direction. The taper, which is a cubic curve, reaches over two thirds of the length, leaving some material at the top for attachment. The plate type (Figure 1-3) can only provide energy dissipation in one direction, but it is cheaper to fabricate. The device has a linearly decreasing width over two thirds of the length while the thickness is kept constant. For both devices, design curves were developed that yield the required length and diameter or width given the maximum strain level, the damping force and the stroke.

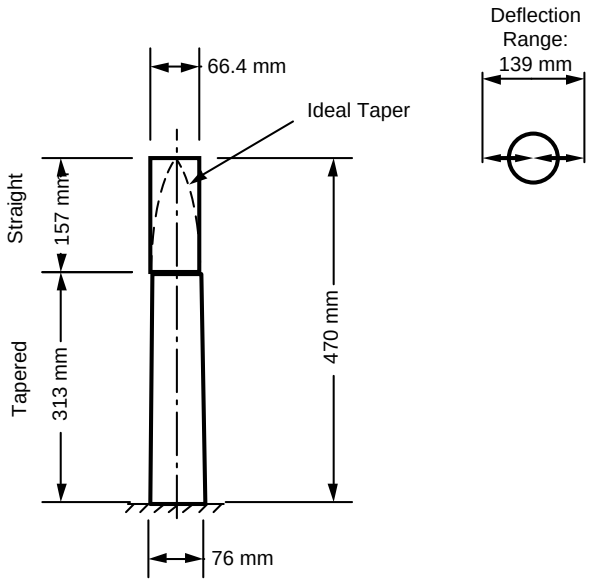

Figure 1-2: Round Tapered Cantilever Damper. Taper over Two Thirds of the Length, then Constant Diameter. From Tyler [1978a]

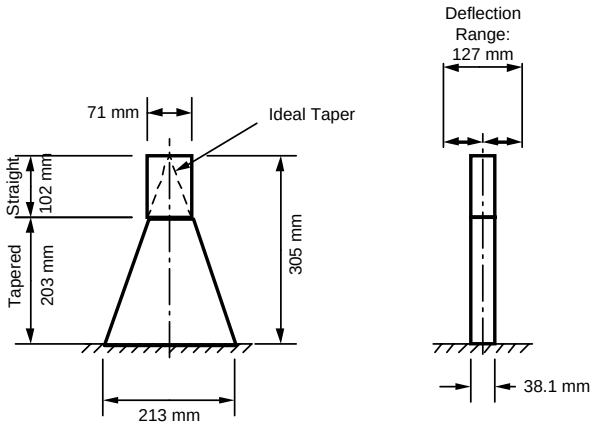

Figure 1-3: Plate-Type Tapered Cantilever Damper, Taper over Two Thirds of the Length, then Constant Width. From Tyler [1978b]

The concept of a triangular plate damper was originally developed in New Zealand by Tyler [1978b]. This device, which consists of some identical triangular structural steel plates positioned in parallel, is typically installed within a frame bay between chevron braces and the overlying beam, as shown in Figure 1-4. The base of each triangular plate is welded into a rigid base plate to approximate a fixed end condition (Figure 1-5). As a result of this configuration, the damper primarily resists horizontal forces, associated with interstory drift, via uniform flexural deformation of the individual plate.

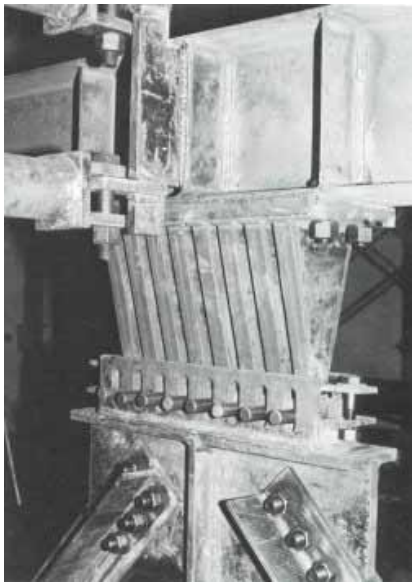

Figure 1-4: Triangular Plate Device Installed between Chevron Braces and the Overlying Beam from Tsai et al. [1993]

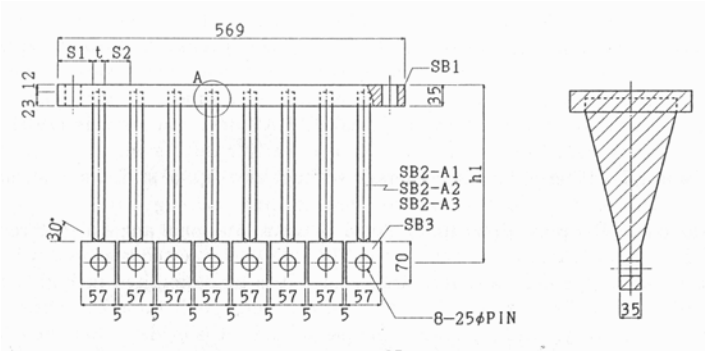

Figure 1-5: Geometries of the Triangular Plate Device from Tsai et al. [1993]

Following the triangular plate energy dissipators, Schneider et al. [1983] reported on development of a tapered X-plate steel device for use as an energy dissipation device in complex spatial piping systems. Scholl [1988] described this so-called added damping and stiffness element (or ADAS) and its applications. ADAS elements (Figure 1-6 and Figure 1-7) consist of multiple X-shaped mild steel plates connected in parallel to each other. Bergman and Goel [1987] carried out a series of cyclic tests to evaluate the properties of ADAS elements, and they pointed out their good fatigue resistance. Alonso [1989] studied in detail the mechanical characteristics of X-plate energy dissipators, and looked for analytical ways to predict their properties. Whittaker et al. [1991] investigated the use of ADAS elements in the retrofit of moment resisting frames. They showed that these energy dissipation devices can successfully reduce the dynamic response of a moment resisting frame, and they proposed to extend their use to other types of structural systems.

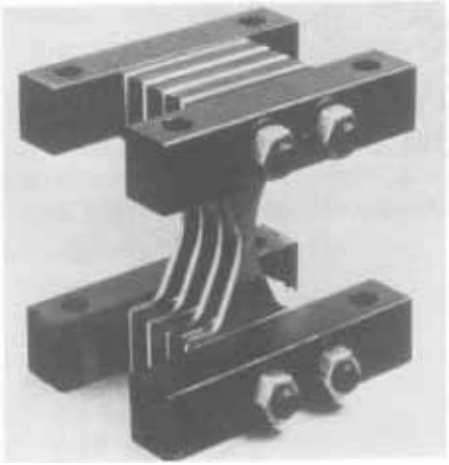

Figure 1-6: Scaled Model of ADAS Element from Perry et al. [1993]

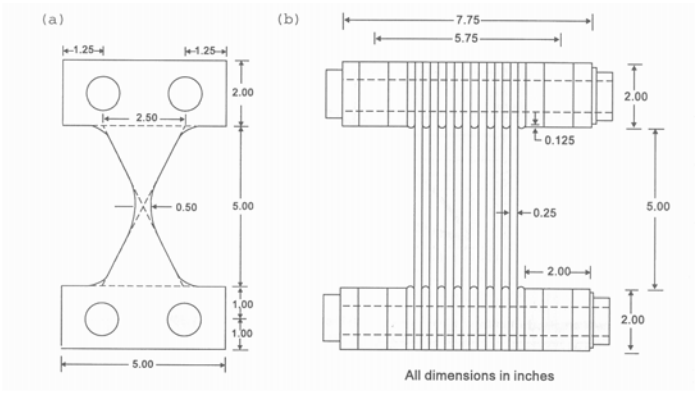

Figure 1-7: ADAS Element Geometry from Whittaker et al. [1991]

At Georgia Tech, Pinelli, et al. [1993] analytically and experimentally investigated a tapered energy dissipation device for use as cladding connections in buildings. The device consists of a section of a square tube, cut away as shown in Figure 1-8, to create two tapered beams. Tapering of the beams ensures that plastification will occur over a significant portion of the material and that the tapered beams will deform with double curvature.

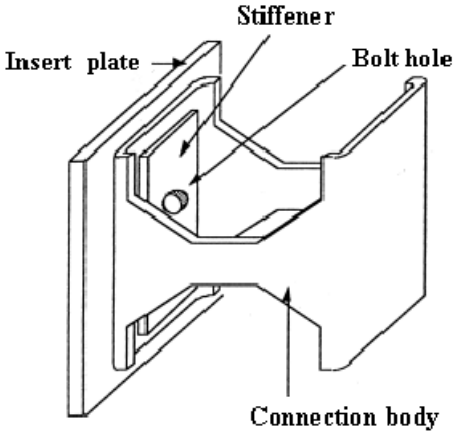

Figure 1-8: Tapered Energy Dissipation Device from Pinelli et al. [1993]

Tests by Pinelli showed that the tapered device provided large and stable hysteresis loops without stiffness degradation or strength deterioration (Figure 1-9). The plastic deformations were distributed uniformly throughout the tapered beams maximizing the amount of energy dissipated. The device also sustained a large number of cyclic load reversals (as high as 37 cycles) before failure representing good fatigue behavior of the tapered device.

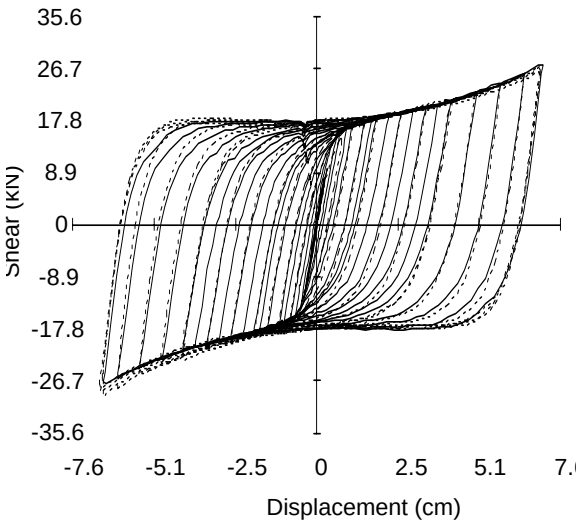

Figure 1-9: Hysteresis Loops for Tested Tapered Device from Pinelli et al. [1993]

Analytical Model

As mentioned in the previous section, the energy dissipation mechanism in metallic dampers results from their inelastic deformations. Most of the time mild steel is used for this purpose. A typical stress-strain curve for mild steel is shown in Figure 1-10. At loads corresponding to stress less than the yield strength σ_y, the behavior of mild steel is fully elastic, with stress linearly proportioned to strain. In this elastic region, the original state is fully recoverable and hence no energy dissipation occurs. Beyond the elastic region, when the stress exceeds the yield strength σ_y, irreversible plastic deformation occurs generating inelastic energy dissipation (shaded area in Figure 1-10).

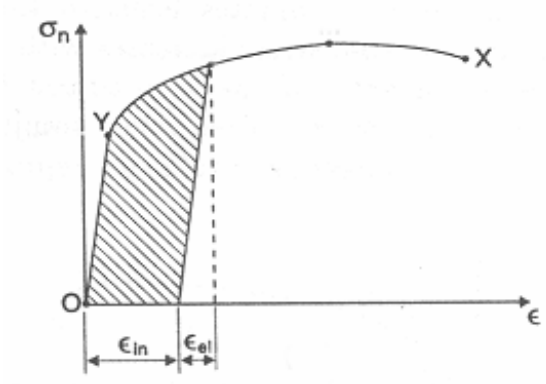

Figure 1-10: Stress-Strain Relationship of Mild Steel from Soong and Dargush [1997]

Numerous mathematical models have been proposed to simplify the stress-strain relationship of metallic substances. Two of the most well known models are the elastic-perfectly plastic model and the elastic-linear strain hardening model (Figure 1-11). These models compare reasonably well with experimental results.

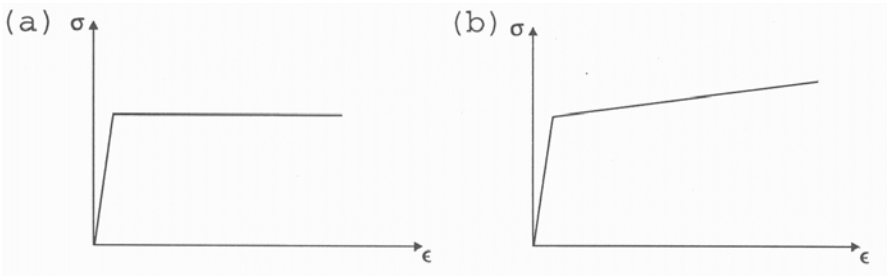

Figure 1-11: Stress-Strain Mathematical Models; a) Elastic-Perfectly Plastic, b) Elastic-Linear Strain Hardening from Soong and Dargush [1997]

Furthermore, in order to develop hysteresis models for metallic dampers, material behavior under load reversals must be considered. The unloading branch of the stress-strain curve is parallel to the initial loading path until it reaches another yield point in the reverse direction. The loading-unloading process will be repeated as the external cyclic loading continues.

Ideally, a very detailed analytical model containing all significant material behaviors is desirable for highest accuracy. Such a detailed nominal model may not be practically possible due to time and computational efforts required. Instead, a design model that provides a reasonable level of fidelity, but is also computationally tractable is preferable. The design model involves a relatively small number of parameters for practical purposes. A simple piecewise bilinear model based on either the elastic-perfectly plastic or the elastic-linear strain hardening material models is generally used. In the case of the elastic-perfectly plastic model, the design parameters are the elastic stiffness and yield force of the damper. An additional design variable, the dimensionless strain hardening ratio, will be needed for the elastic-linear strain hardening model. Figure 1-12 illustrates a typical metallic damper design model.

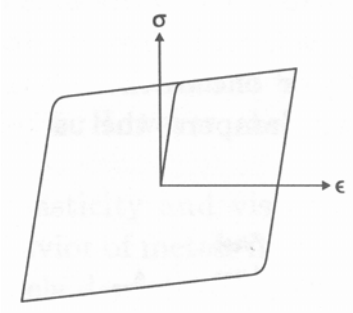

Figure 1-12: Typical Metallic Damper Model Based on the Elastic-Linear Strain Hardening Material Model from Soong and Dargush [1997]

Structural Applications

Having gained some confidence from experimental results, researchers and practitioners have turned their interests to applications of metallic dampers to real structures. The first structural implementation of metallic energy dissipation devices took place in New Zealand. The use of torsional beam metallic dampers in the piers of the Rangitikei Bridge introduced the first-generation of metallic dampers. After that, tapered plate cantilever devices were installed at the base of a chimney in Christchurch and in the Dunedin Motorway Overbridge. Many other metallic damper applications have subsequently been employed in structures in New Zealand.

More recent applications include the Izazaga building, the Cardiology Hospital buildings, and the Reforma buildings in Mexico City, and the Wells Fargo Bank building in San Francisco. The Izazaga building has twelve floors above grade. The building was built in the late 1970s and the structural system is reinforced concrete frames with brick infill walls. The building experienced moderate structural damage from the 1985 Mexico Earthquake, and the first retrofit was made by adding concrete shear walls to increase the lateral stiffness of the building. This was unsuccessful because the building sustained further damage from subsequent earthquakes in 1986 and 1989. The application of metallic dampers was used as a second retrofit method in 1990. Approximately 250 ADAS (added damping and stiffness) devices were installed in 10 outer frame bays of the building to allow building operation during installation. Structural analysis results showed reduction in the fundamental period of the building after the ADAS devices had been installed. For this type of building in Mexico City, reducing the fundamental period results in reduction in building response and, accordingly, damage.

The six-story Cardiology Hospital building in Mexico City was constructed in 1970s. The hospital complex suffered severe damage and collapse of some of its buildings during the 1985 Mexico Earthquake. The retrofit scheme consisted of a series of 18 external steel-trussed buttresses linked to the building floors through 90 ADAS devices (Figure 1-13). Extensive nonlinear analyses were carried out to verify the performance of the retrofit system. The results showed significant reduction in interstory drift and also base shear of the retrofitted building. This reduction resulted from the combined effect of external stiffening action from the buttresses and energy dissipation through the ADAS devices.

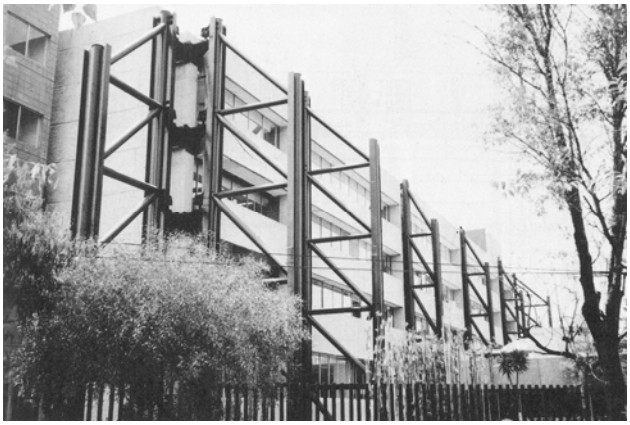

Figure 1-13: Retrofit of the Cardiology Hospital Building from Martinez-Romero [1993]

The Reforma building is a three-building complex built in 1940s. The structural system is composed of cast-in-place reinforced concrete frames. Even though this building had survived major earthquakes over the past 50 years, there was fear that this building remained vulnerable to future major earthquakes. This building underwent a major seismic retrofit in 1992 by installing ADAS devices in 40 frame bays. Results of computational analyses showed reductions of up to 20 percent in roof displacements and 40 percent in maximum story drifts could be obtained by use of ADAS elements.

The Wells Fargo Bank building in San Francisco is a two-story non-ductile concrete frame structure. The building experienced structural and nonstructural damage in the 1989 Loma Prieta earthquake. The retrofit plan was to add steel chevron-braced frames connected with the existing concrete frames by ADAS devices as shown in Figure 1-14. A series of X-shaped mild steel plates was used for this system. The use of the ADAS devices in this building was the first structural application of these devices in the United States. The nonlinear time-history analyses

using DRAIN-2DX confirmed that the maximum displacement of the retrofitted building was within acceptable limits under severe earthquakes.

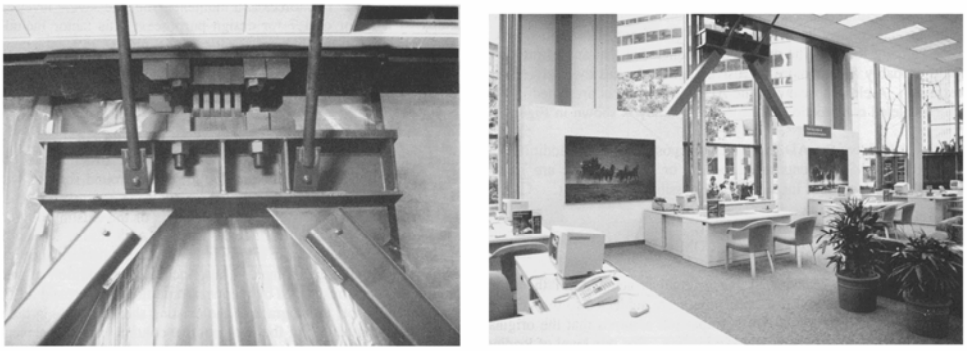

Figure 1-14: Retrofit of the Wells Fargo Bank Building from Perry et al. [1993]

Recently, Goodno et al. [1998] investigated the application of cladding connectors using tapered energy dissipation devices developed by Pinelli [1992]. A 20-story steel frame building located in Oakland was selected to carry out computational analyses and check the performance of the tapered connectors. DRAIN-2DX, which can perform nonlinear time-history dynamic analysis, was used. Over a thousand tapered energy dissipative cladding connectors were added to the building model. A reduction in top floor displacement of up to 40 percent was achieved when tapered cladding connectors were included. Further investigations considered the redesign of the primary framing systems to take advantage of the reduced seismic demand and improved energy dissipation brought about by the cladding connectors, while maintaining the same level of baseline building response. The conclusion of the analytical studies was that by installing the tapered cladding connectors, the primary structural member sizes could be reduced equivalent to a reduction in structural weights of 17 percent in comparison to the baseline building.

1.3.3 Friction Dampers

Friction energy dissipation devices utilize the mechanism of solid friction between two moving surfaces to provide energy absorbing capability. This type of mechanism has long been employed in other industries. The most obvious example is in automobile brakes, in which kinetic energy is dissipated through the friction mechanism. Investigation of friction energy dissipation devices for seismic improvement in structures began in late 1970s.

Past Developments

The study of friction dampers in building applications originated in the late 1970s when Tyler [1977] proposed the use of friction damped PTFE (Teflon) sliding joints between cladding panels, or partitions, and the main structure to reduce the effects of wind and earthquakes.

Based primarily on the concept of friction dampers in automobile brakes, Pall and Marsh [1980] developed a passive friction damper, called the Limited Slip Bolted (LSB) joint, for structural applications. The LSB design integrated brake lining pads between steel plates in order to supply a consistent force-displacement response. The LSB joint configuration is shown in Figure 1-15. Brake lining pads were utilized again in an alternative design proposed by Pall and Marsh [1980] for application in framed structures with cross bracing (Figure 1-16). It consisted of diagonal bracing elements connected by horizontal and vertical link elements with a friction lining pad at their intersection point. Test results verified that adding friction energy dissipation devices to structures would improve their structural performance. It was also discovered that the devices became more effective energy dissipators as the ground motion intensity increased.

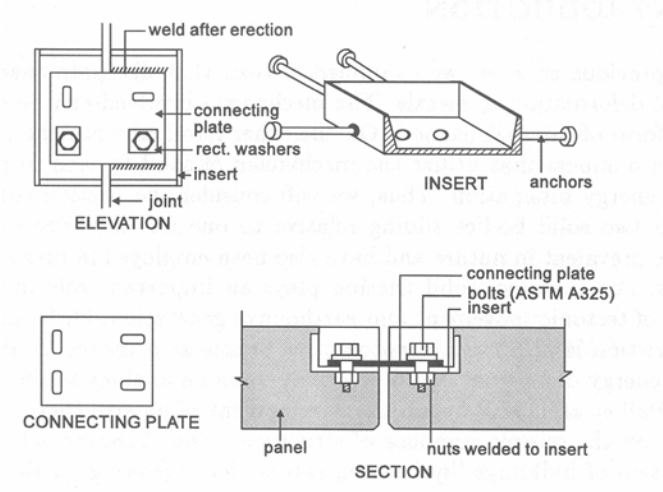

Figure 1-15: Limited Slip Bolted Joint Friction Damper from Pall and Marsh [1980]

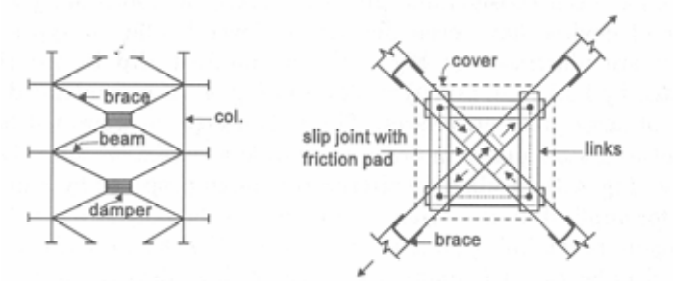

Figure 1-16: X-Braced Friction Damper from Pall and Marsh [1980]

Sumitomo Metal Industries, Ltd., Japan, designed and developed a cylindrical friction damping device with copper alloy friction pads that slide directly on the inner surface of the steel case, as shown in Figure 1-17. The required normal force is exerted through the action of a spring against the inner and outer wedges. The device was first developed for use as a shock absorber in railway rolling stock. Aiken et al. [1993] conducted a shake table test on a 1/4-scale 9-story steel frame with Sumitomo friction dampers installed. The dampers were connected to the steel frames using the Chevron bracing system as shown in Figure 1-18. Both experimental and analytical studies demonstrated an improvement in building response for different ground motions.

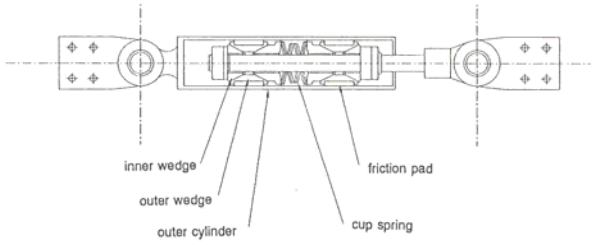

Figure 1-17: Sectional View of Sumitomo Friction Damper from Aiken et al. [1993]

The Energy Dissipating Restraint (EDR) was presented by Nims et al. [1993]. The EDR dissipates input energy by sliding friction through a range of motion with a stop at the end. Internal stops are provided within the cylinder to create tension or compression gaps. The EDR utilizes steel compression wedges and bronze friction wedges to transform the axial spring force into normal pressure acting outward on the cylinder wall creating the required friction surface. The unique characteristics of the EDR device are that it is strongly self-centering and that its friction force is proportional to the displacement. Both characteristics cannot be found in other

friction dampers. An internal view of this device is presented in Figure 1-19. A commercial damping product by Fluor Daniel, Inc. using the EDR concept was tested by Aiken et al. [1993]. The overall effect of the EDR device was to greatly reduce the maximum displacements and interstory drifts in the model. Part of the substantial reduction in response came from the added stiffness and part was from the energy dissipation through the EDR devices. The EDR system was shown to be effective not only for low level seismic or wind forces, but also for high seismic forces.

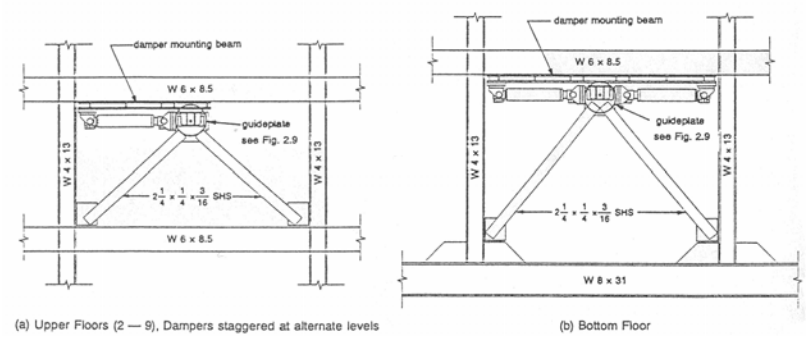

Figure 1-18: Installation of Sumitomo Dampers in Chevron Bracing System Model from Aiken et al. [1993]

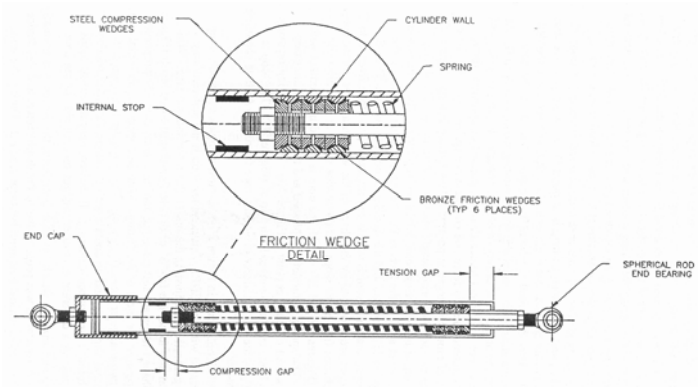

Figure 1-19: Internal View of Energy Dissipating Restraint Device from Nims et al. [1993]

Development of the Slotted Bolted Connection (SBC) energy dissipator by Fitzgerald et al. [1989] and Grigorian et al. [1993] overcame some of the shortcomings in other friction devices. Many of these devices often require precision manufacturing or the use of exotic materials in order to obtain desired performance. In contrast, the SBC system requires only slight modification of standard construction practices. The SBC is composed of a gusset plate

connected to the structural bracing channel elements and cover plates through a bolted connection (Figure 1-20). The elongated bolt slots were parallel to the line of loading. Fitzgerald et al. [1989] employed all structural steel components, while Grigorian et al. [1993] added brass interface plates between friction surfaces. The analytical results by Grigorian et al. [1993] revealed that 85 percent of the input energy in the specimen could be dissipated by the SBC. The SBC also restrained buckling or yielding of the diagonal braces.

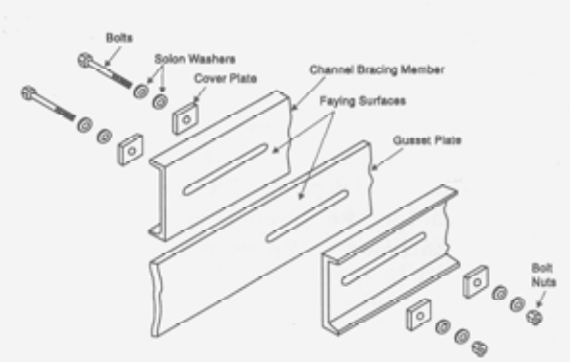

Figure 1-20: Slotted Bolted Connection (SBC) from Fitzgerald et al. [1989]

Analytical Model

Mathematical models for force-displacement of friction dampers depend greatly on the configurations of the dampers and their experimental results. This section reviews both experimental data and corresponding mathematical models for several types of friction energy dissipation devices.

Pall and Marsh [1980] conducted static and dynamic tests on the Limited Slip Bolted (LSB) joints having different surface treatments. The main objective of the experiments was to find the surface treatment that provided a consistent and predictable response, rather than to obtain maximum energy dissipation. Results showed that the use of the heavy-duty brake lining pads inserted between slipping surfaces provided the most consistent and predictable cyclic response (Figure 1-21a). Based upon the experimental results, the elastic-perfectly plastic model appeared to be appropriate so the hysteresis model shown in Figure 1-21b was used for the LSB joints. The behavior is linear elastic as long as the load is less than the slip load P_s and zero stiffness is assumed during the slippage stage. The model also includes a stiff bearing stage for displacement beyond the slip length Δ_b.

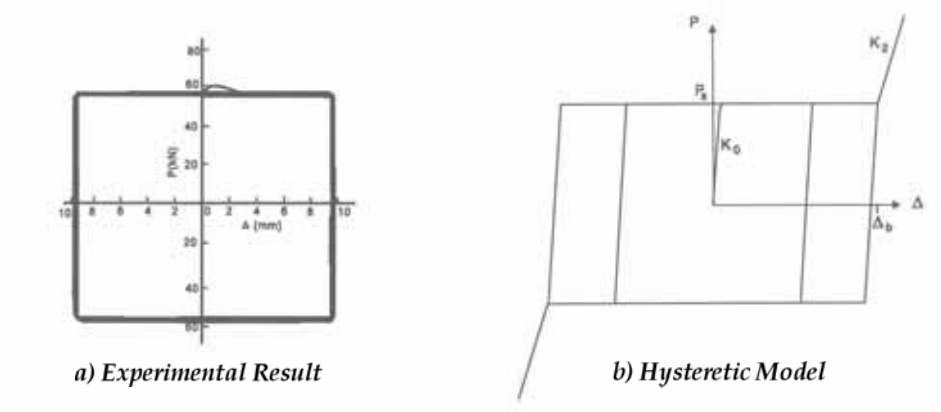

Figure 1-21: Hysteretic Force-Displacement Curves for Limited Slip Bolted Joints; a) Experimental Results from Pall et al. [1980], b) Simplified Hysteretic Model from Soong and Dargush [1997].

Filiatrault and Cherry [1987] carried out experiments on the X-braced friction dampers, developed earlier by Pall and Marsh [1982], with heavy-duty asbestos brake lining pads. Under a cyclic displacement-controlled loading, a consistent response was observed. Contrary to the response of the LSB joints, the response of the X-braced dampers was no longer perfectly rectangular (Figure 1-22a). The notches appearing in the two corners of the hysteresis loops were the result of the difference between the bolt diameters and the bolt holes. A hysteresis model (Figure 1-22b) was then developed to better represent the test findings. Additional required parameters were P_1, Δ_1, and K_1 in the notch regions.

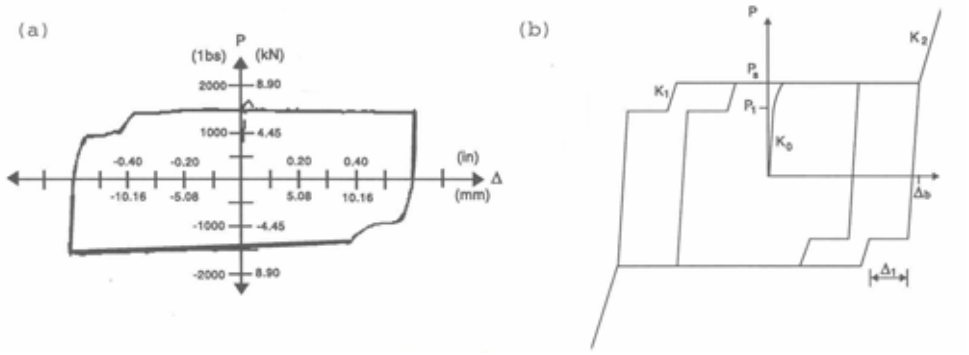

Figure 1-22: Force-Displacement Curves for X-Braced Dampers; a) Experimental Results from Filiatrault and Cherry [1987], b) Hysteretic Model from Soong and Dargush [1997].

A series of laboratory tests have been carried out for the Slotted Bolted Connections (SBC) beginning with the work by Venuti in 1976 at San Jose State University [Venuti 1976]. In 1984

Zsutty conducted further tests on the SBC to improve the earlier test results [Zsutty 1985]. In this experiment, two runs of cyclic loading were applied. Run 1 was limited to the range of deformation involving only central gusset plate slippage (state 1). Run 2 incorporated deformations that developed when the cover plates slipped (state 2). Typical load-deformation diagrams for both state 1 and state 2 were recorded and are shown in Figure 1-23. Fitzgerald et al. [1989] investigated this result and proposed idealized hysteresis models for the SBC. The models, for states 1 and 2, are shown in Figure 1-24.

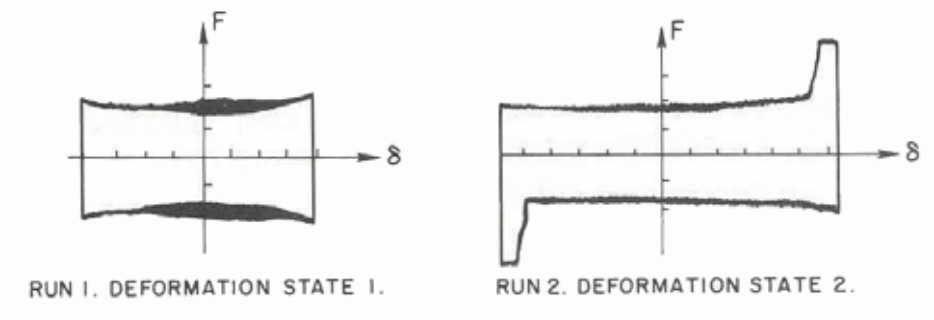

Figure 1-23: Typical Load-Deformation Diagrams for the Slotted Bolted Connections from Fitzgerald et al. [1989]

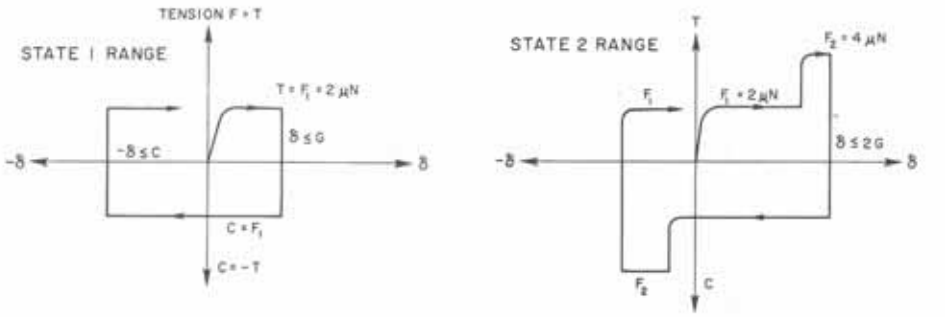

Figure 1-24: Idealized Hysteretic Models for the Slotted Bolted Connections from Fitzgerald et al. [1989]

The final friction damper to be considered here is the Energy Dissipating Restraint (EDR) device. Richter et al. [1990] and Nims et al. [1993] have studied the EDR device manufactured by Fluor Daniel, Inc. Typical experimental hysteresis behaviors are displayed in Figure 1-25 for different configurations. Figure 1-25a represents the response obtained with zero gaps and zero spring preload. Triangular shaped hysteresis loops indicate that the slip force is proportional to

the displacement. With zero initial gaps and non-zero spring preload, the flag-shaped hysteresis loops of Figure 1-25b are achieved. It can be seen that the response characteristics of the EDR are quite different from other friction dampers. Soong and Dargush (1997) suggested two corresponding hysteresis models as shown in Figure 1-26. Parameters K_1, K_2, and K_3 were found to be dependent on one another. Other variables that affected these parameters are K_s (spring stiffness) and a positive factor α incorporating the geometric and Coulomb friction effects. The relationships between various parameters, from Soong and Dargush [1997], are as follows:

$$K_1 = \frac{(1+\alpha)K_s K_3}{(1+\alpha)K_s + K_3} \tag{1.1}$$

$$K_2 = \frac{(1-\alpha)K_s K_3}{(1-\alpha)K_s + K_3} \tag{1.2}$$

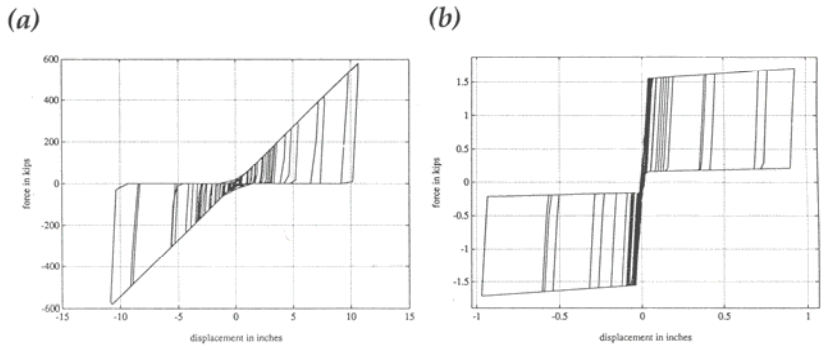

Figure 1-25: Typical Experimental Hysteresis Behaviors of the Energy Dissipating Restraint Device (EDR) from Nims et al. [1993]; a) With Zero Gaps and Zero Spring Preload, b) With Zero Gaps and Non-Zero Spring Preload

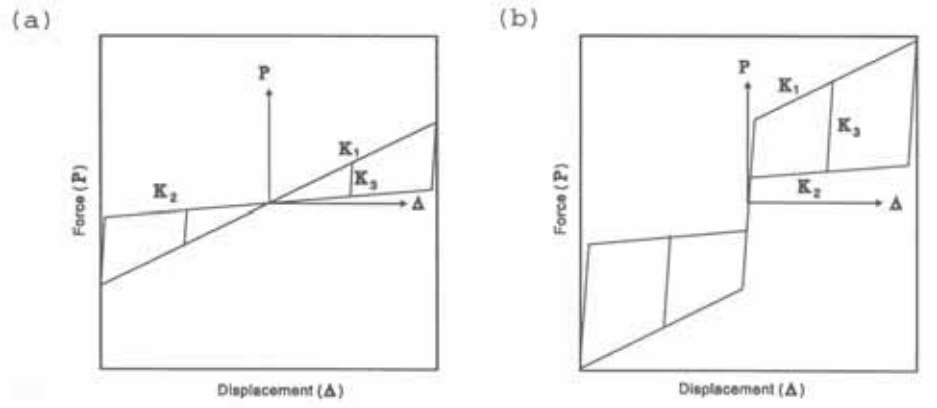

Figure 1-26: Hysteresis Models of the Energy Dissipating Restraint Device (EDR); a) With Zero Gaps and Zero Preload, b) With Zero Gaps and Non-Zero Preload from Soong and Dargush [1997]

Structural Applications

Most of the structural applications of the friction dampers are associated with the use of Pall friction dampers in Canada and Sumitomo friction dampers in Japan. Several of the applications in Canada will be discussed below.

The McConnel Library building at Concordia University in Montreal was the first building that utilized friction devices in its construction. The main structural system of the building was a reinforced concrete frame with reinforced concrete flat slabs. The friction dampers were incorporated in some concrete frames via steel braces and special slab-to-column reinforcement details. A total of 60 friction devices were incorporated into the building, eliminating the need for expensive concrete shear walls. Nonlinear analyses predicted that the optimal slip loads for the devices would range between 600 and 700 kN depending on where the devices were located in the building. The performance of the building equipped with friction dampers was comparable to that of the same building with shear walls, but addition of friction dampers resulted in a net savings of 6.5 percent in structural cost (or 1.5 percent of the total building cost) while its earthquake resistance was significantly increased.

The school buildings at Ecole Polyvalante near Montreal suffered minor structural and nonstructural damage from the 1988 Saguenay Earthquake. The original buildings were constructed of precast concrete beams and columns with welded connections. Floor and roof panels were also precast concrete and the overall structure had very low lateral force resistance. Two alternative retrofit schemes were considered: 1) addition of cast-in-place concrete shear

walls, and 2) steel bracing with the friction dampers. The more expensive cast-in-place shear walls scheme was rejected because the increase in overall stiffness of the building might lead to amplified building responses considering the characteristics of typical earthquakes in the region. Instead, 64 friction devices inserted in steel crossed-bracing were installed within the existing precast concrete frames and 388 friction dampers were installed in the precast wall panel connections. It was reported that inclusion of these friction energy dissipation devices resulted in a 40 percent reduction in construction cost and 60 percent reduction in construction time compared to the alternative retrofit scheme using shear walls.

The main headquarters building of the Canadian Space Agency Complex located near Montreal is a three-story structural steel framed structure clad with aluminum panels. Since this building housed sensitive equipment and instrumentation, special care was taken to ensure that building functionality could be maintained during an earthquake. A protection system using friction damped steel cross braces was included in the construction. A total of 58 braced bays with Pall friction dampers, each having a slip load of 500 kN, were installed. Four alternative structural systems were compared using nonlinear time-history dynamic analyses. These four alternatives included braced frames (BF), moment-resisting frames (MRF), moment-resisting braced frames (MRBF), and friction-damped braced frames (FDBF). The analysis results demonstrated that the performance of the building with FDBF was superior to that of other systems (Pall et al. [1993]).

Soong and Dargush [1997] presented several structural implementations of the Sumitomo friction dampers in Japan. These buildings include the 31-story steel frame Sonic Office building containing eight 22-kip dampers per story and the 22-story Asahi Beer Azumabashi building in Tokyo with four 22-kip dampers per story level.

1.3.4 Viscoelastic Dampers

For roughly 20 years, viscoelastic dampers have been used successfully in high-rise buildings to minimize wind effects. However, the application of viscoelastic dampers to reduce seismic response in buildings is relatively new in comparison to the use of metallic and friction devices. Analytical and experimental investigations on the use of viscoelastic devices under seismic loading have been carried out over only the past decade. The long-term properties and characteristics of these devices are not well defined, and the viscoelastic materials used are also

highly dependent on environmental effects, such as the ambient temperature. For these reasons and because of the long return period of earthquakes in the mid-America region, it was felt that viscoelastic dampers were of limited interest at this time for use in rehab of low-rise URM construction, the focus of this research. Therefore, only brief discussion of past research on these devices will be provided in this report.

Past Developments

Viscoelastic dampers have not been used extensively in seismic rehab applications for buildings. A typical viscoelastic damper consists of viscoelastic material layers bonded between steel plates (Figure 1-27). The seismic energy is dissipated when the structural dynamic response induces relative motion between the outer steel flanges and the center plate.

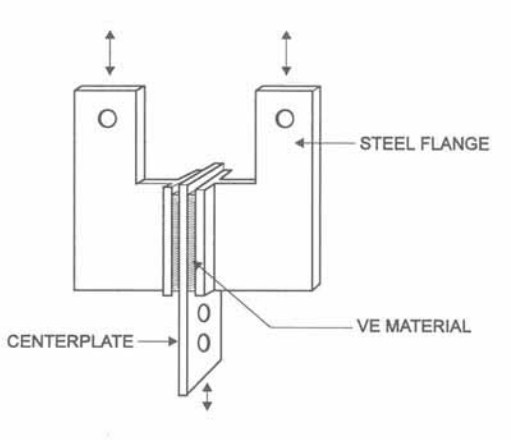

Figure 1-27: Typical Viscoelastic Damper from Soong and Dargush [1997]

Aiken et al. [1993] performed a shake table experiment on a scale model of a 9-story moment resisting steel frame. The viscoelastic dampers were added to the structural frames through single diagonal braces. The viscoelastic material used in this experiment was an acrylic copolymer developed by 3M Co. Fourteen different ground motions were applied to the model. Both experimental and analytical results showed the superior performance of the viscoelastic damped steel frames. Response comparisons for selected ground motions revealed that interstory drifts were reduced by 10 to 60 percent, while floor level accelerations were reduced by 25 to 60 percent over those of the unmodified steel frames.

Chang et al. [1993] studied the relationship between the performance of the viscoelastic dampers and factors affecting their properties such as an ambient temperature. The test structure

was a 2/5-scale 5-story steel frame sitting on a shake table. It was found that as the ambient temperature increased, the viscoelastic materials became softer and their efficiency decreased. Despite the reduction in energy dissipation capacity due to the increase in temperature (as high as 42°C), the performance of the viscoelastic dampers was still remarkable. Reduction in interstory drift and floor acceleration responses of as high as 73 and 78 percent, respectively, were obtained.

An experimental study of the effect of viscoelastic dampers on reinforced concrete structures was carried out by Lobo et al. [1993]. A one-third scaled model of a 3-story lightly reinforced concrete framed building was tested under simulated ground motions using a shake table. The reinforced concrete building model was retrofitted with viscoelastic damped diagonal braces in the interior bay of each frame. The test results revealed that retrofit of reinforced concrete frames using viscoelastic dampers can reduce the overall response, but more importantly, can reduce the risk of a collapse mechanism in the test structure.

More recent studies include experimental investigations by Vulcano and Mazza [2000] and Asano et al. [2000], and an analytical investigation by Soda and Takahashi [2000]. These studies also suggest that there is potential for use of viscoelastic dampers for the seismic protection of building structures.

Analytical Model

Viscoelastic dampers dissipate input seismic energy through shear deformation of viscoelastic material. The mechanical properties of the viscoelastic material depend strongly on the number of repeated cycles, frequency, amplitude, and ambient temperature. As a result, the force-displacement relationship and its hysteresis model are rather complicated. However, a number of researchers have proposed various simplified mechanical models for viscoelastic dampers. Dependency on frequency was the focus of the fading memory model of Izumi et al. [1990], the fractional derivatives model of Kasai et al. [1993], and the multi-Maxwell element model of Soda and Takahashi [1997], etc. Shen and Soong [1995] suggested an analytical model for predicting hysteretic behavior of viscoelastic dampers based on Boltzmann's superposition principle and the method of reduced variables. More recently, Asano et al. [2000] formulated an analytical model considering also the nonlinearity and reaction force degradation properties of

the viscoelastic materials. Several other analytical models have been formulated by other researchers around the world but are not discussed here.

Structural Applications

Early use of viscoelastic damping devices in buildings was primarily to reduce floor vibrations due to wind and increase human comfort in high-rise buildings. In 1969, approximately 10,000 viscoelastic dampers were mounted in each tower of the World Trade Center buildings in New York. The buildings experienced many moderate and severe wind storms over the past 30 years, and the observed performance of the viscoelastic dampers appeared to agree reasonably well with their design values. Another application to reduce wind induced response was the use of as many as 260 viscoelastic devices which were incorporated in 1982 into the Columbia SeaFirst Building in Seattle. Despite these successes in use of viscoelastic dampers to limit wind-induced responses, seismic applications in buildings have begun only recently. The transition from wind to seismic application of these dampers requires some modification in the devices. Larger damping values are required in the case of seismic application in comparison with that of wind application. In addition, the seismic energy input to the building is generally extended over a broader frequency range than the energy input from wind forces.

The first seismic retrofit of an existing building using viscoelastic dampers began in 1993 on a 13-story Santa Clara County building in San Jose, CA. The building, originally built in 1976, provided little lateral resistance and fundamental mode damping value was only one percent. A retrofit method using viscoelastic dampers, with two dampers per building face per floor level, was proposed. The retrofitted building demonstrated significantly increased damping for both frequent small ground motions and larger seismic events.

Viscoelastic damper technology was also applied to the retrofit of a reinforced concrete building. Seismic evaluation of the 3-story Naval Supply Facility building in San Diego concluded that its lateral resistance was not sufficient for possible future seismic events. The main goal of the retrofit of this structure was to reduce interstory drifts in the building. Based on predicted responses from nonlinear dynamic analyses, a total of 64 dampers, connected with the main structural elements through K-braces, were required to achieve this goal.

2 Modeling URM Buildings

The structural behavior of unreinforced masonry (URM) is much more complex than that of other common construction materials such as reinforced concrete. Masonry is essentially a two-phase material and its properties are therefore dependent upon the properties of its constituents, the brick and the mortar. The presence of multiple wythes and the influence of the mortar joint as a plane of weakness are significant features which have no counterpart in the behavior of reinforced concrete. While the behavior or URM at low stress levels is essentially linearly elastic, it quickly becomes highly nonlinear once cracking develops along mortar joints and/or through bricks.

For the analysis of URM structures under earthquake excitation, the most refined approach is to individually model the brick units with continuum elements and the mortar joints with interface elements [Shing et al., 1998]. However, for the analysis of an entire masonry structure, the modeling of every mortar joint can quickly become impractical, especially in design studies where multiple configurations and/or loadings need to be considered. More simplified methods are needed for design purposes, and one such approach is described in the following sections.

2.1 Design Model Approach

Computer-based numerical methods for structural analysis are capable of achieving very high levels of fidelity for many applications, but this almost always requires substantial amounts of computing power, and more importantly, solution times can increase dramatically. For design applications where alternative configurations must be studied and a range of parameter values considered, the use of such high fidelity analysis models can become unwieldy and far too time-consuming to be practical. In such cases, one approach is to consider simpler analytical models that provide less fidelity but still capture the essential behavioral features. These are called "design models" to differentiate them from the higher fidelity "nominal models" to which they are usually calibrated. Design models offer computational simplicity and, more importantly, speed but do not provide the same level of detail as a nominal model would. Good design models simulate the most important features of the nominal model but at a significant savings in computational time and effort. This two-level approach to handling complexity in design analysis is common in many areas of engineering, and the particular terminology used here is widespread in control engineering.

Since the present study assessed the improvement in performance of URM essential facilities in Mid-America, rather than a particular building, it was important in this study to be able to apply any design and evaluation models to a wide range of building configurations in a computationally efficient manner. For this reason, use of simpler design models for the bulk of the study was preferable to use of more costly nominal models. Nominal models are more appropriate for evaluation of the final configurations and designs developed for a specific building using the design models.

2.1.1 Limited Degrees of Freedom

High fidelity nominal models for URM buildings are characterized by large numbers of degrees of freedom and highly nonlinear material behavior, both of which greatly increase the model complexity. Because the nonlinear behavior is an essential and defining characteristic of URM, reduction in the number of degrees of freedom provides the only practical basis for developing suitable design models. In this study, only the lateral loading and response were considered, and the design models reflect this simplification. As a result, design models for components of URM buildings such as foundations, walls (in-plane as well as out-of-plane behavior) and floor and roof diaphragms, incorporating only a few degrees of freedom with lumped masses and nonlinear spring behavior were developed. Further simplification was achieved by lumping wall and floor diaphragm masses at each story level. Details are described in Section 2.4.2.

For increased efficiency in the analysis of a URM building component such as the in-plane behavior of a masonry wall, one can consider only the critical regions that will capture the dominant failure mode of the structure. A further simplification can be achieved by ignoring individual mortar and bricks and treating masonry as a homogenous material. In this approach, the behavior of the masonry system is represented by an equivalent continuum [Shing et al., 1998]. In the present study, this approach was extended, and a URM wall containing one or more openings for doors and windows (*e.g.*, a perforated wall) was considered to be made up of a number of wall segments or components, each of which maintains the integrity of the brick-mortar bond internal to it and therefore behaves largely in a linearly elastic manner. Cracks were assumed to develop between these components and the relative motion involved opening/closing, crushing, or sliding. A simple nonlinear spring element with limited degrees of freedom was

then used for the masonry component model. The spring reflects the initial elastic behavior of the component as well as the nonlinear behavior associated with the inter-component interactions across the cracks.

2.1.2 Composite Nonlinear Behavior

The essential nonlinear behavior of URM was modeled in the present study starting at the component level, as noted above. If the components are carefully chosen, it is possible to model the nonlinear behavior for each component in a relatively simple manner, using for example, bilinear inelastic spring models with or without hysteretic behavior, or simple gap opening/closing models. The model for an entire wall can then be constructed by combining the constituent component models in parallel and series combinations, as appropriate to the particular modeling approach used. The resulting "composite" model was then capable of developing much more complex behavior than any of the individual components, but yet the overall modeling and analysis process was kept at a relatively simple conceptual level.

2.1.3 2D Versus 3D Analysis

Any real building structure–whether URM or not–is obviously three-dimensional, and many have quite irregular layouts. Under the earthquake excitation, the particular direction of seismic loading cannot be anticipated, and therefore, three-dimensional analysis should produce a more accurate description of the behavior of the structure which might include torsional response due to asymmetry of the rigidity and mass distributions of each component with respect to the loading direction. However, in the interest of achieving a simpler analysis model, the design models developed in the present study were based on two-dimensional behavior only. These 2D models considered vertical and horizontal motion in a single plane, and as such are strictly applicable only to buildings with simple plan forms that preclude mass or stiffness cross-coupling between orthogonal horizontal directions. Nonetheless, it is felt that such models captured most of the important structural behavior for the present study. It should be pointed out that a more appropriate, full 3D, design model for low rise URM buildings has been developed under a related MAE Center research project (ST-5). However, this model was developed concurrently with the present study and was not available. It is felt that most of the methodology in the present study can be reapplied using the more accurate 3D design model from ST-5.

2.1.4 DRAIN-2DX approach

DRAIN-2D (Dynamic Response Analysis of INelastic 2-Dimensional Structures) is a research-grade computer program that was first released in 1973 at the University of California at Berkeley, and it has been a useful nonlinear structural analysis tool for many years. The main advantage of the program is that it is both simple and effective. Moreover, additional structural component models, as well as enhancements to the base set, are relatively easily incorporated into the source code distribution. Its capabilities, however, are very limited, and DRAIN-2DX is an improved version that added more powerful capabilities to the program, while retaining its essential simplicity [Prakash et al., 1993]. The commercial code, RAM Perform 2D, is the present successor to the original DRAIN code, and it incorporates a graphical user interface and further computational and modeling improvements.

DRAIN-2DX can be used to perform 2D nonlinear static and dynamic analyses, as well as linear static analysis. Static and dynamic loads can be applied in any sequence, and the structure state can be saved at the end of any analysis. The element library includes an inelastic truss bar element, a plastic hinge beam-column element, a simple connection element, an elastic panel element, a compression/tension link element, and a fiber beam-column element [Prakash et al., 1993, Advanced Structural Concepts, Inc., 1998]. As a result of its versatility and wide recognition, DRAIN-2DX was chosen as the computational modeling basis for the design models developed in the present study. As described in Section 2.3.8, additional nonlinear modeling capabilities were added to one or more of the DRAIN structural components in order to adequately describe the needed in-plane URM wall models

2.2 Building Components

The 2D design models were created to compute response in the vertical and a single horizontal direction for loads applied in the same plane (referred to as the modeling plane). As a result, they are suitable for buildings with well-defined structural properties in two orthogonal planform directions and little or no cross coupling (*e.g.*, mass or stiffness eccentricities). With reference to a particular 2D design model, building lateral response was computed in only the single horizontal direction of the 2D model. Relative to this particular model, building components are defined as being either in-plane or out-of-plane, depending on how they are

oriented with respect to the modeling plane. Figure 2-1 illustrates this definition for a simple one-story building.

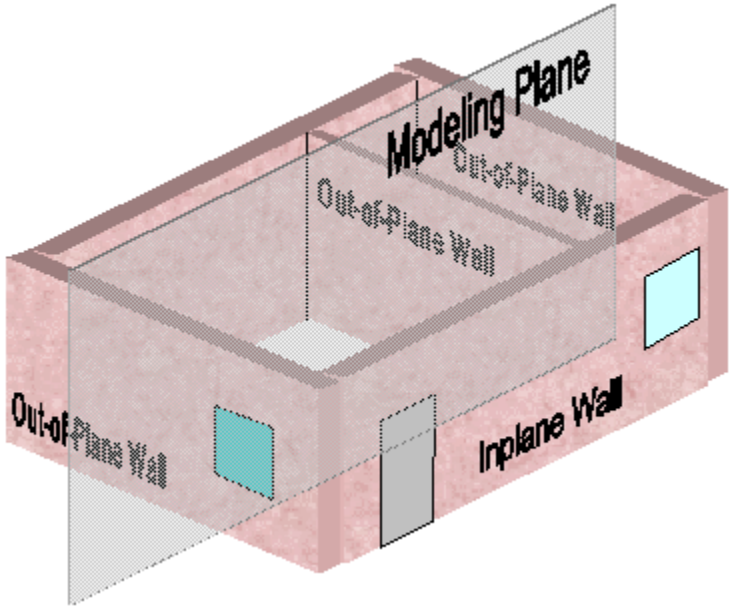

Figure 2-1 Building Components Relative to the 2D Modeling Plane

2.2.1 Out-of-Plane Walls

Building walls that are perpendicular, or nearly so, to the modeling plane are referred to as "out-of-plane" walls. Three such walls are shown in Figure 2-1. Because the lateral stiffness of URM walls perpendicular to their plane is much less than the in-plane stiffness, it is usually ignored in comparison. In the present study, out-of-plane wall stiffnesses were ignored in comparison to the in-plane stiffnesses. The mass, however, cannot so easily be ignored, but usually, only a tributary area of the out-of-plane wall need be considered.

2.2.2 In-plane Walls

Building walls that are oriented parallel to the modeling plane are referred to as "in-plane" walls. Two such walls are shown in Figure 2-1. URM walls develop relatively high values of initial elastic stiffness in their in-plane direction and usually result in a building with high initial stiffness and corresponding low elastic period. Both the in-plane stiffness and the full mass of the wall were incorporated into the 2D model. Multiple parallel walls, either full or partial length, were usually combined in parallel in the 2D model.

2.2.3 Flexible Floor and Roof Diaphragms

The floors and roof of a URM building are supported by the masonry walls. Usually, the connection to the walls involves only support of the gravity load (*e.g.*, with a haunch or pocket), but in some cases, the floors and roof are tied laterally into the wall (*e.g.*, using anchors that tie completely through the masonry wall and are terminated in a large bearing washer on the outside – sometimes called a "star" anchor), or in a few cases, opposite walls are tied together using long threaded rods. As a result, the floors and roof tie together the in-plane and out-of-plane building walls, but the precise manner of this connection is often quite difficult to assess and to model. In the 2D building models, floor bending was not considered, and as a result, the floors were considered as diaphragms with extensional and shear stiffnesses. Floors made from tongue-and-groove or plywood decking over wooden joists are quite common in old URM construction in the central US region although newer construction may involve poured concrete on light steel decking. In either case, and especially for the wooden floors, the shear stiffness is much less than the extensional stiffness and usually is the defining characteristic of the floor. MAE Center studies (see for example, project ST-8) involving laboratory tests of typical and modified wooden flooring systems have confirmed this behavior and have provided representative stiffnesses. It should also be noted that these stiffnesses are nonlinear and are often accurately characterized by a bilinear stiffness with hysteretic behavior.

Floor diaphragms usually are much less massive than the URM walls but in many cases, the floors can support significant masses that should be included in any design model. In such cases, a simple approach is to lump this mass at a point on the floor and couple it into the modeling plane through the shear stiffness of the floor diaphragm.

2.3 Composite In-plane Model of General URM Walls

2.3.1 Characteristics of a Solid URM Wall

For a general understanding of the in-plane behavior of a masonry wall, it is important to begin with the behavior of a solid wall. In FEMA-356, the solid masonry wall and the perforated masonry wall are defined as follows:

- Solid masonry wall: Maximum length or height of an opening in a solid wall must not exceed 10% of the wall width or story height. Openings in a solid wall or infill panel

must be located within the middle 50% of a wall length and story height, and must not be contiguous with adjacent openings.

- Perforated masonry wall: a wall not meeting the requirements for a solid wall.

When subjected to in-plane loading, a solid URM wall behaves elastically under the initial loading, and a simple plane stress model is generally adequate to describe this behavior. Out-of-plane behavior under elastic in-plane loading is usually not of concern owing to relatively large wall thickness. As the in-plane loading is increased on a solid wall, either flexural or shear cracking–or a combination of both–will occur, resulting in deflections that are nonlinear with respect to the applied forces. This behavior occurs for large monolithic walls as well as for components of perforated walls, such as piers, for which the local behavior can often be modeled as small solid wall elements.

There are four kinds of in-plane failure modes for the URM solid wall. The type of failure mode is determined primarily based on the masonry strength, wall aspect ratio, and the vertical compressive stress. The principal failure mechanisms of solid masonry walls, including piers, subjected to seismic actions can be summarized as follows:

(a) Rocking failure: As horizontal load or displacement demand increases, bed joints crack in tension, and shear is carried by the compressed masonry; final failure is obtained by overturning of the wall.

(b) Bed-joint sliding: Due to the formation of horizontal tensile cracks in the bed-joints, subjected to reversed seismic action, potential sliding planes can form along the cracked bed joints; this failure mode is possible for low levels of vertical load and/or low friction coefficients.

(c) Diagonal tension cracking: Peak resistance is governed by the formation and development of inclined diagonal cracks, which may follow the path of bed- and head-joints or may go through the bricks, depending on the relative strength of mortar joints, brick-mortar interface, and bricks.

(d) Toe crushing: When the strength, as limited by toe compression stress, is less than the strength determined by rocking, the wall undergoes a sudden failure due to the crushing of the toe.

A suitable design model for in-plane wall behavior should be capable of representing each of these kinds of failures, depending on the particular design conditions encountered.

2.3.2 Stiffness and Strength of a Solid URM Wall

The in-plane force-deflection behavior of unreinforced masonry shear walls is linearly elastic before net flexural tension stresses at the wall heel or diagonal tension stresses exceed tensile strengths, or bed-joint sliding shear stresses exceed shear strengths. FEMA 356 provides formulas for the calculation of the linear elastic stiffness of an URM shear wall as follows.

$$k = \begin{cases} \dfrac{1}{\dfrac{h_{eff}^{\ 3}}{3E_m I_g} + \dfrac{h_{eff}}{A_v G_m}} & \rightarrow \text{for a cantilevered shear wall} \\ \dfrac{1}{\dfrac{h_{eff}^{\ 3}}{12E_m I_g} + \dfrac{h_{eff}}{A_v G_m}} & \rightarrow \text{for a fixed-fixed shear wall} \end{cases} \qquad (2.1)$$

where,

h_{eff} = Wall height

A_v = Shear area

I_g = Moment of inertia for the gross section

E_m = Masonry elastic modulus

G_m = Masonry shear modulus

This formula is based on the classical theory of bending and shear. However, the strength of the wall is different for each failure mode and must be determined separately. FEMA 356 provides design formulas for the strength of each failure mode of a solid wall under an in-plane force applied along its top. FEMA 356 also notes that unreinforced masonry walls and piers should be considered as deformation-controlled components if their expected lateral strength, limited by bed-joint sliding, shear stress, or rocking, is less than the lower bound lateral strength limited by diagonal tension or toe compressive stress. Otherwise, these components should be considered as force-controlled components.

Strength for Rocking Mode Failure

The expected lateral strength of existing URM walls governed by rocking failure is given by FEMA 356 as:

$$Q_{CE} = 0.9\alpha P_{CE}\left(\frac{L}{h_{eff}}\right) \tag{2.2}$$

where:

P_{CE} = Expected vertical axial compressive force

L = Length of wall

h_{eff} = Height of resultant of lateral force

α = Factor equal to 0.5 for fixed-free cantilever wall, or equal to 1.0 for fixed-fixed wall

Strength for Bed-Joint Sliding

When bed-joint sliding governs the wall failure, FEMA 356 specifies that the expected strength of the wall is:

$$Q_{CE} = v_{me}A_n = \frac{0.75A_n\left(0.75v_{te} + \frac{P_{CE}}{A_n}\right)}{1.5} \tag{2.3}$$

where:

P_{CE} = Expected vertical axial compressive force

v_{me} = Expected bed-joint sliding shear strength, psi

A_n = Area of net mortared/grouted section, in^2

v_{te} = Average bed-joint shear strength, psi

It is further stated that the 0.75 factor on the v_{te} term may be waived for single wythe masonry, or if the collar joint is known to be absent or in very poor condition. Values for the mortar shear strength, v_{te}, should not exceed 100 psi in Eq.(2.3).

Strength for Diagonal Tension Cracking

The strength of a solid wall governed by diagonal shear cracking is given by FEMA 356 as:

$$Q_{CE} = f_{dt}'A_n\left(\frac{L}{h_{eff}}\right)\sqrt{1 + \frac{f_a}{f_{dt}'}} \tag{2.4}$$

where:

f_a = Upper bound of vertical axial compressive stress $\left(=\frac{P_{CE}}{A_n}\right)$, psi

f_{dt}' = Lower bound of masonry diagonal tension strength (may be substituted by the bed-joint shear strength, v_{me}), psi

v_{te} = Average bed-joint shear strength, psi

It is further specified that this equation is only applicable for the range of L/h_{eff} between 0.67 and 1.00. As mentioned earlier, diagonal tension cracking can be divided into two different kinds, depending on the relative strength of mortar joints, brick-mortar interface, and bricks: (a) cracking that follows the path of bed- and head-joints, and (b) cracking that goes through the bricks. Eq.(2.4) above is only applicable to case (b). It would be rational to apply Eq.(2.3) for case (a), because the lateral movement of the wall can only be resisted by the friction of the bed-joints.

Strength for Toe Crushing

The strength of a wall governed by toe crushing is specified in FEMA 356 as:

$$Q_{CE} = \alpha P_{CL}\left(\frac{L}{h_{eff}}\right)\left(1-\frac{f_a}{0.7\,f_m'}\right) \qquad (2.5)$$

where:

P_{CL} = Lower bound of vertical compressive force

f_m' = Lower bound of masonry compressive strength, psi

It is further stated that for this case, the lower bound masonry compressive strength, f_m' should be taken as the expected strength, f_{me} divided by 1.6.

Hysteresis Property for Each Mode

Each of the above failure modes has associated with it a characteristic type of hysteresis that must be incorporated into any practical design model of a solid URM wall under in-plane seismic loading.

Rocking: In the case of a rocking response, very large displacements can theoretically be obtained without significant loss in strength, and this has been born out in experiments. A typical

flexural response is depicted in Figure 2-2, where a nonlinear but nearly elastic behavior with very moderate hysteretic energy dissipation is shown. If no other failure mechanisms occur, the displacements which can be attained in a rocking response are limited only by a decrease in strength due to second order (P-delta) effects associated with overturning. These drift limits can be as high as 10% of the height of the wall and are of no practical use, since other collapse events will usually take place before reaching this drift limit [Magenes, 1997].

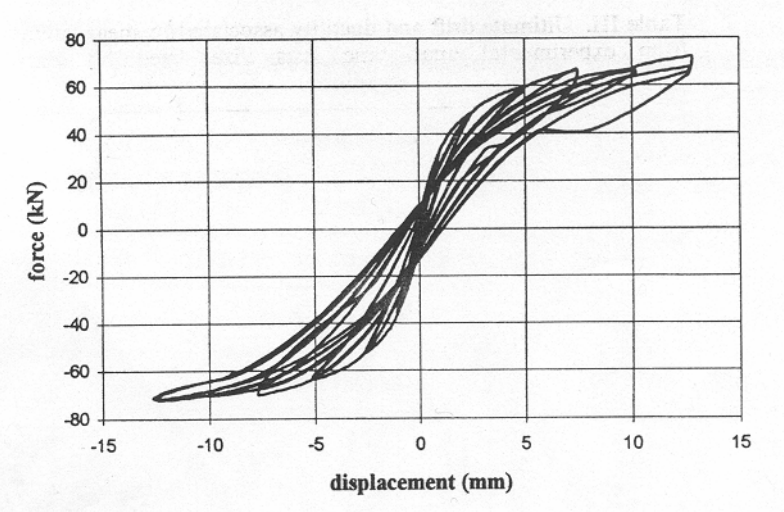

Figure 2-2. Example of Flexural Response (rocking) [Magenes, 1997]

Bed Joint Sliding: When sliding on horizontal bed-joints occur, a very stable mechanism is involved because large displacements are possible without a loss of integrity of the wall. Damage and energy dissipation are concentrated in a bed-joint, and as long as a vertical load is present, high energy dissipation is possible and can be idealized as shown in Figure 2-3.

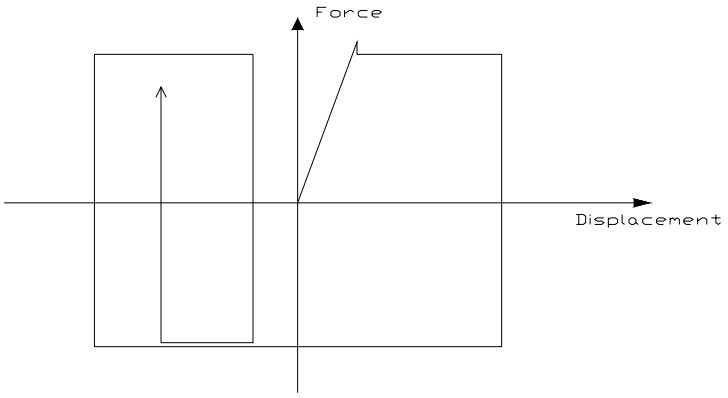

Figure 2-3. Idealized Example of Bed-Joint Sliding Response.

Diagonal Tension Cracking: A typical force-displacement curve for the case of a response dominated by diagonal tension cracking is shown in Figure 2-4 [Magenes, 1997]. The pre-cracking behavior is characterized by moderate hysteresis and by negligible strength and stiffness degradation. Post-cracking response is characterized by higher energy dissipation along with rather rapid strength and stiffness degradation.

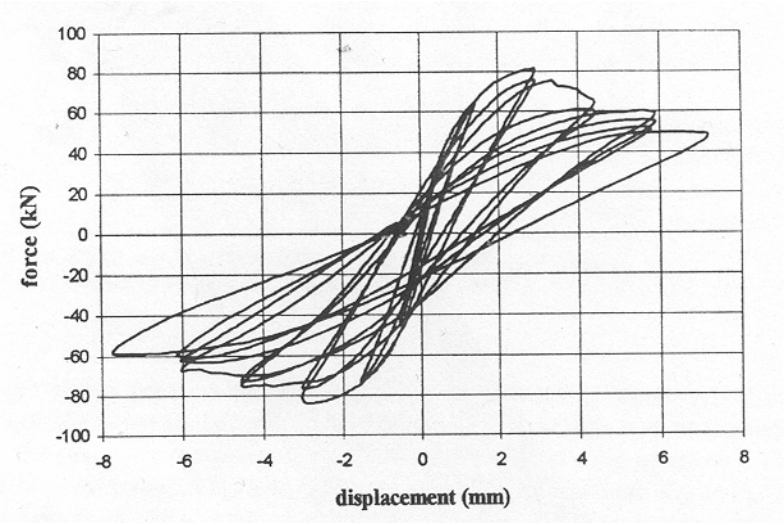

Figure 2-4. Example of Diagonal Shear Cracking Response [Magenes, 1997]

2.3.3 Model Structure for a General URM Wall

As shown in the previous section, the nonlinear behavior of a solid URM wall, including its initial stiffness, strength, and hysteresis property for each kind of failure mode, can be determined based on FEMA 356 [FEMA 2000] (or other relevant design codes). However, few masonry walls exist in a solid wall configuration. Rather, a general masonry wall has one or more major openings such as doors and windows, which comprise more than 10% of the area of the wall. Because almost all of the actual masonry walls are perforated or general masonry walls, it is important to be able to accurately model such walls.

As described in Section 2.1, a lumped parameter model with reduced degree of freedom was developed in this study rather than brick-by-brick modeling with interface elements. Current guidelines [FEMA 2000] suggest a simplified method for the analysis of URM in-plane walls in which the stiffness of the in-plane wall is obtained from finite element analysis and is distributed to each pier based on its aspect ratio. However, this method again requires finite element analysis which in turn requires significant time for development and execution of the computational

models, and therefore quickly becomes impractical for applications involving numerous building models. This section describes the development of a simplified model for the in-plane response of an URM wall subjected to cyclic loading which avoids these computational problems.

Wall Configurations

Under initial levels of in-plane loading, a general URM wall will develop an elastic stress distribution pattern that will, in turn, depend on the number, the size and shape, and the relative arrangement of the perforations. As the loading is increased, the elastic stress intensities will increase until one or more of the failure modes described above develops in some region of the wall. If sufficient post-failure strength can be achieved, additional regions will also experience one or more of the failure modes.

While this process is quite complicated and detailed computational models can be very large and time-consuming to execute, it nonetheless can form the basis for a simpler design model. The anticipated failure zones, as identified by simple elastic behavior (which is relatively easily modeled using commonly available plane stress computational analysis tools) or perhaps by experience and simple heuristics, serve then to define certain regions of the wall that do not fail and continue to exhibit linearly elastic behavior. These regions typically include some of the masonry piers and many of the lintels and spandrel sections. The in-plane force-deformation behavior of these regions, which we will now refer to as wall components, can usually be adequately modeled using classical bending and shear deformation formulations.

The failure modes, failure strengths, and the hysteretic behavior for each wall component can be determined based on the provisions in FEMA-356 as noted in Section 2.3.2 above. These characteristics can readily be incorporated into attributes for nonlinear spring elements for which initial elastic behavior models the elastic properties of the component itself.

Finally, these nonlinear springs can be assembled into a parallel and series arrangement that approximates the topology of the wall components themselves. In this manner, a “composite” wall model consisting of the parallel- and series-connected nonlinear springs can be created.

The single-story wall with two windows and a door shown in Figure 2-5 can be taken as a simple example to illustrate the methodology for this kind of composite modeling of the wall. The wall includes a door and two window openings symmetrically arranged. These perforations effectively break up the single wall into a number of segments such as the two relatively thin

(high aspect ratio) piers on either side of the door as well as the two piers with much lower aspect ratios on the outer sides of the windows (adjoining the wall ends). In addition, the lintels (or spandrel) and the regions below the windows define additional wall segments.

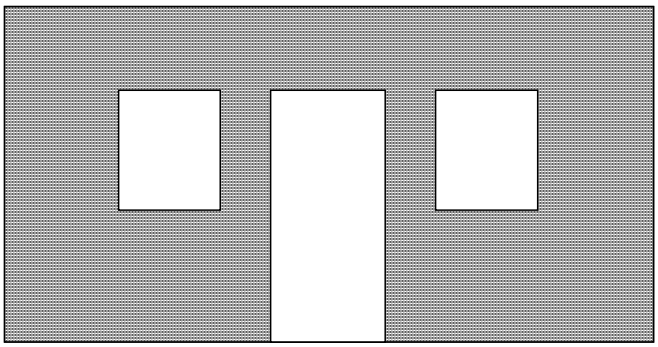

Figure 2-5. Example Perforated URM Wall

Figure 2-6 shows three examples (a, b, c) for modeling this wall using composite spring elements with elastic and nonlinear properties determined by the assumed wall failure modes (which in turn can be determined from heuristics or a plane stress analysis or a combination of both). In this figure, the first row shows the three different assumed failure modes, the second row defines the wall component configurations for each of the corresponding failure modes, and the third row shows the corresponding series-parallel composite nonlinear spring model.

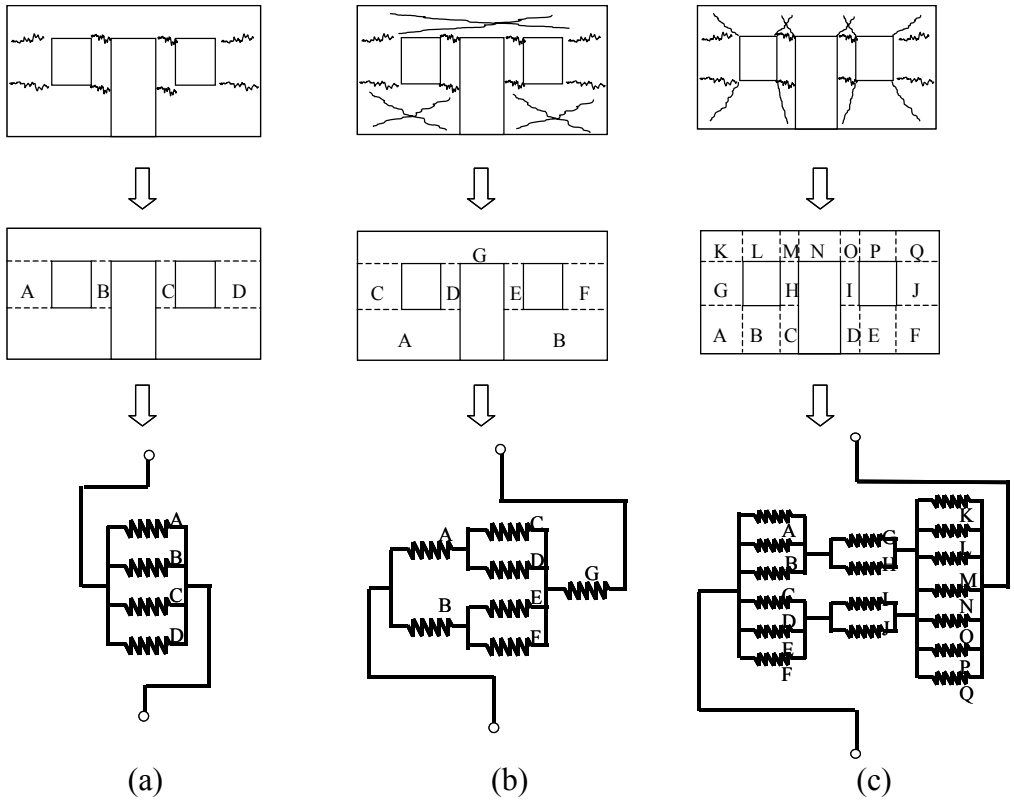

Figure 2-6. Modeling of the Perforated URM Wall

In Figure 2-6(a), the parallel springs are defined based on a model involving pier behavior only [Bruneau, 1994]. In this model, it is assumed that the spandrel beams in a perforated wall will main their integrity but will develop tension cracking at the pier ends, leaving the piers alone to resist the lateral loads. In this case, the unreinforced masonry spandrels either behave as beams or deep-beams, and the failure is initiated when the flexural stresses in the piers exceed the tensile strength of the brick at one course from the beam's bottom surface or when the shear stresses at the head joint near the beam's end exceed the mortar's bond strength, whichever comes first. Although this kind of model represents the structure at its ultimate state, such as might be the case if the spandrels are shallow or not well connected to the piers, it immediately assumes a structure in its degraded condition, neglecting the potentially larger capacity of the structure before cracking develops.

Figure 2-6(b) shows a parallel and series spring model that accounts for the contribution (and failure) of the spandrel beam and the masonry above and below the piers. Although this model can produce more accurate results for the inelastic behavior of the wall, the initial elastic stiffness of the wall based on this model is much stiffer than the real lateral stiffness of the wall.

In order to use this model for the analysis of general URM walls, some kind of calibration should be made to more accurately represent the capacity of the wall before cracking and such a process is described in Section 2.3.

Figure 2-6(c) shows an even more detailed model in the sense that every possible wall component is considered. However, in Figure 2-6(c), it can be a mistake to think that the continuous walls (wall A-C, D-F, and K-Q) act as springs in parallel because the lateral displacement of each segment can be significantly different from each other, and this may preclude their being assumed as springs in parallel. It should also be pointed out that this much greater level of detail is inconsistent with the objectives of a simplified design model.

Calculation of the Elastic Stiffness of the Wall

As shown in Section 2.3.1, the stiffness of a solid wall can be calculated based on the design formula provided in FEMA 356. However, for a general perforated wall, calculation of the lateral stiffness becomes much more complicated. This section describes several existing methods for the calculation of the stiffness of the perforated wall. This section also introduces a new way of calculating the stiffness to obtain a better result with less time.

Finite Element Flexibility Method: The stiffness of the perforated wall can be obtained by using a plane stress finite element formulation. To illustrate, a two-story perforated wall is considered as an example and is shown in Figure 2-7. It is desired to obtain the stiffness matrix of the wall as a function of the average translational degrees of freedom (DOF) at the floor diaphragm levels. U_1 and U_2 are average displacements from all nodes at the roof and the floor level, respectively, due to a given applied force distribution. The flexibility matrix of these two degrees of freedom can be constructed as follows:

$$\overline{F} = \begin{bmatrix} U_{11} & U_{12} \\ U_{21} & U_{22} \end{bmatrix}$$

where,

U_{ij} = the average displacement at DOF i due to the unit load at DOF j.

The stiffness matrix of the wall can then be formulated as follows:

$$\overline{K} = \begin{bmatrix} K_{11} & K_{12} \\ K_{21} & K_{22} \end{bmatrix} = \overline{F}^{-1}$$

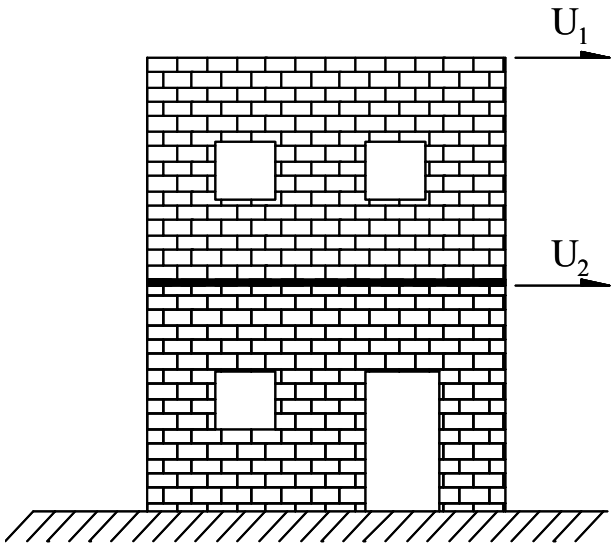

Figure 2-7. Degrees of Freedom of a Two-Story URM Wall

Simplified Methods: There are several simplified ways to calculate the initial elastic stiffness of the general perforated cantilever shear wall suggested in the literature [Tena-Colunga et al., 1992]. However, assuming that a plane stress finite element analysis produces the most accurate results, none of these methods gives a reliable estimate of the lateral stiffness and the top lateral deflection of the general perforated wall. Compared to finite element solution, these methods give considerably stiffer results.

The first method, introduced by Schneider [1987] and named a "pier-spring model," computes the lateral stiffness of a perforated wall as the sum of the rigidities of the individual piers between openings within the wall. This is a very crude assumption, and the method considerably overestimates the lateral stiffness of the perforated walls.

A second method, also due to Schneider [1987], can, perhaps, be called a "composite spring model". This method takes the stiffness of the masonry above and under the openings into account for the calculation of the top displacement of the perforated wall. This method can eliminate the additional stiffness caused by ignoring these spandrel beam parts. However, because the boundary conditions of each wall segment are different from those specified in Eq.1, this method also does not give a reasonable solution.

The third method presented by Tena-Colunga [1992] is called an "interior strip model." This method is much more elaborate and requires five steps:

1.- Obtain the deflection of the cantilever wall as if it were solid.

2.- Subtract the deflection of a cantilever strip having a height equal to the highest opening in the wall

3.- Compute the deflection of all composite piers with openings lying within the strip.

4.- Add the deflections of these individual piers to the modified wall deflection computed in step 2 to obtain the final wall deflection.

5.- Take the reciprocal of this computed deflection to obtain the lateral wall stiffness.

A schematic view of the interior strip model method is illustrated in Figure 2-8. The total top displacement of the wall becomes

$$\Delta t = \Delta s - \Delta i + \Delta p \qquad (2.6)$$

where,

Δt = total displacement of the wall due to the load P.

Δs = displacement of the solid wall due to the load P.

Δi = displacement of the interior strip with a height equal to the highest opening in the wall due to the load P.

Δp = displacement of the piers due to the load P.

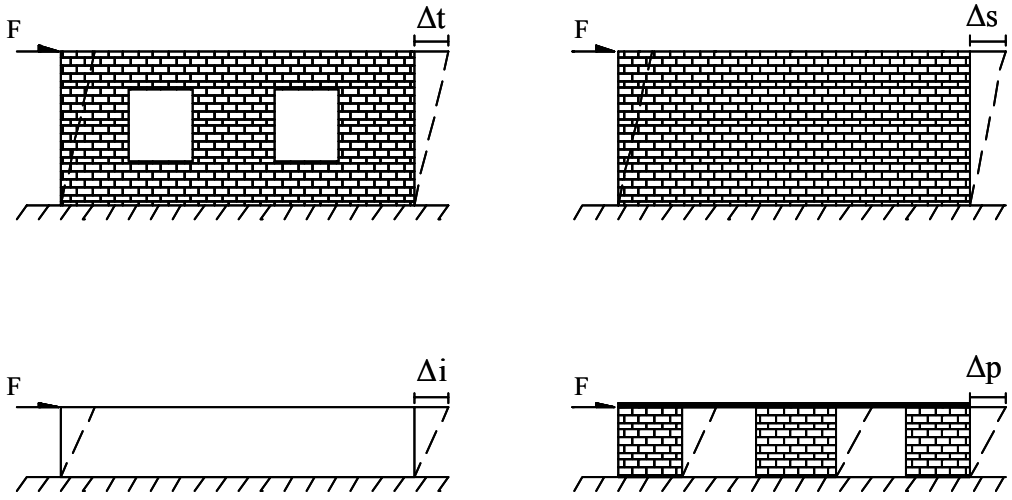

Figure 2-8. Schematic View of Interior Strip Model

The resulting displacement of each method can be compared by applying them to several examples. Figure 2-9 shows the shape and the dimension of the example walls for this trial. The material properties of the masonry are chosen based on the suggested values in FEMA 356 for masonry in good condition. The modulus of elasticity and the Poisson's ratio of the masonry wall

are 495,000 psi and 0.2, respectively, in this study. The self weight of the brick masonry walls was assumed to be 10 psf per inch of thickness [Tena-Colunga et al., 1992].

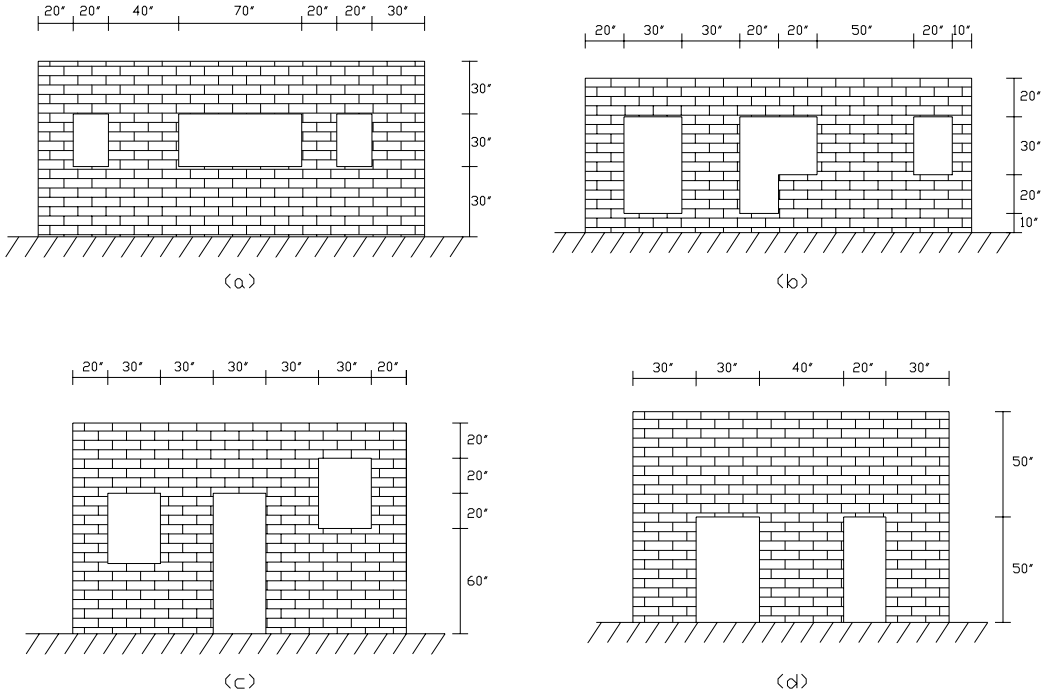

Figure 2-9 Example Walls for Comparison of the Top Displacement

Table 2-1 shows the result of the comparison of the top average deflections of the example perforated masonry walls shown in Figure 2-9. Not unexpectedly, none of these models provide good agreement with the FEM results giving considerably stiffer results than those of the finite element plane stress analyses. As a result, ways to improve the accuracy of the composite spring models is developed in the following section.

Table 2-1. Comparison of the Top Average Deflections in inches of the Perforated Cantilever Walls of Figure 2-9 Predicted by Each Model (percent difference from FEM)

Wall Configuration.	FEM	Pier-only Model	Composite Spring Model	Interior Strip Model
(a)	8.45E-06	2.23E-06 (-74%)	4.12E-06 (-51%)	4.82E-06 (-43%)
(b)	7.96E-06	2.92E-06 (-65%)	4.09E-06 (-52%)	4.18E-06 (-51%)
(c)	1.38E-05	2.67E-06 (-68%)	6.43E-06 (-24%)	5.32E-06 (-37%)

(d)	1.17E-05	5.15E-06 (-39%)	7.39E-06 (-13%)	2.91E-06 (%-66)

2.3.4 Effective Height Method for Estimating Initial Elastic Stiffness of Piers

As described in the previous section, the simplified methods described by Tena-Colunga [1992] give considerably stiffer results than those of the finite element plane stress analyses (considered as the reference solutions). In the present study, a trial method was introduced to obtain a closer value of the initial in-plane elastic stiffness of a general, perforated URM wall compared to the FEM analysis results.

One source for the discrepancy in initial elastic stiffnesses is quickly apparent when one examines the in-plane deformations of the URM wall computed from a plane stress FEM analysis. Figure 2-10 shows such an analysis for a representative URM wall, and it is obvious from the deformation patterns at the upper and lower ends of the piers that the assumption of fixed (clamped) ends for these piers is not accurate. In fact, significant deformation is developed and the end rotation cannot be assumed to be fixed as is implied in the equations from FEMA-356 that are used to compute the initial elastic stiffness of the masonry piers. In fact, the pier boundary conditions are neither fixed nor free as assumed in the FEMA-356 formulas. In the present study, this issue is addressed by incorporating the concept of an "equivalent height" of the piers to account for the different end conditions, but yet still allow use of the classical beam bending and shear deformation formulas in FEMA-356.

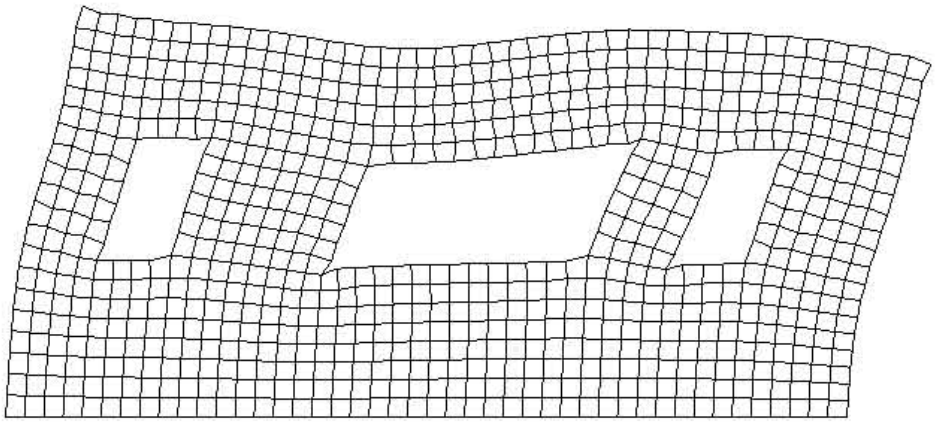

Figure 2-10 Example FEM Plane Stress Analysis of a Perforated URM Wall

The Effective Height Method

As illustrated in Figure 2-10 above, the boundary conditions for the masonry piers in a perforated wall are hard to characterize, but they must be included in order to reasonably approximate the initial elastic in-plane stiffness. One approach to accounting for boundary conditions that are less stiff than the assumed ideal fixed or clamped condition is to instead increase the pier height (*e.g.*, beam length) slightly while maintaining the ideal fixed end conditions. This approach is illustrated in Figure 2-11for a URM pier whose physical height is H_p but whose ends are not ideally fixed to the upper and lower spandrel/lintel components. The flexible ends can be modeled by adding a rotational spring as shown in Figure 2-11(b) or the fixed conditions can be retained but the height increased by a factor, r, as shown in Figure 2-11(c). The increased height will result in a stiffness reduction, that if correctly computed, will equal the reduction due to less than fully fixed end conditions. Since this increased pier height is not real, but is used simply to compute a more accurate stiffness, we will refer to it as an "effective height."

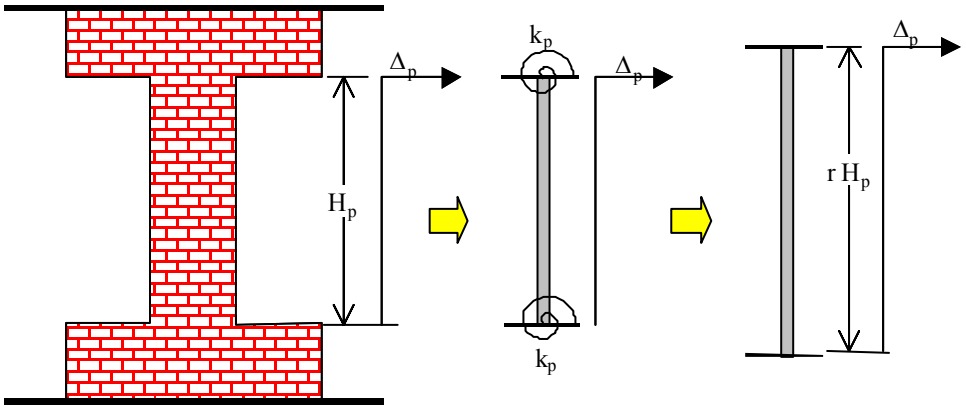

Figure 2-11 Effective Height Formulation for URM Pier

In other words, as can be seen in Eq. 2.7, the effective height, $r\,H_p$, of the pier component is determined so that the in-plane deflection per unit load (*e.g.*, the flexibility) of a pier of this height with fixed ends is equivalent to the deflection of a pier of height, H_p, but with assumed end rotational stiffnesses, k_p.

$$\Delta p = \frac{H_p^{\,3}}{12EI} + \frac{1.2H_p}{GA} + \frac{H_p^{\,2}}{2k_p} = \frac{(r\,H_p)^3}{12EI} + \frac{1.2H_p}{GA} \qquad (2.7)$$

where:

Δp = the horizontal displacement measured from the top to the bottom of the pier

H_p = the height of the pier

k_p = the rotational stiffness of the pier joint area

Note that the effective height factor, *r*, is not applied to the shear term in the pier deflection calculation because the flexibility of the joint area at the pier ends does not affect the shear deformation of the pier. The next sections describe how to calculate the effective height factor for each masonry pier based on the particular configuration of the perforated URM wall.

Variables that Determine the Effective Height of Masonry Pier.

As can be seen in Eq. 2.7, for given material properties the ideal (fixed end) stiffness of a masonry pier is a function of the height, width and thickness of the pier. On the other hand, the end stiffness factor, k_p, which is needed in order to compute the effective height depends on the particular configuration of the spandrel/lintel components at the ends. For this component, the most obvious variables are its height and width, but the situation is not nearly as simple as illustrated in Figure 2-11. These dimensions can and usually are different at the bottom and the top of a pier, and the openings on either side of the pier may themselves be different in height, thereby making it difficult to determine the reference height.

The effect of different end conditions (k_p values) at the top and bottom of the pier can be approximated by breaking the pier into two half-height piers cantilevered from the ends and pinned together in the middle. This is illustrated in Figure 2-12 below. Ideally, the pin joint should be located at the inflection point which is at the mid-height of the pier only if the end conditions are identical. Using half-heights for each segment is therefore an approximation, but it greatly simplifies the formulation.

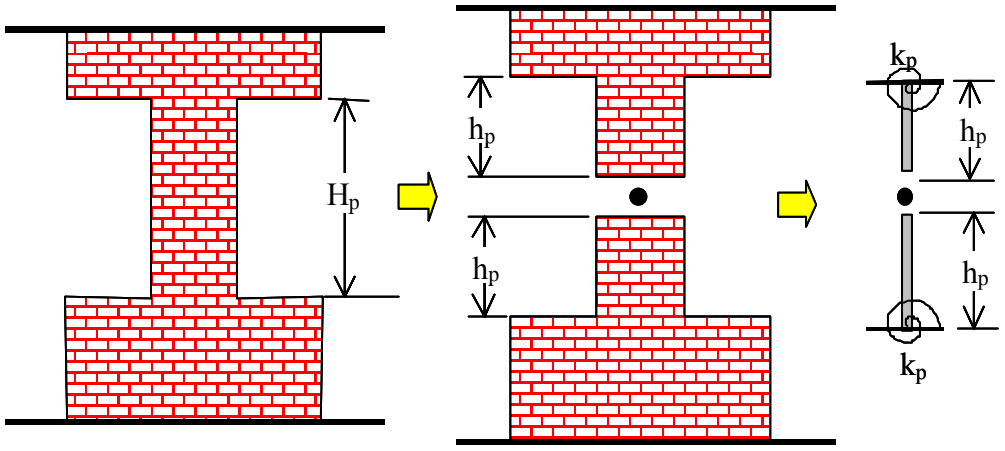

Figure 2-12 Decomposition of Pier into Two Half-Height Components

An appropriate pier model is now a cantilevered pier. Figure 2-13 below shows the same kind of formulation of the effective height as was developed previously in Figure 2-11.

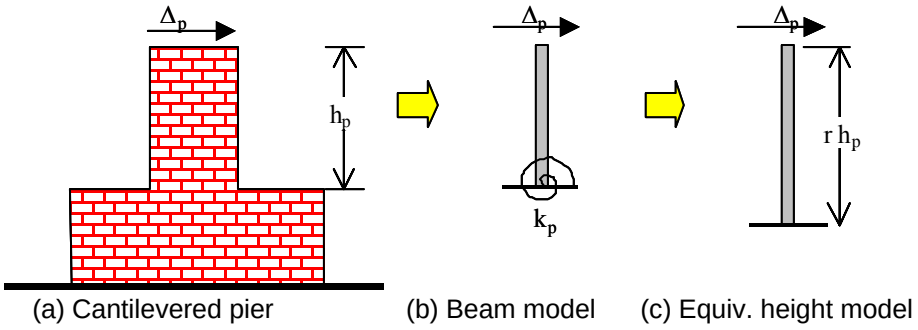

Figure 2-13 Effective Height Formulation for Cantilever Pier

Eq. 2.7 can be modified to represent a cantilevered pier as follows:

$$\Delta p = \frac{h_p^{\,3}}{3EI} + \frac{1.2h_p}{GA} + \frac{h_p^{\,2}}{k_p} = \frac{(r\,h_p)^3}{3EI} + \frac{1.2h_p}{GA} \qquad (2.8)$$

Using this, the in-plane pier flexibility, c_p, (deflection per unit load, Δ_p) is then:

$$c_p = \frac{(r\,h_p)^3}{3E_m I_g} + \frac{1.2h_p}{A_v G_m} \qquad (2.9)$$

where:

r = Effective height factor

h_p = Cantilever pier height (half-height of full pier)

A_v = Shear area

I_g = Moment of inertia for the gross section

E_m = Masonry elastic modulus

G_m = Masonry shear modulus

Eq. 2.9 is then used to compute the initial elastic in-plane pier stiffness as follows. First the pier height, H_p, is divided in half to determine the cantilever heights, h_p, for the upper and lower segments. Next, a value for r for each segment is chosen based on the given end conditions (this is described below). Finally, these values are used along with the geometric and material properties for the pier in Eq. 2.9 to compute flexibilities for both components. The flexibility for the complete pier, c_{pier}, is the sum of these quantities and the pier stiffness, k_{pier}, is the reciprocal:

$$k_{pier} = \frac{1}{c_{pier}} = \frac{1}{c_{top} + c_{bot}} \tag{2.10}$$

Determining of the Effective Height of a Masonry Pier

Pier End Conditions: Accurate estimation of the pier end conditions is difficult to achieve. The depth of the spandrel or lintel component compared to the pier width is obviously an important parameter, but the effect of their widths (*e.g.*, lengths in the horizontal direction) is not so clear. Also, the pier height to width ratio (aspect ratio) is probably important. But as illustrated in Figure 2-14, the pier ends are not always so well-defined because the openings on either side of the pier may be of different heights. In this case a parameter that reflects this asymmetry must be defined.

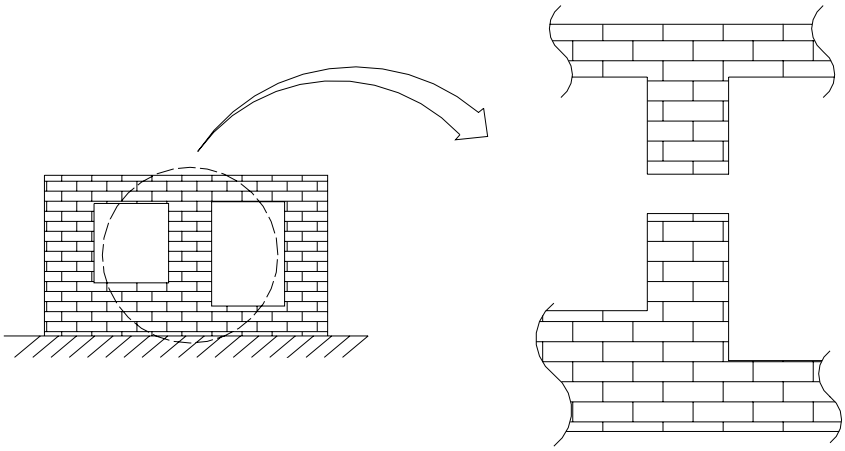

Figure 2-14. Asymmetric End Conditions for a URM Pier

In this study the following three geometric parameters were defined to characterize the geometry of a pier relative to the two openings it separates:

1. W_p/h_p - the aspect ratio of the pier,
2. H_b/W_p - the ratio of the depth of the spandrel component to the pier width,
3. α - a factor that determines the asymmetry of the pier end ($0 \le \alpha \le 1$).

These are illustrated geometrically in Figure 2-15 below. The first two parameters are measures of the pier and spandrel geometries, respectively. The third parameter defines the asymmetry of the end region and is simply the fraction of the spandrel height eliminated by the opening on one side of the pier. The range of values is $0 \le \alpha \le 1$, and α=0 corresponds to a symmetric end while α=1 represents a corner pier or a configuration with a pier adjacent to a doorway. These three parameters have been defined so that practical values are in the range from 0 to less than 10. In addition, when the parameters are equal to 0, the effective height factor should be approximately unity.

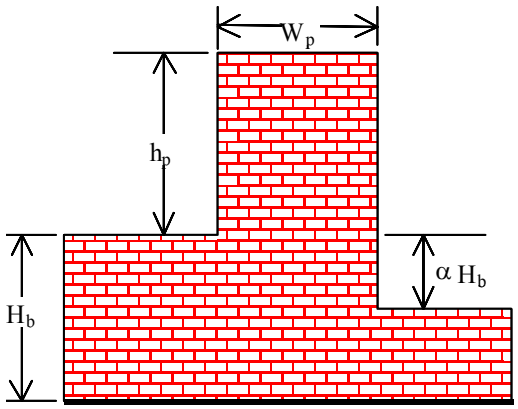

Figure 2-15. Definition of Parameters Defining the Pier End Condition

Reference Solution: As noted earlier, the "exact" solution for this problem is considered to be a plane stress analysis, and in this study it was performed for a URM wall configuration as shown in Figure 2-15 using the ABAQUS finite element program [ABAQUS, 2001]. Values of 495 ksi and 0.2 were used for the elastic modulus and Poisson's ratio for the masonry material and represent average values for commonly used block and mortar combinations. The thickness of the structure was set to a unit value (1.0 inch), and a unit shear force (1.0 lb) was applied horizontally at the top of the pier. The shear force was distributed over the top edge of the pier to avoid any problems that might be caused by stress concentration at a single node. A standard 4-node linear element was used, and the size of the mesh was determined so that either the height or the width of the pier, which ever was smaller, was always divided into more than four elements. The relative horizontal displacement between the top and the bottom of the pier was recorded. This was measured by taking the average displacement of the pier-top nodes and subtracting the average displacement of the pier-bottom nodes. The pier bottom is defined by h_p.

Regression Analysis: Finally, the pier effective height factor, *r*, was determined using regression analysis. In the most general case, a multivariate polynomial regression could be used, and for quadratic degree, the result is usually called a "response surface." However, for the case of three parameters, this would yield up to 9 regression coefficients (many more for higher order polynomials) and would lead to an unnecessarily complicated formulation of the problem. As a result, a simpler solution was sought. The particular choice for the parameters was purposefully made to minimize the interaction between them in determining the *r* factor. Consequently, the approach taken in the present study was to define nominal values for each of the parameters and then to fix two of them while varying the third in order to compute the

regression to determine the *r* factor. Then, under the assumption that the parameters are largely independent of each other (*e.g.*, cross-coupling terms are negligible), the *r* factor for the pier is the product of the 3 *r* factors from each separate regression analysis. For all cases, the overall width of the wall segment(W_b) was set to six times of the pier width (W_p) in order to minimize flexure of the bottom masonry spandrel (which was fixed across the lower base).

The effective height factor was determined for each case using Eq. 2.9 which can be solved for the *r* factor as follows:

$$r^3 = \frac{3E_m I_g}{c_p h_p^3} - \frac{3.6E_m I_g}{h_p^2 G_m A_v} = \frac{E_m}{4c_p}\left(\frac{W_p}{h_p}\right)^3 + \frac{0.3E_m}{G_m}\left(\frac{W_p}{h_p}\right)^2 \qquad (2.11)$$

where the terms have all been defined previously, and the second form is the result of substituting for I_g and A_v in terms of the geometric properties (assuming unit wall thickness). Note that c_p is the computed pier flexibility or the relative in-plane displacement per unit applied horizontal load as determined from the reference FEM analysis. Eq. 2.11 can also be expressed in terms of the computed flexibility and the theoretical flexibility assuming full fixity at the pier base:

$$r^3 = 1 + \frac{E_m}{4}\left(\frac{W_p}{h_p}\right)^3 \left(c_p - c_{p0}\right) \qquad (2.12)$$

where c_{p0} is the tip flexibility with full base fixity. This result clearly shows that if full base fixity is achieved for the pier, the effective height factor will be computed to be unity as expected. These results also show the strong sensitivity of this formulation to the pier aspect ratio.

Figure 2-16 below shows graphically the regression relationships between the effective height factor and each variable as computed from the FEM results using the above equations. The solid line indicates the measured *r* for each case, whereas the dotted line indicates the fitted regression line. The assumed fixed parameter values are also shown for each case.

Finally, the effective height factor, *r*, can be expressed in terms of each variable using the simple exponential regression results for each case. Two of three equations are normalized and multiplied to the last one equation to establish the general expression of r in terms of three variables. As a result, the overall *r* factor can be expressed as follows:

$$r = \left[1.005 + 0.19\left(\frac{H_b}{W_p}\right)^{\frac{1}{5}}\right] \times \left[1 + 0.1\alpha^{\frac{1}{4}}\right] \times \left[0.803 + 0.281\left(\frac{W_p}{h_p}\right)^{\frac{7}{10}}\right] \qquad (2.13)$$

Again, it is noted that this equation is established on the assumption that the finite element analysis gives the correct result, and it is also noted that each parameter must be in the range for which the regression analysis was generated.

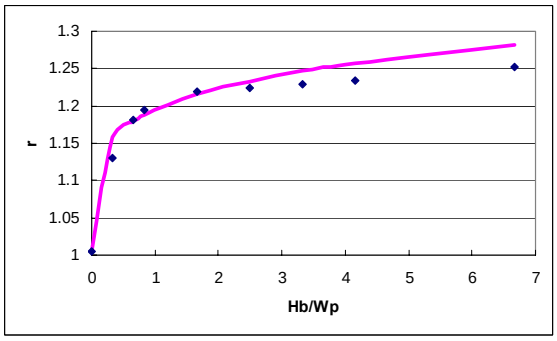

W_p/h_p = 6/10,
α=0,
Vary H_b/W_p

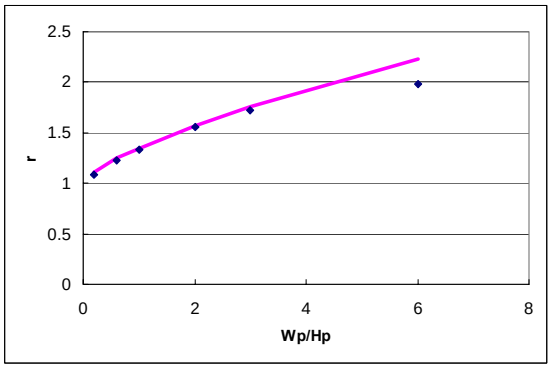

H_b/W_p = 20/6,
α=0,
Vary W_p/h_p

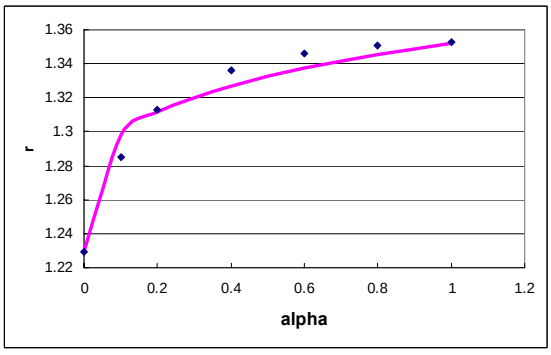

W_p/h_p=6/10,
H_b/W_p=20/6,
Vary α

Figure 2-16. Relationships Between Parameters and the Effective Height Factor, r

2.3.5 Effective Stiffness Method for Estimating Initial Elastic Stiffness of Piers

An alternate approach to incorporating the less than ideally fixed boundary conditions at the pier ends is to try to directly estimate the effective rotational stiffness, that is, the k_p term appearing in the previously described effective height formulation. In this approach, the k_p value was estimated directly, rather than trying to compute a new effective height to reflect a finite rotational stiffness at the pier end.

The Effective Stiffness Method

As illustrated in Figure 2-11(b), a pier can be modeled by putting rotational springs with appropriate stiffnesses at the ends of the pier. The stiffness of each spring can be obtained and used for the calculation of the overall lateral stiffness of the wall. This is in contrast to the effective height method in which the effective height of the pier is applied with ideally fixed end conditions to determine the overall lateral stiffness of the wall. In Eq. 2.7, the rotational stiffness k_p is directly calculated from the regression analysis. An infinite value of k_p indicates that the pier has fixed end condition, whereas a zero value of k_p indicates hinged end conditions. Consequently, for general perforated URM walls, k_p has some value between zero and infinity.

Parameters that Determine the Effective Stiffness of Masonry Pier-End

In the effective stiffness method, similar to the effective height method, the pier is broken into two half-height piers cantilevered from the ends and pinned together in the middle (Figure 2-12). Again, the pin joint should be located at the inflection point for accuracy of the calculation, but the mid-height point is taken for the simplification of the formulation.

From the cantilevered pier model, and from Eq. 2.8, the in-plane pier flexibility, c_p, (deflection per unit load, c_p) is then:

$$c_p = \frac{{h_p}^3}{3E_m I_g} + \frac{1.2h_p}{G_m A_v} + \frac{{h_p}^2}{k_p} \qquad (2.14)$$

where:

k_p = Effective stiffness of the pier-end

h_p = Cantilever pier height (half-height of full pier)

A_v = Shear area

I_g = Moment of inertia for the gross section

E_m = Masonry elastic modulus

G_m = Masonry shear modulus

Similar to the effective height method, after the in-plane flexibilities of both top and bottom half of the pier are obtained, the stiffness for the complete pier, k_{pier}, is calculated from the reciprocal relationship in Eq. 2.10.

Determining of the Effective Stiffness of a Masonry Pier-End

As described in the previous section, the estimation of the pier end conditions is difficult to achieve. Similar to what is discussed in the effective height method, the rotational stiffness at the pier end joint is determined based on some factors. The depth of the spandrel or lintel components compared to the pier width is the parameter that should be considered first. Secondly, the α factor that determines the asymmetry of the pier end as defined in the previous section is considered. Whereas the pier aspect ratio, expressed as *Wp/Hp*, is considered in the effective height method, this factor is left out in the effective stiffness method because the height of the pier does not affect the stiffness of the joint area.

The regression analysis is performed in a similar manner to that used for the effective height method. The relationship between one parameter and the effective stiffness having the other parameter fixed at a specific value is obtained.

The effective stiffness is determined for each case using the following equation that is from Eq. 2.9:

$$k_p = \frac{h_p^{\,2}}{c_p - \frac{h_p^{\,3}}{3E_m I_g} - \frac{1.2h_p}{G_m A_v}} \tag{2.15}$$

where the terms have all been defined previously. In addition, Eq. 2.15 can be expressed in terms of the computed flexibility and the theoretical flexibility assuming full fixity at the pier base:

$$k_p = \frac{h_p^{\,2}}{c_p - c_{p0}} \tag{2.16}$$

where c_{p0} is the tip flexibility with full base fixity as defined in the previous section. This equation shows that if the computed flexibility of the pier gets closer to c_{p0}, the effective stiffness of the pier-end becomes infinite as expected.

However, the effective stiffness is not non-dimensional. That is, it has the dimension which is moment per unit radian. The rotational stiffness at the pier end should change as either the material property or the dimension of the structure varies. Therefore, a non-dimensional factor that should be able to control the effective stiffness needs to be defined, as was the case for *r* in the effective height method. It can be anticipated that k_p, the effective rotational stiffness at the pier end, is proportional to the flexural rigidity of the pier, *EI*, and inversely proportional to the width of the pier, W_p. Therefore, the following equation is the anticipated form of k_p.

$$k_p = \frac{EI}{\xi W_p} \tag{2.17}$$

where,

ξ = effective stiffness coefficient

The effective stiffness coefficient, ξ is in the denominator because it is desired that as the pier-end condition approaches the full fixity, the coefficient goes to zero. Now the regression analysis is performed as described above, and the expression of ξ can be generated in terms of the pre-defined two parameters: α and *Hb/Wp*. Under the assumption that the parameters are largely independent of each other, one of the two expressions for the effective stiffness is normalized and is multiplied by the other expression to determine the expression of ξ. The solid line indicates the measured ξ for each case, whereas the dotted line indicates the fitted regression line. The assumed fixed parameter values are also shown for each case.

Finally, the effective stiffness coefficient, ξ, can be expressed in terms of each variable using the simple exponential regression results for each case. One of two equations is normalized and multiplied by the other equation to establish the general expression of ξ in terms of two variables. As a result, the overall ξ can be expressed as follows:

$$\xi = \left[0.4\left(\frac{Hb}{Wp}\right)^{\frac{1}{5}} \right] \times \left[1 + 0.714\alpha^{\frac{1}{4}} \right] \tag{2.18}$$

As mentioned in the previous section, this equation is established on the assumption that the finite element analysis gives the correct result, and it is noted that each parameter must be in the range for which the regression analysis is generated.

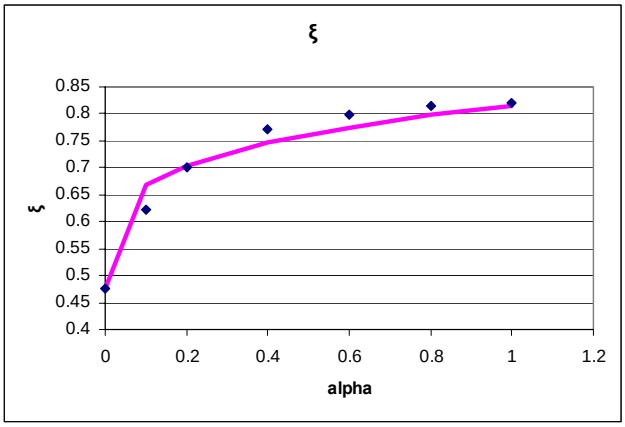

$Hb/Wp = 20/6$,

vary α

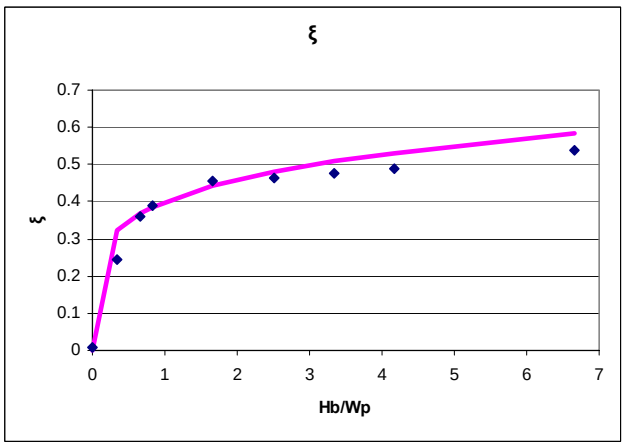

$\alpha = 0$,

vary Hb/Wp

Figure 2-17 Relationships Between Parameters and the Effective Stiffness Coefficient, ξ

Consideration of Bending Effect

Both of these methods are based on a simple shear model that assumes the horizontal displacements of each component are due to the corresponding shear force. However, there will also be in-plane bending action in the wall, and the effect will become larger as the wall aspect ratio increases (wall height/length). An additional bending deflection must be added so that:

$$\Delta_{top} = \Delta_{eff} + \Delta_b \qquad (2.19)$$

where Δ_{top} is the displacement at the top of the wall, Δ_{eff} is the displacement obtained from either the effective height method or the effective stiffness method, and Δ_b is the displacement from the beam bending effect in the wall. The displacement due to the beam effect of the wall, Δ_b, can be estimated as follows.

$$\Delta_b = \frac{H^3}{3EI} \tag{2.20}$$

where H is total height of the wall and I is the moment of inertia of the section of the wall. However, because this equation is for the case of a solid wall (no openings), a correction factor for the effect of the openings has to be considered.

$$\Delta_{top} = \Delta_{eff} + \Delta_b = \Delta_{eff} + \rho \frac{H^3}{3EI} \tag{2.21}$$

where ρ is the correction factor for the opening effect. This correction factor can be determined in the same way done for the effective height and stiffness factors. First, a wall is chosen such that the top displacement due to the lateral load at the top is dominated by bending rather than shear effects. The relationship between the opening ratio, η_p, and the factor was established by performing a regression analysis yielding:

$$\rho = 1 + 0.0035\eta_p + 0.0004\eta_p^{\,2} \tag{2.22}$$

where η_p is the ratio of the area of the openings to the area of the overall wall (%).

2.3.6 Consideration of Vertical Compression

Vertical compression in the pier is one of the important factors for the calculation of the pier strength [FEMA 2000]. The vertical compression acting on the pier is not constant during the seismic excitation due to the time-varying overturning moment as well as the vertical ground acceleration. As a result, the lateral strength and the failure mode of the pier will also vary with time under the seismic loading. This effect can be accounted for when modeling a URM wall using the finite element method by adopting an interface model with a specific yield criterion [Lotfi et al. 1994]. However, for the composite spring model developed in this study, the vertical compression for each pier is initially obtained from the static status of the structure and remains the same throughout the analysis. In other words, the composite spring model does not consider the additional vertical loading from the overturning moment. Accordingly, the strength and the failure mode for each pier do not change during the analysis and the displacement of the top of the pier is purely controlled by the lateral shear force.

2.3.7 Example Calculations

The accuracy of the effective height and the effective stiffness methods for estimating the initial elastic stiffness for masonry piers in a perforated URM wall were evaluated using the four different sample wall configurations previously specified in Figure 2-9. For reference purposes, the overall in-plane stiffness of each wall was determined by computing the average horizontal displacement at the top of the wall from an ABAQUS plane stress analysis. This was used as the reference value for each case.

For both the effective height and effective stiffness methods, the example wall was first decomposed into individual components using the decomposition method given in Figure 2-6(b). Each pier was then considered in two sections: an upper section and a lower section, and each section was half the height of the full pier as measured between the closest bottom/top of the openings on either side of the pier (*e.g.*, vertical distance between the lowest top and highest bottom of the openings). Appropriate values of the geometric parameters were determined for each case, and the effective heights and/or stiffnesses were computed from the regression results. For the effective height method, the in-plane flexibilities were next computed using Eq. 2.9 and these were combined in Eq. 2.10 to determine the total pier stiffness. For the effective stiffness method, the in-plane flexibilities ere computed using Eq. 2.9 and were also combined in Eq. 2.10 to determine the total pier stiffness. Spandrel and lintel in-plane stiffnesses were computed using simple shear stress formulations. Finally, all of the component stiffnesses were combined in series-parallel arrangement according to the initial wall decomposition to determine the overall wall in-plane initial elastic stiffness.

Table 2-2 shows a comparison of the resultant horizontal flexibilities at the top of the wall for each method. The relative percentages are also shown in parentheses. It can be seen that both methods provide essentially the same degree of accuracy. Both methods consistently underestimate the flexibilities for cases (a)-(c) but slightly overestimate the flexibility for case (d). There is a general trend to better agreement at higher flexibilities. For all cases, the results are felt to be acceptable for incorporation into simplified design models for a structure as complex as a URM wall. It should also be noted that these comparisons are only for the initial elastic stiffnesses. The full nonlinear behavior of the URM wall is determined by the strengths of each component and their particular types of hysteretic behavior.

Table 2-2 Computed Overall Wall Flexibility (in/lb) at Top Using Each Method.

Case (Figure 2-9)	Ref. [Abaqus]	Effective Height Method	Effective Stiffness Method
(a)	8.452E-6	6.76E-6 (80.0%)	6.50E-6 (77.0%)
(b)	7.961E-6	6.30E-6 (79.1%)	6.19E-6 (77.7%)
(c)	13.83E-6	11.4E-6 (82.7%)	11.8E-6 (85.0%)
(d)	11.16E-6	12.6E-6 (107.9%)	12.1E-5 (108.1%)

2.3.8 Implementation in DRAIN-2DX

As noted in Section 2.1.4, the URM wall models were designed to be implemented in DRAIN-2DX to form a simple design model. In this approach, the in-plane structural behavior of the URM wall was modeled using an assembly of parallel and series connected nonlinear springs representing the behavior of each component section of the wall. This was accomplished in DRAIN-2DX by using a simple zero-length nonlinear spring element identified as the TYPE 04 element. The basic form of this element can describe a simple bilinear force-deformation characteristic with either elastic, simple hysteretic, or gap hysteretic behavior, depending on the particular "elasticity code" specified for the element. As described in Section 2.2, the mass of the walls and other building elements were lumped at each node to form a relatively simple but highly nonlinear design model.

Additional Nonlinear Capabilities for TYPE 04 Spring Element

As developed in Section 2.3.2, there are four different types of nonlinear behavior that characterize the in-plane response of a URM wall: rocking, sliding, diagonal tension cracking, and toe crushing. Among these, the rocking and sliding behaviors can be idealized with the basic TYPE 04 spring element included in DRAIN-2DX. However, the diagonal tension cracking and toe crushing behavior are more complex and cannot be clearly defined because there are few experimental studies that have reported the associated force-deformation behavior. As can be seen in Figure 2-4, the force-displacement behavior associated with diagonal tension cracking exhibits stiffness degradation and strength deterioration that cannot readily be modeled using the built-in TYPE 04 spring element.

For this study, the Park 3-parameter model for a force-deformation relation [Park, et al., 1987] was adopted to model these additional nonlinear properties. The Park 3-parameter model is built up around a basic tri-linear backbone, or strength, curve that can be unsymmetric (*e.g.*, different shapes for positive and negative deformation). The model also includes a variety of different hysteretic behaviors that can be achieved by specifying the three model parameters α, β, and γ. These parameters define stiffness degradation, strength deterioration, and pinching behavior that are characteristic of a reinforced concrete elements [Park et al., 1987].

The Park 3-parameter model is coded in a force-controlled element in the IDARC program which is a research code for inelastic dynamic analysis of reinforced concrete structures [Park, et al., 1987]. For the present study, this code was extracted and modified for use in the deformation-controlled DRAIN-2DX code. At the start of the study, the Park 3-parameter model was incorporated into a completely new DRAIN-2DX element temporarily identified as a TYPE 03 element. Figure 2-18 below shows a sample of the different kinds of nonlinear behavior over several loading cycles that can be modeled using the Park 3-parameter TYPE 03 element. The required input data and the FORTRAN source code for the associated DRAIN subroutines are described in Appendix D.

Because the Type 03 element ID is designated by the DRAIN developers for other purposes, the Park 3-parameter model behavior should eventually be incorporated directly into the current TYPE 04 nonlinear spring element. This should be done in the form of additional "elasticity codes" that can be specified in the DRAIN input file, much as they now are in the TYPE 03 element developed in this study.

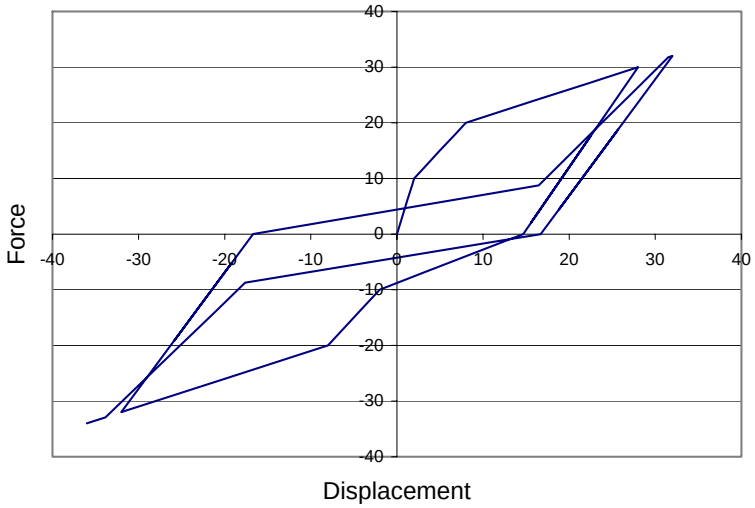

Figure 2-18 Sample Park 3-Parameter Nonlinear Spring Behavior in DRAIN-2dx

Model Comparison

The present lumped parameter model was compared with experimental results developed by Manzouri et al. [1996]. The detail of the particular wall with one opening and its lumped parameter model are shown in Figure 2-19. The in-plane lateral load was applied by a force acting across the top. Each wall component was modeled as a nonlinear spring, and the nonlinear springs were connected to each other to construct a composite spring model. The model was implemented in DRAIN-2DX [Prakash, 1993] using zero length nonlinear spring elements for each spring. The relationship between the lateral force and top displacement obtained from both the experiment and the analysis are plotted in Figure 2-20. The composite spring model provided a reasonable bilinear approximation to the in-plane behavior and closely reproduced the strength (40 kips).

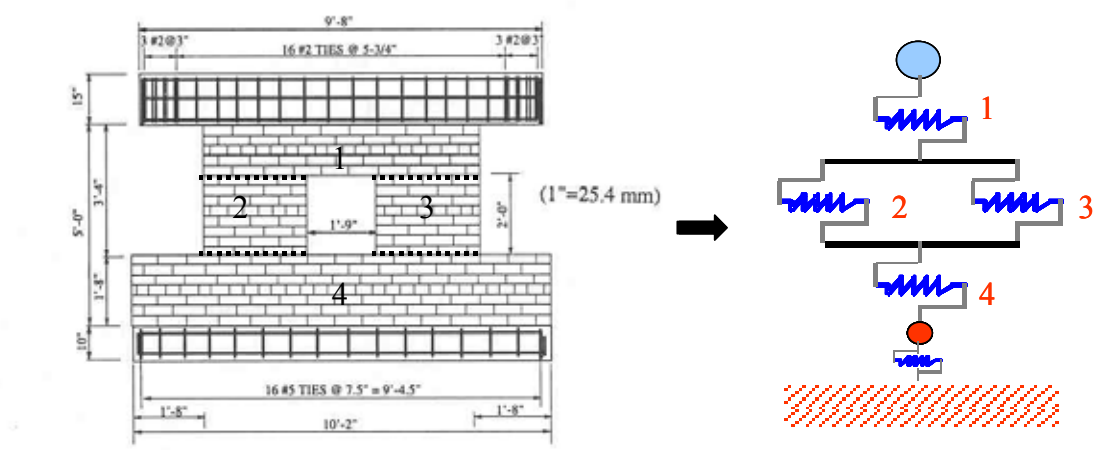

Figure 2-19 Detail of the experimental wall and its modeling

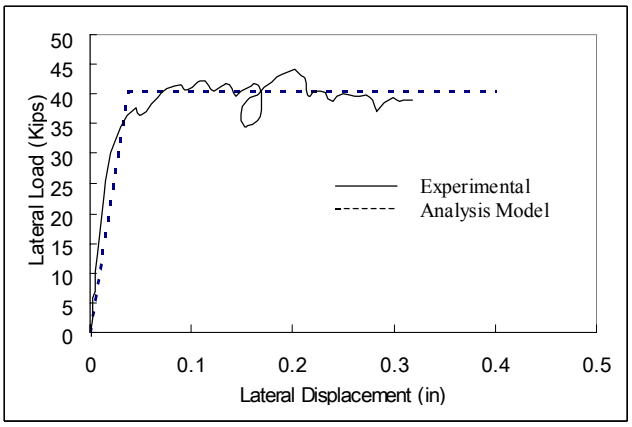

Figure 2-20 Force-displacement curve of wall from both experiment and analysis

2.4 Composite Model of a General URM Building

As described in Section 2.1.3, a general URM building was modeled as a 2D model in this study using DRAIN-2DX as the modeling tool. The out-of-plane wall stiffnesses were ignored, however, the mass of the out-of-plane walls was still considered and was lumped at the story level of the building (see Section 2.2.1). The modeling details are described in the following sections.

2.4.1 Sample Structure

A URM building designed and constructed in a concurrent MAEC project (ST-11) was taken as a sample URM building for the purpose of describing the modeling process. A simple 3-D

view of the building is shown in Figure 2-21, and the detailed dimensions of the building are shown in Figure 2-22. The dimensions shown in the figure were tentative at the time this report was written since construction of the actual structure in the laboratory was not completed. The building is a two-story URM building with wooden floor and roof diaphragms. Each wall of the building is a perforated wall, *i.e.*, it has doors and windows. The walls were designed with three wythes and the thickness of each wall is 12 inch. The same nominal values for the material properties of the masonry and its self-weight as given in Section 2.3.3 were used for this model.

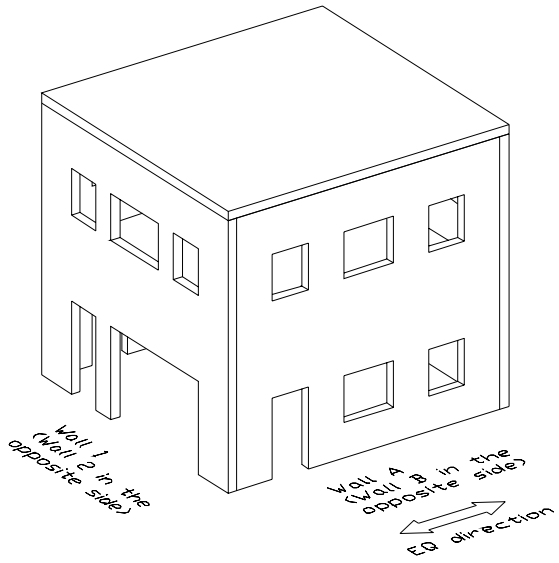

Figure 2-21 The Sample Structure.

The assumed direction of the horizontal ground acceleration due to the earthquake excitation was N-W as shown in Figure 2-21. Therefore, walls A and B are in-plane walls whereas walls 1 and 2 are out-of-plane walls.

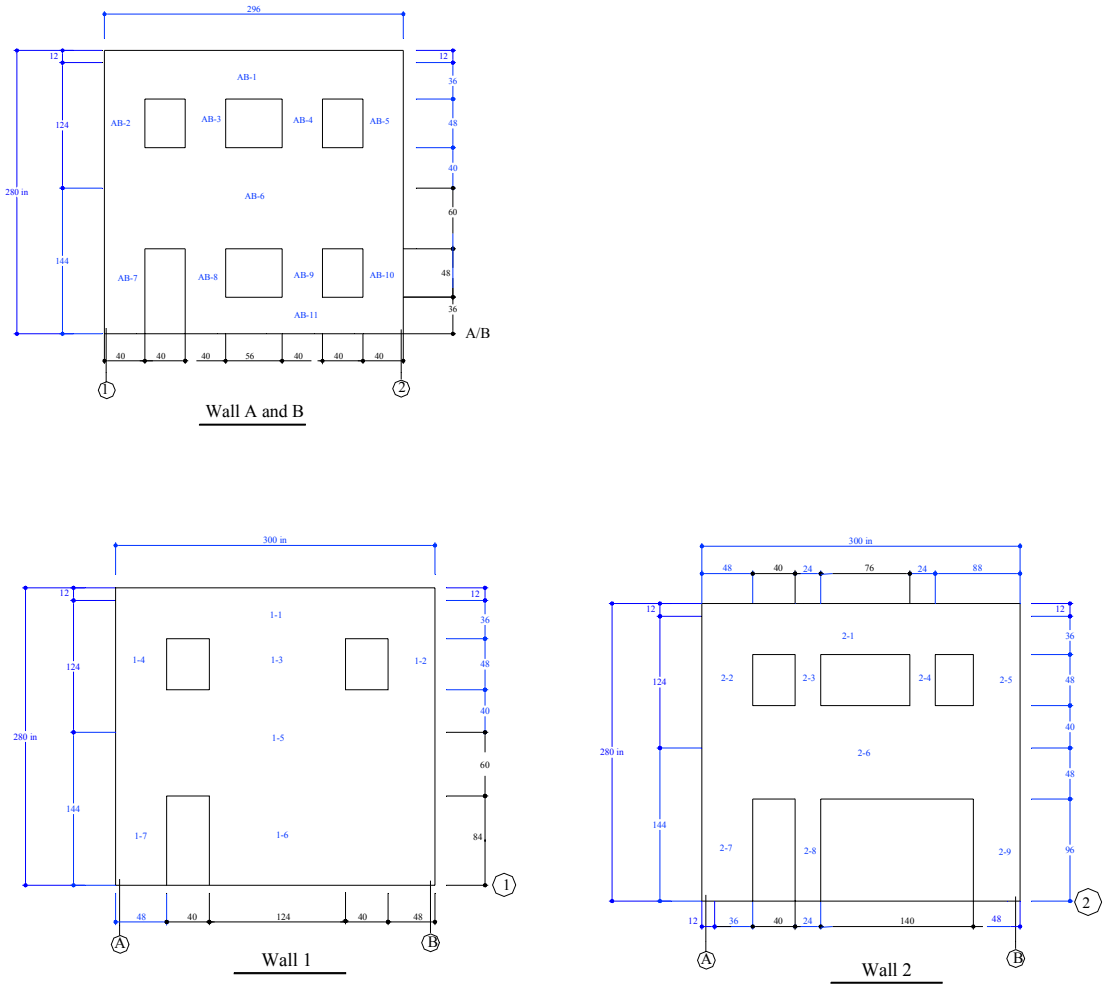

Figure 2-22 Dimensions of Each Wall

2.4.2 Modeling

The 2D model for this building consisted of a single degree of freedom at each floor level for each of the in-plane walls and another degree of freedom for each of the two floor diaphragms as shown in Figure 2-23. The in-plane behavior of each of the walls was modeled with two nonlinear composite springs consisting of series and parallel elements. The individual elements and their properties were determined based on the given wall openings and using the equivalent stiffness methodology described in Section 2.3.3 The out-of-plane wall stiffnesses were ignored but their masses were included. The two in-plane walls were connected with other spring elements which represented the floor and roof diaphragms in the building. The mass of the out-

of-plane wall was lumped at each story level and connected to the diaphragm spring elements. The DRAIN-2DX input file for this model is provided in the Appendix C. Simulation results using this model for design and evaluation of passive response modification are presented in the next chapter.

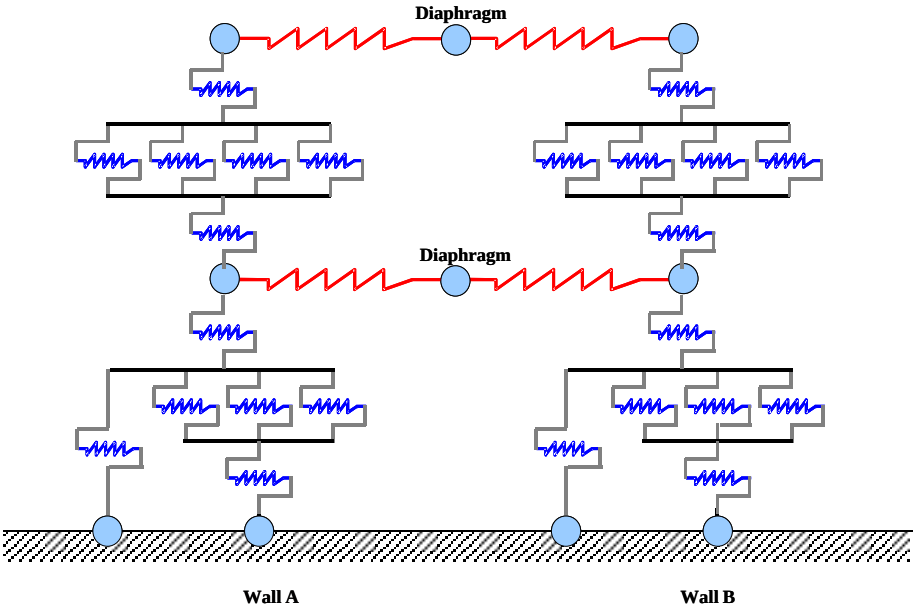

Figure 2-23 2D Modeling of the Sample URM Building.

3 Design of Passive Energy Dissipation Systems

Passive energy dissipators (PED's) can broadly be defined for design purposes as being either displacement sensitive or velocity sensitive or a combination of both. Hysteretic devices based on yielding and ductile deformation of metals are usually considered displacement sensitive while viscous dampers are considered velocity sensitive; however, as noted in Chapter 1, the practical behaviors can sometimes be more complex. Although they are often reduced to generalized design procedures, the design processes for passive energy dissipation systems should reflect these fundamental differences in their behavior. For example, FEMA 356 [FEMA, 2000] specifies linear static, linear dynamic, and nonlinear static procedures (LSP, LDP and NSP) that represent the behavior of passive damping devices by their equivalent viscous damping coefficients. Only the nonlinear dynamic procedure fully considers the behavior of the PED's.

A nonlinear dynamic procedure is used in the present study to size the passive energy dissipation subsystems under investigation. This approach was selected in light of the more complex and highly nonlinear response of URM buildings with flexible wooden floor diaphragms that are characteristic of the target class of buildings (essential facilities). The present analysis procedures is, however, a modified approach that differs from what is outlined in FEMA 356 with regard to several important features:

- The analysis is entirely 2D, and while it considers all multistory mass and lateral force resisting elements in the given (analysis) direction, it does not consider any effects of mass or stiffness eccentricities (and consequent 3D coupling).
- The design procedure is based on a detailed analysis of the energy dissipation developed by the PED's and its maximization with respect to the seismic energy input to the structure.

Only metallic hysteretic damping devices were considered in this study. This was largely based on the extensive experience of the investigators with modeling and analysis of these kinds of PED's as well as with design, fabrication and testing of prototype versions [Pinelli, et al 1996]. In addition, it was felt that such PED's may offer superior levels of reliability compared to viscous, viscoelastic or friction devices, especially over long periods of time (comparable to building lifetimes) that are associated with MCE seismic hazards in the study region. Several

schemes to integrate the metallic PED to the URM buildings are proposed and were evaluated in this investigation.

3.1 Passive Devices

The fundamental role of passive energy dissipation devices is to consume part of the seismic energy transmitted into a structure, thereby reducing energy dissipation demand in its primary structural elements. As a result, damage in the main structural elements is minimized. The use of metallic hysteretic PED's is attractive for a seismic protection system because they offer good long-term reliability with little maintenance actions required, modest cost and relatively simple design.

Tapered beams have received widespread consideration as flexural energy dissipators because of their outstanding performance, analytic simplicity and relative ease of fabrication. As noted above, the investigators have extensive knowledge on the use of tapered devices as an energy dissipating system and have actually fabricated and tested a number of prototypes in the laboratory. Details of a typical tapered flexural energy dissipator design are illustrated in Figure 3-1. The tapered device is fabricated from a steel plate, cut away as shown to create a narrow flexural element with a tapered width to initiate inelastic deformation over a greater portion of material.

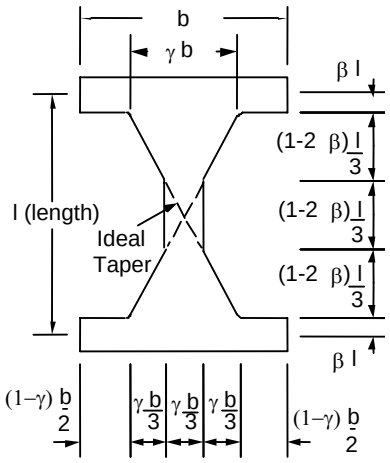

Figure 3-1: Geometry of the Tapered Passive Energy Dissipation Device

Two parameters, β, γ, determine the geometry of a tapered PED device [Moor, 1992; Pinelli, 1993]. They are defined in Figure 3-1. The variable β represents the portion of the length of the beam with full length l (the length itself is computed from center to center of opposite faces).

The variable γ is the ratio between the maximum width of the device and the width of the taper. Both β and γ are dependent on the geometric dimensions and vary with each device.

When the tapered elements deform laterally in double-curvature bending, inelastic deformation will occur at all cross sections along the taper, because both the width of the beam and the bending moment vary linearly. The result will be "fat", almost rectangular, hysteresis loops that reflect the high energy dissipation resulting from the pronounced yielding of a ductile metal used for this purpose (Figure 3-2). In order to get the necessary double-curvature (so that the variation in width and moment coincide), it is important that the beam ends be fixed. This fixity is achieved through an abrupt increase in the beam width (and therefore the flexural rigidity) at the ends of the taper and by end clamping.

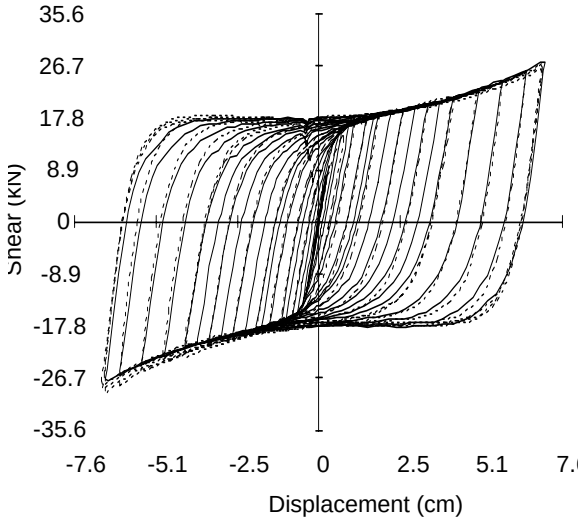

Figure 3-2: Hysteretic Loops for a Tested Tapered Device from *Pinelli et al. [1993]*

The typical behavior of metallic hysteretic PED's illustrated above underscores the obvious requirement that these devices be allowed to develop significant levels of deformation in order to fully realize their superb dissipation capabilities. URM structures, on the other hand, usually exhibit some of the highest lateral stiffnesses encountered in low rise buildings, at least within the elastic range before significant cracking develops. For this reason, it would appear that PED's are unlikely to be effective when applied to these kinds of structures. On the other hand, typical URM structures used for essential facilities in the region are also characterized by the presence of very flexible wooden floor and roof diaphragms. These diaphragms are a significant element in the structural system because they effectively couple together the structural behavior

of parallel as well as orthogonal load-bearing walls (both exterior and interior walls). The result is a much more complex structural system that is capable of developing much greater deformation levels than typically associated with the elastic response of URM walls. For example, simple analysis models such as those included in FEMA 356 [FEMA 2000] suggest that typical wooden diaphragms can routinely be expected to develop in-plane shear deformations at least as large as those indicated in Figure 3-2, and this is born out by recent laboratory testing of both baseline and reinforced configurations [Bracci, et. al., 2001].

Wooden diaphragm flexibility is a complex issue that is not well understood in practice owing to large uncertainty about the construction details and current conditions of most diaphragms. This situation is even more complicated when one considers the connection between the diaphragm and the URM load-bearing walls that support it. It is widely thought that typical connections are capable of supporting only gravity loads and that little or no lateral connection integrity is provided (for example, it is common to find joists supported in pockets in the URM walls with little or no lateral connection between the two). As a result, such structures are highly vulnerable to any kind of lateral seismic loading.

It was assumed for the present study that basic rehabilitation steps have been taken to laterally connect the wooden floor and roof diaphragms to the supporting URM walls. The PED's were then applied using this structure as a baseline. Three rehabilitation concepts were investigated in this study: one that was activated by relative displacements between the "in-plane walls" and the diaphragm (called Type 1), one activated by relative displacements between the diaphragm and the ground (called Type 2), and finally, a system that was activated by the relative displacement between the top of the "in-plane wall" and the ground (called Type 3). The terms "in-plane wall" and "out-of-plane wall" which are used throughout this report are fully defined in Chapter 2.2 and refer to the particular kinds of lateral loading to which the walls are subjected.

3.1.1 Type 1 Scheme

In this rehabilitation scheme, the energy dissipation mechanism is activated by the relative displacement between the in-plane wall and the center of the diaphragm at the same level. The amount of energy dissipated is highly dependent on the deformation of the diaphragm and the in-plane wall (it was assumed that the URM walls subjected to out-of-plane forces offer little or no

resistance). Building applications of the Type 1 rehabilitation scheme can be fabricated by inserting a beam between two in-plane walls at opposite edges of a wooden diaphragm. Provided that this beam is stiff enough, the lateral movement at its midspan will approximately equal the average of the in-plane movement of the supporting (in-plane) walls. Tapered metallic PED devices can be attached between the midspan of the beam and the center of the floor or roof diaphragm immediately above as shown in Figure 3-3. The PED will inelastically deform as the wall and diaphragm move differentially (Figure 3-4).

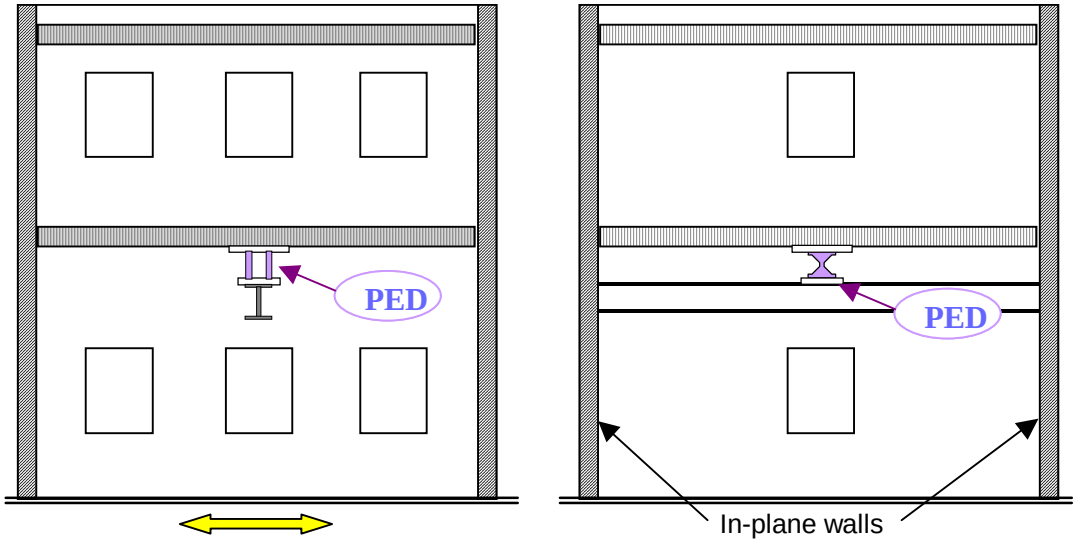

(a) Plane of motion **(b) Normal to plane of motion**

Figure 3-3: Type 1 Rehabilitation Scheme for URM Building

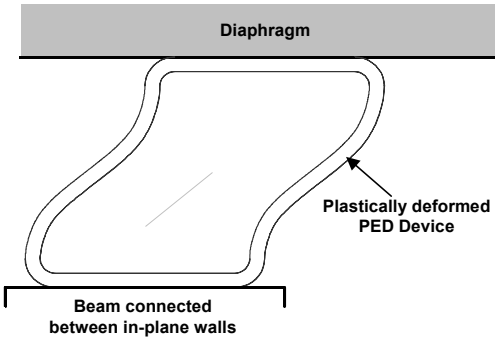

Figure 3-4: Deformation of the Tapered PED Device (in plane of motion)

3.1.2 Type 2 Scheme

The Type 2 rehabilitation scheme makes use of the relative displacement between the center of the diaphragm and the ground or the floor immediately below. The tapered PED devices could be connected between the center of the diaphragm and the ground through a stiff chevron or K-brace as displayed in Figure 3-5. The braces could quite possibly be hidden inside or integrated into interior walls.

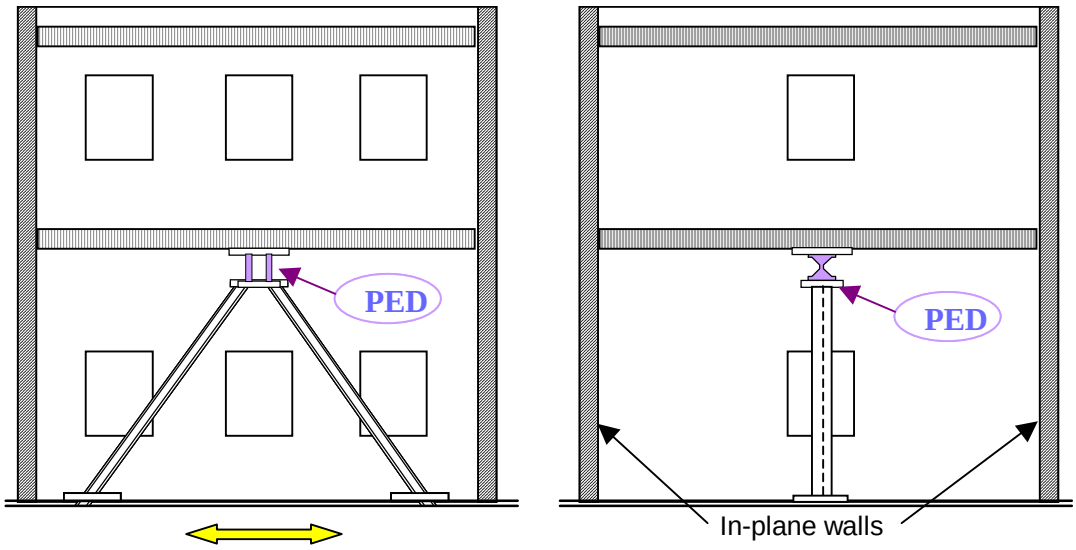

(a) Plane of motion **(b) Normal to plane of motion**

Figure 3-5: Type 2 Rehabilitation Scheme for URM Building

3.1.3 Type 3 Scheme

Relative displacement within the in-plane wall (between top of the in-plane wall and the ground) is employed to activate the Type 3 rehabilitation scheme. The stiff URM wall develops very little in-plane deformation, and as a result, a conventional metallic PED device like one of those used for the Type 1 or 2 schemes may not yield and deform sufficiently to provide significant energy dissipation. Mechanical ways to magnify the deformation in the PED have been studied by others. Constantinou and Sigaher [2000] and McNamara et al. [2000] suggested a concept for motion amplification in structures with high rigidity. It uses what is called a toggle brace to kinematically magnify small displacements of the structure. The amplified displacements could then be used to activate a metallic tapered flexure PED similar to those considered for Type 1 and 2 schemes. One possible application is presented in Figure 3-6 where

the tapered PED is inserted into a motion amplification system. The displacement magnification factor in this scissor-jack system depends solely on the angles θ and ψ. For example if θ = 9° and ψ = 70°, the magnification factor (based on interstory drift) can be as high as 2.16 (Constantinou and Sigaher [2000].)

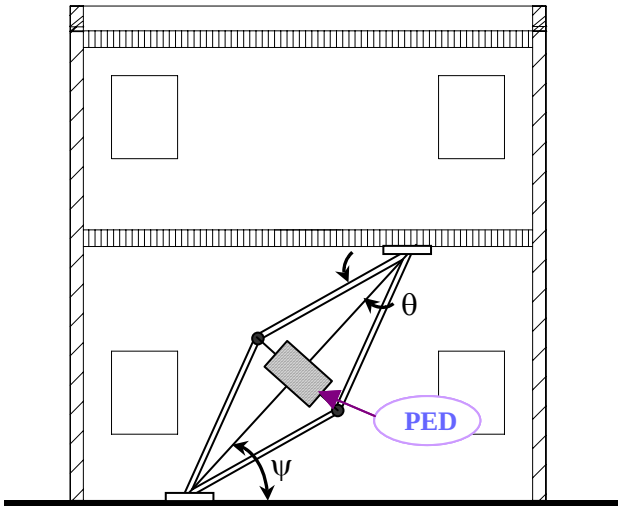

Figure 3-6: Type 3 Rehabilitation Scheme for URM Building

3.2 Energy Formulation

Previous studies of the influence of hysteretic energy dissipation in a tapered flexure PED on the response of a building [Pinelli, et al, 1996; Goodno, et al, 1998] suggest that a suitable design criterion could be formulated in terms of energy dissipation. An energy-based design aims at resisting, or balancing the energy input to the structure by an earthquake with the energy the structure is capable of absorbing. If the equation of motion expressed in terms of the relative displacement with respect to the ground is integrated from the time the ground motion excitation starts, the resulting "relative" energy equation is [Uang and Bertero 1990]:

$$E_i = E_k + E_S + E_d + E_h \qquad (3.1)$$

where:

E_i = the relative energy input by the earthquake;

E_k = the relative kinetic energy;

E_S = the recoverable elastic strain energy;

E_d = the viscous damping energy; and,

E_h = the irrecoverable hysteretic energy.

This type of design approach makes use of a ***global*** quantity (energy in the structure) rather than focusing on a pointwise metric such as interstory drift or maximum deflection. In particular, hysteretic energy dissipation (E_h above) is usually associated with yielding and damage to the structural members, including formation of plastic hinges that could possibly lead to collapse of the structure. If it is possible to eliminate this kind of dissipation in the structural members or to reduce it below some acceptable limit, a structural design that is highly resistant to earthquakes might be achieved.

For a structure to resist an earthquake in a feasible and economical way, a significant part of the input energy must be dissipated through viscous or hysteretic damping outside the primary structural members. Many of the energy dissipators developed in recent years aim at concentrating the dissipation (viscous, hysteretic, friction) away from the structural members and into a few pre-engineered elements. This is exactly the idea behind use of the tapered flexural PED.

In order to design a PED, the following performance criterion is adopted [Pinelli et al., 1996]:

the best design will be the one that provides the highest ratio E_C/E_i,

where E_c is the total hysteretic energy dissipated in all the devices, and E_i is the relative energy input to the structure throughout the motion. At the same time, several practical constraints must also be satisfied:

- the ductility demand on any of the devices should not exceed an allowable value defined for each particular energy dissipator (*e.g.*, from laboratory tests);
- constraints on PED force capacity, physical geometry and the ease of fabrication must be considered.

The E_C/E_i criterion directly takes into account the energy dissipation property of the PED's and tries to maximize it for a given design. While this criterion does not explicitly minimize the hysteretic energy developed in the structural members, Pinelli et al. [1996] showed that

satisfaction of the E_C/E_I design criterion will ensure that little hysteretic energy is dissipated in the structural members and that the overall seismic response of the building is reduced.

A critical issue in the design of energy dissipators is the definition of ductility as it applies to the operation of the PED itself. These devices must be able to sustain quite large levels of inelastic deformation over repeated cycles of loading without failure (low-cycle fatigue fracture). But the traditional definition of ductility, as the ratio of maximum monotonic displacement to yield displacement, provides only limited information to designers in the case of systems subjected to random vibrations with varying amplitudes. It overlooks important parameters like the number of cyclic reversals and the energy dissipated by the system. In this case, a more comprehensive definition of ductility developed by McCabe and Hall [1989] must be adopted. The total ductility of a system, μ, is divided in two parts: an elastic ductility, μ_e, varying from 0 to 1 which corresponds to the elastic behavior of the system (μ_e=1 at yield); and a plastic ductility μ_p, starting from 0 at the yield point. Consequently, once a system has yielded, $\mu = 1 + \mu_p$.

McCabe and Hall assumed that the damage suffered by an elasto-plastic structural steel system during an earthquake is similar to a low cycle fatigue phenomenon. Based on their work, it is possible to predict an equivalent monotonic ductility, μ_p, for a system subjected to an arbitrary cyclic loading. This equivalent monotonic plastic ductility, or ductility demand, is the maximum plastic ductility that the system would exhibit in a monotonic loading test in order to dissipate the same amount of energy as that obtained during cyclic loading. The equivalent monotonic plastic ductility demand on the system expressed in terms of energy, and load reversals, is:

$$\mu_p = \frac{H_t}{f_y u_y \left(2N_f\right)^{0.4}} \tag{3.2}$$

where H_t is the total hysteretic energy dissipated in the system during N_f load reversals; and f_y and u_y are the yield load and yield displacement of the system, respectively.

The design criterion as stated above is a classical constrained optimization problem. The objective function (to be optimized or maximized in this case) is the energy ratio, E_c/E_i. For the design of tapered flexure energy dissipation devices constructed from ductile steel, a simple bilinear stress-strain curve adequately describes the flexural behavior. Thus, suitable properties

that can be used as decision variables are the initial elastic stiffness, k, the yield force, f_y, and the strain hardening ratio, η. For the present cases, the strain hardening ratio was assumed to be very small and only k and f_y were used. In addition, upper/lower bounds must also be specified as side constraints in the minimization process. Finally, the maximum dynamic ductility must also be specified as a constraint to insure the structural integrity of the devices.

For purely practical reasons, additional constraints should also be added. In general, it is unlikely that a given set of tapered flexure PED design properties can be uniquely related to a particular device geometry, that is, more than one given geometric configuration could yield the same design properties. As a result, it might also be necessary that the tapered flexure PED also satisfy practical criteria related to constructability such as:

- the total length of the device should be constrained for manufacturing and installation requirements;
- certain material thicknesses in the tapered elements must be maintained within practical limits.

These can be added in a manner similar to the other constraints noted above, but they have not been utilized in the present study. As a final note, it should be noted that Moor [1992] developed two design formulae for the tapered devices based on laboratory test results as follows:

$$k = \frac{E \cdot b \cdot t^3}{2 \cdot l^3} \tag{3.3}$$

$$f_y = 0.65 \cdot \frac{\sigma_y \cdot b \cdot t^2}{l} \tag{3.4}$$

where k and f_y are the initial stiffness and the yield load of the tapered device, E and σ_y are the elastic modulus and the yield strength of steel, b, t, and l are the width, thickness, and length of the tapered device (see Figure 3-1)

3.3 Application of PED's to URM Building Models

3.3.1 Design Model

From a purely analytical perspective it is always a desirable goal to develop a model that provides the highest degree of fidelity. That is, the model should represent as much physics as possible in the real system so that all significant behavior is incorporated into the model.

However, this ambitious goal all too often results in large, complex and unwieldy models that are impractical for design purposes. In design studies it is often necessary to assess the performance of a range of design variations, and if a great deal of time and (computational) effort are required, it may not be practical to employ such a detailed model.

What is needed, instead, is a "design model" that provides a reasonable level of fidelity but yet is computationally tractable. Such a model frequently omits certain "details" of the actual behavior which, while they may be important issues later when addressing specific features of the design, are nonetheless relatively unimportant in the conceptual stages of design. These "details" may be extremely important for other more refined aspects of the design involving, for example, matters such as localized stresses. Finite element models provide a useful example to consider. One would be unlikely to attempt to carry out a conceptual design for a structural system by using a highly detailed finite element model involving a large number of very accurate, high-order elements. Such a model generally requires very detailed geometric and material information that is not normally available, or even defined, at early conceptual stages of design. In such cases, a much simpler model, perhaps not even involving finite element analysis, might be more practical and useful.

Of course, an obvious problem exists with this situation. At some point, the design model must be converted (or evolve) into a detailed model suitable for more extensive analysis purposes. As a result, the design model must also be fully consistent with more detailed models.

PED Design Model

A design model for a PED must necessarily involve a relatively small number of design variables in order to be practical. In the present study, a structural hysteresis model was based on an assumed elastic-perfectly plastic material behavior. In this case an initial stiffness and a yield force were used to describe the material. As a result the minimum practical number of design variables needed to describe such a device is two, *e.g.*, a stiffness and a yield force. Of course, additional design variables such as strain hardening or the Bauschinger effect could be added to provide more realistic behavior, but for design purposes, these details are of relatively little importance. Figure 3-7 illustrates a typical PED design model based on these assumptions.

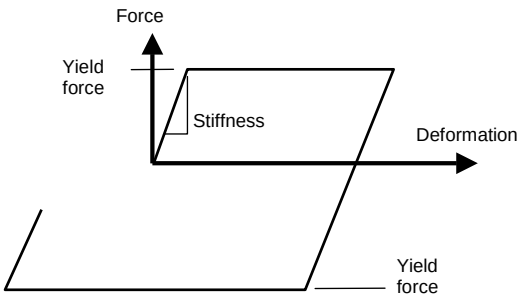

Figure 3-7: Representative PED Design Model

URM Structure Design Model

The design model for the URM structure necessarily represents physical and dynamic characteristics of the structure to an acceptable level, but maintains its computational efficiency. For this design study, it was assumed that a 2D model, such as developed in Chapter 2, would be sufficient for the class of problems to be considered. However, given the presence of energy dissipation devices in the structure and the possible hysteretic, inelastic behavior of structural members, it was important to use a nonlinear structural model.

In the initial "proof-of-concept" studies, a simple rectangular structure with four URM walls and a single flexible wooden floor/roof diaphragm was considered. For either of the two principal directions, the in-plane walls, out-of-plane walls, and diaphragm were represented by a system of the zero-length nonlinear spring elements in DRAIN-2DX (element Type 4) and lumped masses as described in Chapter 2. The basic URM structure design model for this simple building is illustrated in Figure 3-8. The URM elastic stiffnesses were obtained directly from simple shear panel formulas or more precise plane stress analysis (when perforations are present). As noted in Chapter 2, the significant nonlinear properties of the in-plane walls (*i.e.* rocking, bed-joint sliding and shear cracking) were determined following FEMA-356 guidelines while the out-of-plane walls were assumed to be entirely elastic in this study. For example, in-plane wall rocking was modeled using the bilinear behavior with elastic unloading (Elasticity Code = 1 in the Type 04 element) while walls experiencing shear cracking or bed-joint-sliding were modeled using the bilinear behavior with inelastic unloading (Elasticity Code = 0 in the Type 04 element) as shown in Figure 3-9.

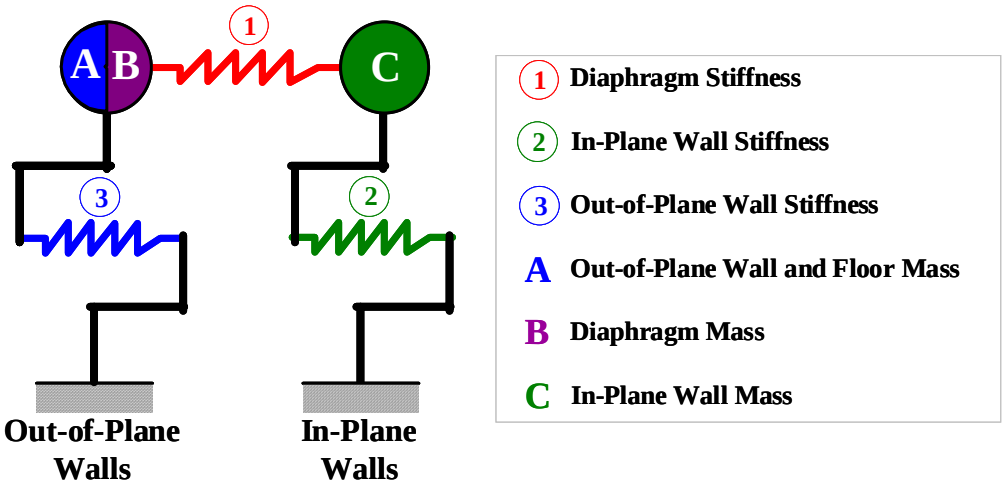

Figure 3-8: URM Structure Design Model

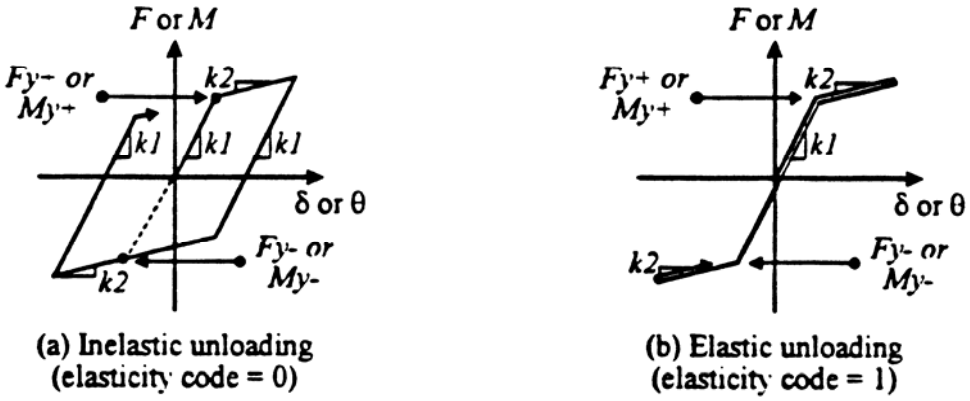

Figure 3-9: Hysteretic Behavior Options in DRAIN-2dx; (a) Inelastic Unloading, (b) Elastic Unloading

3.3.2 Rehabilitated URM Building Models

Application of Type 1, Type 2, or Type 3 rehabilitation schemes in a URM building can be modeled by adding additional spring elements to the existing building model to represent the behavior of the PED. In particular, a nonlinear spring with elastic-perfectly-plastic hysteretic behavior is used to represent a metallic tapered flexure PED. The nonlinear spring is then integrated into the building design model in a way that corresponds to the particular scheme that is used. For the Type 1 scheme, the nonlinear spring representing the PED is attached directly between the in-plane wall mass and the diaphragm mass. It utilizes the relative displacement between the in-plane wall and the diaphragm to dissipate energy. Figure 3-10(a) shows the

configuration schematically (see Figure 3-8 for a key description). As shown in Figure 3-10(b-c), the PED nonlinear spring is added between the diaphragm mass and the ground for a Type 2 scheme and between the in-plane wall mass and ground for a Type 3 scheme.

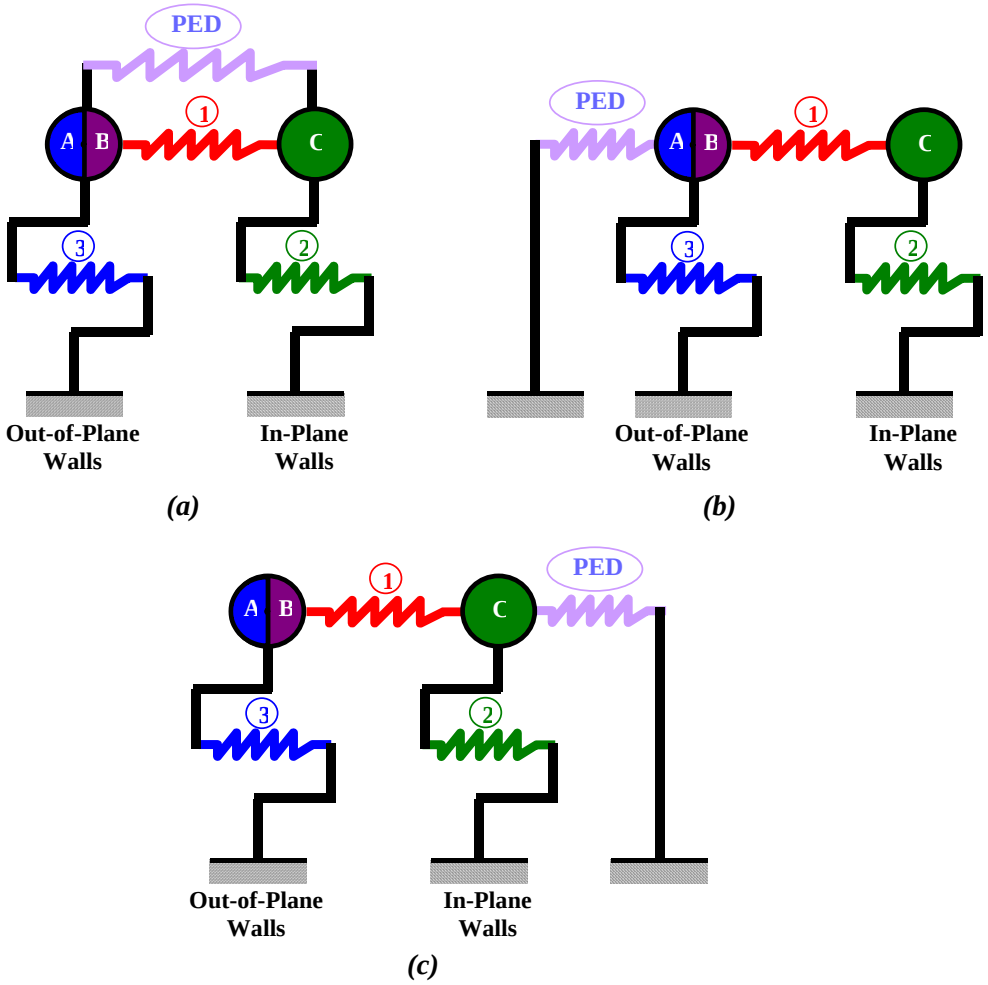

Figure 3-10: Design Models for Rehabilitated Building; (a) Type 1 Scheme, (b) Type 2 Scheme, and (c) Type 3 Scheme

3.4 Concept Validation: ST-10 Experiment

In the initial studies, numerical simulations of the various hysteretic metallic PED schemes were carried out for a greatly simplified URM building. MAEC research project ST-10 involved scale model dynamic testing of out-of-plane URM wall response on the shake table in the Newmark Laboratory at the University of Illinois Urbana-Champaign. The scale model developed for these tests provided the preliminary building for the present project, and additionally, it was anticipated that comparison with actual laboratory test results could be used

to validate the PED design models. In the end, only analytical studies were carried out, and PED designs were not incorporated into the laboratory test program. While the ST-10 test model did not prove to be the best choice for preliminary validation of this response modification approach, a PED design was developed and diaphragm and out-of-plane wall response reductions of as much as 30% were predicted.

3.4.1 Test Structure

The ST-10 test structure was a reduced-scale and highly idealized building placed on the 12′x12′ shake table in the Newmark Lab. It was composed of two (95″ x $71^{5}/_{8}$″ x $3^{5}/_{8}$″) masonry walls positioned parallel to the direction of force (referred to as the in-plane walls) and two (76″ x 39″ x $3^{5}/_{8}$″) masonry walls placed perpendicular to the direction of force (referred to as the out-of-plane walls), as shown in Figure 3-11. The out-of-plane walls were tied together with two stiff beams and the diaphragm flexibility was simulated by tying the in-plane walls together with a flexible steel or aluminum beam (called the "diaphragm beam" below) cross connected at its midpoint to the out-of-plane beams. A floor mass of 7 kips was added to provide pre-compression in the out-of-plane walls. Figure 3-12 shows elevation and plan views of the test structure.

Figure 3-11: ST-10 Test Structure on the Shake Table (out-of-plane URM wall is in foreground)

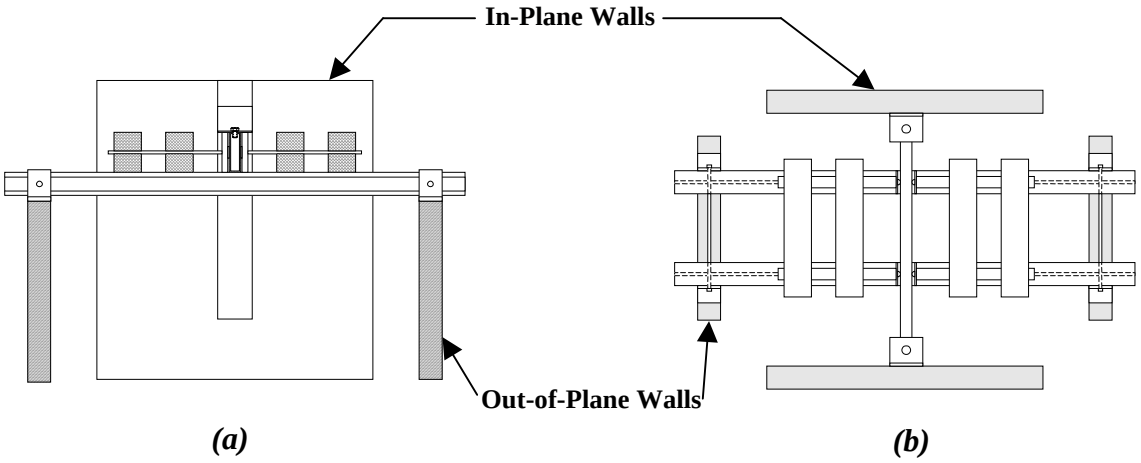

Figure 3-12: Schematics of the ST-10 Test Structure; (a) Elevation View, and (b) Plan View

3.4.2 Nonlinear Modeling of the Test Structure

The in-plane and out-of-plane walls of the ST-10 test structure were modeled in DRAIN-2DX with nonlinear spring elements (element Type 04) using the configuration shown in Section 3.3. A floor mass of 7 kips in combination with the mass of the out-of-plane walls was lumped at the out-of-plane wall node, while the mass of the in-plane walls was lumped at the in-plane wall node. Elastic properties of the walls and diaphragm were obtained directly from preliminary test results of the wall materials.

Calculations following FEMA-356 guidelines yielded a rocking strength of 0.908 kips and a bed-joint-sliding strength of 5.19 kips for the in-plane walls, and therefore it was concluded that rocking would govern the behavior of these particular walls. The rocking was modeled using the elastic unloading hysteretic behavior (Elasticity Code = 1 in the Type 04 element) as shown in Figure 3-9(b). The out-of-plane walls were assumed to offer little or no additional stiffness to the model and therefore were simply treated as elastic. The diaphragm stiffness is represented by a nonlinear spring element.

In order to provide initial validation of the design model, the fundamental period of the structure was compared with preliminary test results. The design model gave a fundamental period of 0.17 seconds, which is reasonably closed to the 0.16 seconds measured in the preliminary tests.

3.4.3 Rehabilitation Schemes

In the ST-10 experiment, a Type 1 scheme was used which utilizes the relative displacement between the in-plane walls and the mid-span of the diaphragm beam to initiate inelastic deformation in the PED's. For this scheme, an additional stiff box beam must be connected between the two in-plane walls. Two tapered flexure PED's can then be installed between mid-spans of the stiff box beam and the diaphragm beam immediately above. Detailed fabrication drawings of this Type 1 scheme are provided in Appendix B. The PED in a Type 2 scheme dissipates energy by making use of the relative displacement between the diaphragm beam and the ground. For this scheme, a PED must be mounted at the mid-span of the diaphragm beam and connect to the ground through a K or chevron brace type structure. Schematic views of these schemes are shown in Figure 3-13 below.

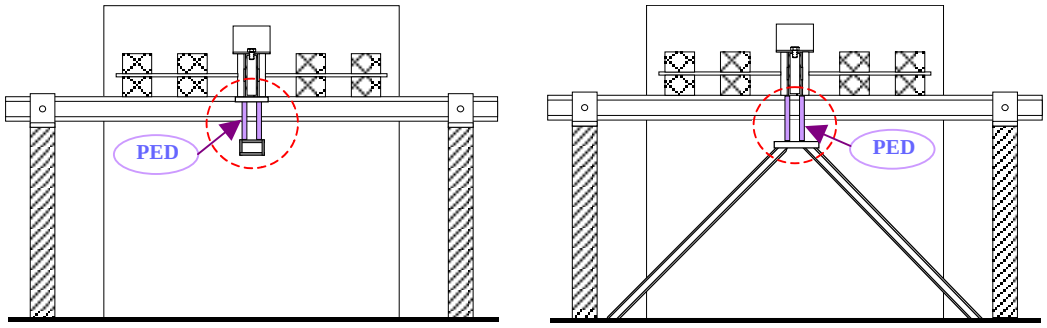

Figure 3-13: Rehabilitation Schemes; (a) Type 1, and (b) Type 2

Finally, another possible way of rehabilitating the URM structures is to use the relative displacement of the in-plane wall alone (*i.e.*, between the in-plane wall and the ground) which is called a Type 3 scheme. Since the deformation of the in-plane walls in this experimental study is very limited, some kind of motion amplification system (*i.e.* toggle brace system) would be necessary in order to activate the PED devices. Extensive fabrication would also be required for such a scheme, and so it was decided to leave this aspect for potential future research.

3.4.4 Design Results

At this point, the design process has been formulated as a straightforward numerical optimization process in which an objective function (E_c/E_i) as computed using DRAIN-2DX must be maximized with respect to PED design variables, k, and f_y, and with constraints on the

maximum allowable dynamic ductility as outlined in Section 3.2. Rather than carry out a purely numerical optimization, a purely graphical process was manually implemented in which the objective function was numerically evaluated for a tabular array of different design variables (PED initial stiffness and yield load) spanning the design space under investigation. In addition, the resulting dynamic ductility demand for each case was also computed and recorded. The result of these calculations was a grid of values of the objective function and constraint values (dynamic ductility demand) that could be plotted as superposed 2D contour plots. A total of 400 test cases were investigated with the design model subjected to the Nahanni* ground acceleration (PGA = 0.4g), shown in Figure 3-14. The yield load and the initial stiffness of the devices ranged from 0.05 to 1 kips and from 1 to 20 kips/in, respectively.

Contour lines of the resulting energy ratios and dynamic ductility demands were superimposed over the design space and are shown in Figure 3-15. The contour lines for the energy ratio are shown as solid lines while the contour lines for the dynamic ductility demand are shown as dashed lines. Figure 3-15 shows two different results, one for the relatively stiff diaphragm beam (a), and one for the relatively flexible diaphragm beam (b) used in the ST-10 design. The optimal points are indicated by the star on the plots, and the logic for selecting these locations is discussed below.

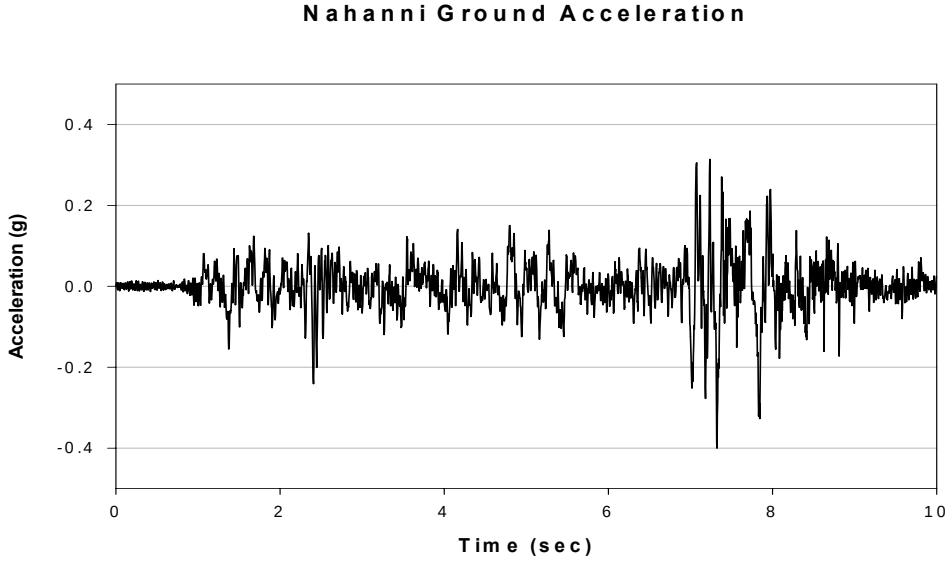

Figure 3-14: Nahanni Ground Acceleration Time-History

* The Nahanni earthquake was used in these preliminary studies carried out early in the project because it was felt that this earthquake was more representative of mid-plate earthquakes like the New Madrid 1811-1812 event than the available synthetic records.

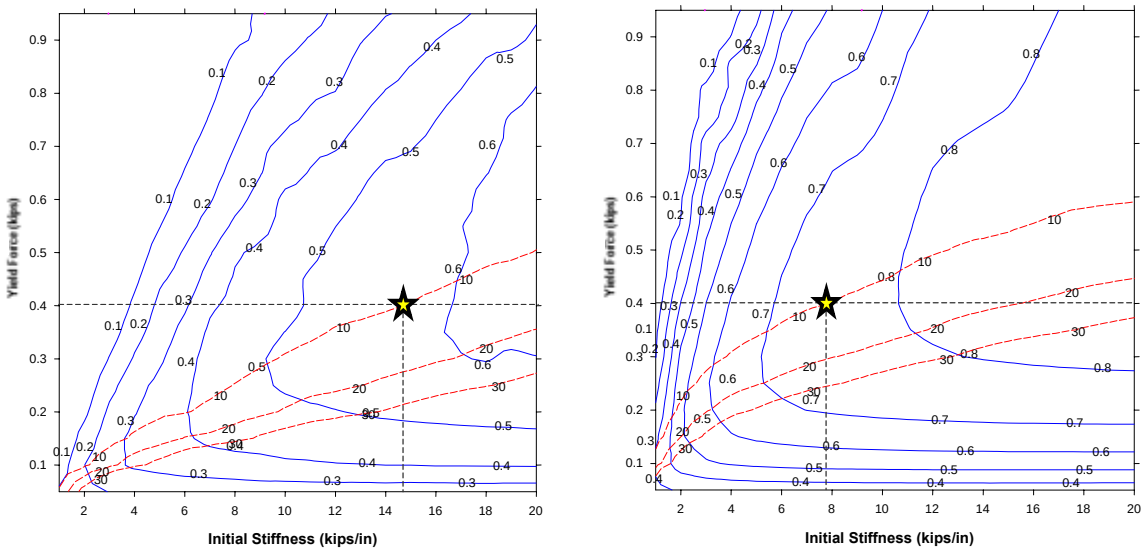

(a) *(b)*

Figure 3-15: Contour Plots for the Energy Ratio (solid blue lines) and the Dynamic Ductility Demand (dashed red lines) for Type 1 PED in ST-10 Test Structure, (a) with Stiff Diaphragm, and (b) with Flexible Diaphragm

Based on laboratory tests of tapered flexure PED's similar to the ones considered here [Pinelli et al, 1996], it is reasonable to allow dynamic ductility demands of no greater than about 10 or 20. In addition, it is reasonable to assume a limit of about 0.4 –0.5 kips for the maximum force that should be developed in the PED. Using these values, the optimal designs are shown by the stars in Figure 3-15, assuming that the device yield load and the dynamic ductility are limited to 0.4 kips and 10, respectively. The optimal designs of the tapered flexural PED give an initial (elastic) stiffness of 14.7 kips/in for the stiff diaphragm case and 7.8 kips/in for the flexible diaphragm case. From the objective function contours, it can be seen that as much as 55% (stiff diaphragm) or 75% (flexible diaphragm) of the input seismic energy can be dissipated in the PED.

Next, for fabrication purposes, the constraints on the geometry of the tapered flexure device can be taken into account. The overall geometry of the tapered device was restricted to 3.6″ to 12″ in width, 3.6″ to 10″ in length, and 0.25″ to 0.5″ in thickness, as reasonable constraints. The elastic modulus and yield strength of mild steel were taken as 29000 and 36 ksi, respectively. On this basis, Moor's [1992] equations provide a constraint plot as shown in Figure 3-16. The feasible design region is an overlapped area between two feasible regions given by Moor's two design constraint equations.

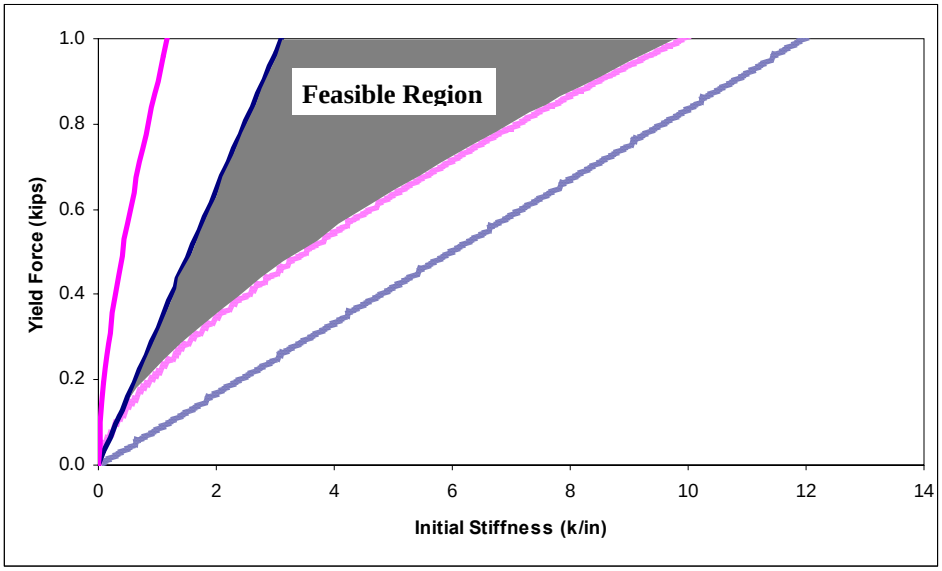

Figure 3-16: Constraints on the Geometry of the Tapered PED Device Obtained from Moor [1992]

Combination of the feasible design region from Figure 3-16 and the contour plots obtained previously in Figure 3-15 results in the contour plots for a Type 1 scheme with added geometry constraints and the optimal feasible designs (circular points) for the tapered flexural PED's illustrated in Figure 3-17. Now, less than 10% energy dissipation (stiff diaphragm case) and 40% energy dissipation (flexible diaphragm case) can be obtained when the PED geometry constraints are applied. The design value for the initial stiffness of the Type 1device was 2.5 kips/in for both the stiff and flexible diaphragm cases. A tapered device that could be fabricated following these design criteria is shown in Figure 3-19.

A similar approach applied for the Type 2 scheme yielded comparable design results except that about 15% (stiff diaphragm) and 40% (flexible diaphragm) of the input seismic energy can be dissipated as shown in Figure 3-18.

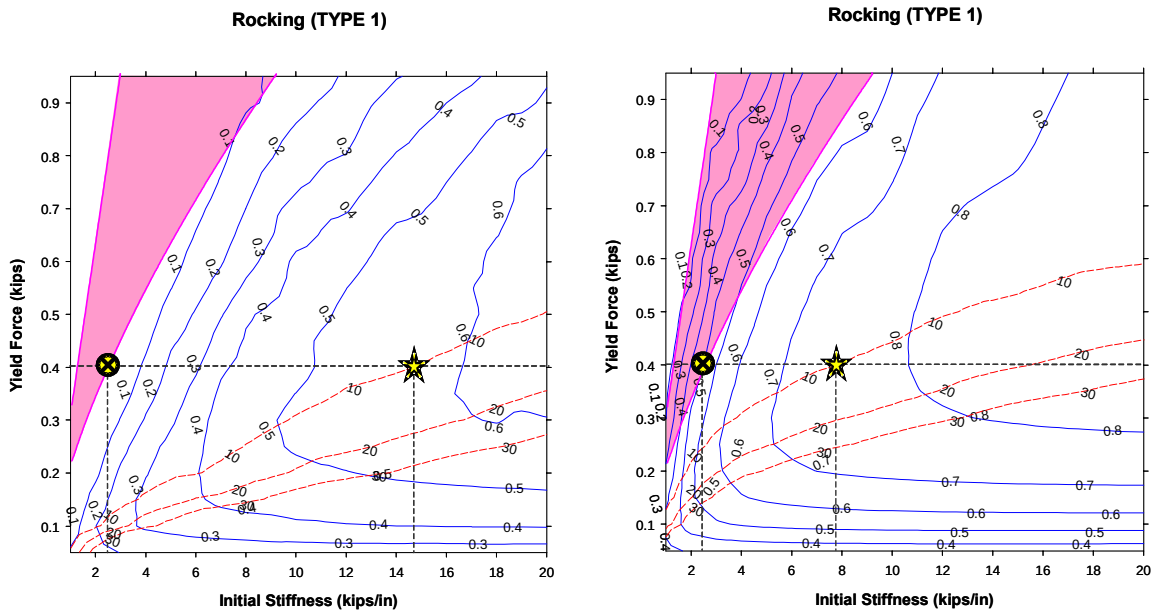

Figure 3-17: Contour Plots showing Feasible Design Point of the Tapered PED in Type 1 Scheme, (a) Stiff Diaphragm, and (b) Flexible Diaphragm

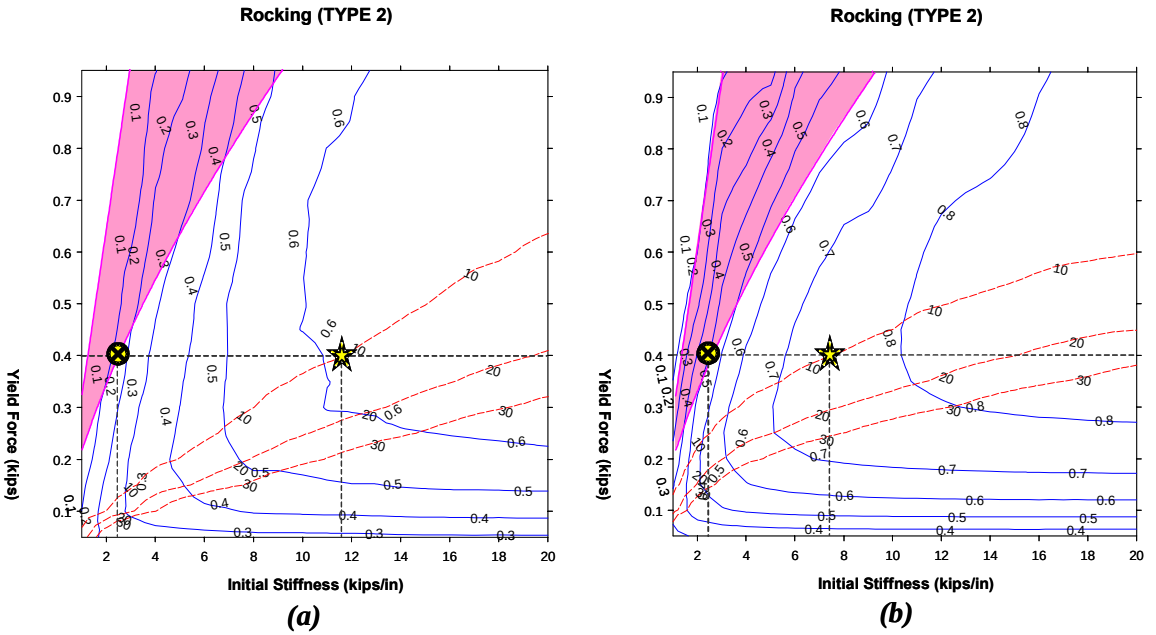

Figure 3-18: Contour Plots showing Feasible Design Point of the Tapered PED in Type 2 Scheme, (a) Stiff Diaphragm, and (b) Flexible Diaphragm

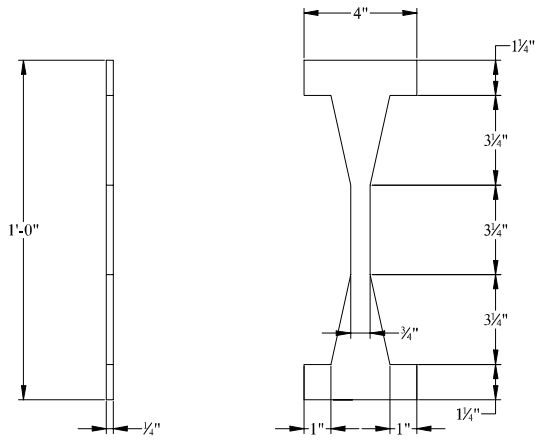

Figure 3-19: Geometry of the Optimally Designed Tapered Passive Energy Dissipator

3.4.5 Performance with Tapered PED

As shown previously in the contour plots, the optimization process resulted in the feasible optimal design of the tapered flexure device which can dissipate as much as 15% (stiff diaphragm) or 40% (flexible diaphragm) of the input seismic energy through the hysteretic behavior of the devices. The amount of energy dissipation in the building models for both stiff and flexible diaphragm cases and with Type 1 and Type 2 rehabilitation schemes are summarized in Table 3-1 and Table 3-2. A reduction in peak structural responses can also be achieved as a result of the rehabilitation.

Table 3-3 and Table 3-4 present the maximum displacement at the top of in-plane wall (IPW) and out-of-plane wall (OPW). The reduction of 26% in maximum displacement for the stiff diaphragm case or 80% for the flexible diaphragm case is quite remarkable.

Table 3-1: Energy Dissipation in the Rehabilitated Building Models with Stiff Diaphragm

Energy Dissipation (% of Total input Energy)			
Rehabilitated (TYPE 1)		**Rehabilitated (TYPE 2)**	
Ideally Optimal Design	Feasible Design	Ideally Optimal Design	Feasible Design
55 %	5 %	60 %	15 %

Table 3-2: Energy Dissipation in the Rehabilitated Building Models with Flexible Diaphragm

Energy Dissipation (% of Total input Energy)			
Rehabilitated (TYPE 1)		**Rehabilitated (TYPE 2)**	
Ideally Optimal Design	Feasible Design	Ideally Optimal Design	Feasible Design
75 %	40 %	75 %	40 %

Table 3-3: Behavior of the Design Model (Stiff Diaphragm) with Optimal Tapered Devices

	Maximum Displacements (in.)				
	Original	**Retrofitted (TYPE 1)**		**Retrofitted (TYPE 2)**	
		Ideally Optimal design	**Feasible Design**	**Ideally Optimal design**	**Feasible Design**
Top OPW	0.2523	0.1957 (22%)	0.2293 (9%)	0.2149 (15%)	0.2348 (7%)
Top IPW	0.1675	0.1197 (29%)	0.1576 (6%)	0.1133 (32%)	0.1233 (26%)

Table 3-4: Behavior of the Design Model (Flexible Diaphragm) with Optimal Tapered Devices

	Maximum Displacements (in.)				
	Original	**Rahabilitated (TYPE 1)**		**Rahabilitated (TYPE 2)**	
		Ideally Optimal design	**Feasible Design**	**Ideally Optimal design**	**Feasible Design**
Top OPW	0.4961	0.2197 (56%)	0.2955 (40%)	0.2217 (55%)	0.2944 (40%)
Top IPW	0.0115	0.0025 (79%)	0.0040 (66%)	0.0020 (83%)	0.0023 (80%)

The displacement time-histories at the top of the in-plane and out-of-plane walls are also computed for the feasible optimal design and compared to those of an unrehabilitated existing structure. These are shown in Figure 3-20 to Figure 3-23.

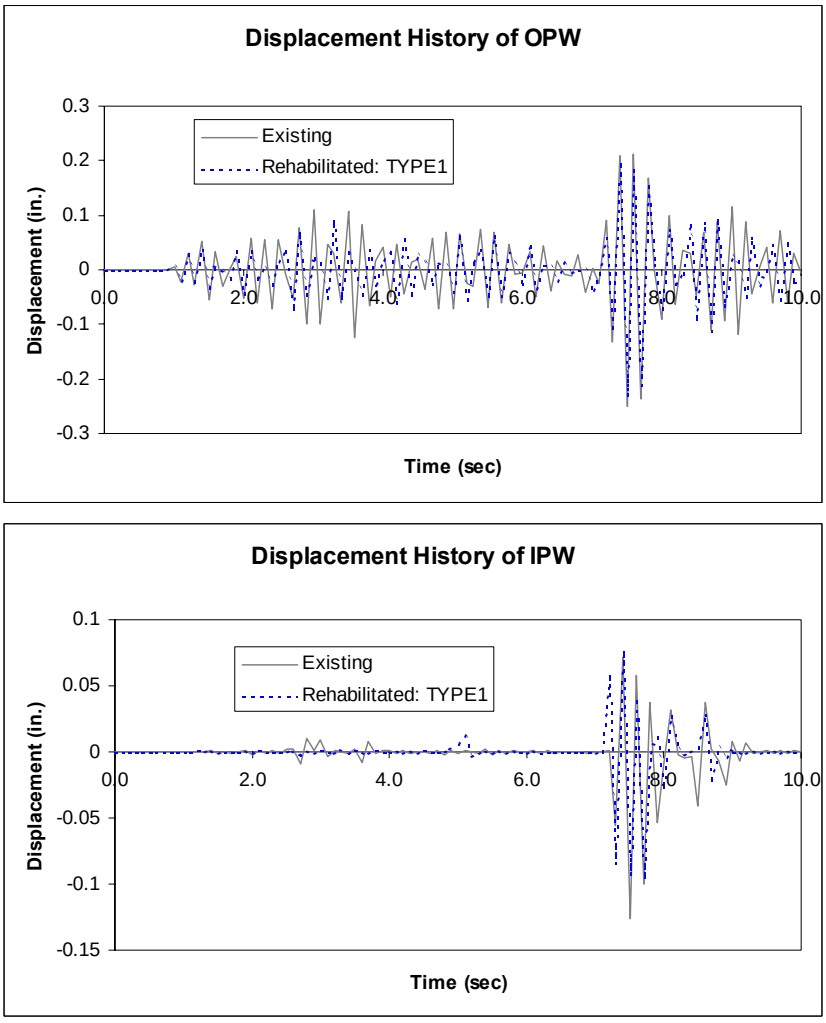

Figure 3-20: Time-History Displacements at (a) Top of Out-of-Plane Wall, and (b) Top of In-Plane Wall for Type 1 Scheme with Stiff Diaphragm

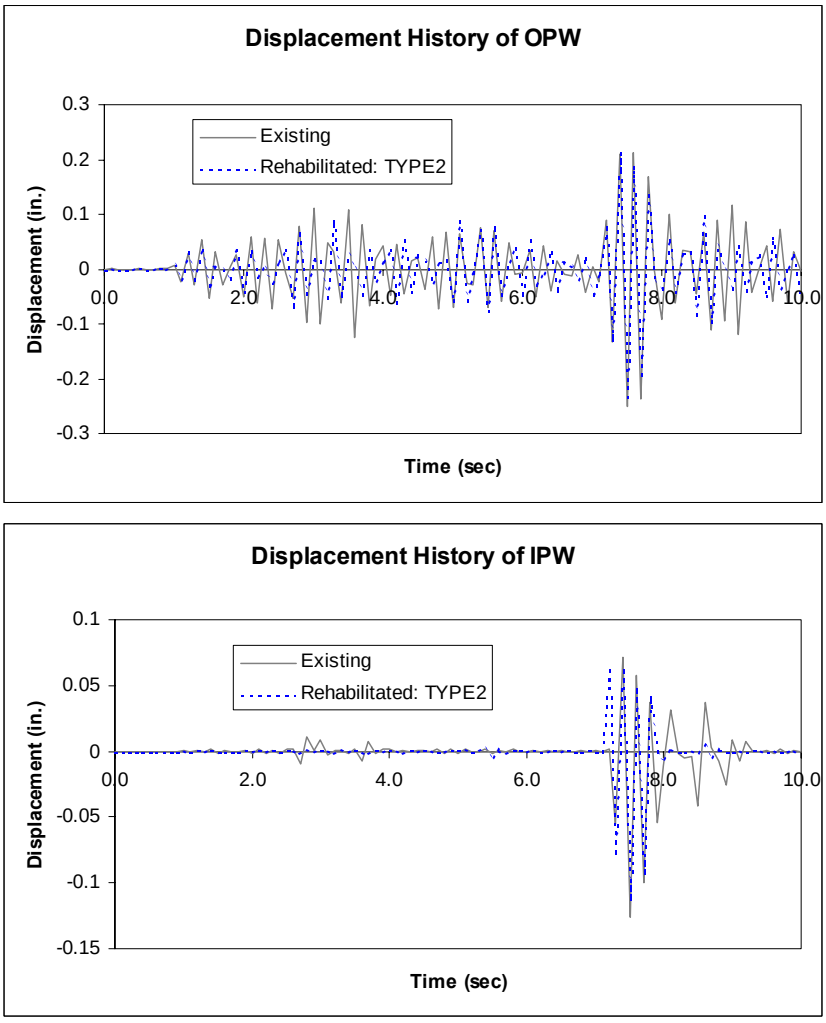

Figure 3-21: Time-History Displacements at (a) Top of Out-of-Plane Wall, and (b) Top of In-Plane Wall for Type 2 Scheme with Stiff Diaphragm

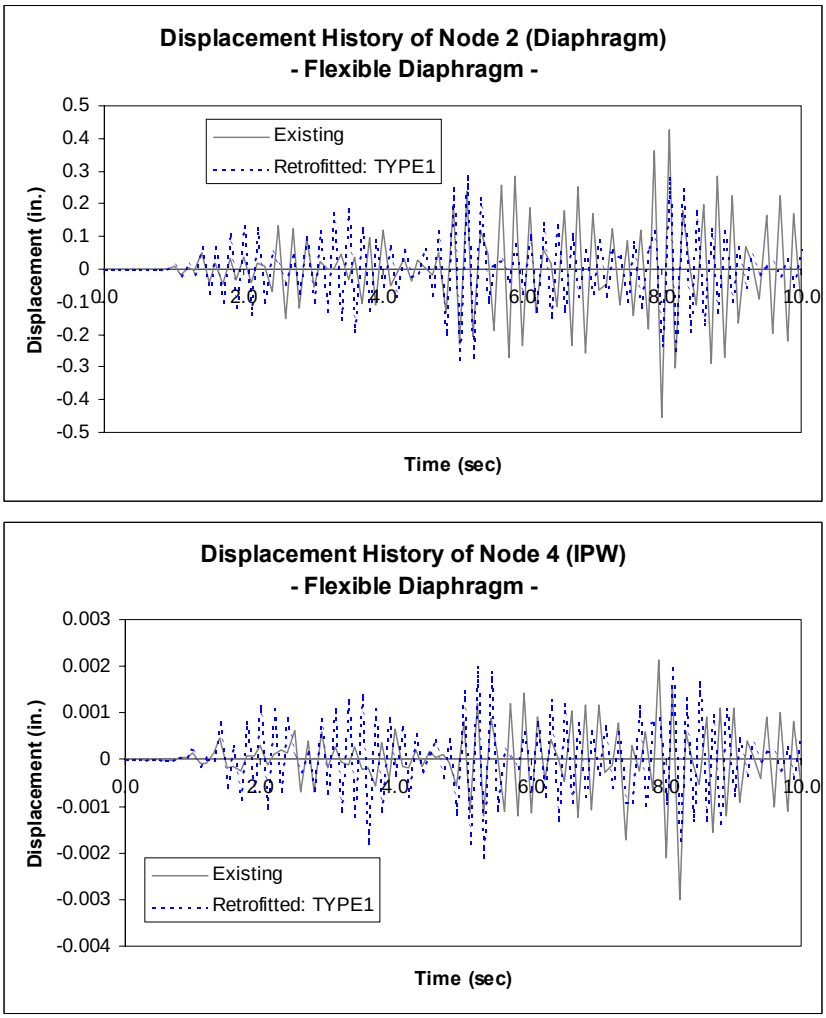

Figure 3-22: Time-History Displacements at (a) Top of Out-of-Plane Wall (Node 2 and Diaphragm), and (b) Top of In-Plane Wall for Type 1 Scheme with Flexible Diaphragm

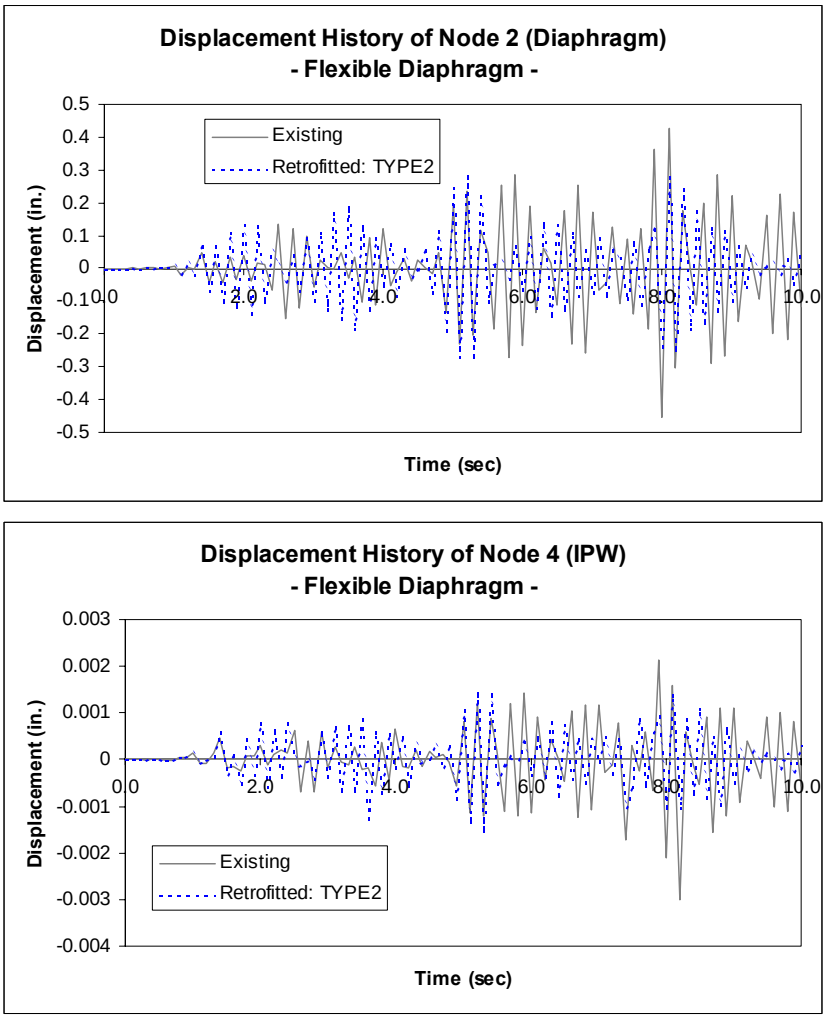

Figure 3-23: Time-History Displacements at (a) Top of Out-of-Plane Wall (Node 2 and Diaphragm), and (b) Top of In-Plane Wall for Type 2 Scheme with Flexible Diaphragm

Each of the figures above shows the displacement time-histories for the design model with the optimal device stiffness and yield parameters. The dashed lines represent the displacements of the model with the optimally designed tapered device, and the solid lines are for an existing building without rehabilitation. These results show the effects of using tapered flexural PED's in the building structure, and as expected, the presence of these devices results in energy dissipation through their hysteretic behavior. The application of the metallic tapered flexure devices results in a significant reduction in the peak displacements compared to that of an existing structure.

3.5 Example Building: ST-11 and ST-22 Test Structures

MAE Center research projects ST-11 and ST-22 involved construction and testing of full-scale (ST-11) and half-scale (ST-22) models of a two story URM building with wooden floor and roof diaphragms that is representative of essential facilities construction in the Midwest. Project ST-11 at Georgia Tech is designed to conduct static pushover type of testing on a full scale model while Project ST-22 at the University of Illinois and the US Army Construction Engineering Research Laboratory (CERL) is designed to carry out dynamic (shake table) tests of a half-scale model of the same building.

These tests were carried out after the completion of the present (ST-4) research project, but the building design nonetheless provides a good opportunity to investigate the potential benefits of using passive response modification for seismic rehabilitation of such structures. This section summarizes analysis and design studies carried out for several possible PED configurations that could be applied to the ST-11/22 building. It is anticipated that the final testing program for these structures might include a PED design to allow experimental assessment of the analysis and simulation results presented in this section.

3.5.1 Test Building

The buildings for the both the ST-11 (static) and ST-22 (dynamic) tests were based on the same design. The detailed dimensions of the full-scale ST-11 test building can be found in Chapter 2, Section 2.4 of this report. The model for dynamic testing is a half-scale version of the full-scale model and was designed to stay within the capacity of the shake table at CERL. The test objective was to learn as much as possible about the dynamic response of the structure before undertaking the much more costly and complex full-scale pushover testing. Because most PED's are inherently dynamic devices, the half-scale dynamic test is the more appropriate test environment, and therefore that model should be the target application for this study. However, the details of the half-scale model were not finalized at the time this report was completed. As a result, the present study is focused on the full-scale model only. It is anticipated that the results should be easy to modify for the half-scale model when further details are available.

3.5.2 Potential Rehabilitation Schemes

Preliminary analysis of the full-scale, 2-story ST-11 model shows that the relative displacement between the center of the floor diaphragm and the top of the in-plane wall is in the

order of 6 times greater than that between the diaphragm center and the out-of-plane wall. This suggests the possible use of PED's, perhaps in connection with floor stiffening, to reduce this flexibility and therefore stabilize the out-of-plane walls. As a result, the devices considered in this study are activated using the flexibility of the floor diaphragm.

Type 1 Rehabilitation Scheme

As described earlier in this chapter, the concept behind the Type 1 rehabilitation scheme is to utilize the differential displacement between the flexible floor (or roof) diaphragm and the much stiffer in-plane walls to activate a PED. Actual application could be in a number of forms involving either: (a) distributed deformation in a ductile bracing member, or (b) transfer (via stiff braces or link beams) to a localized PED. In this study only (b) was considered, and a typical implementation using a link beam and localized PED is shown in Figure 3-24. For this illustration, it was assumed that the device will respond only to seismic input in a direction perpendicular to the link beam. A relatively stiff box section beam was used to connect between the two in-plane walls. The PED was attached between the middle of the box beam and center of the diaphragm. Provided that the lateral stiffness (and the torsional stiffness if an eccentric connection is used) of the link beam is relatively high, movement at the midpoint should be comparable to that of the in-plane walls. The PED will then sustain the relative displacement between center of the diaphragm and the in-plane walls, and energy dissipation will be developed when the device deforms inelastically.

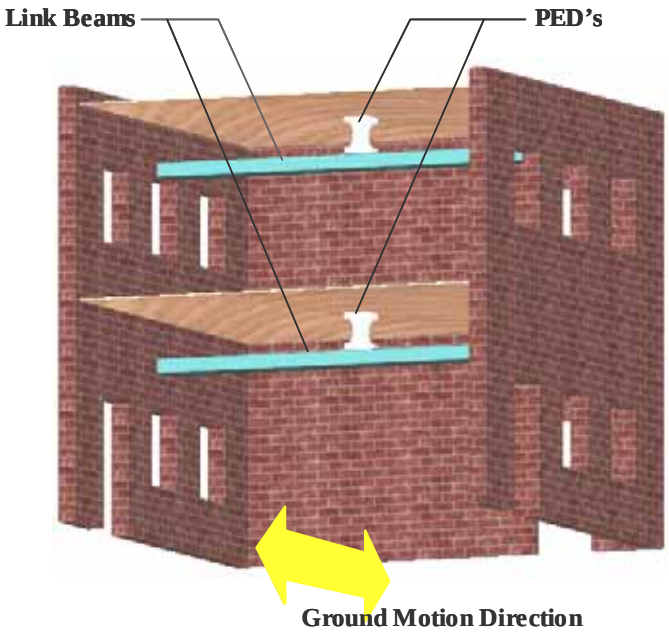

Figure 3-24: Type 1 Rehabilitation Scheme

Type 2 Rehabilitation Scheme

The Type 2 scheme makes use of the differential movement between the center of the diaphragm and the ground to trigger inelastic deformation and, consequently, energy dissipation in a PED connected between the floor diaphragm and the ground. Second floor implementation may be less effective, but definitely is possible. In order to capture this differential displacement, a simple k or chevron brace can be used to support the PED relative to the floor below. A very stiff brace system is desirable in such scheme, and it seems reasonable to think that such a design could be incorporated in a rehabilitation project (*e.g.*, as an interior wall). Figure 3-25 illustrates the application of a Type 2 rehabilitation scheme. In this illustration it is assumed that the device will respond only to seismic input in the plane of the brace.

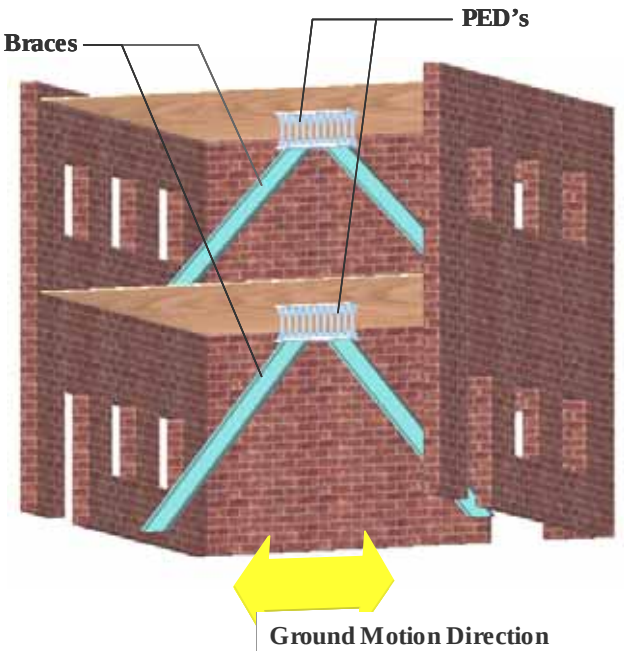

Figure 3-25: Type 2 Rehabilitation Scheme

3.5.3 Design and Analysis Models

A key part of the present study was the development of suitable analysis models for the target building. The initial design study described in Section 3.4 above used DRAIN-2DX [Prakash, Powell 1993] to construct a one-dimensional model of a very simple URM test structure (from Project ST-10) in which zero length nonlinear springs (Type 04 elements) were used to model the walls and floor diaphragm. As will be described below, this simple nonlinear spring element can also be used to develop a more complex two dimensional nonlinear "design" model for a simple URM structure with flexible floor diaphragms subjected to uniaxial loading[†].

The MAE Center has also developed under Project ST-5 a simple nonlinear design modeling tool for URM structures with flexible floor diaphragms that is based around ABAQUS. Much like the above DRAIN-2DX approach, the nonlinear URM wall behavior is modeled using simple nonlinear springs. However, the floor diaphragm is modeled with a special ABAQUS User Element developed specifically for this purpose [Kim et al. 2001]. As a result, the ABAQUS model is capable of handling more realistic building configurations but at the expense

[†] Normally, DRAIN-2DX is used to analyze single axis response of a structure defined in a vertical plane, but by collapsing the design model into a single horizontal plane it is possible to handle 2D horizontal seismic response.

of using a considerably more complex (but far more powerful) analysis tool. Using ABAQUS with the special User Element for the diaphragms, it should be possible to model URM structures with much more irregular configurations than are possible using the simpler DRAIN-2DX models. In light of the relative simplicity and much quicker execution times for the DRAIN-2DX approach versus the greater capabilities and versatility of the ABAQUS models, both approaches will be described in this report and design models will be presented for both.

DRAIN Model with Nonlinear URM Wall Behavior

Chapter 2 of this report describes the basic URM wall model development, and a nonlinear DRAIN-2DX model for the ST-11 full scale test building URM walls is described in Section 2.4. In contrast to the simple one-dimensional wall model used in Section 3.4 above for the project ST-10 test specimen, the ST-11 building wall model developed in this section is a zero-height, 2D model that also includes the effects of a number of wall openings that are present in this design. Such perforated walls can exhibit much more complex behavior associated with localized failures in the masonry piers, lintels and spandrels. The wall model developed in Section 2.4 is a composite spring model created by first decomposing each URM wall into a number of distinct areas or segments. These segments are defined as rectangular regions that can be represented using simple flexural and shear deformation models and for which a single failure mode can be specified. Next, each of these segments is represented by a single elasto-plastic hysteretic spring with elastic properties determined from the deformation model and with strength and hysteretic properties determined from the assumed failure mode.

The boundary conditions for the masonry piers in a perforated wall are hard to characterize, but they must be included in order to reasonably approximate the initial elastic in-plane stiffness. For this study, the pier height is altered to account for the less than ideal end fixity at each end (the “effective height” method described in Section 2.3.4).

Finally, failure modes are assumed for each segment based on empirical formulas [FEMA 356] that reflect the geometry of each segment as well as the vertical compression (gravity) loads. Each type of failure is associated with a particular hysteretic behavior, and this is incorporated in the parameters specified for the DRAIN TYPE 04 nonlinear spring element.

Figure 3-26 shows URM Wall A from the ST-11 building design on the left side and a schematic view of the corresponding composite spring model on the right. In this model, each

segment of the URM wall is represented by a nonlinear spring, and the springs are assembled in series and parallel arrangements to match the segment topology for the wall itself. Table 3-5 shows properties used for each segment in the composite spring model for Wall A and their governing behavior calculated from the FEMA-356 guidelines. Spring 1 represents foundation stiffnesses (assumed to be infinitely stiff) while spring 8 represents the diaphragm stiffness.

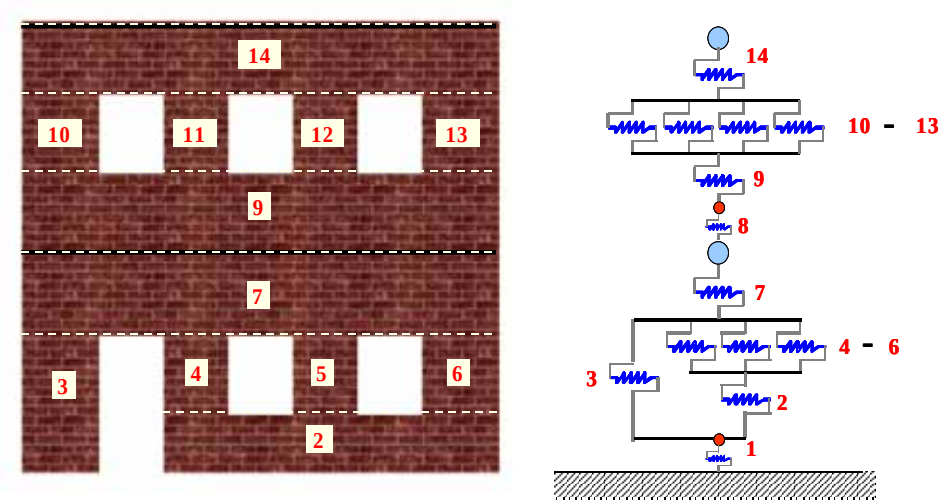

Figure 3-26: Concept of the Composite Spring Model (Wall A)

Table 3-5: Properties of Each Segment in a Composite Spring Model (Wall A)

Segment	Governing Behavior	Elastic Stiffness (k/in)	Strength (kips)
2	Sliding	16678.38	108.72
3	Rocking	1688.14	7.075
4	Rocking	880.73	8.599
5	Rocking	966.34	8.599
6	Rocking	1133.95	12.382
7	Sliding	13612.09	148.98
9	Sliding	21447.34	121.05
10	Rocking	1138.3	4.23
11	Rocking	970.11	2.938
12	Rocking	970.11	2.938
13	Rocking	1138.3	4.23
14	Sliding	17352.35	113.81

The complete 2D zero-height URM structure is then modeled by combining the zero-length composite nonlinear springs for each wall with the lumped wall masses as illustrated in Figure 3-27. The flexible floor diaphragms are modeled using lumped masses and additional nonlinear springs to account for the shear deformation modes only, and these are also illustrated in Figure 3-27. Note that the out-of-plane stiffnesses of the URM walls are ignored (but their masses are considered), and the floor diaphragms are assumed to have very high extensional stiffnesses and therefore to deform in shear modes only.

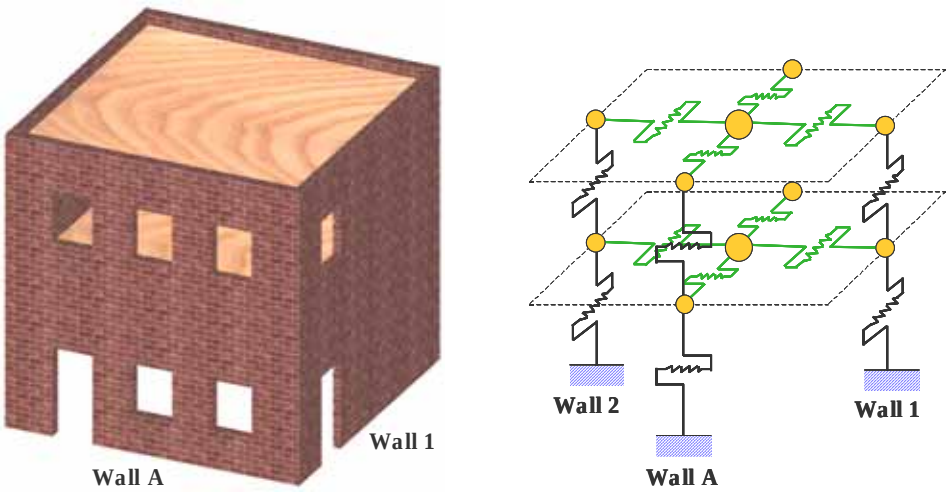

Figure 3-27: DRAIN-2DX Composite Spring Model for the ST-11 URM Building

ABAQUS Model

The ABAQUS model is based on modeling techniques and a special user element for flexible floor diaphragms developed under MAE Center Project ST-5 [Kim et al 2001]. As is the case for the DRAIN-2DX model above, the ABAQUS model is capable of representing the 2D behavior of the structure in a horizontal plane and is basically a zero-height model. As for the DRAIN-2DX model, it is also based on use of nonlinear composite springs to model the URM wall behavior. However, in contrast to the DRAIN model, the ABAQUS model incorporates a special user element to more accurately model the flexible floor diaphragm, especially for irregular structures. This diaphragm element takes into account the shear racking, bending and extensional modes of diaphragm deformation. As a result, the ABAQUS model is capable of handling structures that have nonrectangular floor plans and irregular vertical elevations and which can develop significant torsional response (*e.g.*, a nonrectangular firehouse with a

clerestory for the engines). Figure 3-28 shows a schematic view of an ABAQUS model for the ST-11 building using the same composite nonlinear spring model described above for the DRAIN-2DX model. Similar to the DRAIN-2DX model, out-of-plane wall stiffnesses are also ignored.

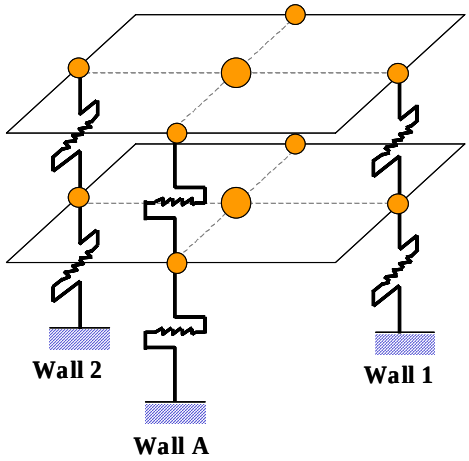

Figure 3-28: ABAQUS Composite Spring Model for the ST-11 URM Building

Generally speaking, the DRAIN-2DX models are more appropriate for the design purposes, whereas the ABAQUS models are more suitable for extended analysis studies or for building configurations that cannot be realistically modeled in DRAIN-2DX because of its less capable diaphragm representation. As can be seen from Table 3-6 and in Figure 3-29 to Figure 3-31, the displacement response for both models are almost identical for the case of single-axis earthquake input that is parallel to one of the URM wall directions. However, while not shown here, the results are slightly different when the earthquake input is not parallel to any wall of the structure. This illustrates the key differences in the two models in the area of diaphragm modeling.

Table 3-6: Comparison between the Results from DRAIN and ABAQUS Models

	DRAIN Model	ABAQUS Model
Fundamental Period (sec)	0.412	0.412
Max Displ of IPW (in.)	0.0290	0.0263
Max Displ of DIA (in.)	0.4073	0.3930
Max Displ of OPW (in.)	0.4528	0.4505

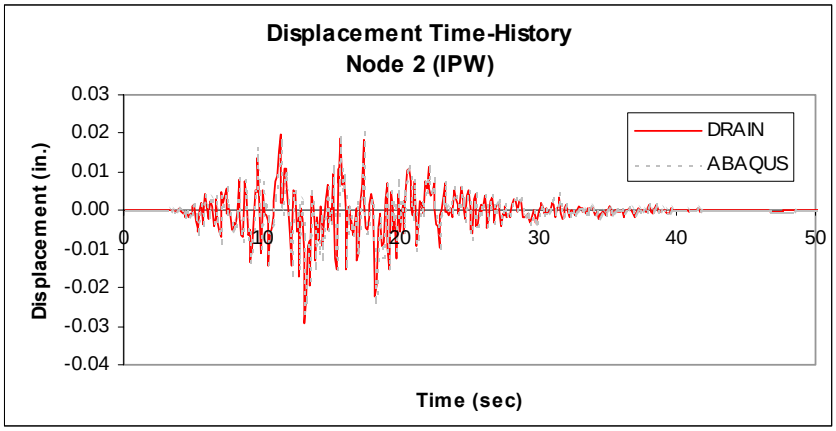

Figure 3-29: Displacement Time-History of the In-Plane Wall

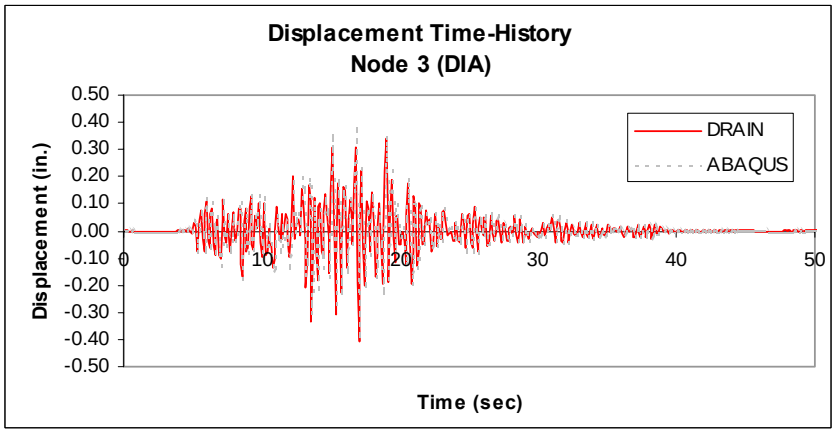

Figure 3-30: Displacement Time-History of the Diaphragm

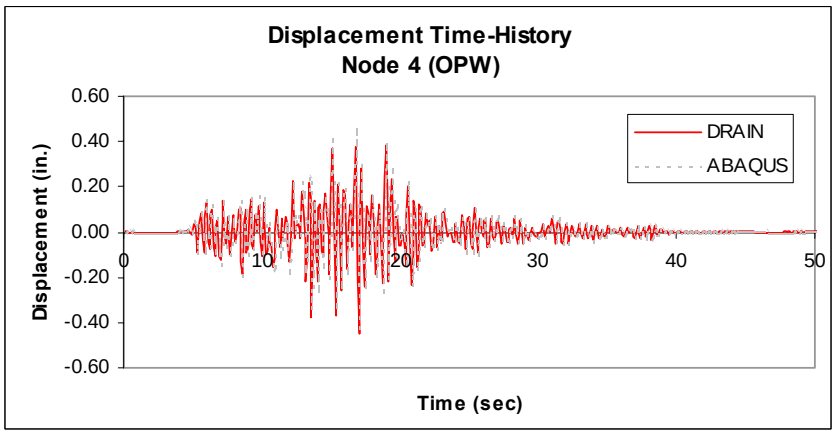

Figure 3-31: Displacement Time-History of the Out-of-Plane Wall

One additional factor that should be considered is the computational time for the DRAIN-2DX and ABAQUS models. Given the same structure, the computational time for the ABAQUS model is much greater than that for the DRAIN-2DX model. For comparison, run times on a 450 MHz Pentium system running Windows NT for a 20 second earthquake record using a building model similar to the one described above ranged from less than a minute for DRAIN-2DX to over 20 minutes for ABAQUS. A good deal of this difference is likely due to the longer setup times, network license access timing and additional file I/O times in ABAQUS. These largely fixed times only become evident when dealing with the very simple models developed in this study.

Finally, it should be pointed out that the ABAQUS model requires use of the special user element to model the flexible floor diaphragm. This is available from the MAE Center Project ST-5 web page [Kim et al.[2001], but it does require use of Visual Fortran 6.0 in order to link it into ABAQUS.

3.5.4 Simulations

In order to relate as closely as possible to the seismic environment in the target Midwest region, representative ground acceleration records were selected from a suite of synthesized records appropriate to the New Madrid Seismic Zone [Wen and Wu ,2000]. Records specifically developed for Carbondale, IL were used from this set and are included in Appendix A. These records were used with both the DRAIN and ABAQUS design models described above.

While both models can be configured for 2D horizontal behavior, for simplicity only single-axis simulations were carried out in this study. Results from the simpler DRAIN spring model closely matched the results obtained using the ABAQUS model for the relatively simple full-scale test structure under consideration. As a result and in view of the greater experience of the researchers with DRAIN-2DX, the remaining studies were all carried out using the DRAIN-2DX model only.

3.5.5 PED Design

Metallic hysteretic PED's can be incorporated into either the ABAQUS or DRAIN building models using specially configured nonlinear springs available in each system to represent the behavior these devices. As noted at the outset, the basic strategy in applying a PED to a

relatively stiff URM structure is to activate the PED through deformations associated with the much more flexible floor diaphragm and its interaction with the URM walls.

Figure 3-32 shows a comparison between the differential displacement of the in-plane walls and diaphragm center compared to a similar differential displacement between the out-of-plane walls and diaphragm center. It is immediately apparent that the relative displacement between the in-plane walls and the diaphragm is much higher. The displacement time-history plots in Figure 3-32 and in Figure 3-30 earlier confirm the basic strategy for applying the proposed Type 1 and Type 2 rehabilitation schemes to URM buildings.

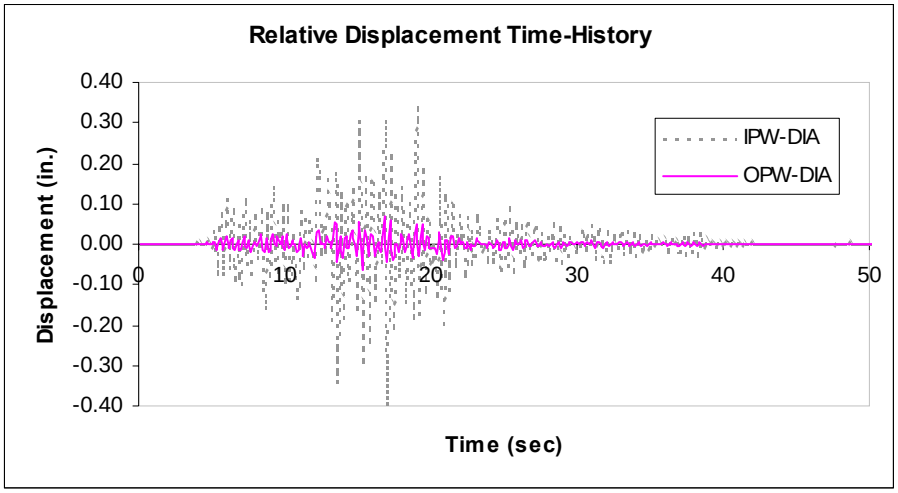

Figure 3-32: Relative Displacement Time-History

DRAIN Model of Building with Metallic Damping Devices

The basic well-designed hysteretic metallic PED can be represented by an elasto-plastic force-displacement model with hysteresis, and this kind of behavior is easily modeled using the DRAIN-2DX TYPE 04 nonlinear zero-length spring element. As a result, it is a relatively simple matter to introduce the PED into the building model simply by adding another TYPE 04 spring in the appropriate place(s). For a Type 1 PED design, this spring is introduced between the in-plane wall and diaphragm masses. On the other hand, the spring is introduced between the diaphragm mass and the ground for the Type 2 PED design.

Design Criteria for PED

The PED to be incorporated in the test building was designed using the energy-based formulation described earlier in Section 3.2. In this approach, the best design for the PED is defined as the design that maximizes the ratio of the amount of energy dissipated in the PED (or PED's if multiple devices are used) to the total amount of input seismic energy. As before, the design variables were taken as the properties of the PED and they included the elastic stiffness and the yield capacity of the metallic flexural devices. In addition, the dynamic ductility demand of each of the PED's was used as a constraint and was not allowed to exceed a value defined for each particular energy dissipator based on monotonically loaded laboratory tests.

As before, the use of only two design variables makes it somewhat easier to graphically describe the design space because a simple Cartesian 3D surface or a 2D contour plot can be used to describe the objective function, and the constraints can be readily superposed as curves. For the present study, a grid of values of the objective (energy ratio) and constraint (dynamic ductility demand) functions were computed and plotted as superposed contour plots. It should be noted that for more complicated or routine cases, a numerical optimization procedure could also be employed to compute the design parameters directly.

3.5.6 PED Design Results (Type 1 Scheme)

A number of test cases were investigated using the Type 1 PED model subjected to a reference Carbondale ground acceleration. The range of yield load and initial stiffness of the PED's ranged from 0.5 to 12 kips and from 5 to 60 kips/in, respectively. The resulting contour plot is shown in Figure 3-33. The contour lines for the energy ratio are shown as solid lines while the contour lines for the plastic ductility demand are shown as dashed lines.

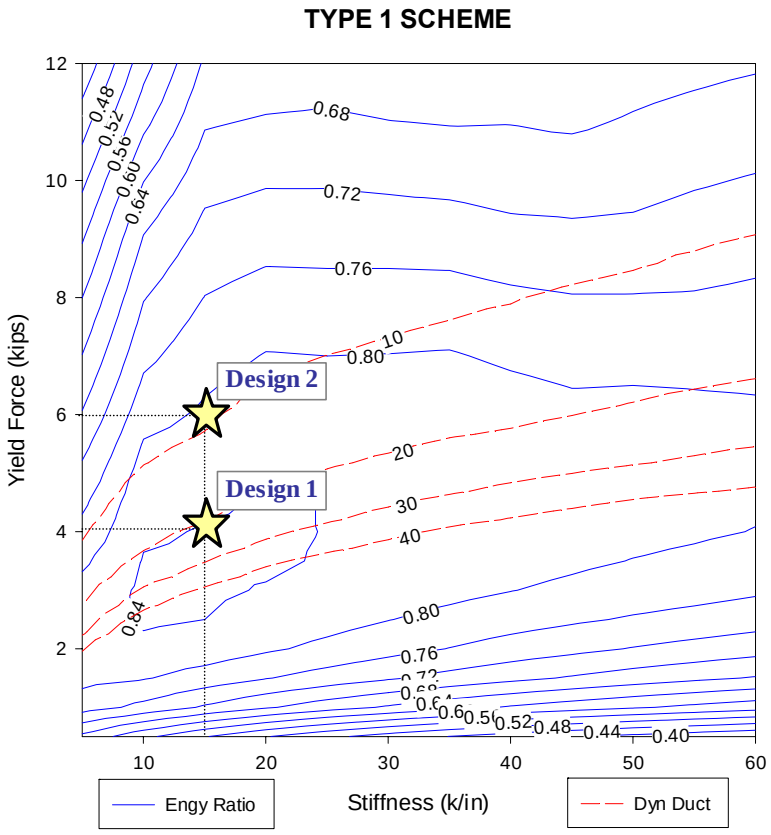

Figure 3-33: Contour plots of the Energy Ratio and the Dynamic Ductility Demand for Type 1 Rehabilitation Scheme Applied to the ST-11 Building for a Carbondale, IL Earthquake

From the plot in Figure 3-33, the objective function is well-behaved and optimal solutions can be obtained. If the dynamic ductility is considered as a constraint in order to represent the finite deformation capacity of the devices (before fracture), the optimal solutions can be limited by the superposed dashed curves. For example, optimal solution for a ductility constraint of 10 lies along the constraint curve where highest energy dissipation occurs. The star points symbolize the constrained optimal solution of the PED design. Assuming that the PED hysteretic ductilities are limited to a practical value of 10 and 20 such as might be representative of a tapered flexural device, the optimal designs will have an initial (elastic) stiffness of 15 kips/in with device yield forces of 4 and 6 kips, respectively. The objective contours indicate that by adding these PED's into the existing structure, from 80-84% of the input seismic energy can be dissipated, depending on dynamic ductility constraints (*i.e.*, reliability) assumed for the devices.

Table 3-7 lists the maximum displacement at the top of in-plane wall (IPW), the center of the floor diaphragm (FDIA), and the center of the roof diaphragm (RDIA). It can be seen that as high as a 73% reduction in the maximum displacement can be obtained when an appropriate PED system is used. Time-history displacements at the center of floor and roof diaphragms are shown in Figure 3-34. Reduction in displacement response is apparent in the rehabilitated building with the properly designed PED system.

Table 3-7: Comparison in Maximum Displacement (Type 1)

Design 1	**Max Displacement (in.)**		**% Reduction**
	Existing	**Rehabilitated**	
Top IPW	0.353	0.097	73
Center FDIA	5.377	3.245	40
Center RDIA	4.489	1.947	57
Design 2	**Max Displacement (in.)**		**% Reduction**
	Existing	**Rehabilitated**	
Top IPW	0.353	0.126	64
Center FDIA	5.377	2.506	53
Center RDIA	4.489	4.489	58

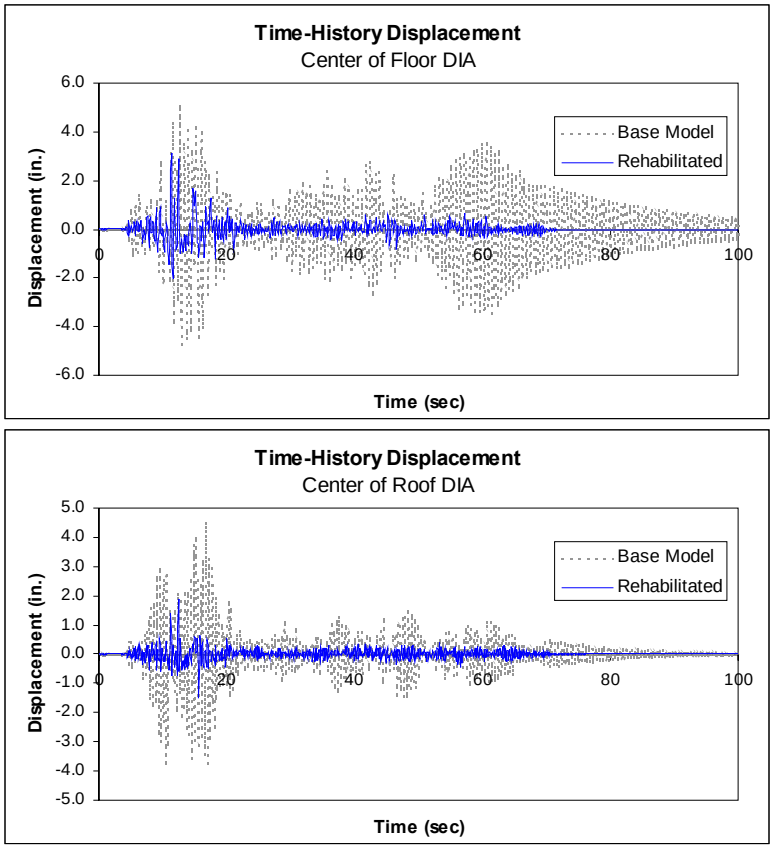

Figure 3-34: Time-History Displacements at the Center of Floor and Roof Diaphragms of the Base Model and Building Equipped with Type 1 PED

Adding a PED system into an unreinforced masonry building also minimizes inelastic action (*i.e.* rocking) in masonry piers. An example of force-deformation relationship from one of the wall piers in the studied building is shown in Figure 3-35.

a)

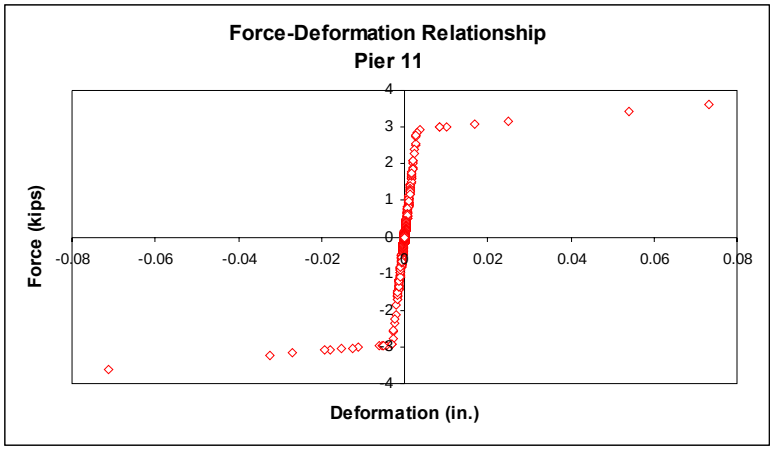

b)

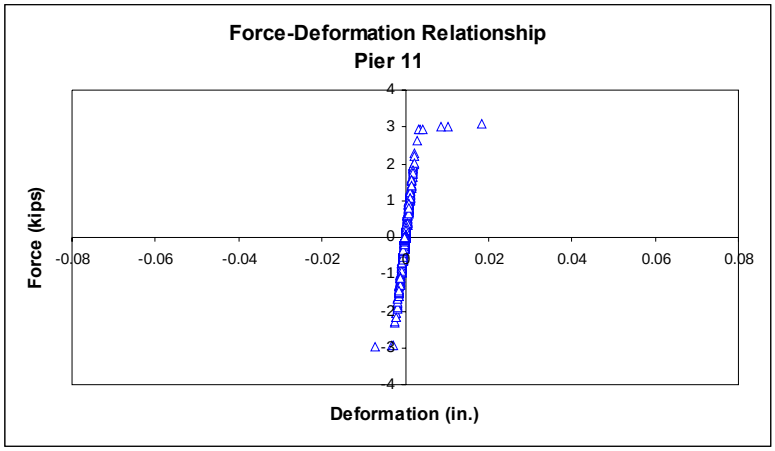

Figure 3-35: Force-Deformation Relationship of Pier 11 (see Figure 3-26) for: (a) the Base Building, and (b) the Building with a Type 1 PED

3.5.7 Effect of Floor Diaphragm Stiffness

As mentioned previously, the flexibility of the floor diaphragms is a key issue in the utilization of a passive rehabilitation system. Further investigations on the effects of diaphragm stiffnesses were performed. The ratio of the energy dissipated in the PED to the total input seismic energy (labeled earlier as the "energy ratio") was computed as the stiffness of the floor diaphragm is varied. Figure 3-36 shows the relationship between the energy ratio and the shear stiffness of the floor diaphragm normalized to the stiffness of the in-plane wall. This figure shows a rapid decrease in the energy dissipation ratio as the diaphragm shear stiffness gets higher. The curve confirms the earlier assumption that the energy dissipation capability of the PED's will be more effective when the floor diaphragm is more flexible.

Generally, the maximum displacements (and drifts) are of interest in the case of unreinforced masonry structures. Figure 3-37 demonstrates how the diaphragm shear stiffness affects the maximum displacement at the diaphragm center for a particular ground motion. Both displacements from the baseline and rehabilitated structures are plotted against the diaphragm shear stiffness ratio. The maximum displacement from the baseline structure is shown with a solid line, while that of a rehabilitated one is shown with a dashed line. The maximum displacements for both cases are almost identical when the stiffness ratio is high (the diaphragm shear stiffness is around 8% or more of in-plane wall elastic stiffness). This means the passive control system is not effective. On the other hand, the maximum diaphragm displacement for the rehabilitated structure is much lower than the baseline when the diaphragm stiffness is less than about 8% of the in-plane wall elastic stiffness. This indicates a greater response reduction can be achieved in the rehabilitated structure, in addition to more energy dissipation, when the diaphragm is more flexible.

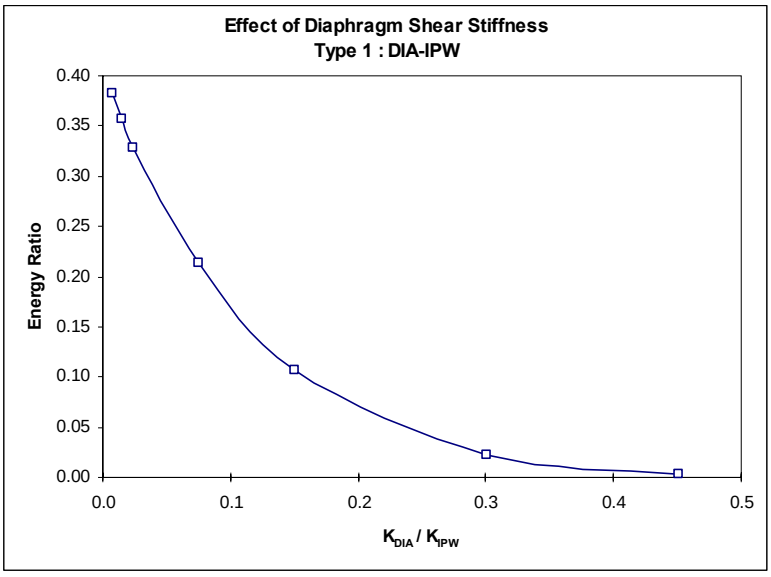

Figure 3-36: Effects of Diaphragm Shear Stiffness on the Energy Dissipation Ratio

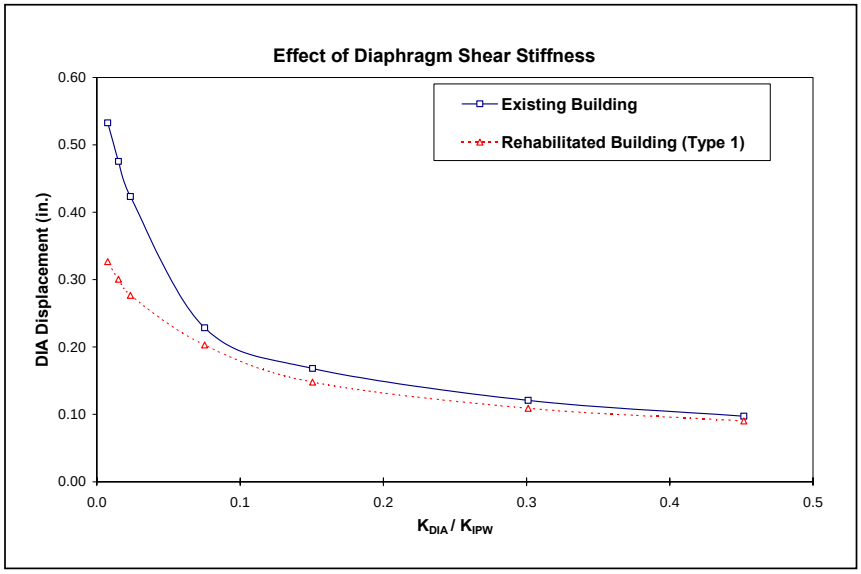

Figure 3-37: Effects of Diaphragm Shear Stiffness on the Maximum Diaphragm Displacement

In order to take into account a variety of potential ground motions in the region, a suite of synthesized Carbondale ground motions were applied to the structure. Similar plots were obtained as shown in Figure 3-38 and Figure 3-39 with vertical lines (error bars) now showing the variation due to different ground motion input.

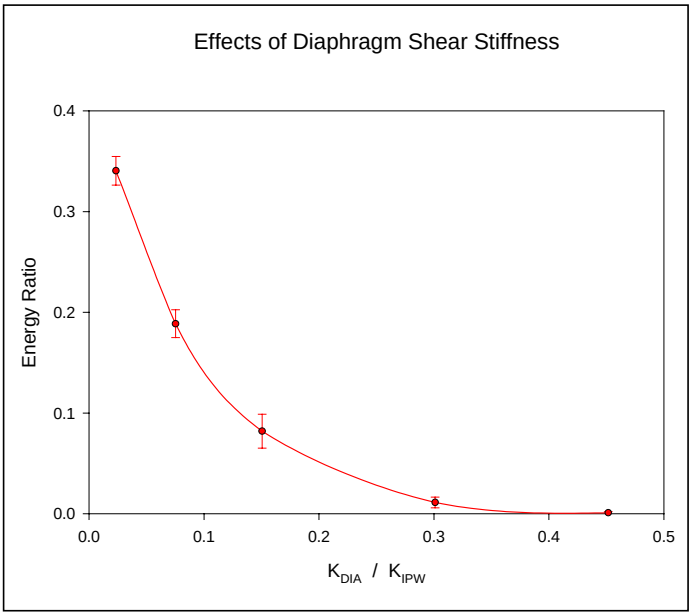

Figure 3-38: Effects of Diaphragm Shear Stiffness on the Energy Dissipation Ratio Considering a Suite of Ground Motions

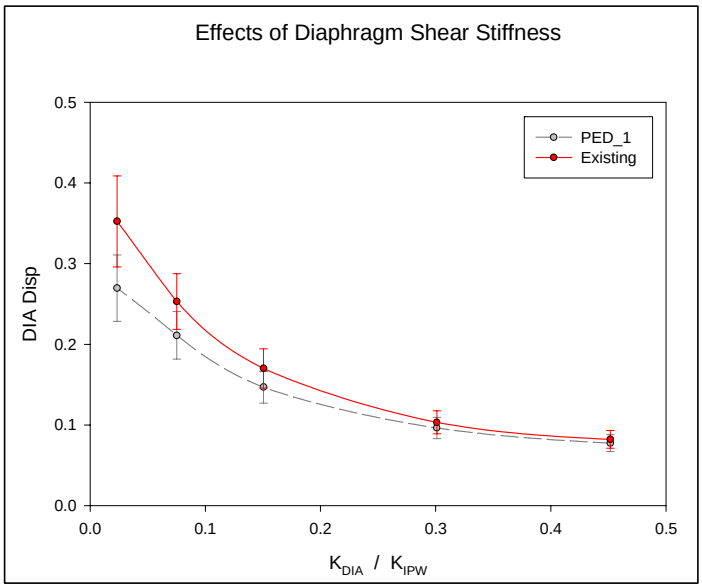

Figure 3-39: Effects of Diaphragm Shear Stiffness on the Diaphragm Maximum Displacement Considering a Suite of Ground Motions

3.5.8 PED Design Results (Type 2 Scheme)

A similar approach can be applied to the design of a Type 2 scheme. The only difference is in where and how the PED is introduced into the building model. The resulting design space contour plot is shown in Figure 3-40. Similar to the Type 1 scheme, the PED yield force and the initial (elastic) stiffness of the device vary from 0.5 to 12 kips and from 5 to 60 kips/in, respectively. The optimal designs for typical metallic flexural PED's can be seen to range from approximately 4 kips (yield load) with 15 k/in (stiffness) for Design 1 and 5.5 kips (yield load) with 15 k/in (stiffness) for Design 2. By adding these PED's into an existing structure, more than 80% of the input seismic energy to the test structure can be dissipated through the devices.

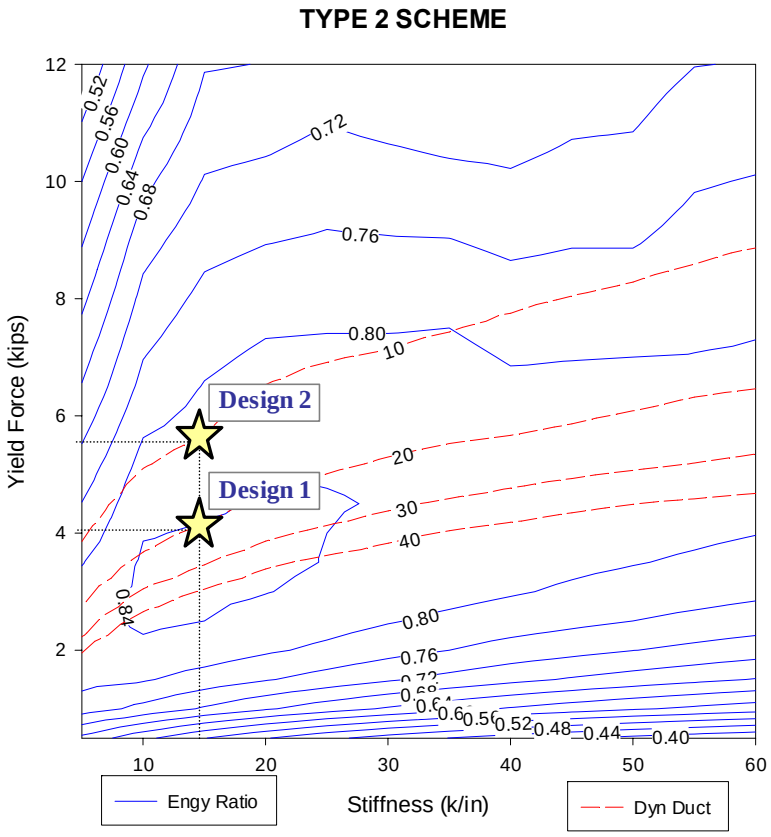

Figure 3-40: Contour plots of the Energy Ratio and the Dynamic Ductility Demand for Type 2 Rehabilitation Scheme

Table 3-8 shows the improvement in seismic response when a Type 2 passive rehabilitation system is applied to an existing structure. As much as 85% reductions in the maximum displacement can be obtained from the analyses. Comparison of the displacement time-histories of the diaphragms for the base and the rehabilitated models are given in Figure 3-41.

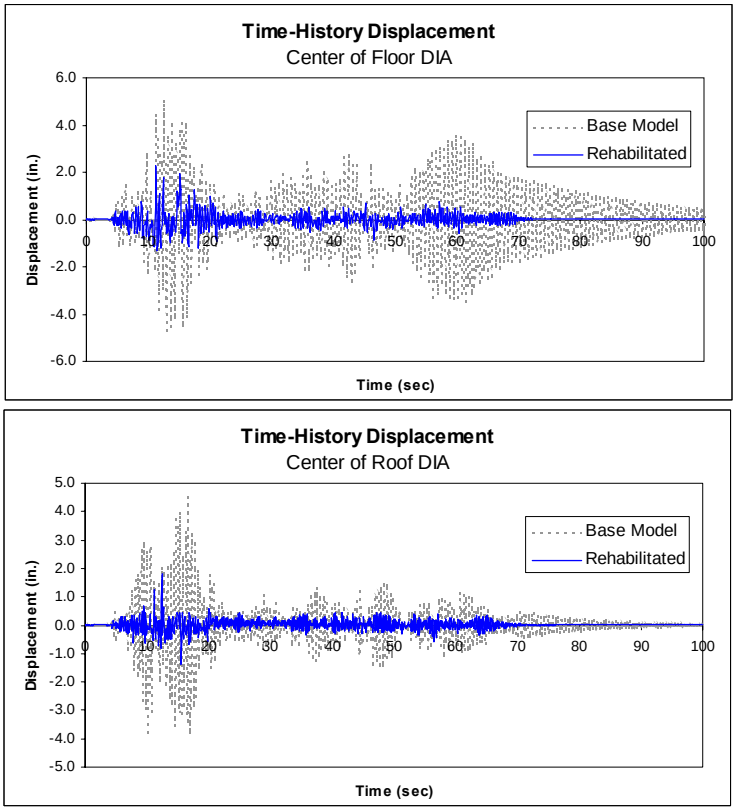

Figure 3-41: Time-History Displacements at the Center of Floor and Roof Diaphragms of the Base Model and Building Equipped with Type 2 PED

Table 3-8: Comparison in Maximum Displacement (Type 2)

Design 1	**Max Displacement (in.)**		**% Reduction**
	Existing	**Rehabilitated**	
Top IPW	0.353	0.056	84
Center FDIA	5.377	3.224	40
Center RDIA	4.489	1.911	57
Design 2	**Max Displacement (in.)**		**% Reduction**
	Existing	**Rehabilitated**	
Top IPW	0.353	0.055	85
Center FDIA	5.377	1.563	71
Center RDIA	4.489	1.848	59

Comparable to the Type 1 PED system, implementation of the Type 2 system significantly reduces rocking in the wall piers as shown in Figure 3-42.

a)

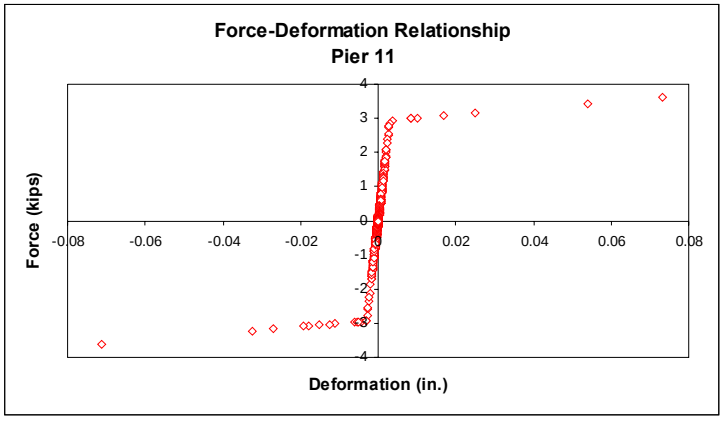

b)

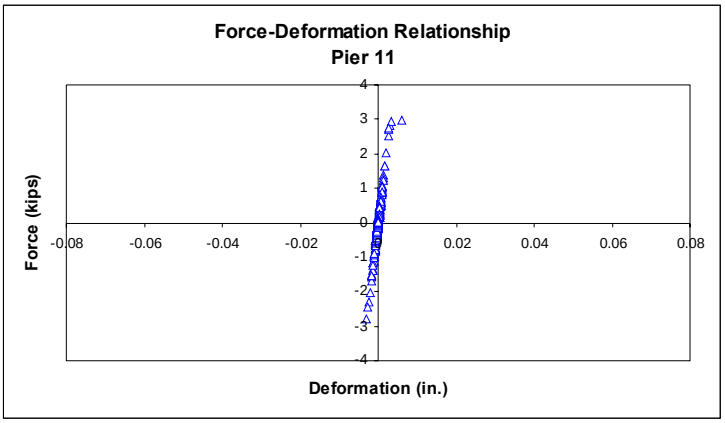

Figure 3-42: Force-Deformation Relationship of Pier 11 for a) Base Model, and b) Building with Type 2 PED

Figure 3-43 shows the performances of both PED types by plotting the curves of the top displacement of the in-plane wall versus the base shear. As can be seen in the figure, the existing building shows highly nonlinear behavior whereas the building rehabilitated with either PED approach exhibits much less nonlinearity with only a small amount of rocking behavior. The stiffness drops remarkably beyond a base shear of about 40 kips in the existing structure, while the rehabilitated structures allow the base shear to go only slightly beyond 40 kips. Between these two types of PED's, the Type 2 scheme can be considered to be giving better results in terms of the maximum displacement.

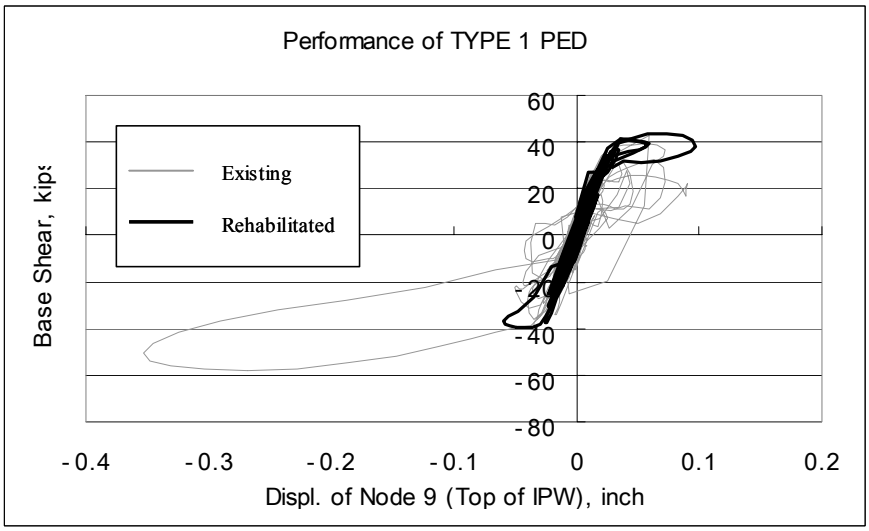

(a)

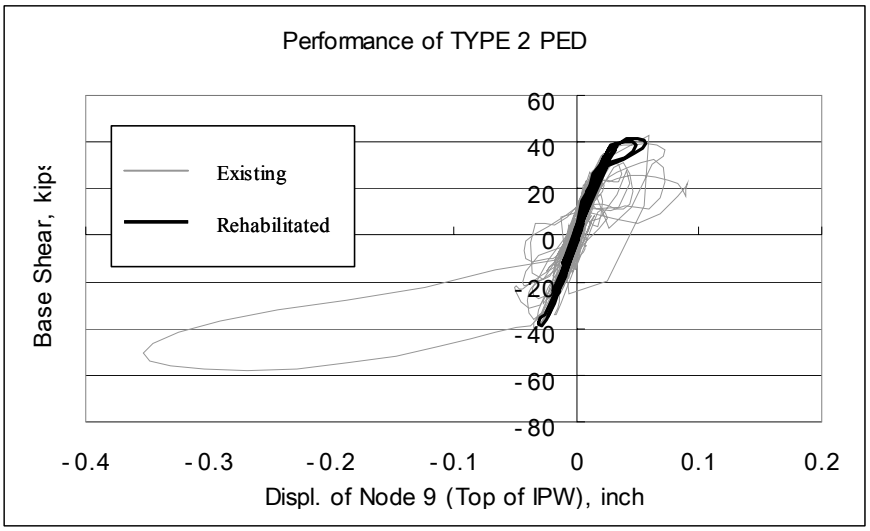

(b)

Figure 3-43: Performance of: (a) TYPE 1 PED, and (b) TYPE 2 PED

3.6 PED Effectiveness

The results from these analytical examples indicated that the incorporation of a properly designed passive energy dissipator in the rehabilitation of certain kinds of URM structures can minimize energy dissipation demand in the primary structure and reduce seismic responses. Given the inherently stiff nature of URM structures, this approach can only be applied in cases where sufficient deformation can be developed, for instance in a flexible floor or roof diaphragm,

to fully activate typical metallic hysteretic dampers considered in this study. Three concepts for passive energy dissipation were investigated: one activated by relative displacements between the in-plane walls and the diaphragm (called Type 1), one activated by relative displacements between the diaphragm and the ground (called Type 2), and the third activated by the relative in-plane displacements within a wall (called Type 3) but not investigated in this study. The primary benefit of this kind of response modification is a significant reduction in out-of-plane wall deformation induced by a flexible floor diaphragm. The effectiveness of this approach is reduced when the diaphragm stiffness for shear mode deformation is more than about 8% of the in-plane wall stiffness, but this is well above the stiffnesses of typical floor and roof diaphragms.

4 Regional Assessment of Fragility Improvement

4.1 Structural Variability

The evaluation of passive energy dissipators (PED's) for response modification of essential facilities in the Midwest was carried out in Chapter 3 in a purely deterministic manner for a single hypothetical building. While the results were quite promising and suggested the possibility of a broader application to this class of building, the results in no way suggest whether there might be a broader potential for significant benefit to a number of essential facilities in the study region. In fact, the results in Chapter 3 are for a single hypothetical earthquake and therefore do not yield any insight into whether PED's would be effective for other similar earthquakes or for larger or smaller seismic events.

The purpose of this chapter is to extend the deterministic analysis developed in Chapter 3 to consider the effectiveness of PED's for a broader class of essential facilities in the New Madrid seismic area of the Midwest. The approach presented in this chapter will take into account not only the variability in the earthquake itself but it will also consider the uncertainties in material and structural properties as well as variability in the structural configuration itself. This approach is in contrast to an alternate methodology that would attempt to identify (or design) a building structure that is entirely representative of essential facilities in the region, and that would then subject this particular structure to a detailed and comprehensive analysis and evaluation.

The analysis and design of any structural system is influenced by:

a. the geometry of the structure,
b. the detailing of the structure,
c. the strength of the materials used in its construction, and
d. the loads acting on the structure.

When dealing with a single structure, there is little uncertainty associated with the structural geometry and in most cases the detailing. When dealing with a class of structures, however, the structural geometry and the detailing may include a significant degree of variability, even for relatively narrow class definitions. On the other hand, strength, stiffness and other material properties are usually not precisely known even for a specific structure and may, in fact, vary throughout the structure, even for a nominally identical material. And finally, seismic loadings

themselves include a large degree of uncertainty, especially when the source mechanisms are not fully understood.

The variation in geometry of a class of structures can be obtained from regional evaluation of the specific type of structure under consideration. The present study is focused on essential facilities in the Midwest region of the US, and as has been noted in Chapter 1, the largest fraction (one third) of these structures are low-rise unreinforced masonry (URM) buildings. This class can be further narrowed by considering particular types of essential facilities, for example, fire stations, police stations, schools, etc. With a class of structures defined to this level, it now becomes practical to consider developing from a regional assessment a probabilistic description of the geometry including variations in both plan and elevation.

Strength is perhaps the material property with the greatest uncertainty because it depends largely on material composition, manufacturing processes and the operational environment over time. Other structural properties such as density, the modulus of elasticity, and Poisson's ratio may also include variability, but are usually well characterized on the basis of laboratory testing.

Variation in seismic loading is particularly significant in the Midwest, not only because of great uncertainty about the nature of the source itself, but also because of large variability in the propagation paths. Hazardous levels of ground motion developed over relatively large distances from epicenters are part of the historical and paleoseismological record. As a result, ground conditions such as the type and thickness of soil layers in the area can be important factors in determining earthquake loads at a building site.

4.2 Generating Fragility Curves

The concept of fragility curves was originally developed from safety and performance studies in the nuclear industry. The fragility curve is defined as a representation of a probability of exceeding a specific level of damage, conditioned on a certain seismic intensity. Generally, fragility curves can be generated using, (1) actual earthquake damage data, (2) engineering judgment, or (3) analytical methods. These approaches are summarized in the following sections.

4.2.1 Fragility Curves Using Actual Damage Data

Damage data obtained from field investigations after an earthquake or from experiments can be used directly for fragility analysis. This type of data is particularly useful for fragility curves

characterizing the seismic performance of a collection of similar structures. Such empirical fragility curves are often used to calibrate the fragility curves developed analytically. Past development of empirical fragility curves is listed as follow.

Yamazaki et al. [1999] constructed a series of fragility curves for the expressway bridges in Japan based on actual damage data from the 1995 Hyogoken-Nanbu (Kobe) earthquake. Data from 216 expressway bridges were collected and investigated after the earthquake. Five damage ranks ranging from no damage to collapse were assigned to each bridge. The ground shaking intensities (peak ground velocity (PGV) and peak ground acceleration (PGA)) at each bridge locations were also recorded. Based on these data, fragility curves for bridge structures were constructed assuming a lognormal distribution for the cumulative probability of damage.

A similar approach was proposed by Shinozuka et al. [2000b] for developing empirical fragility curves for the Hanshin Expressway Public Corporation's bridge columns. The state of damage and PGA values for a sample of 770 simply-supported reinforced concrete columns were considered. It was also assumed that the fragility curve could be represented by a two-parameter lognormal distribution. Contrary to the work done by Yamazaki et al. [1999], which used the method of least squares, the maximum likelihood method was employed to estimate the distribution parameters

O'Rourke and So [1999, 2000] presented a method used to develop empirical fragility curves of on-grade steel liquid storage tanks. The fragility curves were based on the seismic damage records of over 400 tanks in nine earthquake events. One of five damage states and a corresponding PGA were assigned to each tank. The fragility relations were built using regression analysis assuming a logistic distribution function between a probability of damage and the PGA.

Using bridge damage data from the Northridge and Loma Prieta earthquakes, Basöz and Kiremidjian [1999] generated fragility curves to quantify bridge vulnerability. A four level damage measure (minor, moderate, major, and collapse) was used. Similar to the O'Rourke and So approach, a logistic regression analysis was utilized to describe a relationship between the conditional probability and the earthquake intensity, which was also taken as the PGA.

4.2.2 Fragility Curves using Engineering Judgment

When actual earthquake damage and building inventory data are not available, one can develop fragility estimates from experience and judgment of earthquake engineering experts. These data are then processed statistically for earthquake damage estimates of the region. One of the best-known methodologies for generating fragility curves based on engineering judgment is from ATC-13 [1985]. The Applied Technology Council (ATC) conducted project ATC-13 to evaluate the damage of structures in California. The project developed damage probability matrices (DPM) for families of structures with similar structural types. A damage probability matrix describes the probabilities of damage at different damage states for various levels of ground shaking. Structures in California were classified into 78 classes based on size, structural system, and type. Modified Mercalli Intensity (MMI) was selected as an earthquake intensity level in this study. The three-round questionnaire process was carried out involving 71 senior-level specialists in earthquake engineering to obtain damage information for each structure. Damages were expressed in terms of damage factors versus MMI scales. The data obtained from the questionnaires were tested using beta, normal, and lognormal probability distribution functions. The beta distribution fitted the data uniformly and better than the other two, and a beta distribution was used to create damage probability matrices (DPM) for all 78 classes of structures. The damage probability matrix is equivalent to the fragility curve in the sense that both represent a probability of exceeding a specific damage state conditioned on a ground motion intensity level.

Several improvements to the ATC-13 approach were made by Anagnos et al. [1995]. Two major changes related to a new building classification and fragility formulations for those classes were based on the damage probability matrices in ATC-13. Out of a total of 78 classes of structures defined in ATC-13, 40 of them represented building classes, and these were reduced to 17 building classes, considering only framing types and structural materials used. Fragility curves, which could be transformed from ATC-13 damage probability matrices, were then created for each building class. Analogous to ATC-13, the damage factor was used to describe the damage states in the study. For each building class and MMI level, fragility curves were constructed by integrating the beta probability distributions from ATC-13 to develop probabilities of exceeding a particular damage state. Lognormal curves were assumed and fitted

through the resulting points using least-square error techniques. Comparison of these curves suggested a possible consolidation of building classes when the curves were sufficiently close.

4.2.3 Fragility Curves Using Analytical Approaches

When actual earthquake damage data are limited and cannot provide sufficient statistical information, an analytical approach for generating fragility curves is a plausible alternative. This methodology is often applicable in regions with infrequent seismic activities, such as in the Midwest. Because the focus of the proposed research is on this region, only analytically developed fragility curves will be considered in this research.

In general, analytical fragility curves can be constructed following these procedures. The first step is to define an appropriate ground shaking intensity parameter. The use of peak ground acceleration (PGA) and spectral acceleration (SA) are quite common, while the use of the Modified Mercalli Intensity (MMI) scale is not widespread, but it is possible. The ground accelerations corresponding to various ground shaking intensities are then defined, and both actual and synthesized records can be used. Second, appropriate structural models representing actual buildings are established to determine required seismic responses for a variety of ground motion intensities. Structural uncertainties (*i.e.*, material properties) must be included in these models as well. Third, seismic analyses are performed on these models. Fourth, damage states relevant to the structural attributes must be defined. Finally, the seismic responses obtained are statistically processed to evaluate damage probabilities, and the results are shown as fragility curves. A number of researchers have suggested several analytical approaches for assessing fragilities of the structures, and these are discussed in the subsequent paragraphs.

Hwang and Huo [1994a, 1994b] proposed an analytical method for establishing fragility curves and a damage probability matrix for a five-story reinforced concrete frame building. Synthetic ground motions were generated from probability-based scenario earthquakes. Peak ground accelerations ranging from 0.05g to 0.5g were used as the ground shaking parameter. For each PGA level, 50 earthquake acceleration time histories were generated. Five damage states of the building, which varied from nonstructural damage to collapse, were categorized using the building damage index. In this study, uncertainties in the structure were taken into account in the specification of the strength and the stiffness of materials as well as in the specification of a viscous damping ratio. For each of these structural parameters, 50 samples were randomly

generated within two standard deviations around an assumed mean. These samples were then combined using the Latin Hypercube sampling technique to assemble 50 structural models. The Latin Hypercube sampling technique is a method of random sampling which ensures that the entire range of variables is sampled. In contrast to other simple sampling techniques, it can provide response statistics with a reasonable number of samples. The structural models obtained from the sampling process were then paired with 50 samples of ground acceleration records to create 50 samples of earthquake-site-structure systems at each PGA level. A nonlinear time-history analysis was carried out on each sample to determine the building damage index. At the end, 50 values of damage index were obtained in each PGA level. The probability distribution of the building damage index was assumed to follow a lognormal probability function, and regression analysis was performed to determine the distribution parameters. Conditional on this particular PGA level, the probability of damage, or the fragility, was then calculated for each damage state. This process was repeated over other PGA levels to complete the curves.

Analogous methodology with minor difference in details (*e.g.* structural types, damage states, etc.) has been presented by several researchers. Seya et al. [1993] applied this methodology in probabilistic seismic analysis of a five-story steel frame building. Uncertainties in structural and seismic parameters were taken into account. In that study, the damage state was defined in terms of the system ductility ratio obtained from a nonlinear time-history analysis. For a given PGA level, the response data were fitted to a lognormal distribution function, so that the probability of damage could be calculated. The fragility curves were then constructed by evaluating the probability of damage at different levels of PGA. Shinozuka et al. [2000a, 2000b] studied fragility curves for the bridges in the Memphis area. Definitions of uncertainties, ground shaking intensities, and damage levels followed the same approach as the methodology previously described. A major difference appeared in the statistical analyses of the response. Instead of using a regression analysis to approximate the damage probability distribution, a method of maximum likelihood and a test of goodness-of-fit were used instead to estimate the lognormal parameters.

Song and Ellingwood [1999] investigated the role of inherent randomness and uncertainty on the seismic reliability of special moment steel frames with welded connections. Simple damage states based on overall or interstory drifts were implemented. Four parameters from the hysteresis model of degraded connection behavior were treated as structural uncertainties.

Factorial analysis was performed to study the effect and significance of each parameter. It was concluded that only two parameters had a statistically significant effect on the response. Additional structural parameters included material properties and the damping ratio. An ensemble of nine simulated ground accelerations was considered as an equally likely representation of ground motion at the site. The Latin Hypercube sampling was used to define combinations of structural and seismic uncertainties in calculating the dynamic response. The responses were rank-ordered and plotted on lognormal probability scales for each spectral acceleration level. The lognormal distribution parameters were determined from regression analysis and the maximum likelihood estimates (MLE), and seismic fragilities were then calculated from these probability functions.

Dumova-Jovanoska [2000] proposed the use of Modified Mercalli Intensity (MMI) scale as an earthquake intensity indicator in the development of fragility curves and damage probability matrices for reinforced concrete structures in Macedonia. Unlike the other studies, a normal probability distribution was assumed for the damage measures, and the validity of the fitted values was checked by the Chi-square test. Because the MMI could be regarded as a discrete intensity level, the fragility curves were depicted as a piece-wise combination of lines connecting between two MMI levels.

Hwang et al. [2000] further simplified the statistical process by forgoing the process of fitting distribution functions for each PGA level. An overall relationship between the damage measures and ground-shaking parameters (PGA or SA) was set up through a regression analysis. Using the Latin Hypercube technique, 100 earthquake samples and 10 structure samples were combined, and a total of 100 earthquake-structure samples were established. After a number of dynamic analyses, 100 pairs of PGA (or SA) and damage measures were fitted to a regression model. The cumulative probability of damage conditional on a ground shaking parameter or fragility curve was then calculated assuming a lognormal distribution.

Fragility calculations can also be carried out through a Monte Carlo simulation. Monte Carlo simulation is a brute-force but effective tool that can be used for the statistical analysis of uncertainties in engineering problems. It is particularly useful for complex problems in which several random variables are related through nonlinear equations. Monte Carlo simulation involves using a random sampling process to artificially simulate a large number of experiments and then observing the computed results. If each system parameter is known to follow certain

probability distribution, the performance of the system is studied by considering a number of possible values of the parameters and carrying out a simulation for each combination. Mosalam et al. [1997] made use of the Monte Carlo simulation technique in a seismic fragility analysis of frames with infill walls. Five random parameters from the pushover curve were assumed to follow lognormal distributions. A total of 600 synthetic ground motion records were considered, and for each, 200 simulation runs were generated and the probability of exceeding a specific damage state was computed. Fragility curves were plotted by fitting appropriate regression models to these data points. It is important to note that the curves obtained in this manner did not reflect any particular assumed probability distribution for the results.

Finally, it is observed that while a number of methods for generating fragility curves have been proposed, there is no apparent consensus in defining damage states or in selecting the random parameters (structural and seismic) to consider. While the parameters that are selected depend upon the nature of the problem, *i.e.*, the structural type and construction materials used, the major difference arises in characterizing the probabilistic responses (or damage measures) for fragility calculation.

Two different approaches have been suggested. One is through curve-fitting an assumed probability distribution function to the statistically sampled data (the Latin Hypercube method is a popular sampling technique). The distributions considered by researchers include the lognormal distribution [Hwang and Huo 1994; Seya et al. 1993; Shinozuka et al. 2000a, 2000b; Song and Ellingwood 1999b], the normal distribution [Dumova-Jovanoska 2000], and the Extreme Type I distribution [Jaw and Hwang 1988]. The other approach uses the Monte Carlo simulation technique.

Both approaches have advantages and disadvantages to one another. While a sampling process using the Latin Hypercube technique yields few numbers of samples, they may not be sufficiently representative of a population probability distribution for each random parameter. On the other hand, the Monte Carlo technique has the advantage of being capable of representing almost any distribution, but it requires a relatively large number of simulations in order to obtain a sufficiently reliable estimate for probability of damage. However, Mann et al. [1974] suggested that the number of simulations might need to be of the order of 10,000 to 20,000 for approximately 95% confidence limit, depending on the function being evaluated, and this may be

impractical, if not impossible, if carried out using nonlinear time-history integration of complex multi-degree of freedom structural models.

4.3 Response Surface Metamodel

While fundamentally a powerful and versatile approach, Monte Carlo simulation alone may not be practical for problems involving complex structural analysis because of the high computational costs required, especially when repeated executions of numerically intensive analyses are required to obtain statistical stability. The present study considered an alternative methodology in computing building fragilities. It is basically a Monte Carlo approach but one in which a drastically simplified "metamodel" (or model of a model) is used to represent the complex structural performance. This overcomes a major difficulty in traditional Monte Carlo simulations when complex nonlinear structural models, which may involve prohibitive computational efforts, are considered.

4.3.1 Metamodel

A metamodel is a statistical approximation of a complex analysis model, which provides a relationship between a set of independent input variables and a dependent output variable in a function-like manner. Metamodeling involves three main steps: (1) choosing an experimental design for generating data, (2) choosing a type of model for data representation, and (3) fitting the model to the observed data. Several options in each step allow use of different approximation techniques as the basis for the metamodels. A number of different metamodels have been developed and include: response surface equations, artificial neural networks, and so-called fuzzy graph based metamodels. Of these, response surface equations are perhaps the simplest and easiest to apply, and for these reasons were employed for the present study.

Metamodels based on response surfaces statistically approximate desired responses in the form of polynomial functions of random variables. The coefficients of each term in the polynomial can be obtained by conducting a regression analysis using calculated responses obtained from the higher fidelity analyses on which the metamodel is based. Simulations are then performed with much less effort using this response surface equation (metamodel), rather than on the underlying complex and time-consuming numerical analyses.

While the application of a response surface methodology to determine fragility curves is unique, it is not uncommon in other applications. Response surface metamodeling applications

have been extensively employed over the past decade in the area of aerospace system design. Engelund et al. [1993] conducted an investigation to determine a set of optimal aerodynamic configuration design parameters for a space transportation system. The design of such a vehicle is a complex process even at the conceptual level. The response surface methodology was used to optimize a set of configuration parameters in order to achieve minimum vehicle empty weight, while maintaining other constraints. Mavris and Bandte [1995] and Mavris et al. [1996] carried out an economic uncertainty assessment of a High Speed Civil Transport (HSCT) using a combined response surface methodology and Monte Carlo simulation approach. DeLaurentis et al. [1996] incorporated a response surface equation in place of a complex aerodynamic analysis in a preliminary aircraft design in order to more efficiently search the design space for optimum aircraft configurations.

In the field of structural reliability, there have been a number of studies using the response surface methodology to approximate the actual limit state functions when they cannot be represented by closed-form models. Faravelli [1989] and Bucher and Bourgund [1990] introduced an application of the response surface methodology in the field of structural reliability. Rajashekhar and Ellingwood [1993] evaluated an existing response surface approach in structural reliability analysis and proposed an adaptive iterative procedure for inclusion of information on probability distributions of random variables in selecting experimental points. Rajashekhar et al. [1996] compared the reliabilities, for various limit states, of reinforced concrete slabs by response surface approach with reliabilities obtained using traditional approaches. Yao and Wen [1996] described a reliability calculation of structures under earthquake loads utilizing a response surface methodology. A method for measuring the accuracy of the response surface approximation was also presented.

4.3.2 Response Surface Methodology

The origin of the Response Surface Methodology (RSM) can be traced back to the works of several researchers in the 1930's and earlier. However, it was not until Box and Wilson [1951] formally developed the methodology to determine optimal conditions in chemical investigations. Since then, RSM has been successfully applied in many different fields of study such as chemical engineering, industrial engineering, manufacturing, aerospace engineering, structural reliability, and computer simulation.

Response Surface Methodology refers not simply to the use of a response surface as a multivariate function but also to the process for determining the polynomial coefficients themselves. A response surface equation is simply a polynomial regression to a data set. The process is straightforward if a sufficiently large data set is available, that is if the number of members in the data set is at least as large as the number of coefficients in the polynomial. On the other hand, if the data set must be determined and if the process is time-consuming and expensive, then the overall usefulness of the method will depend on the use of an efficient method for selecting the fewest possible members. Design-of-Experiments techniques from applied statistics provide the needed basis for this critical step in the methodology. Response Surface Methodology is a set of techniques that encompasses:

1. Setting up a series of experiments (designing a set of experiments) that will yield the smallest number of adequate and reliable measurements of the response of interest, and
2. Determining a mathematical model that best fits the data collected from the design chosen in (1), by conducting appropriate tests of hypotheses concerning the model's parameters.

If discovering the best value, or values, of the response is beyond the available resources of the experiment, then the response surface methods are aimed at obtaining at least a better understanding of the overall system

The predicted response function is mathematically represented by a polynomial model. The parameters of the polynomials are usually determined by least squares regression analysis by fitting the response surface approximations to existing data. Generally, the success of a response surface investigation depends on whether the degree of the approximating polynomial can be fixed at one or two because low-degree models contain fewer terms than higher-degree models and thus require fewer experiments to be performed. The predicted response function considering a 2-degree polynomial model follows:

$$Y = \alpha_0 + \alpha_1 X_1 + \alpha_2 X_2 + \alpha_{11} X_1^2 + \alpha_{22} X_2^2 + \alpha_{12} X_1 X_2 + \ldots \qquad (4.1)$$

where

Y = Response value

X_i = Input variables

α_i = Coefficients to be estimated

Some of the important properties of the response surface design to be used when fitting a polynomial model proposed by Box and Draper [1975] are as follows:

1. The design should generate a satisfactory distribution of information throughout the region of interest;
2. The design should ensure simplicity of calculation of the model parameter estimates;
3. The design should ensure that the fitted value at any design point, x, be as close as possible to the true value at that point, and
4. The design should require a minimum number of experimental points.

The use response surface methodology in connection with Monte Carlo simulation simplifies the process of generating fragility curves. Because the simulations are not performed on complex structural analyses, but rather on a polynomial equation, a lot of computational time can be saved. Probability of damage conditional on seismic intensity can be calculated from the simulation results and fragility curves can be constructed.

4.4 Example Application

An example application provides a good way to investigate the overall usefulness of the proposed RSM-based Monte Carlo methodology. Ideally, the process begins with the selection of a target class of essential facilities to consider. A baseline structure must be selected and a structural model assembled. Next, the most significant parameters must be determined and a Design-of-Experiments technique used to define a parameter set over which a regression analysis will determine a response surface metamodel. Finally, Monte Carlo simulation can be carried out using the metamodel and selecting appropriate statistical distributions for the parameters.

For this study, a full statistical survey of the structural characteristics of a specific class of building structures in the target region (the New Madrid area) was not available. As a result, the example application considered in this report is necessarily limited in scope, and the results must be considered preliminary. Nonetheless, the effectiveness of the method will be apparent.

4.4.1 Modeling the Gilroy Firehouse

The Gilroy Firehouse in California (Figure 4-1) was chosen as a representative URM essential facilities building in the present study. The seismic behavior of this building was extensively investigated in a prior study by Tena-Colunga and Abrams [1992], and as a result, a considerable body of structural information and simulation models was readily available. The

firehouse is a two-story unreinforced masonry building composed of three walls in the east-west (street) direction and two walls in the north-south direction. The three walls in the east-west direction are called the north, central, and south walls, respectively.

Figure 4-1: The Gilroy Firehouse

In this study, only the east-west direction was considered, and the firehouse was represented using a 2-D structural model. A simplified cut-away of the firehouse showing the three walls and two floors along with the direction of forcing is shown in Figure 4-2. A simplified nonlinear URM building model was next constructed using the methods developed in Chapter 2. To simplify things for this preliminary study, it was assumed that the URM walls would not fail, either due to in-plane or to out-of-plane loadings. Thus the focus was on the interaction of the walls with the flexible wooden floor and roof diaphragms, and it was tacitly assumed that appropriate strengthening had been done to increase the strength of any weak areas (*i.e.*, piers) in the URM walls. As a result, the URM wall stiffnesses (in-plane and out-of-plane) could be reduced from a composite spring model to a single spring element. Only the diaphragm shear deformation modes were modeled using linear springs as described in Chapters 2 and 3. The final DRAIN-2DX model is shown in Figure 4-3 where beam elements were used to represent the in-plane stiffnesses of the North, Central and South walls, and spring elements represent the diaphragm shear stiffnesses. For this model, the stiffnesses of the East and West walls in their out-of-plane directions were neglected (and are not shown).

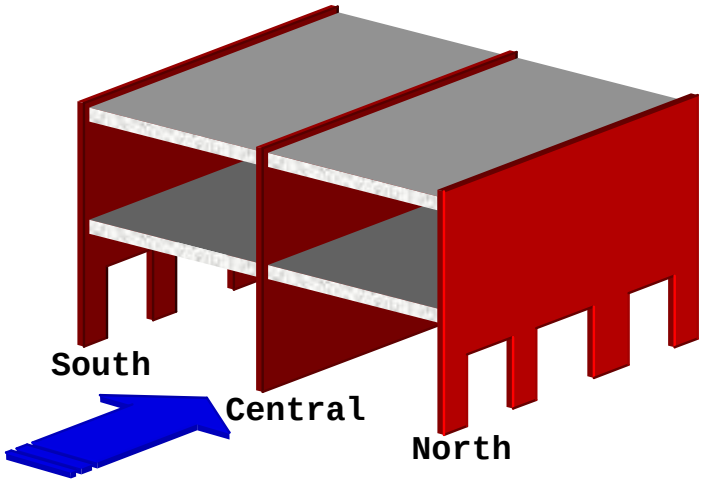

Figure 4-2: Schematic of the Gilroy Firehouse and the Direction of Force

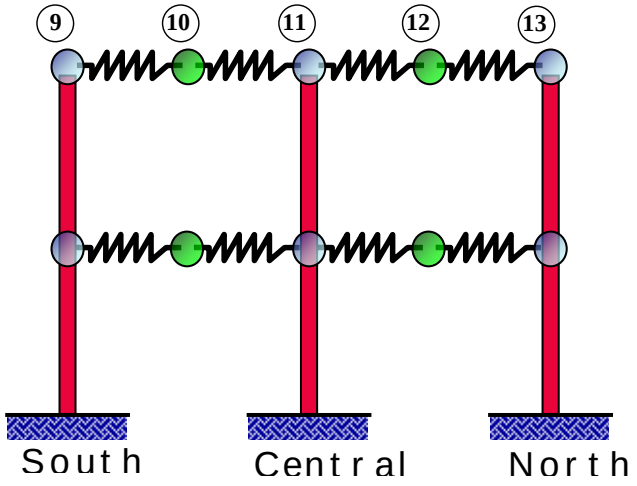

Figure 4-3: East-West Direction Model of the firehouse of Gilroy

For this particular study, the elastic properties of each URM wall in the model were based on plane stress analyses using a conventional finite element model of the perforated wall. A Young's modulus of 515 ksi for the URM walls was assumed based on results reported by Tena-Colunga and Abrams [1992]. Diaphragm stiffness values were also taken from the same report. A comparison between the present simplified DRAIN-2DX model and the measured responses of the actual building reported by Tena-Colunga and Abrams [1992] is shown in Table 4-1. Good agreement was achieved for the fundamental period and reasonable agreement for typical accelerations, but agreement between diaphragm displacements was poorer (likely due to inability to accurately model diaphragm-wall connection).

Table 4-1: Comparison between Drain-2DX Results and Measured Responses of the Gilroy Firehouse

	DRAIN-2DX Model	Measured
Max. Displ @ Center of South Diaphragm (in.)	2.01	1.30
Max. Accel @ Center of South Diaphragm (g)	1.08	0.79
Fundamental Period (sec.)	0.428	0.450

As for the other examples developed in the present report, a suite of ten synthesized uniform hazard ground motions appropriate for the New Madrid area were used in this example [Wen 2000]. The intensity was consistent with a 2%probability of exceedance in 50 years or an MCE level of shaking. Soil conditions were assumed to be representative of those in the Carbondale, IL area.

4.4.2 Damage Criteria

Because the unreinforced masonry in-plane walls are deformation-sensitive, the damage criteria for the URM in-plane walls were defined in terms of a maximum drift ratios for the building. Using Table C1-3, Structural Performance Levels and Damage, in FEMA-356 [FEMA 2000], the damage criteria can be stated as shown below in Table 4-2. The structural performance, defined by the maximum drift ratio, was categorized into three levels which are severe, moderate, and light damage. The corresponding drift ratios for these damage levels are defined by FEMA-356 to be 1.0, 0.6, and 0.3 percent, respectively.

Table 4-2: Damage States and Corresponding Drift Ratios

	Structural Performance Levels		
	Severe	Moderate	Light
Overall Damage	Extensive cracking. Face course and veneer may peel off. Noticeable in-plane and out-of-plane offsets.	Extensive cracking. Noticeable in-plane offsets of masonry and minor out-of-plane offsets	Minor cracking of veneers. Minor spalling in veneers at a few corner openings. No observable out-of-plane offsets.
Drift	1.0%	0.6%	0.3%
FEMA Categories	Collapse Prevention S-5	Life Safety S-3	Immediate Occupancy S-1

4.4.3 Selection of Structural Parameters and their Uncertainties

The structural parameters to be included in the metamodel should be those that have the greatest impact on the output (dependent) variable, but for complex problems, their selection is not always obvious. In this case some kind of screening process should be employed to identify what are often referred to as the "20% of the variables that cause 80% of the response." One of the simplest methods is to systematically make reasonable increments in each variable and compute the response for each case. A rank ordering of the results yields what is often called a Pareto optimal solution [Montgomery 1991].

For this preliminary study, the screening process was omitted, but it should be included in a more comprehensive application of the methodology. Instead, the structural parameters applied to the response surface calculation were selected as the masonry Young's modulus, building floor height, building roof height, wall geometry, and diaphragm stiffness. All structural parameters were assumed to follow the normal distribution as specified in Table 4-3. The wall geometry parameter was subdivided into the area and the moment of inertia of each wall for the response surface calculation, but the area and moment of inertia were assumed to be dependent. Thus the wall geometry parameter in the response surface calculation represented variation of both parameters.

Table 4-3: Uncertainties in Structural Parameters

Parameters	Distribution	Mean	Standard Deviation
Floor Height	Normal	148.0 inches	7.4 inches
Roof Height	Normal	319.0 inches	16.0 inches
Masonry Young's Modulus	Normal	515.0 ksi	25.8 ksi
Wall Area	Normal	1495.8 $in.^2$	74.8 $in.^2$
Wall Moment of Inertia	Normal	1.34×10^7 $in.^4$	0.07×10^7 $in.^4$
Diaphragm Stiffness	Normal	36.4 kips/in	1.8 kips/in

4.4.4 Variability in Seismic Parameters

For the present study, only ten synthesized ground motions representative of an MCE (2% probability of occurrence in 50 years) at the target site were available, but considerably more records are needed for a Monte Carlo simulation. Without additional information, variation in

the acceleration amplitudes of the simulated ground motions was used to create uncertainty in the seismic parameter.

4.4.5 Design of Experiments

A second degree polynomial was chosen for the response function as a good compromise between simplicity and expressiveness. One of the simplest methods for selecting observations (samples) from which to estimate the coefficients in such a model is the Full Factorial Design (FFD) or the 3^k Factorial Design. In this arrangement, each variable is assumed to take on 3 different values, which when equally spaced, produces the coded values –1, 0, +1 (-1 represents minimum, 0 is nominal and +1 represents maximum). In the Full Factorial Design, it is required that the responses are observed at all possible combinations of the levels of k input variables which have three levels each. The total number of variable level combinations (design points) is $N = 3^k$, which can be excessively large, especially when even a moderate number of input variables are under study.

Perhaps the most popular class of designs used for estimating the coefficients in a 2^{nd} degree model is the Central Composite Design (CCD). This consists of:

1. A complete (or fraction of a) 2^k factorial design, where the factor levels are coded to the usual –1 and +1 values. This is called the factorial portion or "cube" points of the design.
2. Two axial points on the axis of each design variable at a distance of α from the design center. This portion is called the axial portion or "star" points of the design.
3. n_0 center points ($n_0 \geq 1$)

The total number of distinct design points is $n = 2^k + 2k + n_0$. Figure 4-4 and Figure 4-5 show CCD's for k = 2 and k = 3 variables, respectively, since these cases permit simple graphical depictions.

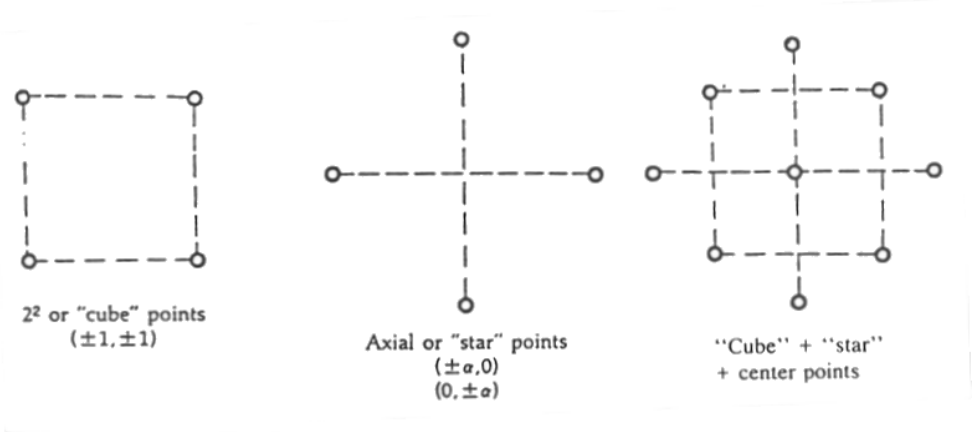

Figure 4-4: CCD for 2 Input Variables

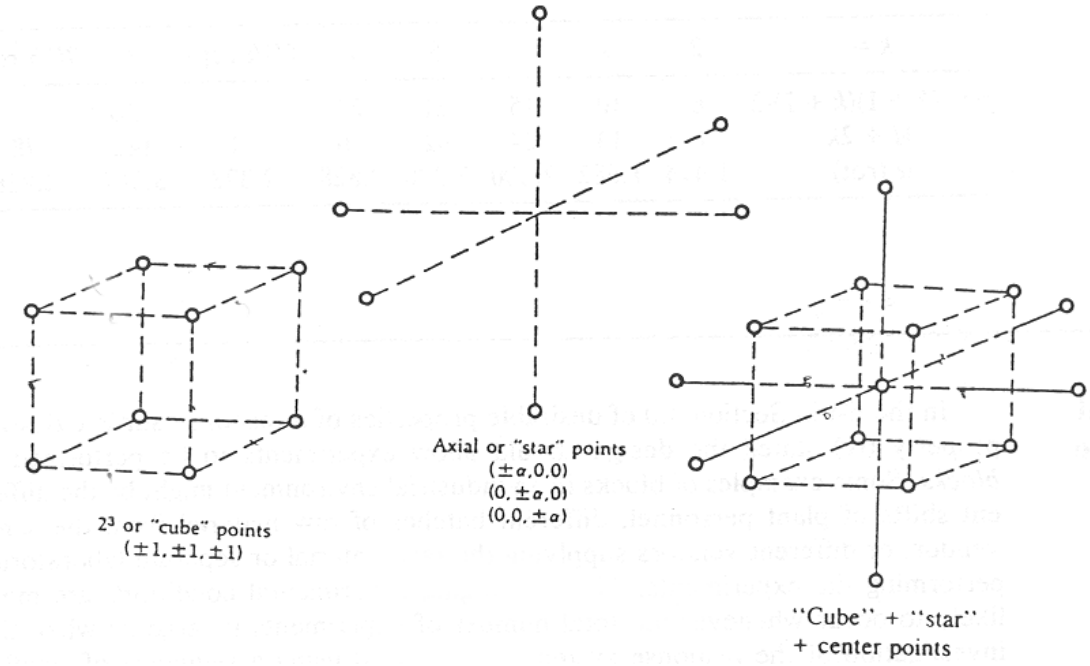

Figure 4-5: CCD for 3 Input Variables

In this study, there are 5 input variables (specified previously). Using a FFD requires 243 design (sample) points while a CCD requires only 43 design points. Figure 4-6 shows a portion of the response surface computed from a CCD.

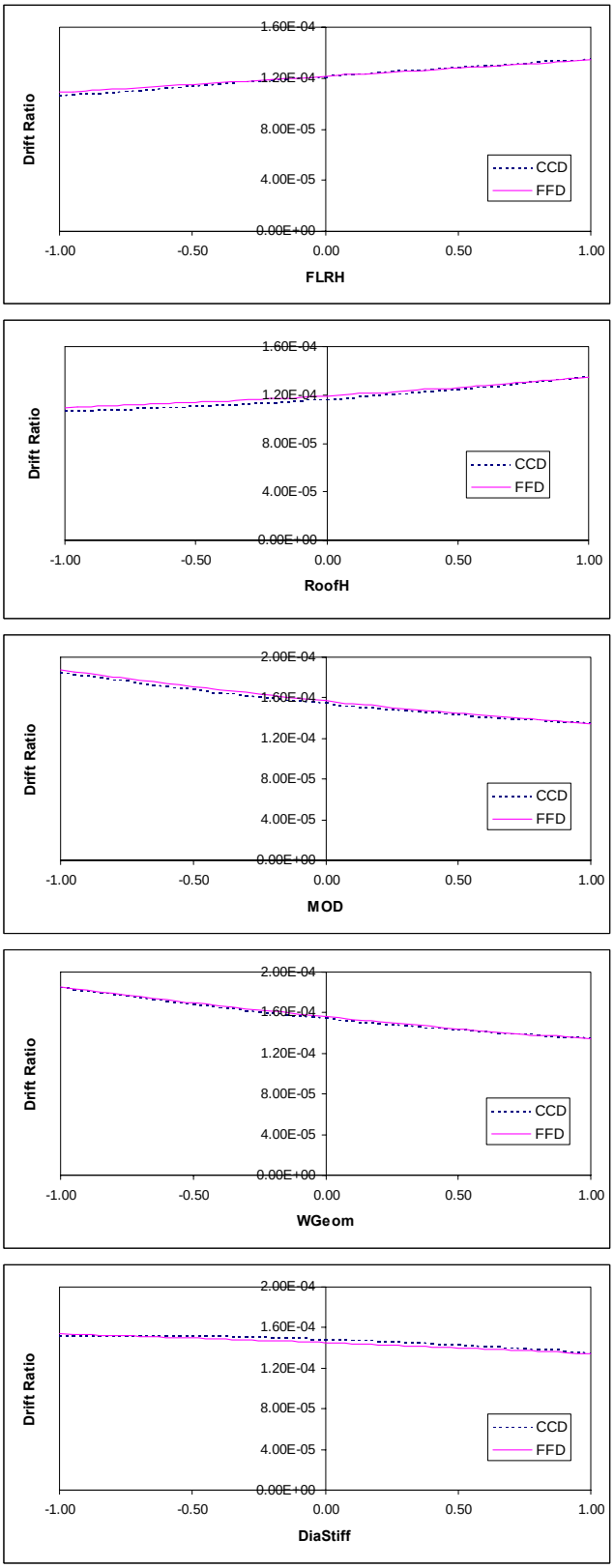

Figure 4-6: Relation between Drift Ratio and each Variable using CCD and FFD

Using the statistical software called JMP [JMP 1995], a response function for the maximum drift ratio resulting from specific ground acceleration can be obtained. Inputs to the program are the response values at those design points (243 design points for FFD or 43 design points for CCD). An example of the results from JMP is shown in Figure 4-7.

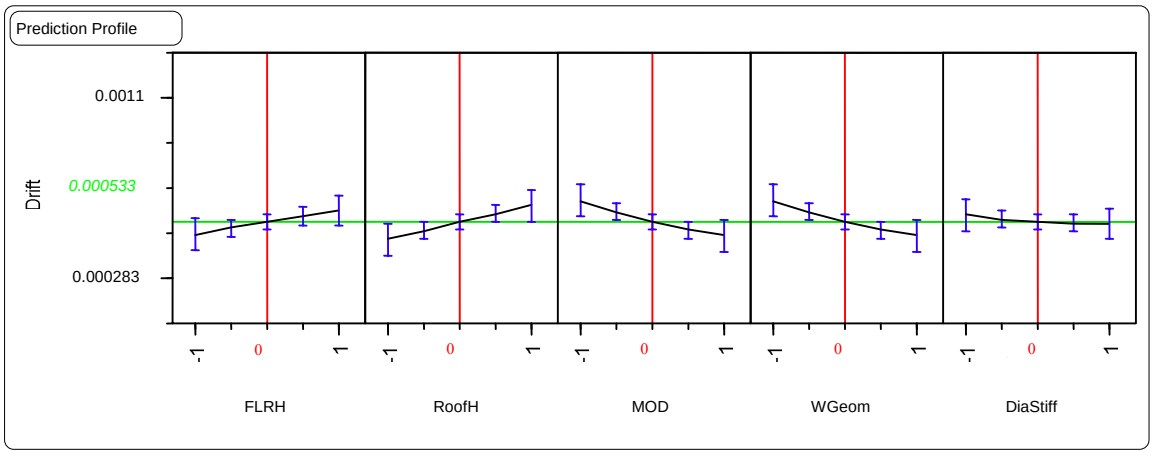

Figure 4-7: Example of Predicted Maximum Drift Ratio from JMP

4.4.6 Response Surface Equation

The response value in this study was the maximum drift ratio in the building and the input variables were those structural uncertainties defined previously. Using a CCD, only 43 cases involving numerically intensive nonlinear structural analyses of specific building configurations were required to define the metamodel. The response function is then described in the form of 2nd degree polynomial as:

$$Y\times 10^4 = 5.328 + 0.537\,X_1 + 0.761\,X_2 - 0.810\,X_3 - 0.800\,X_4 - 0.190\,X_5 - 0.007\,X_1^2 + 0.044\,X_2X_1 - 0.020\,X_2^2 - 0.090\,X_3X_1 - 0.100\,X_3X_2 + 0.180\,X_3^2 - 0.090\,X_4X_1 - 0.100\,X_4X_2 + 0.080\,X_4X_3 + 0.180\,X_4^2 - 0.090\,X_5X_1 - 0.170\,X_5X_2 + 0.100\,X_5X_3 + 0.100\,X_5X_4 + 0.130\,X_5^2$$

where

Y = Predicted Building Maximum Drift Ratio

X_1 = Building Floor Height

X_2 = Building Roof Height

X_3 = Masonry Young's Modulus

X_4 = Wall Geometry

X_5 = Diaphragm Stiffness

and each X_i ranges between –1 and +1 representing minimum and maximum values for each variable.

For verification purposes, analyses using DRAIN-2DX were performed at the design points to check the predicted response equations for both the CCD and FFD. Figure 4-8 shows the comparison between actual DRAIN-2 DX results and predicted values obtained from the response surface equation. The response surface equation predicts the maximum drift ratios (at the design points) acceptably close to the actual DRAIN-2 DX analyses. Both Central Composite Design (CCD) and Full Factorial Design with 5 degree (FF-5deg) provide good results.

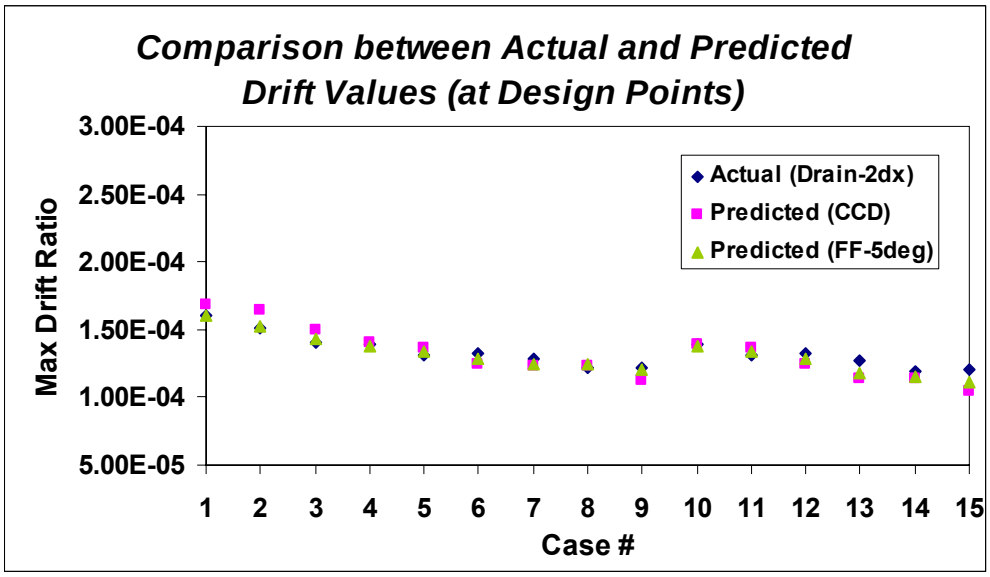

Figure 4-8: Comparison between Actual and Predicted Responses

4.4.7 Fragility Analysis

Because an acceptable metamodel (response function) is available, an efficient Monte Carlo simulation was possible. A Microsoft Excel add-in program called Crystal Ball [Crystal Ball 1996] was used for the Monte Carlo analyses. The selection of particular distribution shapes for each of the design variables should follow from a statistical analysis of actual inventory data for the target class of buildings. Lacking this kind of information in the present study, representative normal distributions as specified previously in Table 4-3 were used to describe the target classes of buildings. Table 4-4 summarizes the results of the Monte Carlo simulation.

Table 4-4: Statistics of Maximum Drift Ratio

PGA ($x10^{-1}$)	Maximum Drift Ratio (%)	
	Mean	Std Dev
0.026	5.36E-02	4.50E-03
0.052	1.07E-01	9.00E-03
0.078	1.61E-01	1.35E-02
0.104	2.15E-01	1.80E-02
0.130	2.68E-01	2.25E-02
0.156	3.22E-01	2.69E-02
0.182	3.76E-01	3.14E-02
0.208	4.29E-01	3.59E-02
0.234	4.83E-01	4.04E-02
0.260	5.37E-01	4.50E-02
0.286	5.90E-01	4.95E-02
0.312	6.44E-01	5.39E-02
0.338	6.98E-01	5.84E-02
0.364	7.51E-01	6.28E-02
0.390	8.05E-01	6.73E-02
0.416	8.59E-01	7.18E-02
0.442	9.13E-01	7.62E-02

The damage probability matrix and corresponding fragility curves are shown respectively in Table 4-5 and Figure 4-9.

Table 4-5: Damage Probability Matrix

PGA ($x10^{-1}$)	Light Damage	Moderate Damage	Severe Damage
0.026	0.00	0.00	0.00
0.052	0.00	0.00	0.00
0.078	0.00	0.00	0.00
0.104	0.00	0.00	0.00

0.130	0.09	0.00	0.00
0.156	0.79	0.00	0.00
0.182	0.99	0.00	0.00
0.208	1.00	0.00	0.00
0.234	1.00	0.03	0.00
0.260	1.00	0.09	0.00
0.286	1.00	0.41	0.00
0.312	1.00	0.79	0.00
0.338	1.00	0.96	0.05
0.364	1.00	0.99	0.22
0.390	1.00	1.00	0.51
0.416	1.00	1.00	0.79
0.442	1.00	1.00	0.94

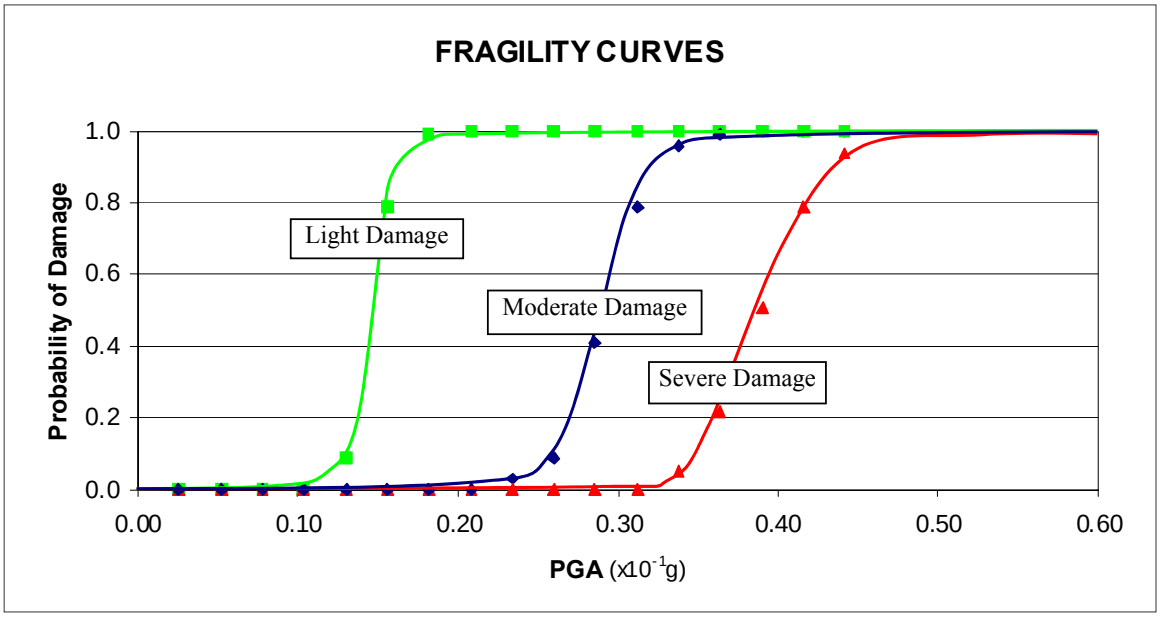

Figure 4-9: Fragility Curves for Example Problem

4.4.8 Effect of Passive Energy Dissipation Devices

The fragility curves shown in Figure 4-9 represent the baseline performance for URM firehouses with the general characteristics assumed for the target class of structures. The question at this point is, then, to what degree will response modification using passive energy dissipators improve the performance, that is, reduce the estimated fragility? The results presented in Chapter 3 for a specific URM building configuration with flexible floor/roof diaphragms suggest that installation of what were defined as Type 1 or Type 2 PED's could reduce the peak drift by 50% or more.

The Type 2 design utilizes relative displacements between the center of the diaphragms and the ground to activate an energy dissipation mechanism. Such a PED could be mounted atop a simple k- or chevron brace and attached to the floor/roof diaphragm above as shown in Figure 4-10. The PED can be introduced into the structural model by adding a nonlinear spring connected between the diaphragm center node and the ground for each bay of the east-west 2D model as shown in Figure 4-11. For this example, PED's were considered on the ground floor only.

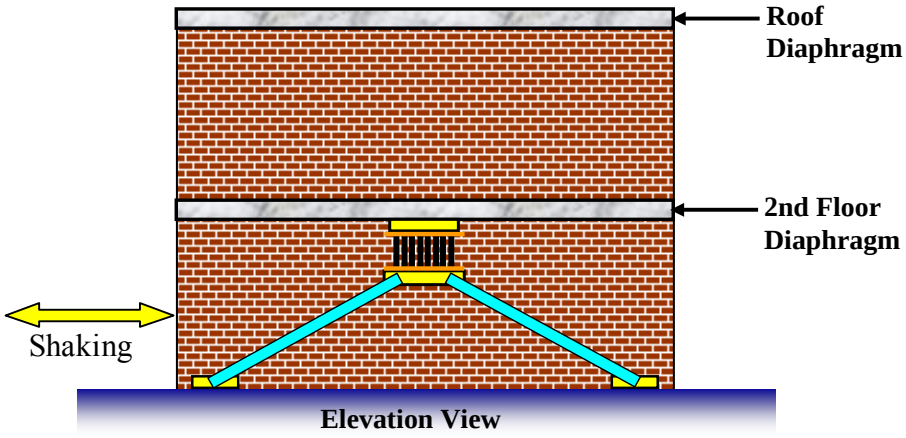

Figure 4-10: Type 2 Passive Energy Dissipator on Ground Floor Only

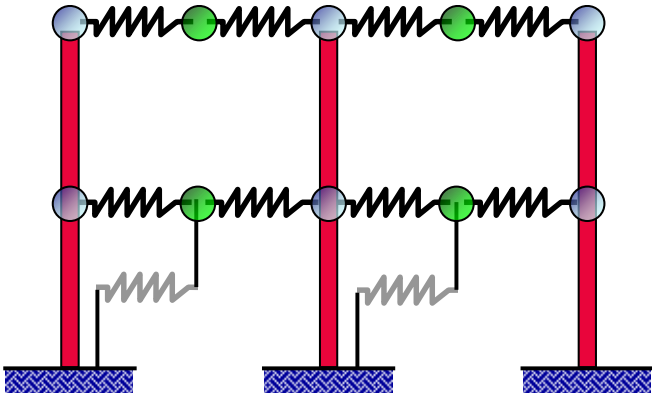

Figure 4-11: DRAIN-2DX Model with Type 2 Passive Devices

The Type 1 design is activated by relative displacements between the center of the diaphragm and the edge of the diaphragms. The possible practical implementations of this concept are more varied and speculative. A simple approach using a stiff link beam between the URM walls was illustrated in Chapter 3, (Section 3.1.1). An alternate concept could involve replacing the link beam and PED with a ductile link beam attached to the center of the diaphragm. In this case, energy dissipation would be developed through inelastic deformation of the link beam itself rather that in a discrete PED. To be effective such a ductile link beam would have to have minimal bending rigidity while at the same time developing ductile shear deformation. (A specially designed bar-joist with light flanges and ductile (kinked) diagonal web members oriented horizontally is a possible concept.) Another more elaborate configuration is shown below in Figure 4-12. In this concept, a cable and pulley system is configured so that diaphragm shear deformations in the direction shown will cause movement of the cable which in turn will activate a PED attached between the cable and one of the in-plane walls[*].

[*] An in-plane is a wall that is subjected primarily to in-plane loads for the particular example being considered.

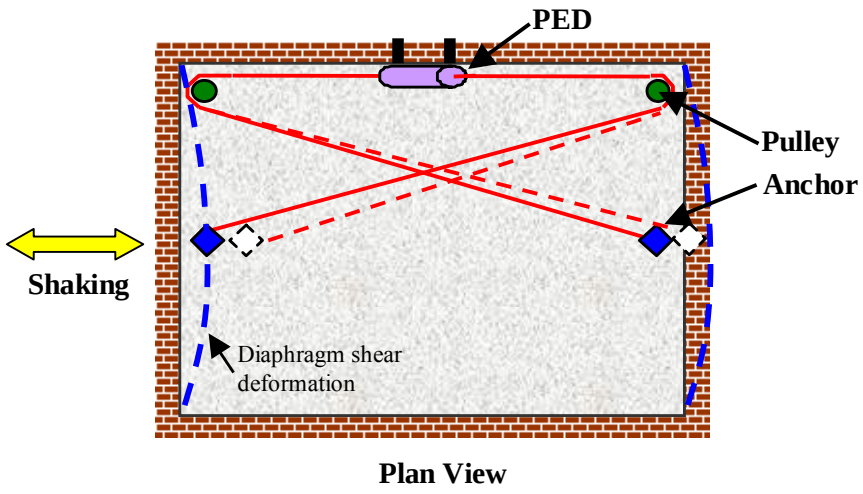

Figure 4-12: Type 1 Passive Energy Dissipation Device

A structural model for a Type 1 configuration involves adding a nonlinear spring between the in-plane wall node and the diaphragm (center) node at the same level as shown in Figure 4-13.

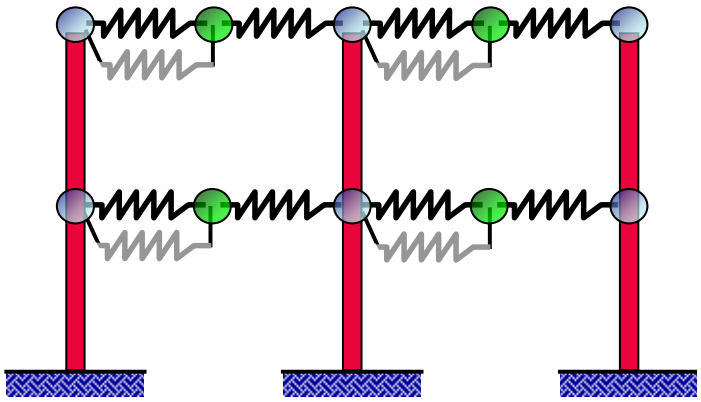

Figure 4-13: DRAIN-2DX Model with Type 1 Passive Devices

In order to gain most benefit out of the passive energy dissipation devices, the spring stiffness and yield force can be determined using the energy-based methodology described in Chapter 3. The objective function to be maximized is the ratio between the energy dissipated in the device and the total input seismic energy, and the design variables are the initial stiffness and yield force of the PED. The dynamic ductility demand on the device is used as a constraint to reflect the low-cycle fatigue limits of the PED. The dynamic ductility demand on the PED can be calculated from

$$\mu_p = \frac{H_t}{f_y u_y (2N_f)^{0.4}} \tag{4.2}$$

where :

H_t is the total hysteretic energy dissipated in the device,

f_y is the yield force of the device,

u_y is the corresponding yield displacement, and

N_f is the total number of load reversals experienced by the device.

The dynamic ductility should always be less than the monotonic plastic ductility observed in monotonically loaded laboratory tests of similar devices. Additional constraints (sometimes called side constraints) must also be placed on the design variables themselves in order to limit the maximum forces in the devices in accordance with FEMA 356 guidelines [FEMA 2000]. Without such constraints on strength and stiffness, the optimization process could quickly converge on solutions with large values for these parameters that effectively result in supplementary lateral bracing to the structure.

As noted in Chapter 3, a number of powerful numerical optimization algorithms are widely available to handle constrained optimization problems like this, for example, DOT [Vanderplaats 1993]. However, in order to more clearly illustrate the actual nature of this optimal design problem, a contour plot of the objective function (including the dynamic ductility constraint contours) for each model were computed and are shown in Figure 4-14 and Figure 4-15.

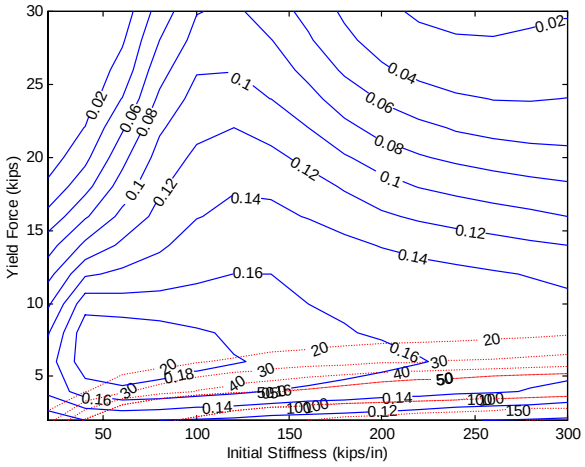

Figure 4-14: Objective Function for the Gilroy Firehouse Model with Type 2 Passive Devices (solid blue lines are energy dissipation contours while dashed red contours are ductility demand contours)

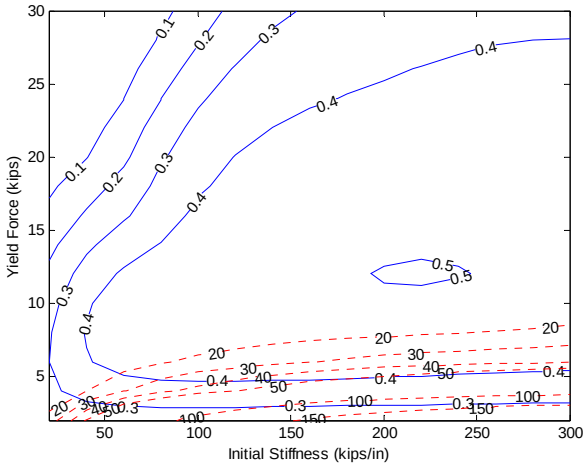

Figure 4-15: Objective Function for the Gilroy Firehouse Model with Type 1 Passive Devices (solid blue lines are energy dissipation contours while dashed red contours are ductility demand contours)

The contour plots show that the Type 1 configuration should be more effective than the Type 2 design because of the larger value of its objective function (ratio of energy dissipated in the PED to the input energy) which is roughly 0.5 as compared to 0.18 for the Type 2 design. For both configurations, the constraint lines for dynamic ductility lie close to the stiffness axis so that solutions satisfying this constraint lie above these dashed lines. Following the FEMA 356 guidelines [FEMA 2000], an additional practical constraint should be placed on the maximum force developed in the PED. If not, the optimization process may converge on very large values for force and stiffness, so that the presence of the PED becomes essentially an additional lateral bracing system for the main structure. Using a reasonable force limit of 12 kips, the optimal PED stiffness is 220 kips/in and the dynamic ductility constraint of 20 or less was met. This maximum force in each damping device accounted for about 2% of the total base shear of the building. The improvements in the dynamic responses at selected locations in the model are shown in Table 4-6. The peak displacements were reduced by 64% while the peak accelerations were reduced by 67% from the baseline values.

For the fragility analysis of the rehabilitated building, a new response surface based metamodel must be developed for use in the Monte Carlo simulation. However, this now adds an additional complication if the structural performance is highly sensitive to the PED design parameters. To test the sensitivity of the optimal passive device design to variations in structural and seismic uncertainties a series of four extreme cases were selected. Design parameters were

drawn at +3 and –3 times standard deviation of each assumed probability distribution. The optimization process was performed on each of these cases and the corresponding PED objective function contour plots and optimal design points were compared. It can be observed from Figure 4-16 that these contours follow the same pattern and are only slightly different in quantitative terms. Therefore, it will be assumed in this study that the design of the passive device can be implicitly incorporated into the response surface and need not be included as an added input variable.

Table 4-6: Comparison Between Baseline Model and Model with Type 1 Devices

	Baseline Model		Modified (Passive) Model	
	Displacement (in.)	Acceleration (g)	Displacement (in.)	Acceleration (g)
Center of Top Floor Diaphragm	1.880	1.030	0.680	0.339
Top of the In-Plane Wall	0.070	0.120	0.058	0.076

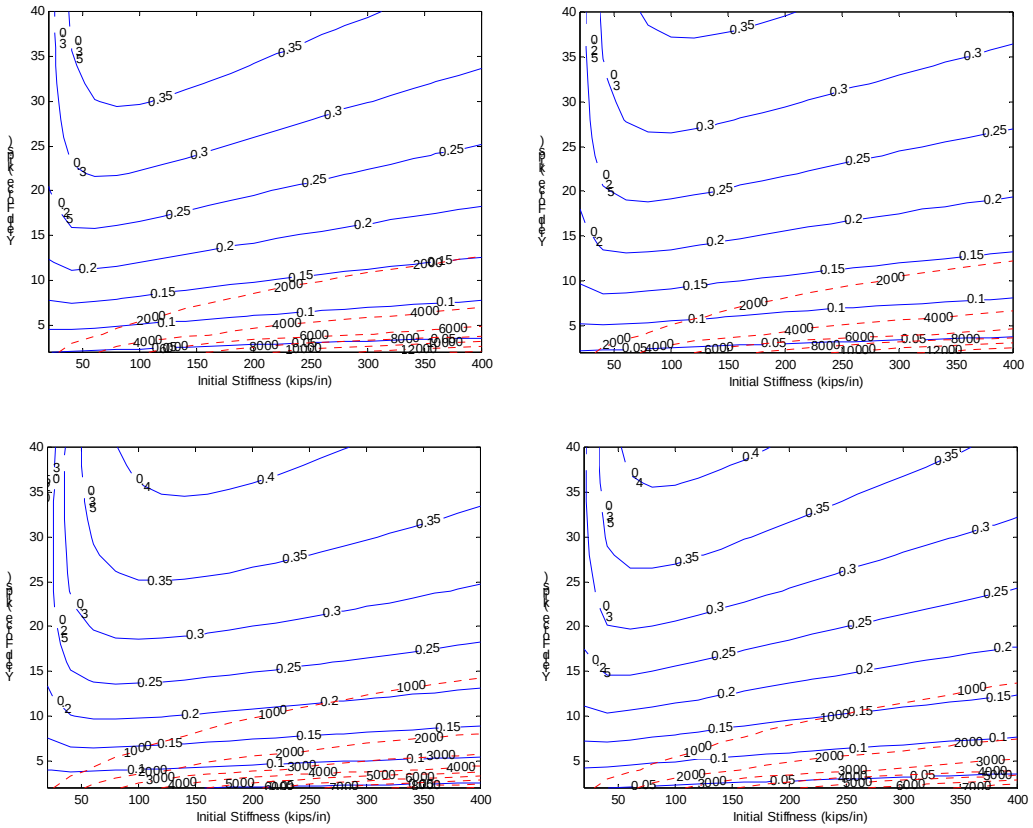

Figure 4-16: Sensitivity of the Type 1 Passive Device Design

4.4.9 Improvement in Structural Response

A similar approach to that used for the baseline building was followed for the fragility analysis of the rehabilitated building. Given that the passive energy dissipation device design would not be affected by the changes in structural and seismic parameters, the response surface methodology and Monte Carlo simulation were applied again for the building rehabilitated with the addition of a Type 1 PED. Fragility curves showing the improvement in dynamic response of the firehouse when the Type 1 passive energy dissipation system was added to the baseline building are shown in Figure 4-17. The solid lines represent the curves for baseline buildings, while the dashed lines represent rehabilitated buildings. The shift to the right from solid to dashed lines indicates lower probability of damage (relative to PGA) when the passive energy dissipation system is used to rehabilitate the structure. On first glance, the improvements might appear to be relatively small, especially given the rather large (more than 50%) reduction in peak displacements and accelerations noted earlier. However, the quantitative improvement in fragility at a given level of ground motion is indicated by the vertical separation between the curves for each assumed level of damage. For example, at a PGA of 0.3, the PED system will have little or no effect on light damage (which is almost certain to occur), but the probability of moderate damage drops from about 70% to around 30%, a reduction of over 50%.

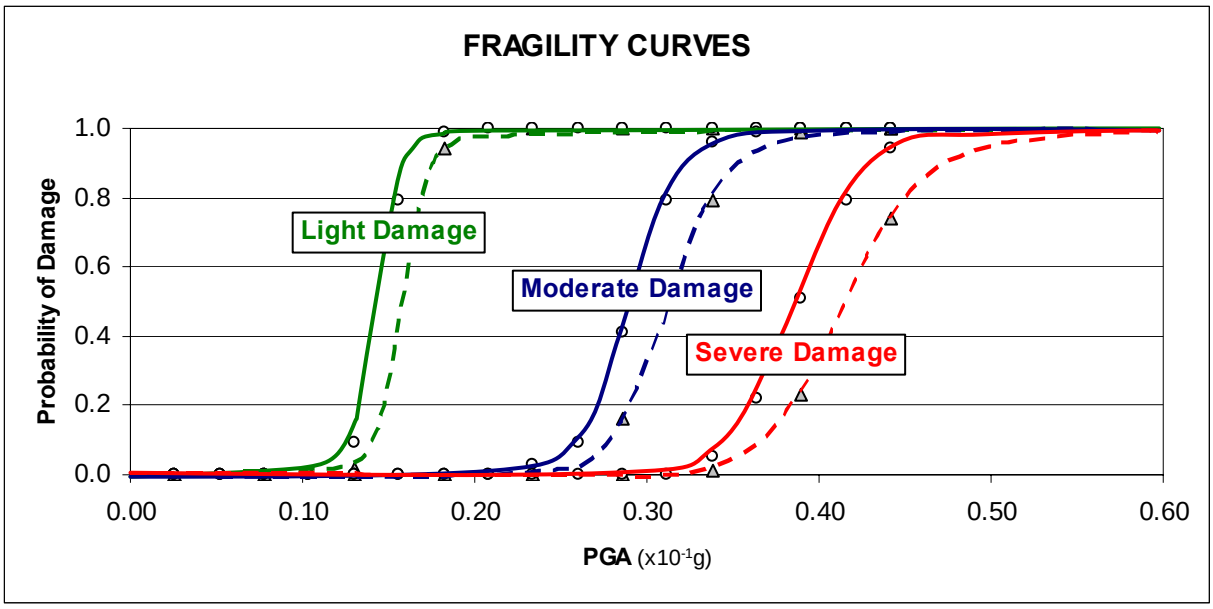

Figure 4-17: Fragility Curves of the Baseline (solid curves) and Rehabilitated (dashed curves) Buildings

5 Conclusions

5.1 Findings

This study has examined the application of passive energy dissipation systems for response modification of essential facilities in the Mid-America region. Essential facilities are defined as buildings that support functions related to post-earthquake emergency response and disaster management. These include fire stations, police stations, emergency management offices, schools and hospitals. For such buildings simply ensuring life safety and preventing collapse are not sufficient and the buildings must remain operational during or at least suitable for immediate occupancy after a major earthquake. A regional inventory of essential facilities carried out in another MAE Center project (SE-1) revealed that unreinforced masonry (URM) is the most common type of construction for essential facilities in the region, and such material is well known to be highly vulnerable to strong earthquakes. As a result, response modification for this type of building, and particularly for low-rise URM firehouses, was the focus of this study.

Based on prior experience, the research team chose to study the use of the tapered metallic flexure passive damping devices for response modification purposes. It was felt that metal hysteresis offers good energy dissipation with excellent long-term stability and reliability, and therefore are particularly well-suited for scenarios with infrequent earthquakes. Passive energy dissipation has not been considered for response modification of URM structures because of the very high initial elastic in-plane stiffnesses of URM walls. However, a large number of URM essential facilities commonly include flexible wooden floor and roof diaphragms that couple the URM walls into structures that are more flexible (and complex) that the URM walls alone.

Three concepts for passive energy dissipation were investigated: one activated by relative displacements between the in-plane walls and the diaphragm (called Type 1), one activated by relative displacements between the diaphragm and the ground (called Type 2), and the third activated by the relative in-plane displacements within a wall (called Type 3). Only Type 1 and 2 configurations were considered in this report, and both were studied through several examples. The passive energy dissipation devices were designed using an energy-based criterion with the objective being to maximize the ratio of the energy dissipated in the devices to the total input seismic energy subject to selected constraints on peak forces and dynamic ductility.

For modeling URM buildings, an efficient and simple approach was sought so that the methods could be applied to a large number of different representative structures. A novel approach was developed for modeling the in-plane response of a perforated URM wall. First the wall was decomposed into characteristic regions such as piers and spandrels. The in-plane behavior of each region was modeled by a single nonlinear spring, and these regions were then assembled into a 2-D parallel-series composite spring model. Linear and nonlinear properties for each spring were pre-determined empirically and integrated into the model. The varying boundary conditions for each of these regions were modeled by using either an "effective height" or an "effective end stiffness" approach to account for less than ideal end conditions. An additional factor based on overall wall aspect ratio was applied to reflect the degree of in-plane bending action in the wall. These factors were determined by a regression analysis using plane stress finite element models for basic wall regions as well as complete walls. The model was verified by comparison with an experimental result and showed good agreement for the wall stiffness and strength. Finally, a simple 2-D lumped-parameter building model was developed in DRAIN-2DX and ABAQUS using these in-plane wall models and with springs to model the shear deformation modes for flexible floor/roof diaphragms. No consideration was given to out-of-plane wall stiffness but the masses were considered.

The response modification concepts were then evaluated in analytical studies, first using a relatively simple structural model for a highly idealized laboratory test model used in MAE Center project ST-10, and second, using a structural model for the full-scale project ST-11/22 test structures. The results from these analytical examples indicated that the incorporation of a properly designed passive energy dissipator in the rehabilitation of certain kinds of URM structures could minimize energy dissipation demand in the primary structure, reduce seismic responses, and lessen the possibility of damage. Given the inherently stiff nature of URM structures, this approach can only be applied in cases where sufficient deformation can be developed in a flexible floor or roof diaphragm to fully activate typical metallic hysteretic dampers considered in this study. The primary benefit of this kind of response modification is a significant reduction in out-of-plane wall deformation induced by a flexible floor diaphragm. The effectiveness of this approach is reduced when the diaphragm stiffness for shear mode deformation is more than about 8% of the in-plane wall stiffness, but this is well above the stiffnesses of typical floor and roof diaphragms. Thus the use of a passive energy dissipator as

outlined in this study might be considered as part of a potential rehabilitation scheme aimed to reduce deleterious effects of an overly flexible diaphragm system.

Finally, the probabilistic nature of the problem, specifically the variation in building configuration for a regional class of buildings such as firehouses, were taken into account. Fragility curves and damage probability matrices were used to describe the likelihood of damages under different ground shaking intensities. This research made use of meta-modeling techniques through a combined response surface methodology and Monte Carlo simulation approach to include randomness in configurations over a class of buildings in a region. Improvement in the seismic responses when a passive energy dissipation system is implemented were shown to lead to a lowered probability of damage in the buildings.

5.2 Recommendations

The preliminary results described in this report suggest that the use of metallic passive damping devices may contribute to response reduction in actual URM buildings in the Mid-America region. However, more research and study is needed before this kind of a high-risk approach is actually attempted. In this connection, the following recommendations are made:

1. Rehabilitation schemes developed in this study only apply to URM buildings with regular floor plans. It is essential to continue to investigate the effect of building irregularities that may result in torsional effects.
2. The model developed in this study was a 2-D lumped parameter model and therefore it did not properly represent multiaxis behavior including torsional movement of the building due to stiffness asymmetry. It is recommended that the modeling methods be incorporated into 3D analyses using newly developed analysis tools developed under MAE Center project ST-5.
3. The URM wall model was developed under the assumption that failure occurs along the boundaries of pre-defined regions. However, in reality, cracks can occur at any place in the wall. Even though it is generally understood that only a refined model, or a finite element model can ultimately represent this failure mode, it is strongly recommended that the simplified model be more fully tested and evaluated in comparison to more refined models and actual test results.

4. The tapered metallic flexural dampers can only dissipate energy when the seismic force acts perpendicular to them, other configurations or even other types of devices may be better suited for multidirectional earthquakes.
5. The current PED design approach is ground motion dependent. Each contour plot results in an optimal design for the PED fitted into a building under a specific ground motion. The entire process must be repeated as different seismic loading is considered. This design approach should be further improved to be general to different earthquakes.
6. An alternative way of rehabilitating URM buildings using metallic dampers might involve activating a PED using in-plane wall deformation that could arise through inelastic behavior involving, for example, pier rocking and bed joint sliding mechanisms. Such a scheme will require much stiffer PED's than the ones considered for this report. Research at SUNY-Buffalo and MCEER [Constantinou and Sigaher 1997; McNamara et al. 2000]) has examined novel concepts for stiff "toggle" brace systems and motion amplification devices that might be appropriate for such applications. Devices like these could be applied in parallel with a URM wall to reduce in-plane response and thereby protect the wall. Such schemes are referred to as Type 3 designs to differentiate them from the earlier schemes considered for use with the floor diaphragm system.
7. Finally, while the present study has focused on the use of the metallic hysteretic PED because of its potentially high reliability and durability over a long period of time, other passive energy dissipation devices such as viscous and viscoelastic dampers might prove equally or perhaps more effective in similar applications.

6 References

Advanced Structural Concepts, Inc. (1998). The RAM Structural System, RAM International.

Aiken, I. D., Nims, D. K., Whittaker, A. S., and Kelly, J. I. (1993). "Testing of Passive Energy Dissipation Systems." Earthquake Spectra, Vol. 9, No. 3, pp. 335-370.

Alonso, L. J. (1989). "Mechanical Characteristics of X-Plate Energy Dissipators." *CE 299 Report*, University of California, Berkeley, CA.

Anagnos, T., Rojahn, C., and Kiremidjian, A. S. (1995). "NCEER-ATC Joint Study on Fragility of Buildings." *Technical Report NCEER-95-0003*, National Center for Earthquake Engineering Research, State University of New York, Buffalo, NY.

Applied Technology Council (1985). "Earthquake Damage Evaluation Data for California." Report ATC-13, Applied Technology Council, Redwood City, CA.

Asano, M., Masahiko, H., and Yamamoto, M. (2000). "The Experimental Study on Viscoelastic Material Dampers and the Formulation of Analytical Model." *Proceedings of the 12th World Conference on Earthquake Engineering,* Auckland, New Zealand. Paper 1535.

Basöz, N., and Kiremidjian, A. S. (1999). "Development of Empirical Fragility Curves for Bridges." *Proceedings of the 5th U.S. Conference on Lifeline Earthquake Engineering*, Seattle, WA, pp. 693-702.

Bergman, D. M., and Goel, S. C. (1987). "Evaluation of Cyclic Testing of Steel-Plate Devices for Added Damping and Stiffness." *Report No. UCME 87-10*, Department of Civil Engineering, University of Michigan, Ann Arbor, MI.

Box, G. E. P., and Draper, N. R. (1975). "Robust Designs." *Biometrika*, Vol. 62, No. 2, pp. 347-352.

Box, G. E. P., and Wilson, K. B. (1951). "On the Experimental Attainment of Optimum Conditions." *Journal of the Royal Statistical Society*, Series B, Vol. 13, Issue 1, pp.1-45.

Bruneau, M. (1994). "Seismic Evaluation of Unreinforced Masonry Buildings – a State-of-the-Art Report." *Canadian Journal of Civil Engineering*, Vol. 21, No. 3, pp. 512-539.

Bucher, C. G., and Bourgund, U. (1990). "A Fast and Efficient Response Surface Approach for Structural Reliability Problems." *Structural Safety*, Vol. 7, No. 1, pp. 57-66.

Chang, K. C., Soong, T. T., Lai, M. L., and Nielsen, E. J. (1993). "Viscoelastic Dampers as Energy Dissipation Devices for Seismic Applications." *Earthquake Spectra*, Vol. 9, No. 3, pp. 371-387.

Constantinou, M. C., and Sigaher, A. N. (2000). "Energy Dissipation system Configurations for Improved Performance." *Proceedings of the 2000 Structures Congress & Exposition*, Philadelphia, PA.

Crystal Ball User Manual – Version 4.0. (1996). Decisioneering, Inc., Denver, CO.

DeLaurentis, D., Mavris, D. N., and Schrage, D. P. (1996). "System Synthesis in Preliminary Aircraft Design using Statistical Methods." *Proceedings of the 20th Congress of the International Council of the Aeronautical Sciences*, Sorrento, Italy.

Dumova-Jovanoska, E. (2000). "Fragility Curves for Reinforced Concrete Structures in Skopje (Macedonia) Region." *Soil Dynamics and Earthquake Engineering*, Vol. 19, No. 6, pp.455-466.

El-Gazairly, L. F. (1993). "Three Dimensional Nonlinear Dynamic Response of an RC Structure with Advanced Cladding." Ph.D. thesis, Georgia Institute of Technology, Atlanta, GA.

Engelund, W. C., Stanley, D. O., Lepsch, R. A., McMillan, M. M., and Unal, R. (1993). "Aerodynamic Configuration Design using Response Surface Methodology Analysis." *Proceedings of the AIAA Aircraft Design, Systems, and Operations Meeting*, Monterey, CA.

Faravelli, L. (1989). "Response-Surface Approach for Reliability Analysis." *Journal of Engineering Mechanics*, Vol. 115, No. 12, pp. 2763-2781.

FEMA - Federal Emergency Management Agency (2000). "Prestandard and Commentary for the Seismic Rehabilitation of Buildings." *Report No. FEMA-356*, Washington, DC.

Filiatrault, A., and Cherry, S. (1987). "Performance evaluation of friction damped braced steel frames under simulated earthquake loads." *Earthquake Spectra*, Vol. 3, No. 1, pp. 57-78.

Fitzgerald, T. F., Anagnos, T., Goodson, M., and Zsutty, T. (1989). "Slotted Bolted Connections in Aseismic Design for Concentrically Braced Connections." *Earthquake Spectra*, Vol. 5, No. 2, pp. 383-391.

French, S., and Olshansky, R. (2000). "Inventory of Essential Facilities in Mid-America." *Project SE-1 Final Report*, Mid America Earthquake Center, The University of Illinois, Champaign, IL.

Goodno, B. J., Craig, J. I., Dogan, T., and Towashiraporn, P. (1998). "Ductile Cladding Connection Systems for Seismic Design." *Report GCR 98-758*, Building and Fire Research Laboratory, NIST.

Grigorian, C. E., Yang, T.-S., and Popov, E. P. (1993). "Slotted Bolted Connection Energy Dissipators." *Earthquake Spectra*, Vol. 9, No. 3, pp. 491-504.

Hwang, H. H. M., and Huo, J.-R. (1994a). "Generation of Hazard-Consistent Fragility Curves." *Soil Dynamics and Earthquake Engineering*, Vol. 13, No. 5, pp. 345-354.

Hwang, H. H. M., and Huo, J.-R. (1994b). "Generation of Hazard-Consistent Fragility Curves for Seismic Loss Estimation Studies." *Technical Report NCEER-94-0015*, National Center for Earthquake Engineering Research, State University of New York, Buffalo, NY.

Hwang, H., Liu, J. B., and Chiu, Y.-H. (2000). "Seismic Fragility Analysis of Highway Bridges." Center of Earthquake Research and Information, The University of Memphis, Memphis, TN.

Izumi, M., et al. (1990). "Development and Application of Finite Nonlinear Viscoelastic Constitutive Law." *Journal of Structural and Construction Engineering*, Vol. 407, pp. 79-85.

Jaw, J.-W., and Hwang, H. H. M. (1988). "Seismic Fragility Analysis of Shear Wall Structures." *Technical Report NCEER-88-0009*, National Center for Earthquake Engineering Research, State University of New York, Buffalo, NY.

JMP User's Guide – Version 3.1. (1995). SAS Institute Inc., Cary, NC.

Kasai, K., Munshi, J. A., and Maison, B. F. (1993). "Viscoelastic Dampers for Seismic Pounding Mitigation." *Structural Engineering in Natural Hazards Mitigation: Proceedings of Papers Presented at the Structures Congress '93*, Vol. 1, New York, pp. 730-735.

Kelly, J. M., Skinner, R. I., and Heine, A. J. (1972). "Mechanisms of Energy Absorption in Special Devices for Use in Earthquake Resistant Structures." *Bulletin of New Zealand Society for Earthquake Engineering*, Vol.5, No 3, pp. 63-88.

Kim, S.-C. and White, D. W. (2001). "MDOF Response of Low Rise Buildings." *draft report for Project ST-5*, Mid-America Earthquake Center, School of Civil and Environmental Engineering, Georgia Institute of Technology, Atlanta, GA.

Lobo, R. F., Bracci, J. M., Shen, K. L., Reinhorn, A. M., and Soong, T. T. (1993). "Inelastic Response of R/C Structures with Viscoelastic Braces." *Earthquake Spectra*, Vol. 9, No. 3, pp. 419-446.

Lotfi, H. R., and Shing, P. B. (1994). "Interface Model Applied to Fracture of Masonry Structures." *Journal of Structural Engineering*, Vol. 120, No.1, pp. 63-80.

Lourenco, P. B. (1996). *Computational strategies for Masonry Structures*, Delft University Press.

Magenes, G., and Calvi, G. (1997). "In-plane seismic response of brick masonry walls." *Earthquake Engineering and Structural Dynamics,* Vol. 26, No. 11, pp.1091-1112.

Mann, N. R., Schafer, R. E., and Singpurwalla, N. D. (1974). *Methods for Statistical Analysis of Reliability and Life Data*, John Wiley & Sons, Inc., New York.

Manzouri, T., Schuller, M. P., and Shing, P. B. (1996). "Repair and Retrofit of Unreinforced Masonry Structure.s" *Earthquake Spectra*, Vol. 12, No. 4, pp. 903-922.

Martinez-Romero, E. (1993). "Experiences on the Use of Supplementary Energy Dissipators on Building Structures." *Earthquake Spectra*, Vol. 9, No. 3, pp. 581-625.

Mavris, D. N., and Bandte, O. (1995). "Economic Uncertainty Assessment using a Combined Design of Experiments/Monte Carlo Simulation Approach with Application to an HSCT." *Proceedings of the 17th Annual Conference of the International Society of Parametric Analysts*, San Diego, CA.

Mavris, D. N., Bandte, O., and Schrage, D. P. (1996). "Effect of Mission Requirements on the Economic Robustness of an HSCT Concept." *Proceedings of the 18th Annual Conference of the International Society of Parametric Analysts*, Cannes, France.

McCabe, S. L., and Hall, W. J. (1989). "Assessment of Seismic Structural Damage," *Journal of Structural Engineering*, Vol. 115, No. 9, pp. 2166-2183.

McNamara, R. J., Huang, C. D., and Wan, V. (2000). "Viscous-Damper with Motion Amplification Device for High Rise Building Applications." *Proceedings of the 2000 Structures Congress & Exposition*, Philadelphia, PA.

Mongomery, D. C. (1991). *Design and Analysis of Experiments*, John Wiley & Sons, Inc.

Moor, C. (1992). "Analytical and Experimental Evaluation of Advanced Cladding Connections," M.S.C.E. Thesis, School of Civil Engineering, Georgia Institute of Technology, Atlanta, GA.

Mosalam, K. M., White, R. N., and Gergely, P. (1997). "Computational Strategies for Frames with Infill Walls: Discrete and Smeared Crack Analyses and Seismic Fragility." *Technical Report NCEER-97-0021*, National Center for Earthquake Engineering Research, State University of New York, Buffalo, NY.

Nims, D. K., Richter, P. J., and Bachman, R. E. (1993). "The Use of the Energy Dissipating Restraint for Seismic Hazard Mitigation." *Earthquake Spectra*, Vol. 9, No. 3, pp 467-489.

O'Rourke, M. J., and So, P. (1999). "Seismic Behavior of On-Grade Steel Tanks; Fragility Curves." *Proceedings of the 5th U.S. Conference on Lifeline Earthquake Engineering*, Seattle, WA, pp. 849-858.

O'Rourke, M. J., and So, P. (2000). "Seismic Fragility Curves for On-Grade Steel Tanks." *Earthquake Spectra*, Vol. 16, No. 4, pp. 801-815.

Pall, A. S., and Marsh, C. (1980). "Optimum Seismic Resistance of Large Panel Structures Using Limited Slip Bolted Joints." *Proceedings of the Seventh World Conference on Earthquake Engineering*, Istanbul, Turkey, Vol. 4, pp. 177-184.

Pall, A. S., and Marsh, C. (1982). "Response of Friction Damped Braced Frames." *Journal of the Structural Division*, ASCE, 108, ST6, pp. 1313-1323.

Park, Y. J., Reinhorn, A. M., and Kunnath, S. K. (1987). "IDARC: Inelastic Damage Analysis of Reinforced Concrete Frames-Shearwall Structure." *Technical Report NECCR-87-0008*, National Center for Earthquake Engineering Research, State University of New York, Buffalo, NY.

Perry, C. L., Fierro, E. A., Sedarat, H., and Scholl, R. E. (1993). "Seismic Upgrade in San Francisco Using Energy Dissipation Devices." *Earthquake Spectra*, Vol. 9, No. 3, pp. 559-579.

Pinelli, J. P. (1992). "Development of Energy Dissipating Cladding Connections for Passive Control of Building Seismic Response." Ph.D. dissertation, School of Civil Engineering, Georgia Institute of Technology, Atlanta, GA.

Pinelli, J. P., Moor, C., Craig, J. I., and Goodno B. J. (1996). "Testing of Energy Dissipating Cladding Connections." *Earthquake Engineering and Structural Dynamics*, Vol. 25, pp. 129-147.

Pinelli, J.-P., Craig, J. I., Goodno, B. J., and Hsu, C. C. (1993). "Passive Control of Building Response Using Energy Dissipating Cladding Connections." *Earthquake Spectra*, Vol. 9, No. 3, pp.529-546.

Prakash, V., Powell, G. H., and Campbell, S. (1993), "DRAIN-2dx Base Program Description and User Guide." Version 1.10, Dept. of Civil Engineering, University of California Berkeley, CA.

Rajashekhar, M. R., Adidam, S. S. R., and Ellingwood, B. R. (1996). "Structural Reliability Analysis Through Response Surfaces." *Journal of Structural Engineering*, Structural Engineering Research Centre, Madras, India, Vol. 22, No. 4, pp. 179-192.

Rajashekhar, M. R., and Ellingwood, B. R. (1993). "A New Look at the Response Surface Approach for Reliability Analysis." *Structural Safety*, Vol. 12, No. 3, pp. 205-220.

Richter, P. J., Nims, D. K., Kelly, J. M., and Kallenbach, R. M. (1990). "The EDR-Energy Dissipation Restraint, A New Device for Mitigating Seismic Effects." *Proceedings of the 1990 Structural Engineers Association of California*, Lake Tahoe, CA.

Schneider, R., and Dickey, W. L. (1987). *Reinforced Masonry Design*, Prentice Hall, Second Edition.

Schneider, S., Lee, H. M., and Godden, W. G. (1983). "Piping Seismic Test with Energy-Absorbing Devices." *Final Report EPRI-NP-2902 for Research Project 1586-1*, EERC, College of Engineering, University of California, Berkeley, CA.

Scholl, R. E. (1988). "Added Damping and Stiffness Elements for Earthquake Damage and Loss Control." *Proceedings of Conference XLI: A Review of Earthquake Research Applications in the National Earthquake Hazards Reduction Program: 1877-1987*, U.S. Geological Survey Open File, Report No. 88-13-A, San Diego, CA.

Seya, H., Talbott, M. E., and Hwang, H. H. M. (1993). "Probabilistic Seismic Analysis of a Steel Frame Structure." *Engineering Mechanics*, Vol. 8, No. 2, pp. 127-136.

Shen, K. L., and Soong, T. T. (1995). "Modeling of Viscoelastic Dampers for Structural Applications." *Journal of Engineering Mechanics*, Vol. 121, No. 6, pp. 694-701.

Shing, P. B., and Klingner, R.E. (1998). "Nonlinear Analysis of Masonry Structures." *Structural Engineering World Wide T125-2*, Elsevier Science Ltd.

Shinozuka, M., Feng, M. Q., Kim, H.-K., and Kim, S.-H. (2000a). "Nonlinear Static Procedure for Fragility Curve Development," *Journal of Engineering Mechanics*, Vol. 126, No. 12, pp. 1287-1295.

Shinozuka, M., Feng, M. Q., Lee, J., and Naganuma, T. (2000b). "Statistical Analysis of Fragility Curves," *Journal of Engineering Mechanics*, Vol. 126, No. 12, pp. 1224-1231.

Skinner, R. I., Kelly, J. M., and Heine, A. J. (1973). "Energy Absorption Devices for Earthquake Resistant Structures." *Proceeding of the Fifth World Conference on Earthquake Engineering*, Rome, Italy, pp. 2924-2933.

Skinner, R. I., Kelly, J. M., and Heine, A. J. (1975). "Hysteretic Dampers for Earthquake-Resistant Structures." *Earthquake Engineering and Structural Dynamics*, Vol.3, pp. 287-296.

Skinner, R. I., Beck, J. L., and Bycroft, G. N. (1975). "A Practical System for Isolating Structures from Earthquake Attack." *Earthquake Engineering and Structural Dynamics*, Vol.3, pp. 297-309.

Soda, S., and Takahashi, Y. (1997). "Quantification of Frequency-Dependent Property of Visco-Elastic Damper by Random Loading Method." *Journal of Structural and Construction Engineering*, Vol. 498, pp. 43-49.

Soda, S., and Takahashi, Y. (2000). "Performance Based Seismic Design of Building Structures with Viscoelastic Dampers." *Proceedings of the 12th World Conference on Earthquake Engineering,* Auckland, New Zealand. Paper 1236.

Song, J., and Ellingwood, B. R. (1999). "Seismic Reliability of Special Moment Steel Frames with Welded Connections: II." *Journal of Structural Engineering*, Vol. 125, No. 4, pp. 372-384.

Soong, T. T., and Dargush, G. F. (1997). *Passive Energy Dissipation Systems in Structural Engineering*, John Wiley & Sons Ltd., West Sussex, England.

Tena-Colunga, A., and Abrams, D. P. (1992). "Response of an Unreinforced Masonry Building During the Loma Prieta Earthquake." *UILU-ENG-92-2024*, Structural Research Series 576, 0069-4274, Dept. of Civil Engineering, Univ. of Illinois, Urbana, IL.

Tsai, K.-C., Chen, H.-W., Hong, C.-P., and Su, Y.-F. (1993). "Design of Steel Triangular Plate Energy Absorbers for Seismic-Resistant Construction." *Earthquake Spectra*, Vol. 9, No. 3, pp. 505-528.

Tyler, R.G. (1977), "Damping in Building Structures by Means of PTFE Sliding Joints." *Bulletin of the New Zealand Society for Earthquake Engineering*, Vol.10, No. 3, pp. 129-138.

Tyler, R.G. (1978a). "A Tenacious Base Isolation System Using Round Steel Bars." *Bulletin of the New Zealand Society for Earthquake Engineering*, Vol.11, No. 4, pp. 273-281.

Tyler, R.G. (1978b). "Tapered Steel Energy Dissipators for Earthquake Resistant Structures." *Bulletin of the New Zealand Society for Earthquake Engineering*, Vol.11, No. 4, pp 282-294.

Vanderplaats, G. N., 1993, *DOT Users Manual*, Version 4.00, VMA Engineering, Goleta, CA.

Venuti, W. J. (1976). "Energy Absorbtion of High Strength Bolted Connections." *Test Report*, Structural Steel Educational Council, CA.

Vulcano, A., and Mazza, F. (2000). "Comparative Study of the Seismic Performance of Frames using Different Dissipative Braces." *Proceedings of the 12th World Conference on Earthquake Engineering,* Auckland, New Zealand**.** Paper 1982.

Wen, Y. K., and Wu, C. L. (2001). "Uniform Hazard Ground Motions for Mid-America Cities." *Earthquake Spectra*, Vol. 17, No. 2, pp. 359-384.

Whittaker, A. S., Bertero, V. V., Thompson, C. L., and Alonso, L. J. (1991). "Seismic Testing of Steel Plate Energy Dissipation Devices." *Earthquake Spectra*, Vol. 7, No. 4, pp. 563-604.

Yamazaki, F., Hamada, T., Motoyama, H., and Yamauchi, H. (1999). "Earthquake Damage Assessment of Expressway Bridges in Japan." *Proceedings of the 5th U.S. Conference on Lifeline Earthquake Engineering*, Seattle, WA, pp. 361-370.

Yao, T. H.-J., and Wen Y.-K. (1996). "Response Surface Method for Time-Variant Reliability Analysis." *Journal of Structural Engineering*, Vol. 122, No. 2, pp. 193-201.

Zhuge, Y., Thambiratnam, D., and Corderoy, J. (1998). "Nonlinear Dynamic Analysis of Unreinforced Masonry." *Journal of Structural Engineering*, Vol. 124, No. 3, pp. 270-277.

Zsutty, T. C. (1985). *Slotted Bolted Connections in Seismic Resistant Bracing Systems,* T.F. Fitzgerald & Associations, San Francisco, CA.

APPENDIX A: Simulated Carbondale Ground Acceleration Records

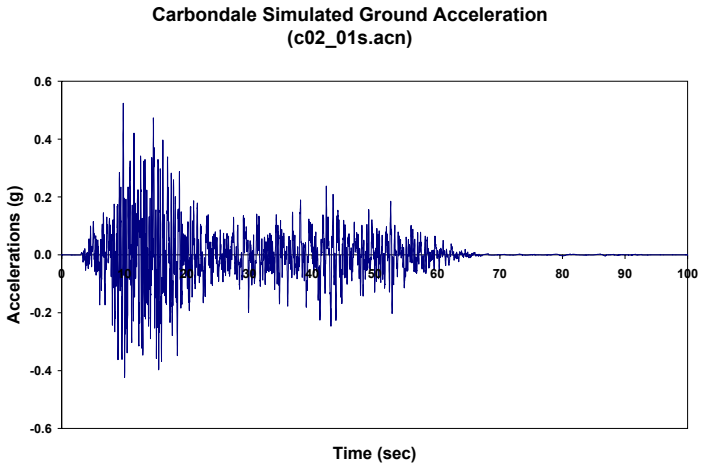

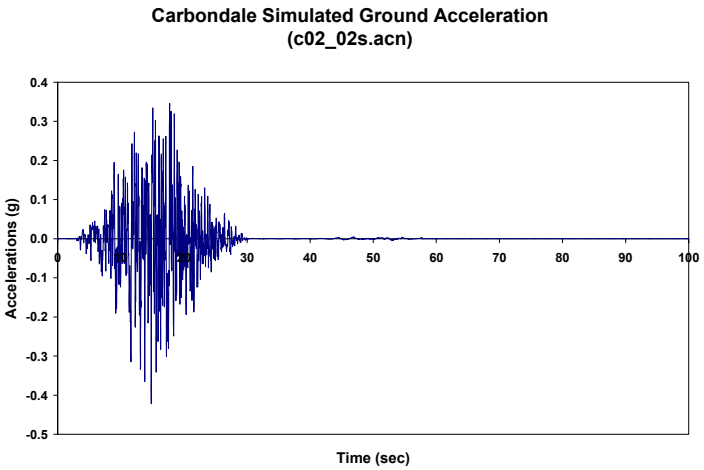

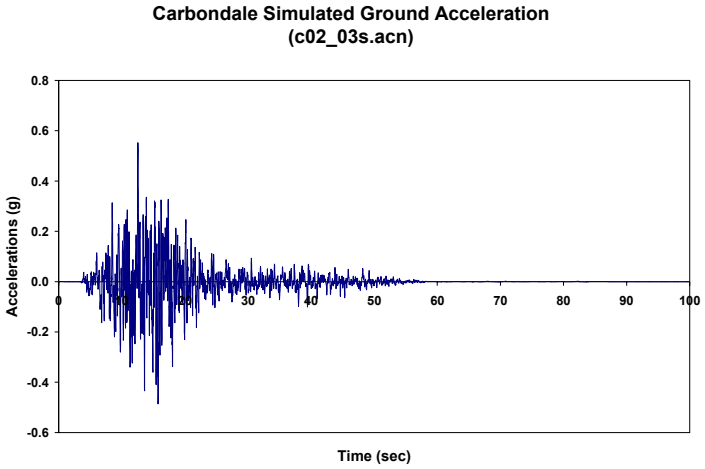
Carbondale Simulated Ground Acceleration
(c02_03s.acn)
Accelerations (g)
Time (sec)

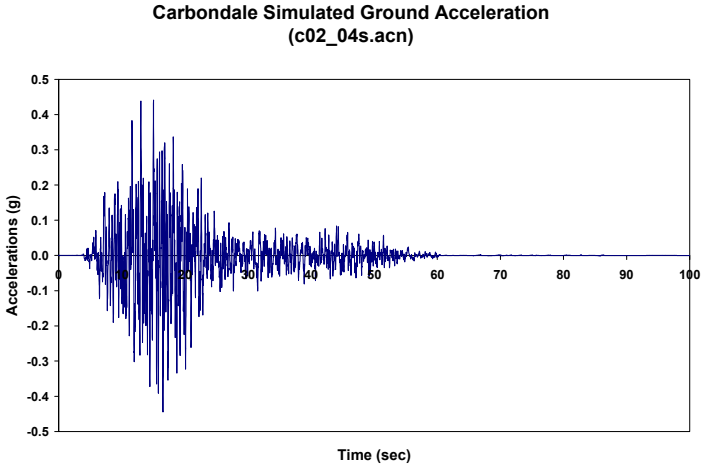
Carbondale Simulated Ground Acceleration
(c02_04s.acn)
Accelerations (g)
Time (sec)

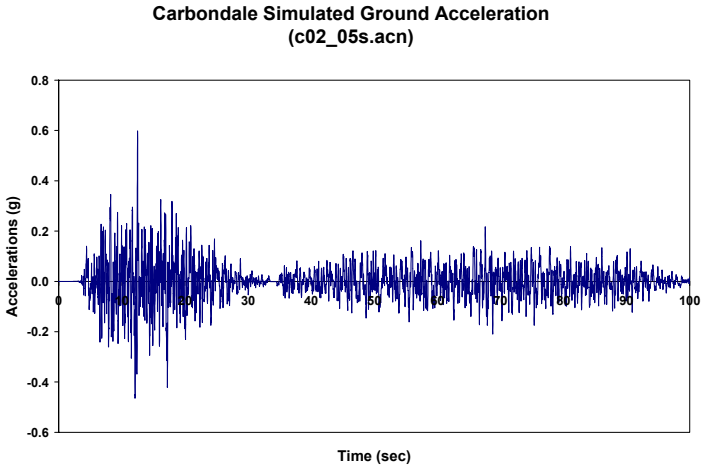
Carbondale Simulated Ground Acceleration
(c02_05s.acn)
Accelerations (g)
Time (sec)

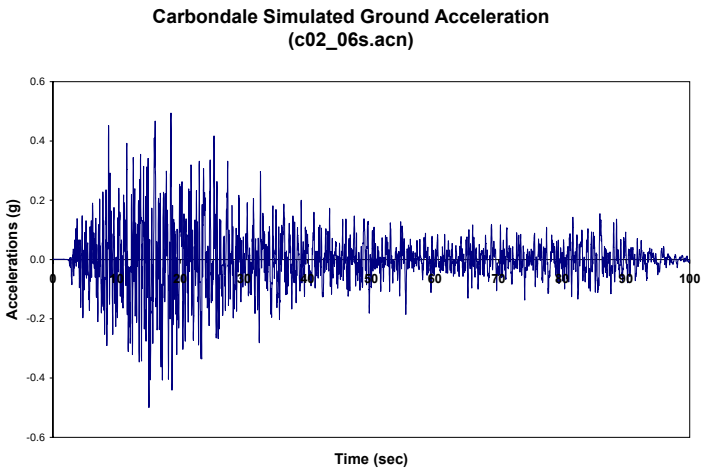
Carbondale Simulated Ground Acceleration
(c02_06s.acn)
Accelerations (g)
Time (sec)

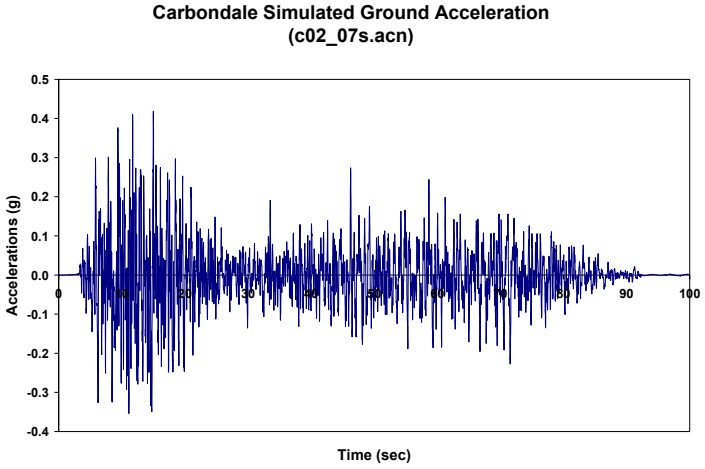
Carbondale Simulated Ground Acceleration
(c02_07s.acn)
Accelerations (g)
Time (sec)

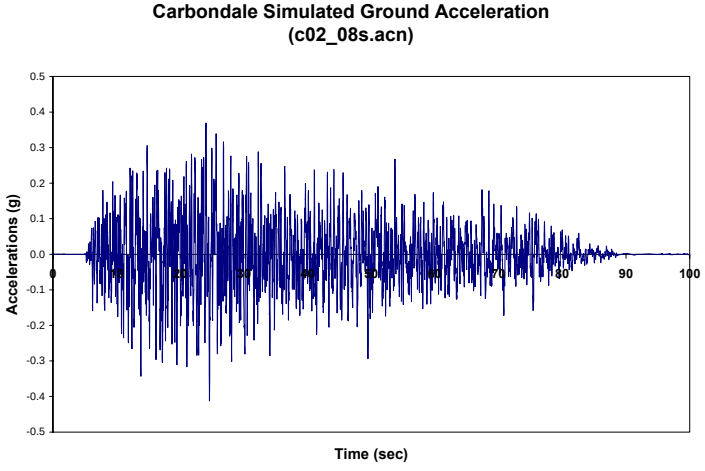
Carbondale Simulated Ground Acceleration
(c02_08s.acn)
Accelerations (g)
Time (sec)

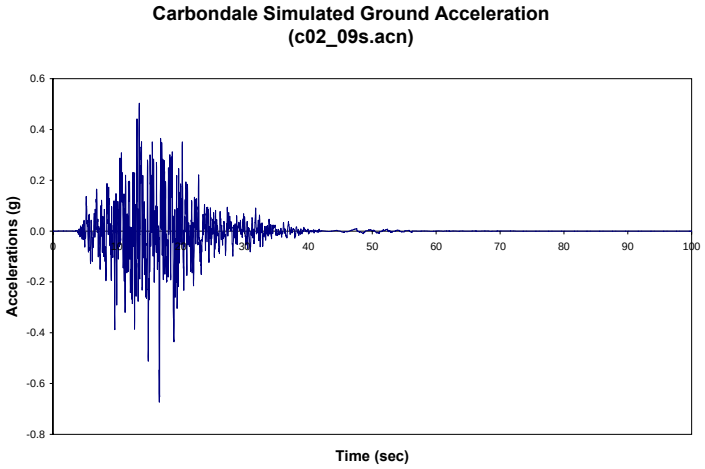
Carbondale Simulated Ground Acceleration
(c02_09s.acn)
Accelerations (g)
Time (sec)
0.6
0.4
0.2
0.0
-0.2
-0.4
-0.6
-0.8
0
10
20
30
40
50
60
70
80
90
100

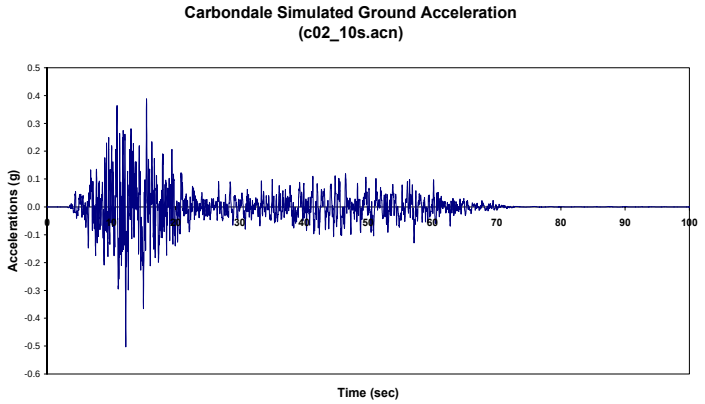
Carbondale Simulated Ground Acceleration
(c02_10s.acn)
Accelerations (g)
Time (sec)
0.5
0.4
0.3
0.2
0.1
0.0
-0.1
-0.2
-0.3
-0.4
-0.5
-0.6
0
10
20
30
40
50
60
70
80
90
100

APPENDIX B: Detailed Fabrication Drawings for ST-10 Rehabilitation

The drawings shown in this appendix were provided by project ST-10 and were used to create the simplified structural models used in the present study. The dimensions and materials specified in these drawings were used to formulate the nonlinear spring models used to represent the in-plane URM walls and the diaphragm stiffness.

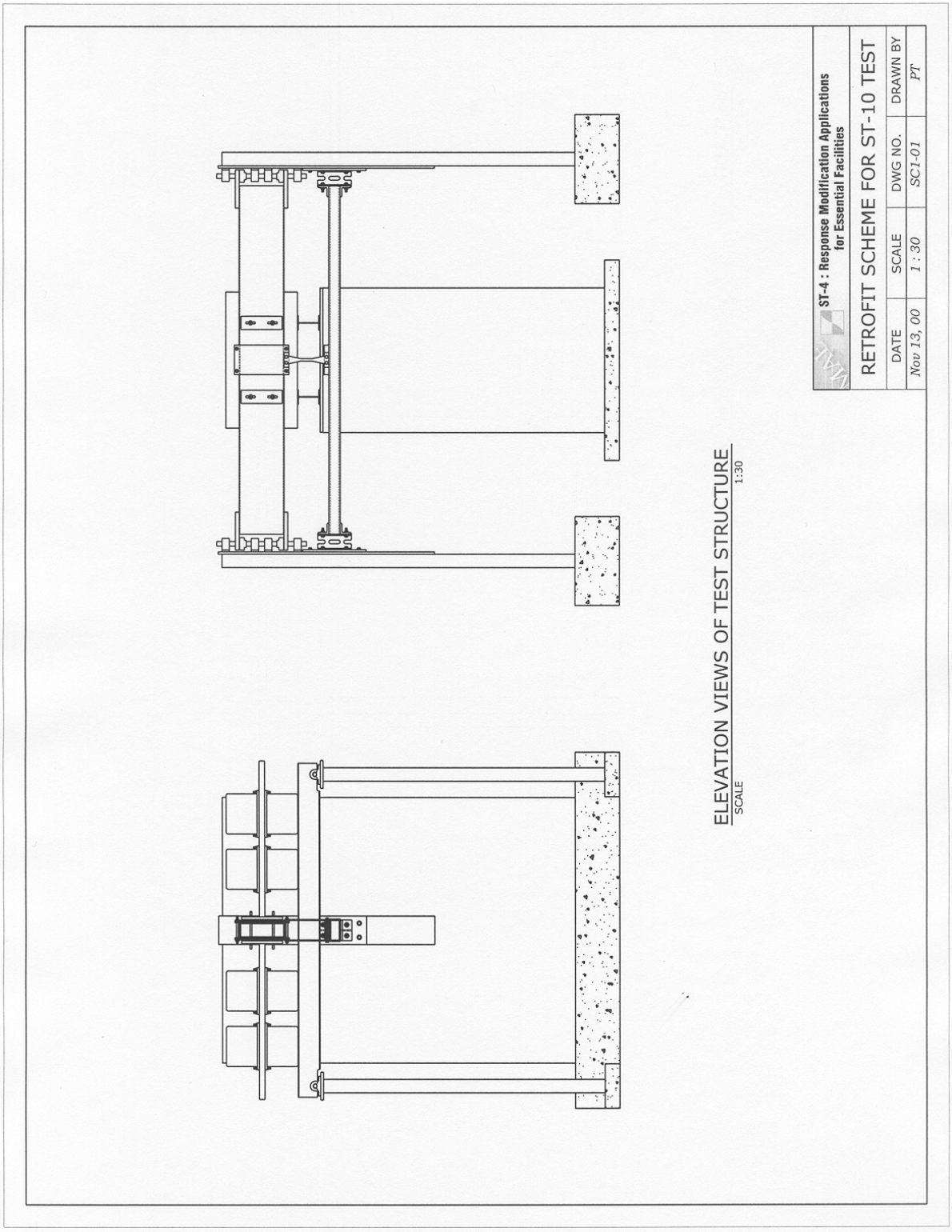
ST-4 : Response Modification Applications for Essential Facilities
RETROFIT SCHEME FOR ST-10 TEST
DATE
Nov 13, 00
SCALE
1 : 30
DWG NO.
SC1-01
DRAWN BY
PT
ELEVATION VIEWS OF TEST STRUCTURE
SCALE
1:30

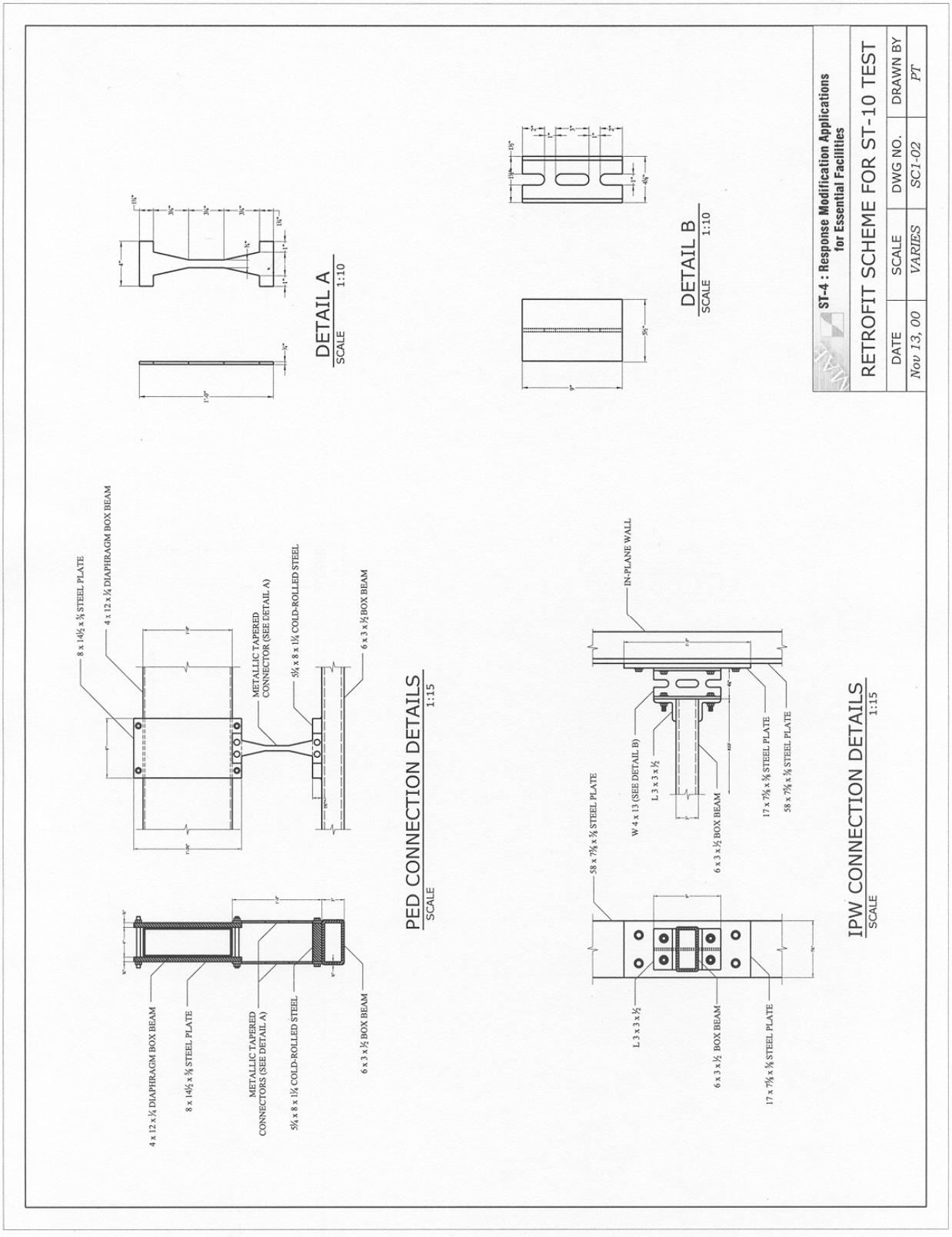
DETAIL A
SCALE 1:10
DETAIL B
SCALE 1:10
PED CONNECTION DETAILS
SCALE 1:15
8 x 14½ x ⅜ STEEL PLATE
4 x 12 x ¼ DIAPHRAGM BOX BEAM
METALLIC TAPERED CONNECTOR (SEE DETAIL A)
5¼ x 8 x 1¼ COLD-ROLLED STEEL
6 x 3 x ½ BOX BEAM
4 x 12 x ¼ DIAPHRAGM BOX BEAM
8 x 14½ x ⅜ STEEL PLATE
METALLIC TAPERED CONNECTORS (SEE DETAIL A)
5¼ x 8 x 1¼ COLD-ROLLED STEEL
6 x 3 x ½ BOX BEAM
IPW CONNECTION DETAILS
SCALE 1:15
IN-PLANE WALL
58 x 7⅞ x ⅜ STEEL PLATE
W 4 x 13 (SEE DETAIL B)
L 3 x 3 x ½
6 x 3 x ½ BOX BEAM
17 x 7⅞ x ⅜ STEEL PLATE
58 x 7⅞ x ⅜ STEEL PLATE
L 3 x 3 x ½
6 x 3 x ½ BOX BEAM
17 x 7⅞ x ⅜ STEEL PLATE
ST-4 : Response Modification Applications for Essential Facilities
RETROFIT SCHEME FOR ST-10 TEST
DATE Nov 13, 00
SCALE VARIES
DWG NO. SC1-02
DRAWN BY PT

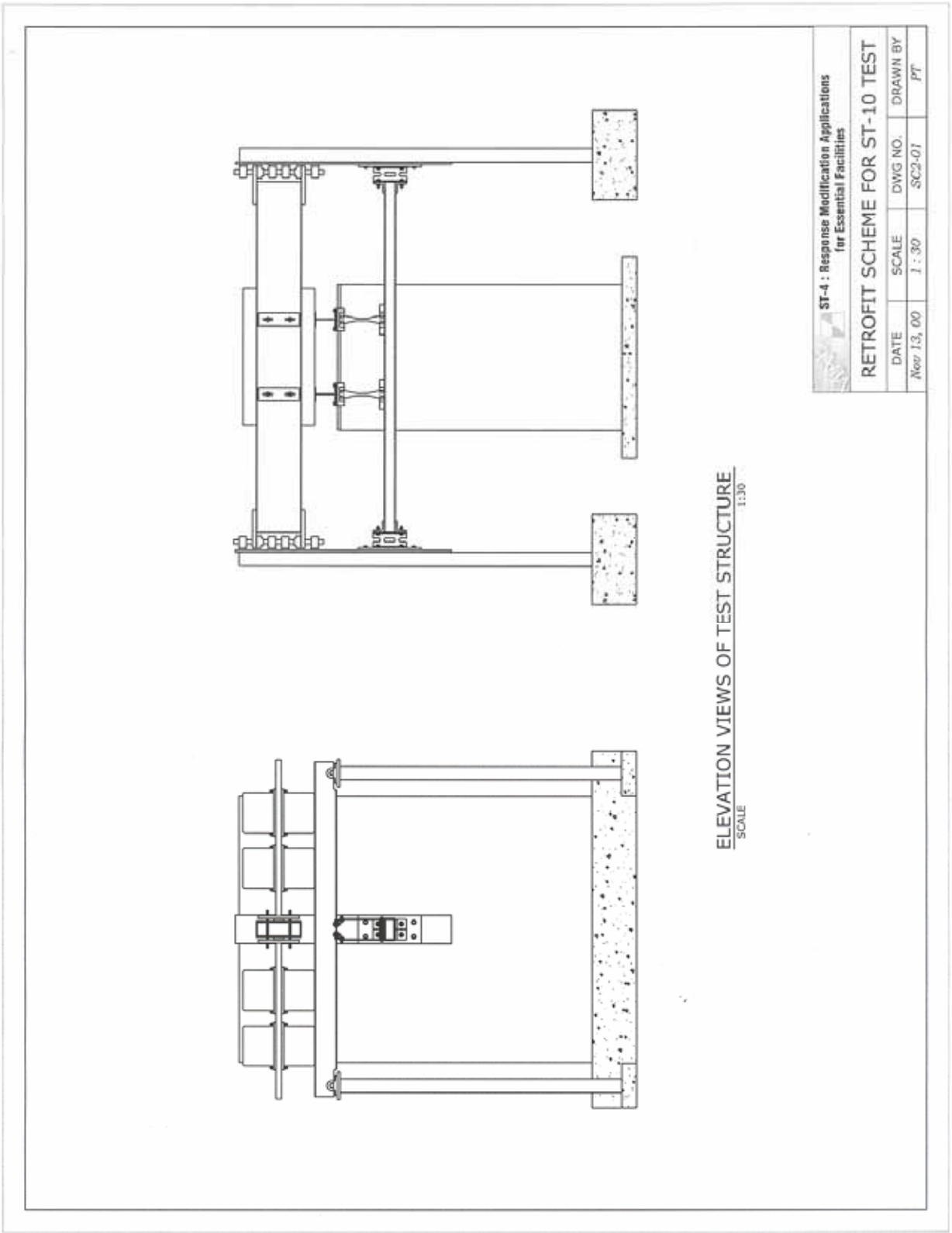
ST-4 : Response Modification Applications for Essential Facilities
RETROFIT SCHEME FOR ST-10 TEST
DATE
Nov 13, 00
SCALE
1 : 30
DWG NO.
SC2-01
DRAWN BY
PT
ELEVATION VIEWS OF TEST STRUCTURE
SCALE
1:30

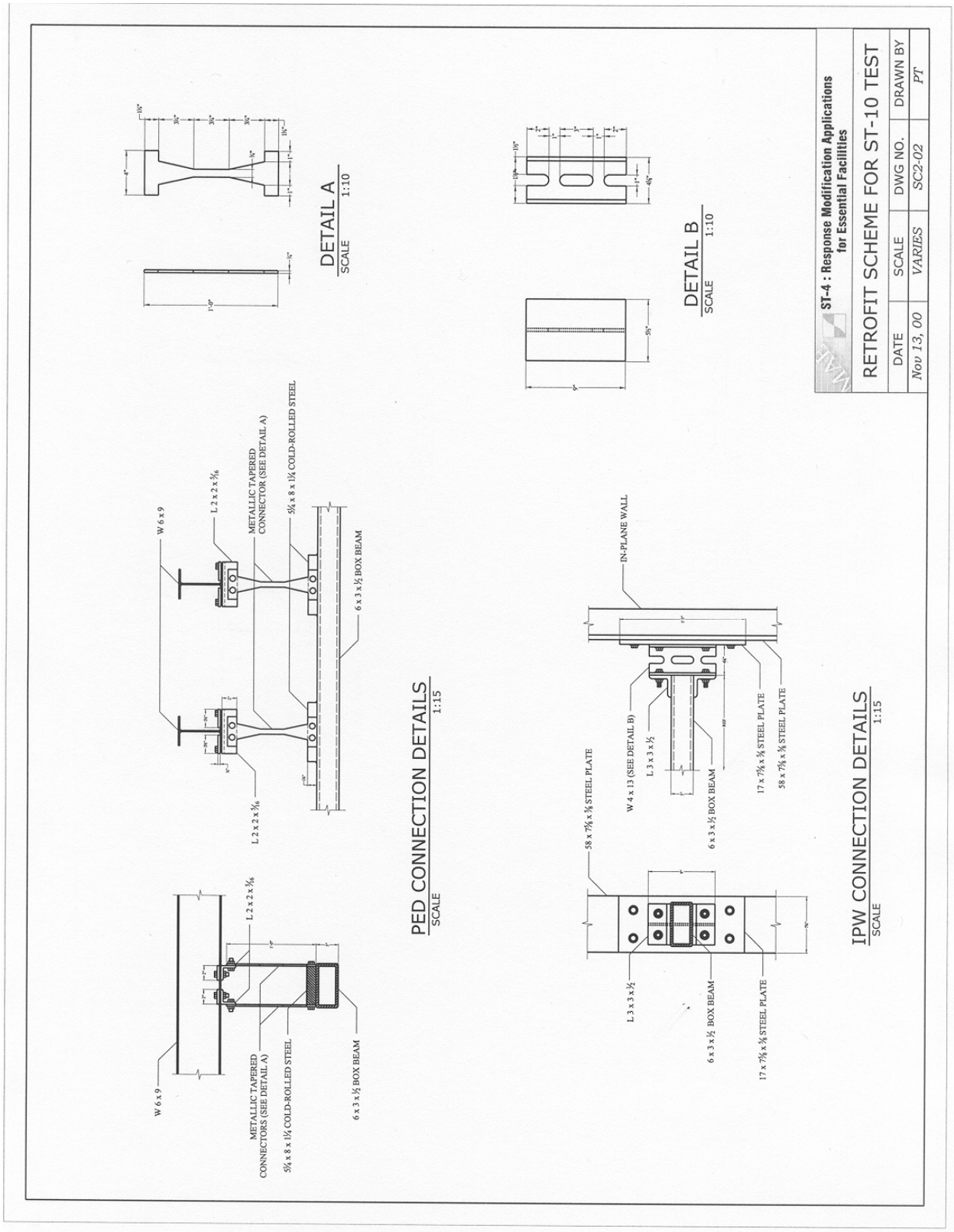
DETAIL A
SCALE 1:10
DETAIL B
SCALE 1:10
PED CONNECTION DETAILS
SCALE 1:15
IPW CONNECTION DETAILS
SCALE 1:15
W 6 x 9
L 2 x 2 x 5/16
METALLIC TAPERED CONNECTOR (SEE DETAIL A)
5/16 x 8 x 1/4 COLD-ROLLED STEEL
6 x 3 x 1/2 BOX BEAM
IN-PLANE WALL
W 4 x 13 (SEE DETAIL B)
L 3 x 3 x 1/2
58 x 7/8 x 5/8 STEEL PLATE
17 x 7/8 x 5/8 STEEL PLATE
ST-4 : Response Modification Applications for Essential Facilities
RETROFIT SCHEME FOR ST-10 TEST
DATE Nov 13, 00
SCALE VARIES
DWG NO. SC2-02
DRAWN BY PT

APPENDIX C: DRAIN-2DX Input File for ST-11 Building

This appendix contains lists the DRAIN-2DX input file for the analysis of the example structure which is described in Section 3.5. The stiffness and strength of each pier are pre-calculated and input as the spring properties. The PED element is attached in the manner that is described in Section 3.5. The analysis is performed with x-direction ground acceleration only making wall A and wall B in-plane walls.

C.1 With Type 1 Rehabilitation Scheme

```
!SPRING MODEL FOR REPRESENTING THE ST-11 STRUCTURE UNDER X-DIR ACCELARATION
!APPLY GROUND ACCELERATION
! PED Device is incorporated into the model using a bilinear spring element
!
!WALL A AND B ARE MOVING IN X DIRECTION
!WALL 1 AND 2 ARE MOVING IN Y DIRECTION
!NO OUT-OF-PLANE STIFFNESS
!ANALYSIS STEP = one increment (smaller)
!ANALYSIS SEGMENT = whole unit of analysis
!
!234567890123456789012345678901234567890123456789O
!
!
!
*STARTXX
  ST-11_PED        0 0 0 1   F          ST-11 Composite Spring Model (with PED 1)
!
!
!
*NODECOORDS
! OPTION   NODE#   X-COOR   Y-COOR
!Wall A
C         1         0.         0.     ! base
C         2         0.         0.
C         3         0.         0.
C         4         0.         0.
C         5         0.         0.
C         6         0.         0.
C         7         0.         0.
C         8         0.         0.
C         9         0.         0.
!Wall B
C        11         0.         0.
C        12         0.         0.
C        13         0.         0.
C        14         0.         0.
C        15         0.         0.
C        16         0.         0.
C        17         0.         0.
C        18         0.         0.
C        19         0.         0.
!Wall 1
C        21         0.         0.
C        22         0.         0.
C        23         0.         0.
C        24         0.         0.
C        25         0.         0.
C        26         0.         0.
C        27         0.         0.
C        28         0.         0.
```

```
!Wall 2
C       31        0.        0.
C       32        0.        0.
C       33        0.        0.
C       34        0.        0.
C       35        0.        0.
C       36        0.        0.
C       37        0.        0.
C       38        0.        0.
!Diaphragm 1 and 2
C       41        0.        0.
C       42        0.        0.
!
!
!
*RESTRAINTS
!0=FREE, 1=FIXED, 2=SPRING SUPPORTED, 3=NO CHANGE
! XYR   S-NODE   E-NODE  INCREMENT
S 111         1        31        10
S 011         2         9         1
S 011        12        19         1
S 101        22        28         1
S 101        32        38         1
S 001        41        42         1
!
!
!
!
*MASSES
! XYZ MASS-VAL.    S-NODE    E-NODE   INCREMENT                        F     ALPHA
!1st floor
S 111     0.085         5         5         1                      1.0     0.003
S 111     0.085        15        15         1                      1.0     0.003
S 111     0.085        24        24         1                      1.0     0.003
S 111     0.085        34        34         1                      1.0     0.003
S 111     0.088        41        41         1                      1.0     0.003
!2nd floor
S 111     0.044         9         9         1                      1.0     0.003
S 111     0.044        19        19         1                      1.0     0.003
S 111     0.044        28        28         1                      1.0     0.003
S 111     0.044        38        38         1                      1.0     0.003
S 111     0.047        42        42         1                      1.0     0.003
!
*ELEMENTGROUP    !   01 Wall A
!234567890123456789012345678901234567890123456789012345678901234567890
!!!!!!!!!!!!!!!!!!!!!!!!!!!!!
!!!!!!                 !!!!!!!
!!!!!!  Wall A        !!!!!!!
!!!!!!                 !!!!!!!
!!!!!!!!!!!!!!!!!!!!!!!!!!!!!
!TYPE CODE  P-D          BETHA          G-TITLE
    4    1    0           .001          wall A
   14         !TOTAL # OF PROPERTY TYPES --- THERE ARE 14 TYPE OF PROPERTIES OF
!   #         K      Kh/K       Syt       Syc TOLERANCE CODE  E-CODE
!1st story,    ROT 01,      ROCKING
    1  15825.31      0.01    100.00     100.0       0.1    1    1
!1st story,    BOT,         SLIDING
    2  16678.38      0.01    100.00    100.00       0.1    1    0
!1st story,    PIER 01,     ROCKING
    3   1688.14      0.01     7.075     7.075       0.1    1    1
!1st story,    PIER 02,     ROCKING
    4    880.73      0.01     8.599     8.599       0.1    1    1
!1st story,    PIER 03,     ROCKING
    5    966.34      0.01     8.599     8.599       0.1    1    1
!1st story,    PIER 04,     ROCKING
    6   1133.95      0.01    12.382    12.382       0.1    1    1
!1st story,    TOP,         SLIDING
    7  13612.09      0.01    100.00    100.00       0.1    1    0
!
!2nd story,    ROT 02,      ROCKING
    8   2491.51      0.01    100.00    100.00       0.1    1    1
!2nd story,    BOT,         SLIDING
```

```
    9  21447.34      0.01    100.00    100.00       0.1    1    0
!2nd story,    PIER 01,     ROCKING
   10    1138.3      0.01      4.23      4.23       0.1    1    1
!2nd story,    PIER 02,     ROCKING
   11    970.11      0.01     2.938     2.938       0.1    1    1
!2nd story,    PIER 03,     ROCKING
   12    970.11      0.01     2.938     2.938       0.1    1    1
!2nd story,    PIER 04,     ROCKING
   13    1138.3      0.01      4.23      4.23       0.1    1    1
!2nd story,    TOP,         SLIDING
   14  17352.35      0.01    100.00    100.00       0.1    1    0
!
! ELEMENT GENERATION
! Wall A
!   #       N-1       N-2       INC  PRO.
    1         1         2         1    1
    2         2         3         1    2
    3         2         4         2    3
    4         3         4         1    4
    5         3         4         1    5
    6         3         4         1    6
    7         4         5         1    7
    8         5         6         1    8
    9         6         7         1    9
   10         7         8         1   10
   11         7         8         1   11
   12         7         8         1   12
   13         7         8         1   13
   14         8         9         1   14
!
*ELEMENTGROUP    !   02 Wall B
!234567890123456789012345678901234567890123456789012345678901234567890
!!!!!!!!!!!!!!!!!!!!!!!!!!!!!!
!!!!!!                 !!!!!!!
!!!!!!  Wall  B       !!!!!!!
!!!!!!                 !!!!!!!
!!!!!!!!!!!!!!!!!!!!!!!!!!!!!!
!TYPE CODE  P-D          BETHA          G-TITLE
    4    1    0           .001          wall B
   14         !TOTAL # OF PROPERTY TYPES --- THERE ARE 14 TYPE OF PROPERTIES OF
!   #         K      Kh/K       Syt       Syc TOLERANCE CODE  E-CODE
!1st story,    ROT 01,      ROCKING
    1  15825.31      0.01    100.00    100.00       0.1    1    1
!1st story,    BOT,         SLIDING
    2  16678.38      0.01    100.00    100.00       0.1    1    0
!1st story,    PIER 01,     ROCKING
    3   1688.14      0.01     7.075     7.075       0.1    1    1
!1st story,    PIER 02,     ROCKING
    4    880.73      0.01     8.599     8.599       0.1    1    1
!1st story,    PIER 03,     ROCKING
    5    966.34      0.01     8.599     8.599       0.1    1    1
!1st story,    PIER 04,     ROCKING
    6   1133.95      0.01    12.382    12.382       0.1    1    1
!1st story,    TOP,         SLIDING
    7  13612.09      0.01    100.00    100.00       0.1    1    0
!
!2nd story,    ROT 02,      ROCKING
    8   2491.51      0.01    100.00    100.00       0.1    1    1
!2nd story,    BOT,         SLIDING
    9  21447.34      0.01    100.00    100.00       0.1    1    0
!2nd story,    PIER 01,     ROCKING
   10    1138.3      0.01      4.23      4.23       0.1    1    1
!2nd story,    PIER 02,     ROCKING
   11    970.11      0.01     2.938     2.938       0.1    1    1
!2nd story,    PIER 03,     ROCKING
   12    970.11      0.01     2.938     2.938       0.1    1    1
!2nd story,    PIER 04,     ROCKING
   13    1138.3      0.01      4.23      4.23       0.1    1    1
!2nd story,    TOP,         SLIDING
   14  17352.35      0.01    100.00    100.00       0.1    1    0
!
! ELEMENT GENERATION
```

```
! Wall A
!   #       N-1       N-2       INC  PRO.
    1        11        12         1    1
    2        12        13         1    2
    3        12        14         2    3
    4        13        14         1    4
    5        13        14         1    5
    6        13        14         1    6
    7        14        15         1    7
    8        15        16         1    8
    9        16        17         1    9
   10        17        18         1   10
   11        17        18         1   11
   12        17        18         1   12
   13        17        18         1   13
   14        18        19         1   14
!
*ELEMENTGROUP    !   03 Wall 1
!234567890123456789012345678901234567890123456789012345678901234567890
!!!!!!!!!!!!!!!!!!!!!!!!!!!!
!!!!!!                !!!!!!!
!!!!!!  Wall 1        !!!!!!!
!!!!!!                !!!!!!!
!!!!!!!!!!!!!!!!!!!!!!!!!!!!
!TYPE CODE  P-D          BETHA          G-TITLE
    4    1    0           .001          wall 1
   10         !TOTAL # OF PROPERTY TYPES --- THERE ARE 9 TYPE OF PROPERTIES OF T
!   #         K      Kh/K       Syt       Syc TOLERANCE CODE  E-CODE
!1st story,    ROT 01,      ROCKING
    1  11396.83      0.01    100.00     100.0       0.1    2    1
!1st story,    PIER 01,     ROCKING
    2    328.44      0.01     4.499     4.499       0.1    2    1
!1st story,    PIER 02,     SLIDING
    3   3632.07      0.01    67.844    67.844       0.1    2    0
!1st story,    TOP,         SLIDING
    4   8784.54      0.01    100.00    100.00       0.1    2    0
!
!2nd story,    ROT 02,      ROCKING
    5    1794.3      0.01    100.00    100.00       0.1    2    1
!2nd story,    BOT,         SLIDING
    6  13823.52      0.01    100.00    100.00       0.1    2    0
!2nd story,    PIER 01,     ROCKING
    7    723.77      0.01      2.69      2.69       0.1    2    1
!2nd story,    PIER 02,     ROCKING
    8   3443.24      0.01    17.951    17.951       0.1    2    1
!2nd story,    PIER 03,     ROCKING
    9    723.77      0.01      2.69      2.69       0.1    2    1
!2nd story,    TOP,         SLIDING
   10  11192.75      0.01    100.00    100.00       0.1    2    0
!
!
! ELEMENT GENERATION
! Wall 1
!   #       N-1       N-2       INC  PRO.
    1        21        22         1    1
    2        22        23         1    2
    3        22        23         1    3
    4        23        24         1    4
    5        24        25         1    5
    6        25        26         1    6
    7        26        27         1    7
    8        26        27         1    8
    9        26        27         1    9
   10        27        28         1   10
!
*ELEMENTGROUP    !   04 Wall 2
!234567890123456789012345678901234567890123456789012345678901234567890
!!!!!!!!!!!!!!!!!!!!!!!!!!!!
!!!!!!                !!!!!!!
!!!!!!  Wall 2        !!!!!!!
!!!!!!                !!!!!!!
!!!!!!!!!!!!!!!!!!!!!!!!!!!!
```

```
!TYPE CODE  P-D          BETHA          G-TITLE
    4    1    0           .001          wall 2
   12         !TOTAL # OF PROPERTY TYPES --- THERE ARE 10 TYPE OF PROPERTIES OF
!   #         K      Kh/K       Syt       Syc TOLERANCE CODE  E-CODE
!1st story,    ROT 01,      ROCKING
    1   8321.13      0.01    100.00     100.0       0.1    2    1
!1st story,    PIER 01,     ROCKING
    2    250.37      0.01      4.27      4.27       0.1    2    1
!1st story,    PIER 02,     ROCKING
    3     54.52      0.01     0.984     0.984       0.1    2    1
!1st story,    PIER 03,     ROCKING
    4    250.37      0.01      4.27      4.27       0.1    2    1
!1st story,    TOP,         SLIDING
    5  11192.75      0.01    100.00    100.00       0.1    2    0
!
!2nd story,    ROT 02,      ROCKING
    6   1310.07      0.01    100.00    100.00       0.1    2    1
!2nd story,    BOT,         SLIDING
    7  13823.52      0.01    100.00    100.00       0.1    2    0
!2nd story,    PIER 01,     ROCKING
    8    723.77      0.01      2.69      2.69       0.1    2    1
!2nd story,    PIER 02,     ROCKING
    9    220.39      0.01     0.741     0.741       0.1    2    1
!2nd story,    PIER 03,     ROCKING
   10    220.39      0.01     0.741     0.741       0.1    2    1
!2nd story,    PIER 04,     ROCKING
   11    723.77      0.01      2.69      2.69       0.1    2    1
!2nd story,    TOP,         SLIDING
   12  11192.75      0.01    100.00    100.00       0.1    2    0
!
! ELEMENT GENERATION
! Wall 2
!   #       N-1       N-2       INC  PRO.
    1        31        32         1    1
    2        32        33         1    2
    3        32        33         1    3
    4        32        33         1    4
    5        33        34         1    5
    6        34        35         1    6
    7        35        36         1    7
    8        36        37         1    8
    9        36        37         1    9
   10        36        37         1   10
   11        36        37         1   11
   12        37        38         1   12
!
*ELEMENTGROUP    !   05 Diaphragm
!234567890123456789012345678901234567890123456789012345678901234567890
!!!!!!!!!!!!!!!!!!!!!!!!!!!!
!!!!!!                !!!!!!!
!!!!!!  Diaphragm     !!!!!!!
!!!!!!                !!!!!!!
!!!!!!!!!!!!!!!!!!!!!!!!!!!!
!TYPE CODE  P-D          BETHA          G-TITLE
    4    1    0           .001            DIA
!   #         E      Eh/E       Syt       Syc TOLERANCE  DIR  E-CODE
    2         !TOTAL # OF PROPERTY TYPES --- THERE ARE 4 TYPE  PROPERTIES OF THI
    1       4.0      0.01     125.6     125.6      0.01    1    0  ! shear-X DIR
    2       4.0      0.01     125.6     125.6      0.01    2    0  ! shear-Y DIR
!
! ELEMENT GENERATION
! Diaphragm 1 and 2
!   #       N-1       N-2       INC  PRO.
    1         5        41        36    1
    2        15        41        26    1
    3        24        41        17    2
    4        34        41         7    2
!
    5         9        42        33    1
    6        19        42        23    1
    7        28        42        14    2
    8        38        42         4    2
```

```
!
! GROUP#6 NONLINEAR SPRINGS (PED Device)
!
*ELEMENTGROUP
    4    1    0       0.001602          SPRING (PED Device) HORIZ
    1
! Property Types
!   #    init K   str hrdng    Fy+       Fy-    overshoot dir  elst
!-------------------------------------------------------------------
![PAR04]
    1     15.00      0.00      4.00      4.00      0.01    1    0
!
! Element Generation
!   #       node i    node j    incr prop
!-----------------------------------------
    1         5         41         0    1
    2         9         42         0    1
!
!
*RESULTS
NSD    111          9          9          1
NSD    111          5          5          1
NSD    111         42         42          1
E      111    1     1     1     1
E      111    2     2    14     1
E      111    5
E      111    6
!
!
!
*ACCNREC      ![Inserted by NONLIN-Pro]
 c-10    c02_10s.acn            (2F15.0) WEN'S CARBONDALE EQ - REP SOIL
! Wen's accelerations are in unit of cm/s^2
! Output needed are in unit of inches
! Convert the accel from cm/s^2 to in/s^2 by multiplying 0.3937 (1/2.54)
15000    1     1    1       1.0    0.3937      0.01       0.0
!
*PARAMETERS
OD       0          0    0          0    1                          20000
DC  1    0     0    0
DT    0.01 !TIME STEP (INCRESE BY 0.010)
!
*ACCN                                     WEN'S CARBONDALE EQ - REP SOIL
100.0     99999    1
1     c-10       1.5       1.0
!
*STOP
```

C.2 With Type 2 Rehabilitation Scheme

```
!SPRING MODEL FOR REPRESENTING THE ST-11 STRUCTURE UNDER X-DIR ACCELARATION
!APPLY GROUND ACCELERATION
! PED Device is incorporated into the model using a bilinear spring element
!
!WALL A AND B ARE MOVING IN X DIRECTION
!WALL 1 AND 2 ARE MOVING IN Y DIRECTION
!NO OUT-OF-PLANE STIFFNESS
!ANALYSIS STEP = one increment (smaller)
!ANALYSIS SEGMENT = whole unit of analysis
!
!234567890123456789012345678901234567890123456789
!
!
!
*STARTXX
  ST-11_P2         0 0 0 1   F              ST-11 Composite Spring Model (PED 2)
!
!
!
```

```
*NODECOORDS
! OPTION   NODE#   X-COOR   Y-COOR
!Wall A
C         1        0.       0.     ! base
C         2        0.       0.
C         3        0.       0.
C         4        0.       0.
C         5        0.       0.
C         6        0.       0.
C         7        0.       0.
C         8        0.       0.
C         9        0.       0.
!Wall B
C        11        0.       0.
C        12        0.       0.
C        13        0.       0.
C        14        0.       0.
C        15        0.       0.
C        16        0.       0.
C        17        0.       0.
C        18        0.       0.
C        19        0.       0.
!Wall 1
C        21        0.       0.
C        22        0.       0.
C        23        0.       0.
C        24        0.       0.
C        25        0.       0.
C        26        0.       0.
C        27        0.       0.
C        28        0.       0.
!Wall 2
C        31        0.       0.
C        32        0.       0.
C        33        0.       0.
C        34        0.       0.
C        35        0.       0.
C        36        0.       0.
C        37        0.       0.
C        38        0.       0.
!Diaphragm 1 and 2
C        41        0.       0.
C        42        0.       0.
!
!
!
*RESTRAINTS
!0=FREE, 1=FIXED, 2=SPRING SUPPORTED, 3=NO CHANGE
! XYR   S-NODE   E-NODE  INCREMENT
S 111         1        31        10
S 011         2         9         1
S 011        12        19         1
S 101        22        28         1
S 101        32        38         1
S 001        41        42         1
!
!
!
!
*MASSES
! XYZ MASS-VAL.    S-NODE    E-NODE   INCREMENT                        F     ALPHA
!1st floor
S 111     0.085         5         5         1                      1.0     0.003
S 111     0.085        15        15         1                      1.0     0.003
S 111     0.085        24        24         1                      1.0     0.003
S 111     0.085        34        34         1                      1.0     0.003
S 111     0.088        41        41         1                      1.0     0.003
!2nd floor
S 111     0.044         9         9         1                      1.0     0.003
S 111     0.044        19        19         1                      1.0     0.003
S 111     0.044        28        28         1                      1.0     0.003
S 111     0.044        38        38         1                      1.0     0.003
```

```
S 111     0.047        42        42         1                        1.0     0.003
!
*ELEMENTGROUP    !   01 Wall A
!234567890123456789012345678901234567890123456789012345678901234567890
!!!!!!!!!!!!!!!!!!!!!!!!!!!!
!!!!!!                !!!!!!!
!!!!!!  Wall A        !!!!!!!
!!!!!!                !!!!!!!
!!!!!!!!!!!!!!!!!!!!!!!!!!!!
!TYPE CODE  P-D          BETHA          G-TITLE
    4    1    0           .001          wall A
   14         !TOTAL # OF PROPERTY TYPES --- THERE ARE 14 TYPE OF PROPERTIES OF
!   #         K      Kh/K       Syt       Syc TOLERANCE CODE  E-CODE
!1st story,    ROT 01,      ROCKING
    1  15825.31      0.01    100.00     100.0       0.1    1    1
!1st story,    BOT,         SLIDING
    2  16678.38      0.01    100.00    100.00       0.1    1    0
!1st story,    PIER 01,     ROCKING
    3   1688.14      0.01     7.075     7.075       0.1    1    1
!1st story,    PIER 02,     ROCKING
    4    880.73      0.01     8.599     8.599       0.1    1    1
!1st story,    PIER 03,     ROCKING
    5    966.34      0.01     8.599     8.599       0.1    1    1
!1st story,    PIER 04,     ROCKING
    6   1133.95      0.01    12.382    12.382       0.1    1    1
!1st story,    TOP,         SLIDING
    7  13612.09      0.01    100.00    100.00       0.1    1    0
!
!2nd story,    ROT 02,      ROCKING
    8   2491.51      0.01    100.00    100.00       0.1    1    1
!2nd story,    BOT,         SLIDING
    9  21447.34      0.01    100.00    100.00       0.1    1    0
!2nd story,    PIER 01,     ROCKING
   10    1138.3      0.01      4.23      4.23       0.1    1    1
!2nd story,    PIER 02,     ROCKING
   11    970.11      0.01     2.938     2.938       0.1    1    1
!2nd story,    PIER 03,     ROCKING
   12    970.11      0.01     2.938     2.938       0.1    1    1
!2nd story,    PIER 04,     ROCKING
   13    1138.3      0.01      4.23      4.23       0.1    1    1
!2nd story,    TOP,         SLIDING
   14  17352.35      0.01    100.00    100.00       0.1    1    0
!
! ELEMENT GENERATION
! Wall A
!   #       N-1       N-2       INC  PRO.
    1         1         2         1    1
    2         2         3         1    2
    3         2         4         2    3
    4         3         4         1    4
    5         3         4         1    5
    6         3         4         1    6
    7         4         5         1    7
    8         5         6         1    8
    9         6         7         1    9
   10         7         8         1   10
   11         7         8         1   11
   12         7         8         1   12
   13         7         8         1   13
   14         8         9         1   14
!
*ELEMENTGROUP    !   02 Wall B
!234567890123456789012345678901234567890123456789012345678901234567890
!!!!!!!!!!!!!!!!!!!!!!!!!!!!
!!!!!!                !!!!!!!
!!!!!!  Wall  B       !!!!!!!
!!!!!!                !!!!!!!
!!!!!!!!!!!!!!!!!!!!!!!!!!!!
!TYPE CODE  P-D          BETHA          G-TITLE
    4    1    0           .001          wall B
   14         !TOTAL # OF PROPERTY TYPES --- THERE ARE 14 TYPE OF PROPERTIES OF
!   #         K      Kh/K       Syt       Syc TOLERANCE CODE  E-CODE
```

```
!1st story,    ROT 01,      ROCKING
    1  15825.31      0.01    100.00    100.00       0.1    1    1
!1st story,    BOT,         SLIDING
    2  16678.38      0.01    100.00    100.00       0.1    1    0
!1st story,    PIER 01,     ROCKING
    3   1688.14      0.01     7.075     7.075       0.1    1    1
!1st story,    PIER 02,     ROCKING
    4    880.73      0.01     8.599     8.599       0.1    1    1
!1st story,    PIER 03,     ROCKING
    5    966.34      0.01     8.599     8.599       0.1    1    1
!1st story,    PIER 04,     ROCKING
    6   1133.95      0.01    12.382    12.382       0.1    1    1
!1st story,    TOP,         SLIDING
    7  13612.09      0.01    100.00    100.00       0.1    1    0
!
!2nd story,    ROT 02,      ROCKING
    8   2491.51      0.01    100.00    100.00       0.1    1    1
!2nd story,    BOT,         SLIDING
    9  21447.34      0.01    100.00    100.00       0.1    1    0
!2nd story,    PIER 01,     ROCKING
   10    1138.3      0.01      4.23      4.23       0.1    1    1
!2nd story,    PIER 02,     ROCKING
   11    970.11      0.01     2.938     2.938       0.1    1    1
!2nd story,    PIER 03,     ROCKING
   12    970.11      0.01     2.938     2.938       0.1    1    1
!2nd story,    PIER 04,     ROCKING
   13    1138.3      0.01      4.23      4.23       0.1    1    1
!2nd story,    TOP,         SLIDING
   14  17352.35      0.01    100.00    100.00       0.1    1    0
!
! ELEMENT GENERATION
! Wall A
!   #       N-1       N-2       INC  PRO.
    1        11        12         1    1
    2        12        13         1    2
    3        12        14         2    3
    4        13        14         1    4
    5        13        14         1    5
    6        13        14         1    6
    7        14        15         1    7
    8        15        16         1    8
    9        16        17         1    9
   10        17        18         1   10
   11        17        18         1   11
   12        17        18         1   12
   13        17        18         1   13
   14        18        19         1   14
!
*ELEMENTGROUP    !   03 Wall 1
!234567890123456789012345678901234567890123456789012345678901234567890
!!!!!!!!!!!!!!!!!!!!!!!!!!!!
!!!!!!                !!!!!!!
!!!!!!  Wall 1        !!!!!!!
!!!!!!                !!!!!!!
!!!!!!!!!!!!!!!!!!!!!!!!!!!!
!TYPE CODE  P-D          BETHA          G-TITLE
    4    1    0           .001          wall 1
   10         !TOTAL # OF PROPERTY TYPES --- THERE ARE 9 TYPE OF PROPERTIES OF T
!   #         K      Kh/K       Syt       Syc TOLERANCE CODE  E-CODE
!1st story,    ROT 01,      ROCKING
    1  11396.83      0.01    100.00     100.0       0.1    2    1
!1st story,    PIER 01,     ROCKING
    2    328.44      0.01     4.499     4.499       0.1    2    1
!1st story,    PIER 02,     SLIDING
    3   3632.07      0.01    67.844    67.844       0.1    2    0
!1st story,    TOP,         SLIDING
    4   8784.54      0.01    100.00    100.00       0.1    2    0
!
!2nd story,    ROT 02,      ROCKING
    5    1794.3      0.01    100.00    100.00       0.1    2    1
!2nd story,    BOT,         SLIDING
    6  13823.52      0.01    100.00    100.00       0.1    2    0
```

```
!2nd story,    PIER 01,     ROCKING
    7    723.77      0.01      2.69      2.69       0.1    2    1
!2nd story,    PIER 02,     ROCKING
    8   3443.24      0.01    17.951    17.951       0.1    2    1
!2nd story,    PIER 03,     ROCKING
    9    723.77      0.01      2.69      2.69       0.1    2    1
!2nd story,    TOP,         SLIDING
   10  11192.75      0.01    100.00    100.00       0.1    2    0
!
!
! ELEMENT GENERATION
! Wall 1
!   #       N-1       N-2       INC  PRO.
    1        21        22         1    1
    2        22        23         1    2
    3        22        23         1    3
    4        23        24         1    4
    5        24        25         1    5
    6        25        26         1    6
    7        26        27         1    7
    8        26        27         1    8
    9        26        27         1    9
   10        27        28         1   10
!
*ELEMENTGROUP    !   04 Wall 2
!234567890123456789012345678901234567890123456789012345678901234567890
!!!!!!!!!!!!!!!!!!!!!!!!!!!!
!!!!!!                !!!!!!!
!!!!!!  Wall 2        !!!!!!!
!!!!!!                !!!!!!!
!!!!!!!!!!!!!!!!!!!!!!!!!!!!
!TYPE CODE  P-D          BETHA          G-TITLE
    4    1    0           .001          wall 2
   12         !TOTAL # OF PROPERTY TYPES --- THERE ARE 10 TYPE OF PROPERTIES OF
!   #         K      Kh/K       Syt       Syc TOLERANCE CODE  E-CODE
!1st story,    ROT 01,      ROCKING
    1   8321.13      0.01    100.00     100.0       0.1    2    1
!1st story,    PIER 01,     ROCKING
    2    250.37      0.01      4.27      4.27       0.1    2    1
!1st story,    PIER 02,     ROCKING
    3     54.52      0.01     0.984     0.984       0.1    2    1
!1st story,    PIER 03,     ROCKING
    4    250.37      0.01      4.27      4.27       0.1    2    1
!1st story,    TOP,         SLIDING
    5  11192.75      0.01    100.00    100.00       0.1    2    0
!
!2nd story,    ROT 02,      ROCKING
    6   1310.07      0.01    100.00    100.00       0.1    2    1
!2nd story,    BOT,         SLIDING
    7  13823.52      0.01    100.00    100.00       0.1    2    0
!2nd story,    PIER 01,     ROCKING
    8    723.77      0.01      2.69      2.69       0.1    2    1
!2nd story,    PIER 02,     ROCKING
    9    220.39      0.01     0.741     0.741       0.1    2    1
!2nd story,    PIER 03,     ROCKING
   10    220.39      0.01     0.741     0.741       0.1    2    1
!2nd story,    PIER 04,     ROCKING
   11    723.77      0.01      2.69      2.69       0.1    2    1
!2nd story,    TOP,         SLIDING
   12  11192.75      0.01    100.00    100.00       0.1    2    0
!
! ELEMENT GENERATION
! Wall 2
!   #       N-1       N-2       INC  PRO.
    1        31        32         1    1
    2        32        33         1    2
    3        32        33         1    3
    4        32        33         1    4
    5        33        34         1    5
    6        34        35         1    6
    7        35        36         1    7
    8        36        37         1    8
```

```
    9        36        37         1    9
   10        36        37         1   10
   11        36        37         1   11
   12        37        38         1   12
!
*ELEMENTGROUP    !   05 Diaphragm
!234567890123456789012345678901234567890123456789012345678901234567890
!!!!!!!!!!!!!!!!!!!!!!!!!!!!!!
!!!!!!                 !!!!!!!
!!!!!!  Diaphragm     !!!!!!!
!!!!!!                 !!!!!!!
!!!!!!!!!!!!!!!!!!!!!!!!!!!!!!
!TYPE CODE  P-D          BETHA          G-TITLE
    4    1    0           .001            DIA
!   #         E      Eh/E       Syt       Syc TOLERANCE  DIR  E-CODE
    2         !TOTAL # OF PROPERTY TYPES --- THERE ARE 4 TYPE  PROPERTIES OF THI
    1       4.0      0.01     125.6     125.6      0.01    1    0  ! shear-X DIR
    2       4.0      0.01     125.6     125.6      0.01    2    0  ! shear-Y DIR
!
! ELEMENT GENERATION
! Diaphragm 1 and 2
!   #       N-1       N-2       INC  PRO.
    1         5        41        36    1
    2        15        41        26    1
    3        24        41        17    2
    4        34        41         7    2
!
    5         9        42        33    1
    6        19        42        23    1
    7        28        42        14    2
    8        38        42         4    2
!
! GROUP#6 NONLINEAR SPRINGS (PED Device)
!
*ELEMENTGROUP
    4    1    0       0.001602          SPRING (PED Device) HORIZ
    1
! Property Types
!   #    init K   str hrdng    Fy+       Fy-    overshoot dir  elst
!-------------------------------------------------------------------
![PAR04]
    1     15.00      0.00      4.00      4.00      0.01    1    0
!
! Element Generation
!   #       node i    node j    incr prop
!-----------------------------------------
    1         1        41         0    1
    2         5        42         0    1
!
!
*RESULTS
!TYPE  MAN.P28   N-1       N-2       INC
NSD    111         9         9         1
NSD    111         5         5         1
NSD    111        42        42         1
E      111    1    1    1    1
E      111    2    2   14    1
E      111    5
E      111    6
!
!
!
*ACCNREC      ![Inserted by NONLIN-Pro]
 c-10    c02_10s.acn            (2F15.0) WEN'S CARBONDALE EQ - REP SOIL
! Wen's accelerations are in unit of cm/s^2
! Output needed are in unit of inches
! Convert the accel from cm/s^2 to in/s^2 by multiplying 0.3937 (1/2.54)
15000    1    1    1       1.0    0.3937      0.01       0.0
!
*PARAMETERS
OD       0         0    0         0    1                         20000
DC  1    0    0    0
```

```
DT    0.01 !TIME STEP (INCRESE BY 0.010)
!
*ACCN                                    WEN'S CARBONDALE EQ - REP SOIL
100.0     99999    1
1     c-10       1.5       1.0
!
*STOP
```

APPENDIX D: DRAIN-2DX Park 3-Parameter Element

This appendix describes the DRAIN-2DX element (called the Type 03 element and replacing the default element of the same name) developed in this study. The Type 03 element is a nonlinear spring element capable of representing stiffness degradation, strength deterioration, and pinching effect in its hysteresis property. Park's 3 parameter model (Park et al, 1987) is adopted and the subroutine is integrated in DRAIN-2DX source code (replacing the default Type 03 element). The modified source code can be downloaded from *http://www.maec.gatech.edu/st4/html/st4.htm*

The following text is the guide for preparing the input file for the Type 03 element. The format follows that used in the RAM (Advanced Structural Concepts, Inc., 1998) manual for the commercial version of DRAIN-2DX, and as a result it can be inserted as a part of that manual.

E03.2 INPUT DATA FOR *ELEMENTGROUP

E03.2.1 Control Information

One line

Columns	Notes	Variable	Data
1-5(I)			No. of property types (min. 1, max. 40)

E03.2.2 Property Types

Values are all sign sensitive, *i.e.*, compression force and negative deformation should be input as negative.

Three lines for each property type.

First line

Columns	Notes	Variable	Data
1-10(I)			Property type number, in sequence beginning with 1.
11-20(R)			Initial stiffness, E0
21-30(R)			Positive post-yielding stiffness, Eyp
31-40(R)			Negative post-yielding stiffness, Eyn

41-50(R)			Positive cracking force, Pcp
51-60(R)			Negative cracking force, Pcn

Second line

Columns	Notes	Variable	Data
1-10(R)			Positive yielding force, Pyp
11-20(R)			Negative yielding force, Pyn
21-30(R)			Positive yielding deformation, Uyp
31-40(R)			Negative yielding deformation, Uyn
41-50(R)			Alpha (stiffness degradation factor) positive, $\alpha+$
51-60(R)			Alpha (stiffness degradation factor) negative, $\alpha-$

Third line

Columns	Notes	Variable	Data
1-10(R)			Beta (strength deterioration factor) positive, $\beta+$
11-20(R)			Beta (strength deterioration factor) negative, $\beta-$
21-30(R)			Positive slipping yielding force ($\gamma*$Pyp), Psp (set to be larger than Pyp when no slip is expected)
31-40(R)			Negative slipping yielding force ($\gamma*$Pyn) Psn (set to be smaller than Pyn when no slip is expected)
41-50(R)			Slip factor to change the slip point, SLPF (set to 1.0 to avoid this effect)
51-60(R)			Overshoot tolerance (force value)
61-65(I)			Direction code, as follows. 1 = X translation 2 = Y translation 3 = Z translation